

UNCLASSIFIED

AD NUMBER

AD917373

LIMITATION CHANGES

TO:

Approved for public release; distribution is unlimited.

FROM:

Distribution authorized to DoD only; Test and Evaluation; MAR 1974. Other requests shall be referred to Army Ballistic Missile Defense Agency, Safeguard Systems Command, PO Box 1500, Huntsville, AL 35807.

AUTHORITY

usassc ltr, 10 may 1974

THIS PAGE IS UNCLASSIFIED

UNCLASSIFIED

AD NUMBER

AD917373

LIMITATION CHANGES

TO:

Distribution authorized to DoD only; Test and Evaluation; MAR 1974. Other requests shall be referred to Army Ballistic Missile Defense Agency, Safeguard Systems Command, PO Box 1500, Huntsville, AL 35807.

FROM:

Distribution authorized to U.S. Gov't. agencies only; Test and Evaluation; 12 NOV 1971. Other requests shall be referred to Army Ballistic Missile Defense Agency, Safeguard Systems Command, PO Box 1500, Huntsville, AL 35807.

AUTHORITY

mar 1974 per document marking

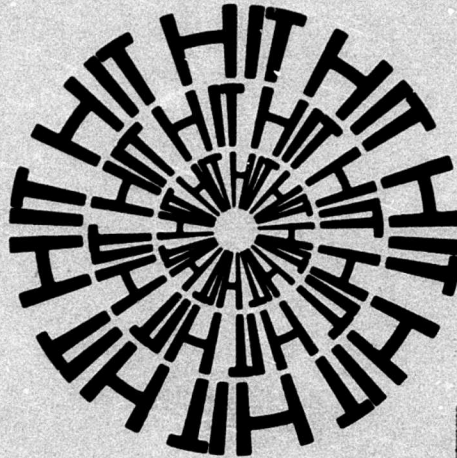
THIS PAGE IS UNCLASSIFIED

HIT-TO-KILL HOMER GROUND TEST (HIT PHASE II)

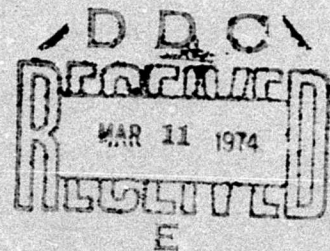
CONTRACT DAHC60-71-C-0072

TASK COMPLETION REPORT MANEUVER MOTOR ARRAY

AD917373



MARCH 1974



**SPONSORED BY THE U.S. ARMY ADVANCED
BALLISTIC MISSILE DEFENSE AGENCY**

The findings of this report are not to be construed
as an official Department of the Army position



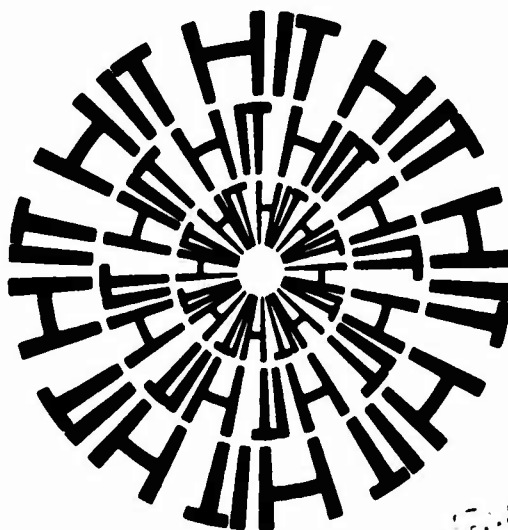
VOUGHT SYSTEMS DIVISION
LTV AEROSPACE CORPORATION

"Limiting Statement: Distribution limited to U.S. Government
Agencies Only; Test and Evaluation; 12 November 1971.
Other requests for this document must be referred to
ABMDA, ATTN: RDMD-MD"

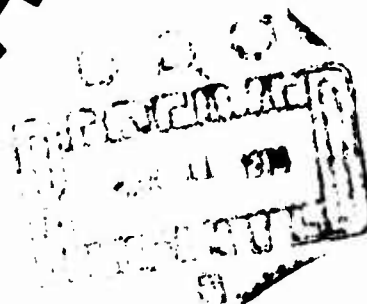
HIT-TO-KILL HOMER GROUND TEST (HIT PHASE II)

CONTRACT DAHC60-71-C-0072

TASK COMPLETION REPORT MANEUVER MOTOR ARRAY



MARCH 1974



SPONSORED BY THE U.S. ARMY ADVANCED
BALLISTIC MISSILE DEFENSE AGENCY

The findings of this report are not to be construed
as an official Department of the Army position



VOUGHT SYSTEMS DIVISION
LTV AEROSPACE CORPORATION

"Limiting Statement: Distribution limited to U.S. Government
Agencies Only; Test and Evaluation, 12 November 1971.
Other requests for this document must be referred to
ABMDA, ATTN: RDMD-MD"

TABLE OF CONTENTS

<u>Section No.</u>	<u>Title</u>	<u>Page</u>
1.0	<u>INTRODUCTION AND SUMMARY</u>	1
1.1	INTRODUCTION	1
1.2	SUMMARY	2
2.0	<u>MMA DESCRIPTION</u>	6
2.1	DESIGN	6
2.1.1	<u>Assembled MMA</u>	6
2.1.2	<u>Nozzle Ring</u>	6
2.1.3	<u>Motor Tube</u>	12
2.1.4	<u>Igniter</u>	13
2.1.5	<u>End Plug</u>	14
2.1.6	<u>Support Rings</u>	14
2.1.7	<u>Spacers</u>	16
2.1.8	<u>Insulator</u>	16
2.1.9	<u>Nozzle Seal</u>	16
2.1.10	<u>Propellant Grain</u>	17
2.2	PERFORMANCE	17
2.3	MASS PROPERTIES	17
3.0	<u>DEVELOPMENT DISCUSSION</u>	21
3.1	PROPELLANT CHARACTERIZATION	21
3.1.1	<u>Ballistic Test Program</u>	21
3.1.2	<u>Laboratory Study</u>	23
3.1.3	<u>Process and Physical Properties Controls</u>	28
3.2	IGNITER DEVELOPMENT	30
3.2.1	<u>Initial Development</u>	30
3.2.2	<u>Reliability Testing</u>	32
3.2.3	<u>Igniter Qualification</u>	32
3.2.4	<u>Igniter Requalification</u>	33

TABLE OF CONTENTS (Continued)

<u>Section No.</u>	<u>Title</u>	<u>Page</u>
3.3	MOTOR DEVELOPMENT TESTS	34
3.3.1	<u>Initial Tests</u>	34
3.3.2	<u>Failure Diagnosis Tests</u>	38
3.3.3	<u>Heavywall Confirmatory Tests</u>	44
3.3.4	<u>Pressure Oscillation Phenomena Tests</u>	45
3.3.5	<u>Design Verification Tests</u>	48
3.4	MOTOR CASE TESTS	64
3.4.1	<u>Burst Tests</u>	64
3.4.2	<u>Tube/Overwrap Bond Tests</u>	64
3.5	ANALYTICAL SUPPORT PROGRAMS	72
3.5.1	<u>MMA Sizing Analysis</u>	72
3.5.2	<u>Performance Variability Analysis</u>	75
3.5.3	<u>Thermal Analysis</u>	79
3.5.4	<u>Mass Properties Analysis and Measurement</u>	85
3.5.5	<u>Structural Analysis</u>	96
3.6	HIT STRUCTURAL MODEL ANALYSIS AND TEST	108
3.6.1	<u>HIT Structural Model Analyses</u>	108
3.6.2	<u>HIT Structural Model Test</u>	112
3.7	PROCESSING AND ASSEMBLY	113
3.7.1	<u>Component Part Manufacture</u>	113
3.7.2	<u>Motor Case Preparation</u>	113
3.7.3	<u>Propellant/Grain Manufacture</u>	113
3.7.4	<u>Assembly</u>	117
3.8	DESIGN EVOLUTION SUMMARY	119
3.8.1	<u>Nozzle Ring</u>	119
3.8.2	<u>Motor Case</u>	120

TABLE OF CONTENTS (Continued)

<u>Section No.</u>	<u>Title</u>	<u>Page</u>
	3.8.3 <u>Igniter</u>	121
	3.8.4 <u>End Plug</u>	121
	3.8.5 <u>Support Rings and Spacers</u>	122
	3.8.6 <u>Intertube Spacers</u>	122
	3.8.7 <u>Insulator</u>	122
	3.8.8 <u>Nozzle Seal</u>	123
	3.8.9 <u>Propellant Grain</u>	123
4.0	<u>CONCLUSIONS AND RECOMMENDATIONS</u>	124
	4.1 CONCLUSIONS	126
	4.2 FUTURE ACTIVITIES	127
	4.3 RECOMMENDATIONS	128
5.0	<u>BIBLIOGRAPHY</u>	129
	5.1 VSD DOCUMENTS	129
	5.2 ARC DRAWINGS	129
	5.3 ARC SPECIFICATIONS	130
	5.4 ARC REPORTS AND RELATED DOCUMENTS	130

LIST OF APPENDICES

<u>Number</u>	<u>Title</u>	<u>Page</u>
1.	Propellant Characterization Motor Test Data	133
2.	Typical Traces	152
3.	Thrust Alignment Test Plan	191
4.	Array Pendulum Test Plan	213
5.	Array Spin Test Plan	229
6.	Array Static Test Plan	240
7.	Key Personnel	256
8.	DD Form 1473	258

LIST OF FIGURES

<u>Figure No.</u>	<u>Title</u>	<u>Page</u>
2-1	Prototype Maneuver Motor Array	7
2-2	Profile and Cutaway View of MMA	8
2-3	Maneuver Motor Array	9
2-4	Motor Configuration	10
2-5	MMA Igniter	15
2-6	Nominal MMA Pressure and Thrust Histories	19
3-1	ATI Test Setup	37
3-2	Plume Impingement Test Setup	42
3-3	MMFC and Structural Model Subsystem Installation	57
3-4	Pendulum Test Fixture	58
3-5	Pendulum Test Setup	59
3-6	Spin Test Setup	61
3-7	MMA Static Test Setup	63
3-8	Prototype MMA Thermocouple Locations	67
3-9	Tube/Overwrap Bond Test Specimen Assembly	69
3-10	Typical Failure Modes - Tube/Overwrap Bond Tests	70
3-11	Tube/Overwrap Bond Test Setup	71
3-12	Nozzle Ring - Local Temperature Predictions	83
3-13	Thermocouple Data Comparisons	86
3-14	Mass Property Measurement Instruments	90
3-15	Mass Property Measurement Fixtures	91
3-16	MMA Stress Analysis Locations	103
3-17	Pressure vs Time-Firing No. 39900	106
3-18	HIT Structural Model	109
3-19	Typical Structural Model Shock Test	114
3-20	MMA Process Flow Chart	115

LIST OF TABLES

<u>Table No.</u>	<u>Title</u>	<u>Page</u>
2-I	MMA Materials and Gauges	11
2-II	Nominal MMA Performance	18
2-III	MMA Consumables Mass Properties	20
2-IV	Nominal MMA Mass Properties Summary	20
3-I	Propellant Characterization Mix History	22
3-II	Propellant Characterization Motor Ballistic Data Summary	24
3-III	Propellant Physical Properties	28
3-IV	Propellant Control Limits	29
3-V	Heavywall Confirmatory Test Ballistic Data Summary	46
3-VI	Pressure Oscillation Test Ballistic Data Summary	49
3-VII	Flightweight Test Ballistic Data Summary	51
3-VIII	Thrust Alignment Test Ballistic Data Summary	53
3-IX	Array Batch Check Test Ballistic Data Summary	55
3-X	Prototype Array Test Ballistic Data Summary	65
3-XI	Array Thermocouple Data Summary	66
3-XII	Individual Motor Performance Variability	76
3-XIII	Maximum Predicted MMA Temperatures	80
3-XIV	Mass Properties Controls	87
3-XV	Mass Properties Measurement Errors	89
3-XVI	Individual Motor Propellant Weights	92
3-XVII	Array Fire Down POI Measurements	94
3-XVIII	Consumables Mass Properties Summary	97
3-XIX	MMA Structural Safety Factor Summary	102
3-XX	MMA Component Parts	116
4-I	MMA Design Requirement Compliance Summary	125

GLOSSARY OF TERMS

ABMDA	Advanced Ballistic Missile Defense Agency
AP	Ammonium perchlorate
ARC	Atlantic Research Corporation
ATI	Adjacent tube interaction
CF	Thrust coefficient
CFO	Reference thrust coefficient
CG	Center of gravity
CP	Specific heat
CPS	Cycles per second
C_v	Coefficient of variation
DOT	Department of Transportation
FFB	Free-free beam
F_{max}	Maximum thrust
g	Mass conversion factor
G	Mass velocity
h	Convective heat transfer coefficient
HIT	Homing Interceptor Terminal
HTPB	Hydroxy-terminated polybutadiene
Hz	Hertz (cycles per second)
ID	Inside diameter
I_{sp}	Specific impulse
I_{spo}	Reference specific impulse
I_{sps}	Smearred specific impulse
I_{spin}	Spin moment of inertia
I_{pitch}	Pitch moment of inertia
I_T	Total impulse
IST	Integrated Systems Test
KDNBF	Potassium Dinitrobenzofuroxan
L/D	Length/diameter
MEOP	Maximum expected operating pressure
MMA	Maneuver Motor Array

GLOSSARY OF TERMS (Continued)

MMFC	Maneuver Motor Firing Circuit
MOI	Moment of inertia
N/A	Not applicable or not available
OD	Outside diameter
\bar{P}_b	Average pressure during burn time
PDR	Preliminary Design Review
P_{max}	Maximum pressure
POI	Product of inertia
Pr	Prandtl number
\bar{F}_b	Average burn rate during burn time
RE	Reynolds number
RPS	Revolutions per second
S	Smear factor
S. F. u	Ultimate Safety Factor
S. F. y	Yield Safety Factor
SM	Structural Model
SOS	Space Ordnance Systems, Inc.
t_a	Action time
t_b	Burn time
t_d	Ignition delay time
TVOPA	1, 2, 3-tris [$\alpha\beta$ -bis(difluoramino)ethoxy] propane
VSD	Vought Systems Division
VVM	Vibration Validation Model
W_i	Propulsion system inert weight
W_p	Propellant weight
W_{pl}	Payload weight
ΔPOI	Change in Product of Inertia
ΔV	Ideal velocity increment
σ	Standard deviation

1.0 INTRODUCTION AND SUMMARY

1.1 INTRODUCTION

The objective of the Maneuver Motor Array (MMA) Development program was to conduct the analyses, design, and testing necessary to develop a lightweight and integrated array of maneuver motors suitable for HIT systems ground flight testing. This objective has been achieved. A lightweight prototype MMA has been successfully developed and tested, thereby providing verification of the design for use in HIT integrated systems tests.

The MMA consists of 56 "T" burning solid propellant rocket motors, arranged in two concentric cylindrical rows of 28 motors each. These motors provide the lateral velocity increments to the HIT vehicle which are required to execute intercept. The nozzles for all motors are machined into a common, centrally located ring such that all 56 thrust vectors are directed through the HIT vehicle center of gravity. With the MMA rotating about its central axis, maneuvers can be made in any direction normal to the axis of rotation by firing a selected motor when it rotates into the proper position. The MMA also serves as the primary structural element of the HIT vehicle. Toward this end, system stiffness is enhanced by bonding all tubes together as a unit using longitudinal carbon phenolic intertube spacers and epoxy resin.

Stringent requirements were placed on the MMA as a consequence of the HIT system mechanization. Some of the more unique and critical requirements are: (1) provide a minimum ΔV of 970 fps to the MMA with a 6.608 lb payload; (2) individual motor thrust misalignment shall not exceed $\pm 0.25^\circ$; (3) time to impulse centroid, defined as the time interval between ignition command (current to initiation) and centroid of the thrust-time pulse (point at which half the pulse total impulse is delivered), shall be repeatable within ± 1.25 msec from pulse to pulse;

(4) individual motor action time shall not exceed 15 msec, and (5) mass properties of consumables (center of gravity, ratio of pitch to roll moment of inertia, and products of inertia) must be uniquely controlled.

This Task Completion Report covers the analysis, design, and testing efforts conducted since PDR to develop the HIT MMA Propulsion System. The work was accomplished by Vought Systems Division (VSD) of LTV Aerospace Corporation, under U. S. Army Contract DAHC60-71-C-0072. The major portion of the development activity was subcontracted to Atlantic Research Corporation (ARC). Detailed design, envelope, interface, performance, structural, and mass properties requirements were specified to ARC by means of VSD Source Control Drawing Number 371B-10010 and Procurement Specification Number 3-371-04-O-10185. Schedule, deliverable hardware, and documentation requirements were likewise established by means of Statement of Requirements Specification Number 3-371-13-O-10186.

The MMA design configuration established at PDR forms the baseline for the development work described herein. A discussion of the design, analysis, and testing efforts conducted prior to PDR, including the rationale by which the baseline MMA configuration and materials were selected, may be found in VSD Report Number 3-371-3R-Y-20023, dated 25 January 1972.

1.2 SUMMARY

Design and analysis efforts were conducted to define in detail a configuration capable of meeting the stringent performance, structural, and mass properties requirements. A propellant characterization program was conducted to define required propellant processing controls. Component tests were conducted to characterize, develop, and demonstrate the filament-wrapped motor tube, igniter, nozzle, insulator, end plug, nozzle closure, and grain end configurations. Adequacy of the resultant design was demonstrated by 25 successful heavywall motor tests and 31

successful flightweight motor tests. The program culminated in fabrication of a complete prototype MMA and successful test of all 56 motors.

The MMA development program was initiated in March 1972, and completed in November 1973. A series of 39 heavywall firings were performed in April 1972 to characterize the ARCEF 143 B propellant. Concurrently the igniter development program was initiated and efforts were directed toward the extremely detailed analyses required to define and justify the MMA design. During the month of May, analytical studies were conducted to optimize the system frequency by making the structure as stiff as possible without overstressing the bond joints. The resulting structural design was approved during a design review meeting held at the end of May 1972, and ARC was released to proceed with the fabrication of a structural model. With the approval of the structural design, motor case orders were released. Near the end of June squib assemblies capable of meeting the MMA ignition requirements became available.

In early July, the individual flightweight motor tests were initiated. Two tests were conducted to gather further ballistic data to confirm the flightweight motor case design, and four were conducted to evaluate thrust alignment. Five of the motors fired as expected, but the fourth thrust alignment test motor suffered a case rupture at ignition due to an excessively high chamber pressure, and a failure analysis was undertaken. The results of the investigation showed the primary problem to be unbonded areas between the carbon phenolic motor case insulator and the propellant grain. Other factors that could have contributed to the failure included damage to the propellant from igniter blast and overstress of the propellant.

While techniques to improve the propellant-case bond were studied, two more tests were conducted to evaluate the effects of adjacent motor tube interaction (ATI) in late August 1972. The first motor fired normally but the second resulted in another failure. Post-test analysis

showed that the motor case threads burned through at the nozzle ring. In addition, movies and heat flux data taken during the ATI tests revealed the exhaust plume would impinge on the battery and telemetry subsystems.

At this point a plan was defined for a series of single motor tests to diagnose and eliminate the design defects. Specifically, the tests evaluated the following items: (1) the effect of igniter impingement on the propellant grain; (2) the effect of unbonded areas at different locations in the propellant to motor case interface; (3) the effect of softened ignition, and (4) the effect of lengthening the nozzle on plume impingement. These tests involving 37 motor firings, were successfully concluded in January 1972 and appropriate corrective changes were incorporated into the MMA motor design.

In early February 1973, a series of design confirmation tests were initiated. Following a program stop-work in mid-February 1973, work was resumed in late March 1973 and by the end of the month a total of 15 heavywall titanium motors incorporating all of the design changes were successfully static-fired.

In May, June and July 1973, 6 heavywall and 7 flightweight motors were fired to evaluate oscillations recurring in the pressure time traces. All 13 motors performed as expected.

In May 1973, 6 flightweight motors were subjected to shock and vibration testing. Three of the units and a control unit were then static fired. The other 3 units were fired at a simulated spin rate of 25 rps. All motors operated as expected and showed no significant difference in ballistic performance under spin conditions. In June 1973, 10 thrust alignment tests were successfully conducted, 6 with flightweight motors and 4 with heavywall motors. This constituted completion of the component development phase of the program, which had involved firing 102 heavywall and 25 flightweight motors.

Due to limited funding, the prototype phase of the program was re-scoped to the assembly and test of a single array, and the IST production phase was postponed. During the months of August through October 1973, the prototype inert array was assembled and balanced, disassembled and cast with propellant, reassembled, bonded, balanced and inspected. In November, the array was successfully fired under static, spin and self-induced shock conditions. All 56 motors were successfully fired with ballistic performance which met the VSD specification limits, as discussed in section 4.0 of this report. These 56 motors, plus the last 56 motors fired during the component development program, brought the total number of consecutive successful motor firings to 112.

Based on these accomplishments, it is concluded that the MMA development has been successfully completed and that the existing prototype MMA design is suitable for use in HIT Integrated Systems Tests.

2.0 MMA DESCRIPTION

2.1 DESIGN

2.1.1 Assembled MMA

The MMA consists of 56 "T" burning solid propellant rocket motors, arranged in two concentric cylindrical rows of 28 motors each. The nozzles for all motors are machined into a common, centrally located ring such that all 56 thrust vectors are directed through the HIT vehicle center of gravity. One hundred and twelve motor tubes are threaded into the nozzle ring in opposing pairs to form the 56 motors. With the MMA rotating about its central axis, incremental maneuvers can be made in any direction normal to the axis of rotation by firing a selected motor when it rotates into the proper position. To provide stiffness, all tubes are bonded together using longitudinal carbon phenolic spacers and epoxy resin. Four equipment mounting rings are bonded onto the resultant tube bundle to form the MMA assembly.

The current design (Prototype) MMA is depicted in Figures 2-1 and 2-2. Comparisons between the current and PDR MMA designs are illustrated in Figures 2-3 and 2-4, and summarized in Table 2-I. The current design differs from the PDR design only at the detail level. The more significant design changes since PDR include: (1) making inner and outer row motor lengths equal to provide commonality; (2) lengthening nozzle exit cones to prevent plume impingement on external subsystems; (3) lengthening and changing insulator material to prevent burn throughs; and (4) increasing case and overwrap wall thicknesses to improve burst margin of safety. Each of the MMA components is described in the following sections.

2.1.2 Nozzle Ring

The nozzle ring is a single piece structure which contains all 56 nozzles of the Maneuver Motor Array. The ring has threaded openings to accept the 112 motor tubes which make up the 56 individual motors.

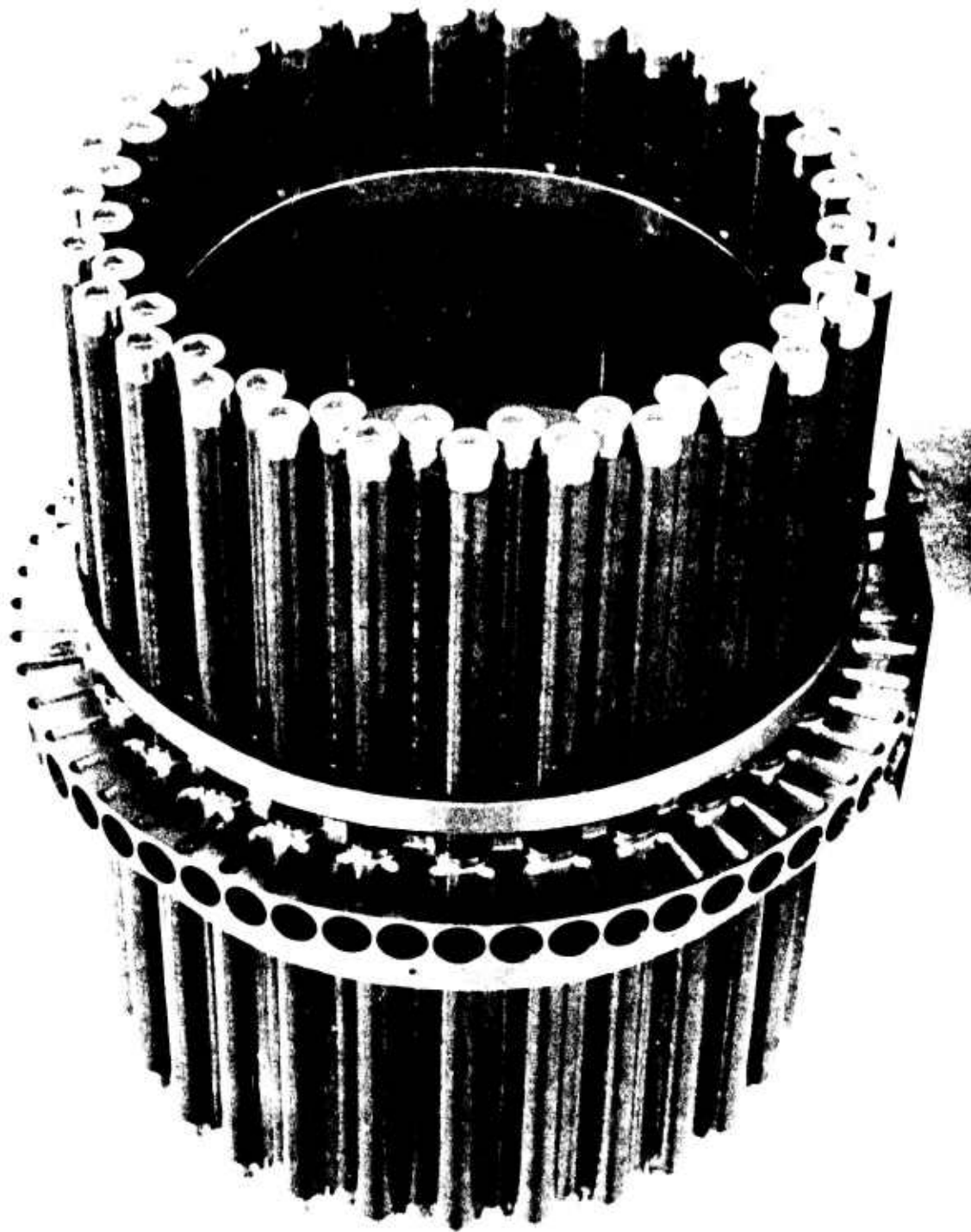


FIGURE 2-1 Prototype Maneuver Motor Array

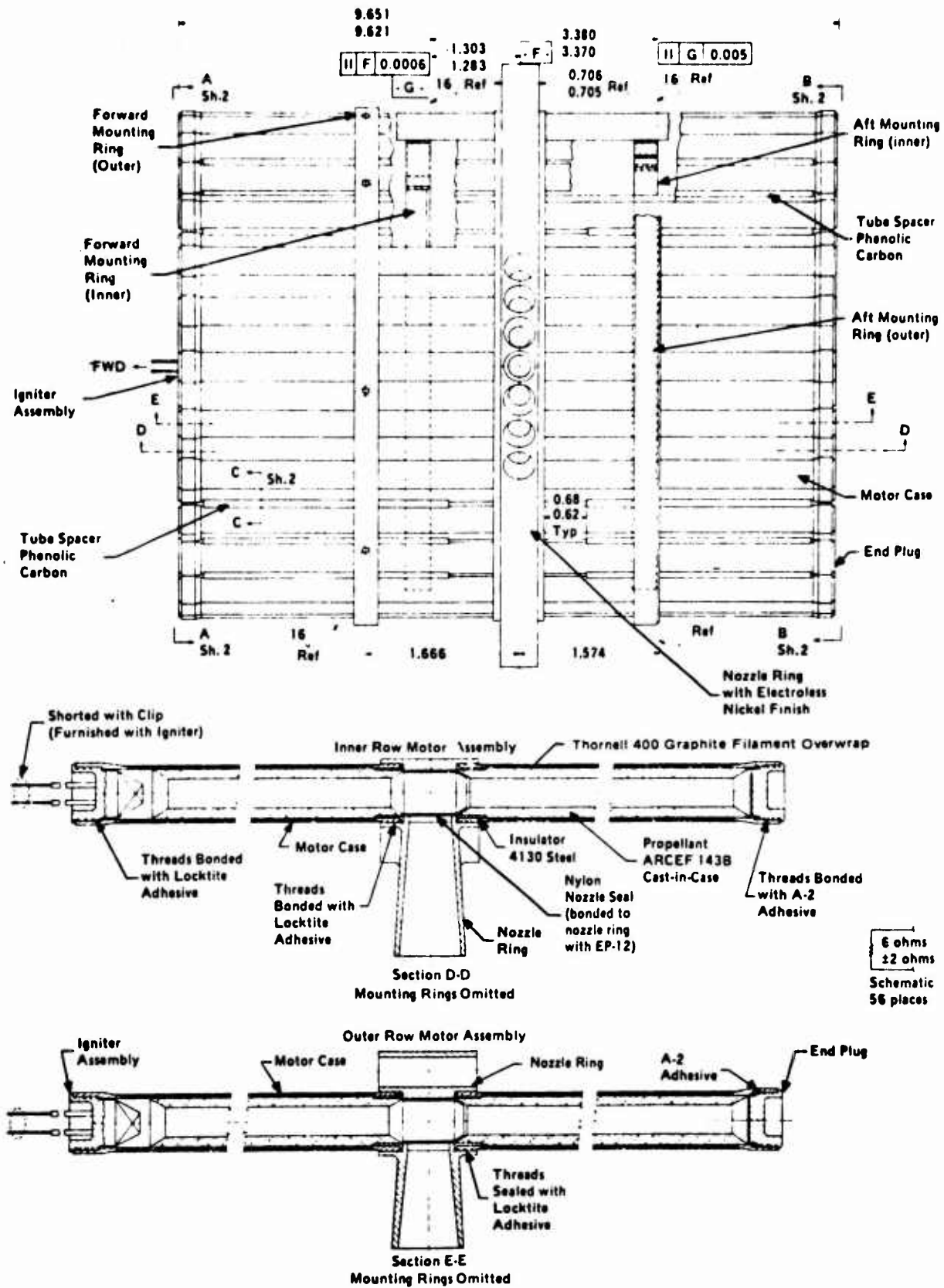


FIGURE 2-2 Profile and Cutaway View of MMA

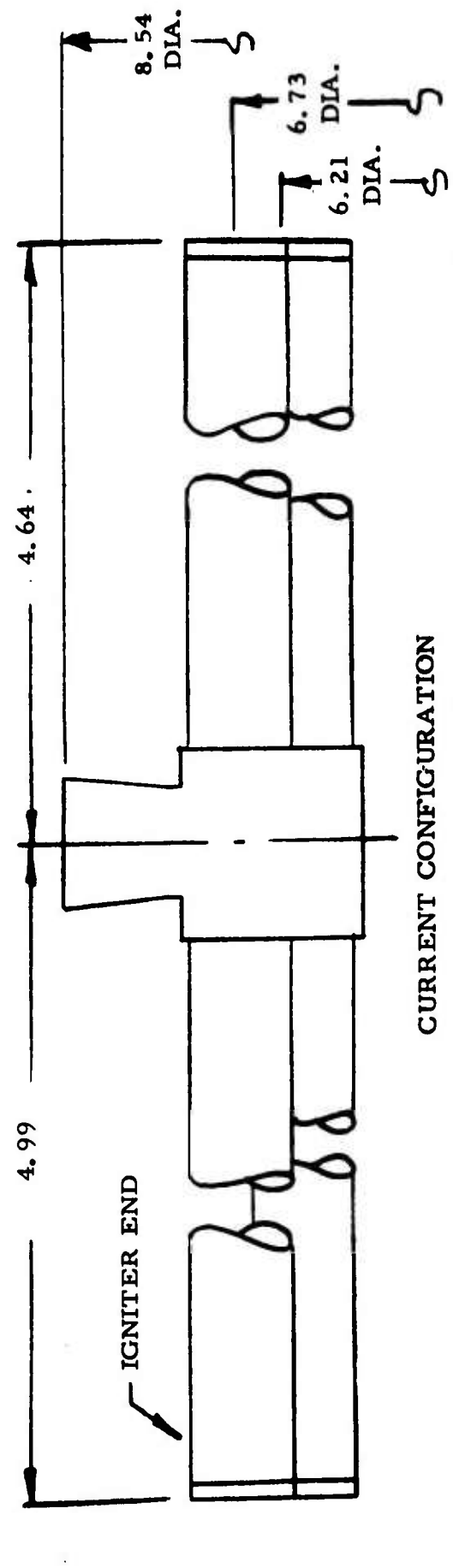
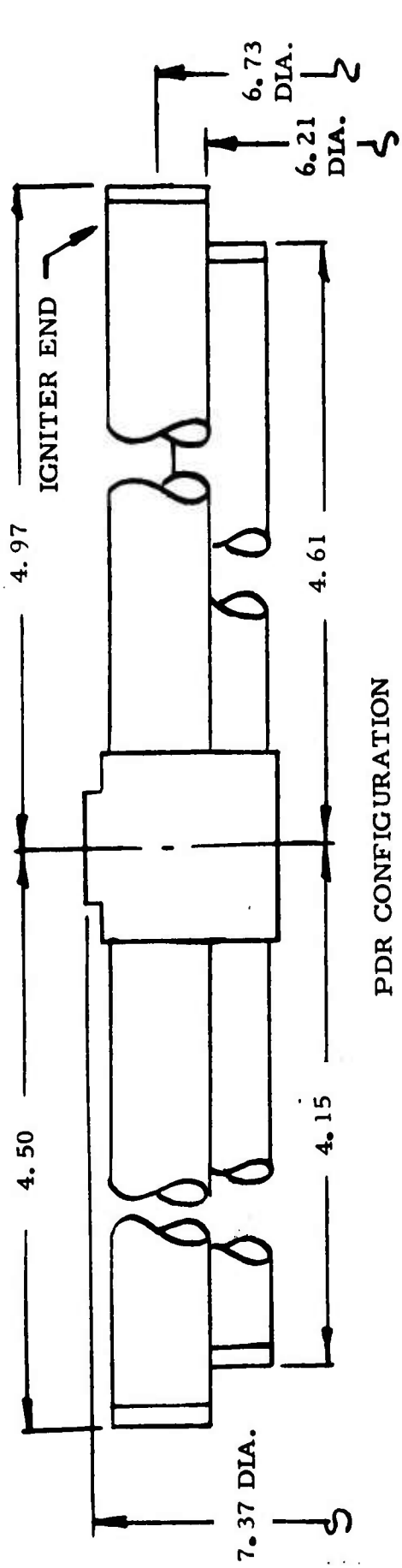
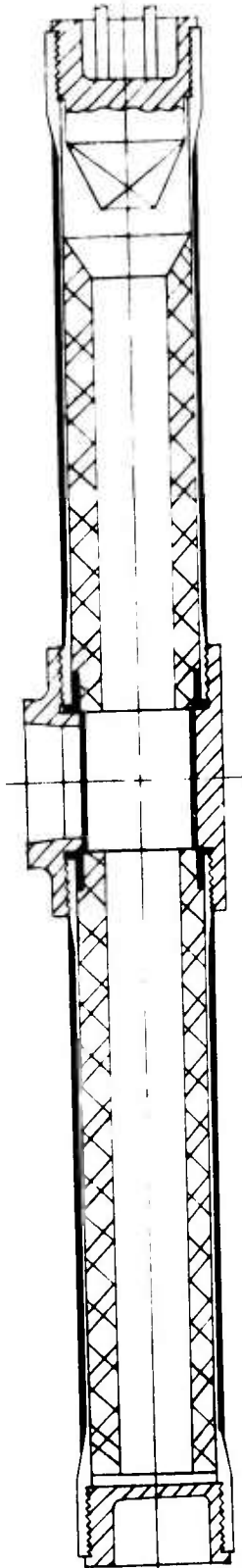


FIGURE 2-3 Maneuver Motor Array

PDR DESIGN



CURRENT DESIGN

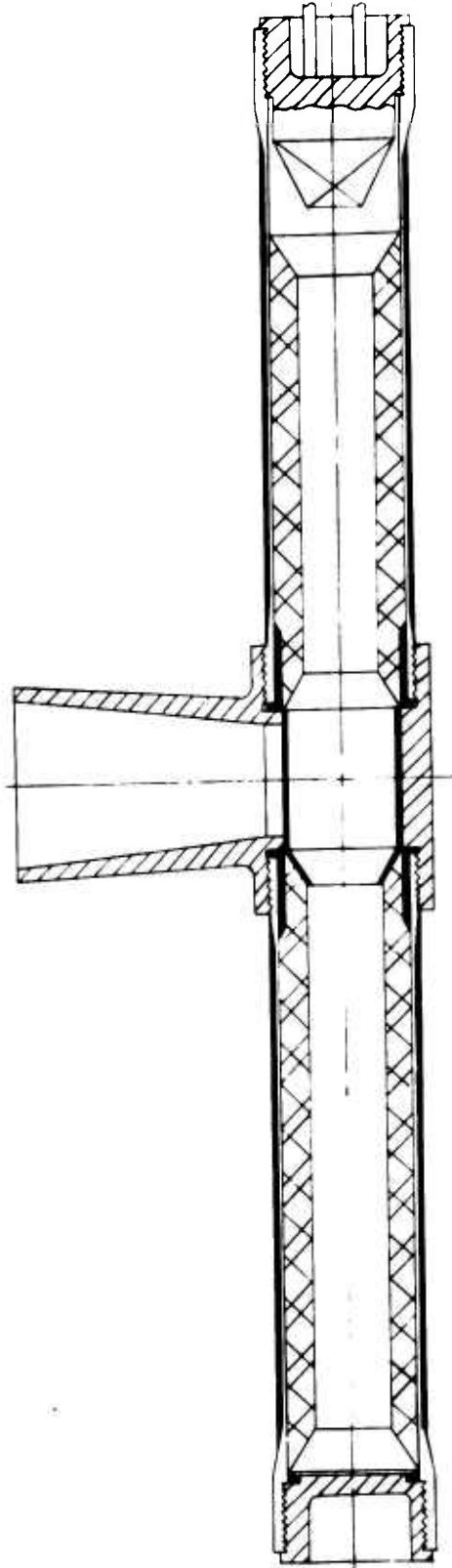


FIGURE 2-4 Motor Configuration

TABLE 2-I

MMA MATERIALS AND GAUGES

Component	PDR Design	Current Design
Nozzle Ring	4130 Steel, 0.1 in. long exit cone	Same, 0.7 in. long exit cone
Motor Tube	6 Al-4V Titanium; 0.0075 in.	Same; 0.010 inch
Tube Overwrap	Thornel 400T Graphite; 0.0095 inch	Same; 0.014 inch
End Plugs	7075-T6 Aluminum	Same
Igniter	110 mg Charge/Guilding Metal Can	Same/Same
Propellant Grain	ARCEF 143 B	Same
Insulator	Carbon Phenolic, 0.020 x 0.171 inch	4130 Steel, 0.020 x 0.432 inch
Nozzle Closure	Cylindrical Mylar; 0.007 inch	Conical Nylon; 0.008 inch
Equipment Rings	Beryllium, 0.25 inch wide	Same, 0.35 inch wide
Inter-Tube Spacers	Carbon Phenolic, 1 piece	Same, 2-piece
Equipment Ring Spacers	Carbon Phenolic	Same

Those areas of the structure between motors not required for strength or nozzle geometry have been lightened by judicious removal of material.

The ring is made of 4130 steel alloy heat treated to 145,000 psi ultimate strength. The final-machined nozzle receives a electroless nickel coating (.0002 inch) to protect against corrosion.

Several of the dimensional features of the nozzle ring are of note. The perpendicularity and parallelism between the inside and outside diameters and the sides of the ring are maintained to less than 0.0005 inch. Close control has been placed on these surfaces since they are used to position the nozzle ring with respect to the pitch, roll, and yaw axes of the MMA. Accurate positioning of the ring with respect to these references is critical to the pick-up and balancing operations required as part of the HIT vehicle manufacture. TIR tolerances of 0.001 inch have been applied to the nozzle throats and exits to ensure that the nozzle falls within the 1/4 degree thrust misalignment requirement. Additionally, close control is maintained on the angularity of the exit cones. All faces requiring critical tolerances are ground and lapped, producing a 16 microinch finish in almost all cases.

2.1.3 Motor Tube

The MMA motor tube is a thin-walled titanium alloy tube overwrapped with graphite filament. The tube is threaded at both ends to mate with the nozzle ring, and either the tube end plug or igniter.

The tube has been designed to take the best advantage of material properties while minimizing weight. The metallic portion of the motor tube is titanium alloy 6Al-4V, heat treated to an ultimate tensile strength of 165,000 psi. In the thin-walled section of the tube, wall thickness is held to 0.010 ± 0.0005 inch. This thickness has been chosen as the minimum thickness required to provide the required axial strength. Additional hoop loading capability is derived by overwrapping the titanium with a graphite filament designated Thornel 400T (Union Carbide),

impregnated with epoxy. This overwrap is machined to a thickness of 0.014 inch. The titanium has been locally thickened (0.0155 to 0.0165 inch) on the internally threaded end of each tube in the area left exposed (without propellant cast against it), to accept the end plug or igniters. Heating of these exposed sections reduces the material properties such that a thicker section is required to maintain axial strength during the firing.

As part of the overwrapping process, two primer coats of NARMCO 2021-10 Nitrile Phenolic Primer are applied to the external surface of the titanium motor tube. This primer is dried and the overwrap wound directly onto the primer. Full cure of the primer is accomplished as part of the cure of the overwrap. This primer is required to develop adequate overwrap-to-case bond strength.

The inside diameter of the motor case is dry-honed to a 22 to 32 micron uniform finish prior to casting propellant. This finish serves to provide a uniform surface for propellant bonding.

2.1.4 Igniter

The MMA motor is ignited from one end of the motor by a squib that serves not only as the igniter, but also one of the motor end closures.

The basic housing of the igniter is an aluminum 7075-T6510 body with protective finish. A glass-to-metal header is bonded into the body with Scotchcast EC-1838. This header contains two 15-mil KOVAR leadwires onto which the bridgewire is subsequently welded. The bonded assembly is designed to withstand a proof pressure of 12,000 psi. The seal is also hermetic to a level of 10^{-6} cc/sec leak rate.

A 0.00012 inch diameter tungsten bridgewire is welded between the two leadwires. A primer charge of 18 milligrams of KDNEBF (Potassium Dinitrobenzofuroxan) is buttered onto the bridgewire. The main squib charge consists of 92 milligrams of "Bullseye" (Hercules) smokeless powder. The charge is compacted to a packing density of 0.60 gram/cc in a copper alloy can which is roll-crimped onto the 7075 aluminum body. Packing is required to prevent a cg shift prior to motor operation.

The 0.010 inch thick can is crimped at the squib output end into a six-prong star crimp which remains closed until squib ignition. Upon ignition, the burning squib mix opens the star-crimped can, releasing the hot gasses down the bore of the grain.

The can has been sized just under the motor case inside diameter, such that the opening can will be supported by the motor case wall. This requirement became evident during heavywall testing when the squib can released from its header because the can overexpanded. Release of the can could produce, (a) burning metal in the motor exhaust, and/or (b) damage to the grain from metal pieces cutting the grain surface, both of which are unwanted effects.

To ensure can retention at the roll crimp/body joint, a bead of EC 1838 epoxy is inserted into the roll crimp joint. At the output star crimp, the prongs are dip soldered to ensure a tight seal. This tight seal permits a rapid pressure buildup (hence good powder ignition) prior to expulsion of the burning Bullseye powder charge. The igniter is depicted in Figure 2-5.

2.1.5 End Plug

The motor tube end plugs are similar to the igniter bodies. They are made from aluminum alloy 7075-T6510 and contain an identical pentagon-shaped recess to provide a torquing location for installation. The internal face of the plug extends inboard of the threads to provide a retaining barrier for the Armstrong A2 thread sealant.

2.1.6 Support Rings

Four beryllium rings are provided as part of the MMA. These rings serve two major functions: (a) to stiffen the structure, thus increasing the system natural frequency; and (b) as attachment points for the various subsystems that mate with the MMA to produce the HIT vehicle.

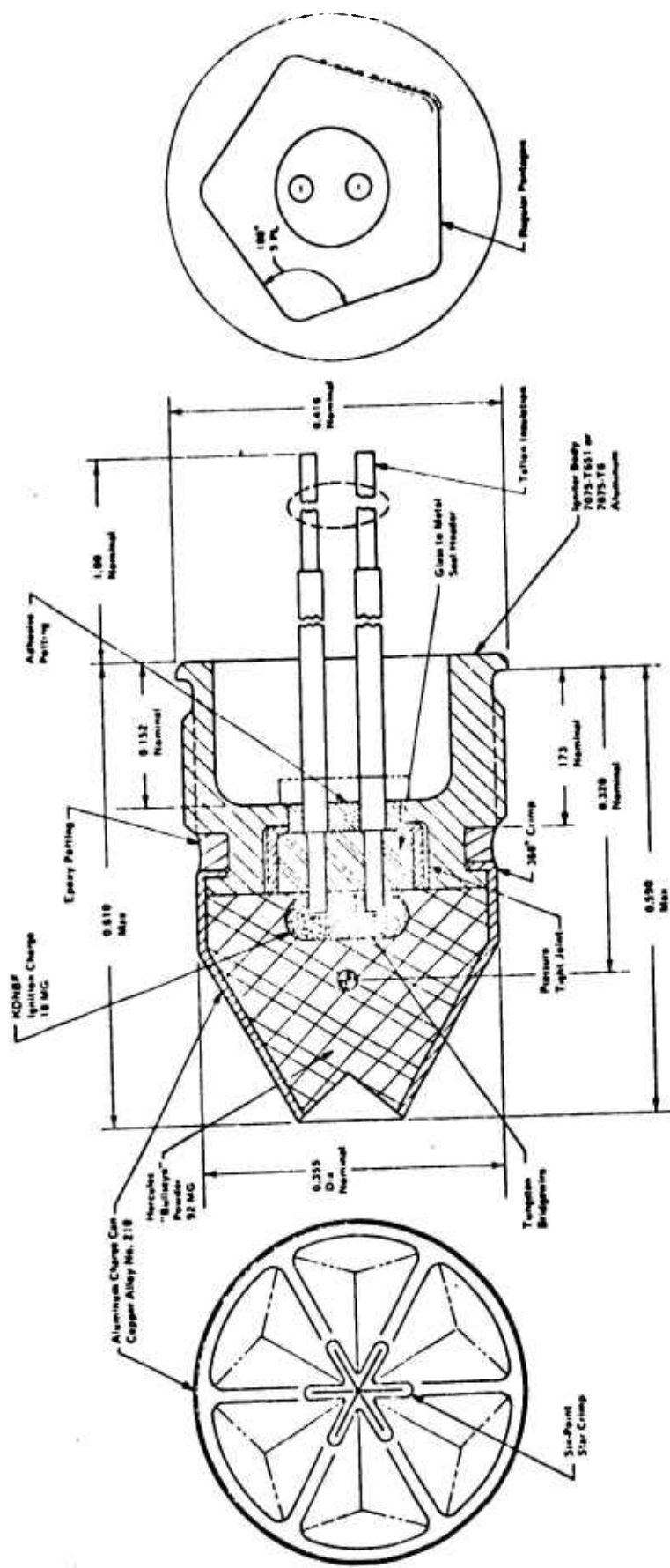


FIGURE 2-5 MMA Igniter

The rings are mounted in pairs on either side of the nozzle ring, one inboard and the other outboard of the motor tube bundle. Movement of the outer rings relative to the nozzle ring and to each other provides flexibility in initial balancing of the HIT vehicle.

Beryllium has been selected as the ring material because of its stiffness and low density. The specific requirements placed on the beryllium are as follows: ultimate tensile strength = 50,000 psi; yield strength = 40,000 psi; elongation = 2.3 percent. The rings receive a protective finish of "Berylcoat D", a conductive protective finish.

The rings are contoured to fit the shape of the motor tube bundle. Carbon phenolic spacers are bonded to the radii, which mate with the motor tubes. These spacers minimize the strain incompatibility between the rings and motor tubes during motor pressurization. EA 943 epoxy is used as the adhesive.

2.1.7 Spacers

The motor tubes of the MMA are tied together for structural purposes by means of molded carbon-phenolic spacers which are bonded longitudinally between the motor tubes. The spacers are contoured to fit between adjacent tubes. This contouring provides alignment as the spacer is slipped into place and prevents the spacer from slipping through between tubes. Spacers are bonded both from the outside and inside of the tube bundle utilizing EA 943 epoxy adhesive.

2.1.8 Insulator

The motor tube insulator is a 0.020 inch thick, 0.432 inch long cylinder of 4130 steel. Its function is to protect the end of the motor case nearest the nozzle from the severe heating and erosion effects caused by the combustion gas. Insulator bonding surfaces are roughened to enhance bonding to the motor tube and the propellant grain.

2.1.9 Nozzle Seal

The nozzle closure is a thin-walled (0.005 to 0.008 inch thick) cylinder of Nylon bonded into the nozzle ring in the 0.322 inch diameter

port perpendicular to the throat. The closure end opposite the igniter is tapered to serve as a buffer to the pressure wave produced at motor ignition. This taper forces the closure against the grain surface, thus sealing the joint. The closure is bonded in place with EP 12 epoxy.

2.1.10 Propellant Grain

The propellant used in the MMA is a non-aluminized difluoro-amino designated ARCEF 143 B. The major constituents are 1, 2, 3-tris [$\alpha\beta$ -bis (difluoroamino) ethoxy] propane (TVOPA) and 7 micron ammonium perchlorate.

The cast grain is configured with a cylindrical center port. Each motor contains two cylinders of case-bonded propellant. The cylinders are of different lengths to compensate for the cg offset caused by having the motor igniter at one end of the motor. All grain ends are tapered at 30 degrees to the bore. The stand-off distance between the fully opened igniter and the beginning of the grain taper is approximately 50 mils. A port-to-throat ratio of approximately 1.0 has been employed in the MMA configuration to achieve maximum loading density while minimizing weight.

2.2 PERFORMANCE

Nominal (average) and 1σ performance parameters for the MMA are summarized in Table 2-II. Nominal pressure vs time and thrust vs time traces are shown in Figure 2-6. These parameters were derived by a statistical analysis of the data obtained from motors fired subsequent to finalization of the internal motor design (Heavywall Confirmatory through Array Batch Check motors). These data encompassed 56 motor firings from 7 propellant batches for most parameters.

2.3 MASS PROPERTIES

A mass property summary of the MMA consumables is presented in Table 2-III. Table 2-IV presents a detailed breakdown of MMA component weights and Moments of Inertia.

TABLE 2-II
NOMINAL MMA PERFORMANCE

Parameter	Value
Action Time, msec	12.76
Ignition Delay, msec ⁽¹⁾	0.56
Time to Impulse Centroid, msec ⁽²⁾	6.72
Maximum Thrust, lb.	802
Maximum Pressure, psi	8453
Total Impulse, lb-sec	7.93
Specific Impulse, sec	234.7
Smear Factor ⁽²⁾	0.869
Total ΔV , ft/sec ⁽³⁾	1009
<p>(1) Includes only those firings utilizing final design igniter.</p> <p>(2) Includes only thrust alignment and subsequent firings.</p> <p>(3) Calculated assuming a 6.608 lb. payload.</p>	

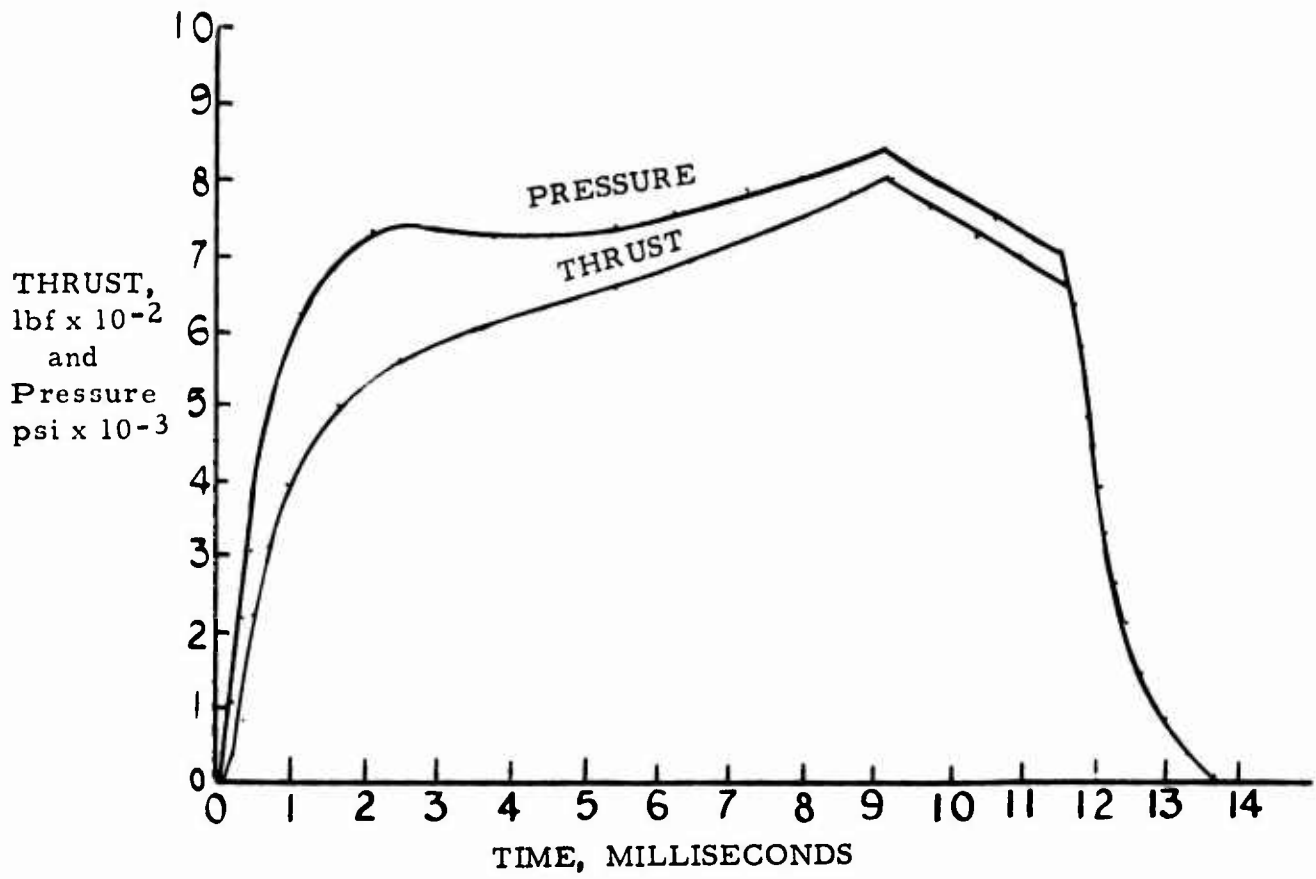


FIGURE 2-6 Nominal MMA Pressure and Thrust Histories

TABLE 2-III

MMA CONSUMABLES MASS PROPERTIES

Parameter	Value
I_{Pitch} (Inner)	10.96155
I_{Spin} (Inner)	9.09841
I_{Pitch}/I_{Spin} (Inner)	1.20478
I_{Pitch} (Outer)	11.75023
I_{Spin} (Outer)	10.67575
I_{Pitch}/I_{Spin} (Outer)	1.10065
Axial CG (in. from point C)	0.00004 Fwd.

TABLE 2-IV

NOMINAL MMA MASS PROPERTIES SUMMARY

Item	I_{Pitch}	I_{Spin}	Weight (lb)
Propellant*	22.71178	19.77416	1.893
Nozzle Ring	11.66315	23.64561	1.860
Motor Tubes	23.43164	17.07354	1.623
Insulators	1.66422	3.22394	0.307
Spacers	4.50771	3.42697	0.327
Equipment Rings	2.88582	3.79651	0.392
End Closures	<u>7.65213</u>	<u>2.87039</u>	<u>0.274</u>
Total	74.51645	73.81112	6.676

* Includes 0.01358 lb. igniter charge

3.0 DEVELOPMENT DISCUSSION

This section describes the detailed step-by-step development of the MMA and presents results of test and analysis efforts conducted to evolve and verify the MMA design.

3.1 PROPELLANT CHARACTERIZATION

3.1.1 Ballistic Test Program

The ballistic test program was designed to study the effects of process variables in propellant manufacturing on motor performance and to assess candidate grain end inhibitors.

Ten 400-gram mixes were prepared with the following variations. Six mixes were made with identical formulations and used the same lot of ammonium perchlorate (AP). Three AP batches which were ground at different times were utilized. The percentage of TVOPA was decreased by 1/2% in the seventh batch and increased by 1/2% in the eighth batch. The nominal 7-micron AP particle size was reduced to 6.3 microns in the ninth batch and increased to 7.6 microns in the tenth batch. The batches and the variables are listed in Table 3-I. Propellant from each of the 19 batches was cast into heavywall steel motors. The units were static-fired at 60°F and monitored for thrust and pressure versus time. The propellant grains were tapered at a 30° angle at the igniter end only. The distance between the igniter and the grain was 0.350 inch. Several different grain inhibitors were evaluated in the tests.

A total of 39 motors were tested including 4 retests necessitated due to hangfires. Two motors failed at ignition. The two failures were attributed to the separation of the undersized igniter charge can from the igniter body due to over expansion of the gilding metal. After the two failures, which occurred in the first group of firings, a sleeve of 3016 rubber insulation was added to the remaining motors. This sleeve supported the outside diameter of the squib can and prevented any further anomalies in the remaining tests. This condition was later eliminated by increasing the igniter can OD to a close tolerance fit with the motor tube ID.

TABLE 3-I

PROPELLANT CHARACTERIZATION MIX HISTORY

Mix Sequence	Batch No.	AP Grind No.	Formulation
1	1	193	Standard
2	1R	193	Standard
3	2	194	Standard
4	2R	194	Standard
5	3	195	Standard
6	3R	195	Standard
7	4L	195	- 1/2% TVOPA
8	4H	195	+ 1/2% TVOPA
9	5A	196 R2(6.3 μ)	Standard
10	5B	196 R1(7.6 μ)	Standard

Detailed ballistic data and typical pressure and thrust traces from these tests are given in Appendix 1. An analysis of these data indicated excessive variability in specific impulse and burn rate (Table 3-II). A between-batch burn rate variability of 4.1% (1σ) was observed for the first 6 batches (supposedly identical). However, the corresponding within-batch variability was generally on the order of 2% (1σ). Likewise, a between-batch variability of 3.8% (1σ) was observed between the seventh and eighth batches (variable TVOPA). An analysis of the effect of burn rate on the critical parameters of maximum pressure, smear factor, and time to impulse centroid indicated that burn rate should be controlled to $\pm 2\%$ (1σ).

It was also noted that moderate ignition spikes occurred when grain ends were not inhibited, that specific impulse was approximately 2% lower, and that specific impulse variability was higher as compared to inhibited grains. Based upon these observations, the following conclusions were reached:

- (a) Particle size of the ultrafine AP should be controlled between 6.5 - 7.1 microns to control burn rate variability to within $\pm 2\%$ (1σ).
- (b) TVOPA content should be controlled to within $\pm 0.25\%$ to control burn rate variability to within $\pm 2\%$ (1σ).
- (c) The igniter blast on uninhibited grains sometimes produces ignition spikes and corresponding low specific impulse.

3.1.2 Laboratory Study

The purposes of the laboratory study were to:

- (a) Develop criteria and control limits for physical properties, viscosity, and burn rate.

TABLE 3-II

PROPELLANT CHARACTERIZATION MOTOR BALLISTIC DATA SUMMARY

<u>Propellant Burn Rates Corrected to 7000 psi</u>					
Propellant Batches	AP Grind No.	No. of Samples	Avg. Burn Rate, in/sec	1 σ in/sec	C _v %
1, 1R	193	5	6.13	0.14	2.3
2, 2R	194	3	6.26	0.05	0.8
3, 3R	195	5	5.77	0.15	2.6
1, 1R, 2, 2R, 3, 3R	- -	13	6.02	0.25	4.1
4L, 4H	195	6	5.85	0.22	3.8
<u>Delivered Specific Impulse (Isp)</u>					
Nozzle Type, Row	Grain End Configuration	Samples	Avg. Isp, sec.	1 σ sec.	C _v %
Inner	Inhibited	8	226.5	2.13	0.9
Outer	Inhibited	3	216.5	0.75	0.3
Inner	Uninhibited	9	221.5	2.77	1.3
Outer	Uninhibited	11	212.5	2.61	1.2

- (b) Study the bonds between the motor case, the insulator and the propellant.
- (c) Perform tests needed to obtain DOT propellant ratings.

3.1.2.1 Burning Rate and Physical Properties

Under the first portion of the study, mylar straws, approximately 3/16 inch in diameter were filled with uncured propellant from the 10 mixes. Strand burning rates were determined at 2000 psi in nitrogen and at 11,500 psi in an oil bomb. Strand burning rate molds were filled with propellant and cured with the motors for the ballistic test program. The cured sheets were sliced into 3/16 inch square strands and combusted in the oil bomb.

Small blocks of propellant, 2 inches by 1.5 inches by 0.375 inch were cast and cured from the 10 mixes. The blocks were micro-measured and weighed to determine propellant density. The samples were then die-cut to provide microtensile specimens with a one-inch gauge length. The specimens were pull-tested at a rate of one inch per minute.

The major results and conclusions drawn from the data were as follows:

- (a) The end of mix viscosity will range from 4 to 6 Kilopoise at mix temperatures between 120-130°F.
- (b) Strand burning data cannot be used to predict the burning rate variations that occur in motors since no significant change in strand burning rate was obtained for the 10 mixes.
- (c) Variations in propellant density and mechanical properties were larger than desired. Additional data are required to establish control limits for physical properties. (See 3.1.3)

3. 1. 2. 2 Bond and Inhibitor Studies

Two approaches were explored to bond the propellant grain to the motor case. One approach was to cast the propellant directly against a mechanically prepared surface. The other was to cast the propellant against a liner or coating bonded to the case. The materials studied under the second approach included the acrylic propellant binder, cellulose nitrate lacquer and HTPB polymers. Tests were conducted to evaluate adhesion and determine the propellant compatibility under both approaches. Under the direct bonding approach, two methods were evaluated: (1) grit blasting the titanium alloy (Ti-6Al-4V) motor case with a 180 grit to a microsurface of 40-43 microinch, and (2) vapor honing with MF glass beads to a microsurface of 25-30 microinch. Vapor honing produced the best bonds. Under the second approach, preliminary tests led to the selection of two candidate adhesive liners, cellulose nitrate and Chemlok #231. In the liner screening tests, propellant was cast and cured against the following substrates, 313 carbon phenolic, Ti-5Al-4V titanium, and 4130 steel. After further testing, in which the liners were bonded against the substrates, cellulose nitrate was shown to produce the strongest bond regardless of surface preparation. Consequently, both vapor honing the case and application of a thin cellulose nitrate coating were selected to enhance case bonding. The cellulose nitrate liner was later eliminated from the design when it was discovered to be moisture-sensitive. The current design utilizes direct bonds to dry honed cases and insulators which produces adequate bond strengths.

In conjunction with the propellant adhesion studies, numerous materials designed to inhibit the grain were bonded to cured propellant samples and tested for bond strength. Four of these materials, EA 943, Uralane 8089, Nitrocellulose and Ethyl Acrylate were tested in motors under the Ballistic Test Program. Subsequent design changes, i. e., tapering of all grain ends, etc., eliminated the need for grain end inhibitors.

3. 1. 2. 3 DOT Propellant Rating

Samples of cured ARCEF 143B propellant, in the form of two-inch by two-inch cylinders, were shipped to the Association of American Railroads, Bureau of Explosives, where the following tests were performed:

- (a) One cylinder was maintained at 75°C (167°F) for 48 hours. It did not ignite, decompose or change in appearance.
- (b) One cylinder was initiated with a No. 8 electric blasting cap. It did not explode but ignited and burned very rapidly.
- (c) Four cylinders were placed in intimate contact on a bed of Kerosene-soaked sawdust which was ignited. When the fire reached the propellant, the cylinders burned very rapidly without explosion.

Based on the above tests, the propellant was given a Department of Transportation rating of Class B Explosive.

Drawings of the MMA and its Packaging were also transmitted to the Bureau of Explosives. Based on a review of the drawings, the MMA and its packaging assembly were assigned the following ratings:

- (a) MMA - Class B
- (b) Packaging Assembly - Class B - BA 1261

These low-hazard ratings reflect the low sensitivity and good stability characteristics of the ARCEF 143B propellant utilized in the MMA.

3.1.3 Process and Physical Properties Controls

Because the propellant characterization batches yielded greater than expected variation in physical properties, it was decided to defer establishment of control limits until additional batches had been mixed and evaluated. The next batches to be mixed after the propellant characterization batches were Numbers 6, 7, 8, and 9. The physical properties data from Batch 9 exhibited extremely low modulus values; a review of Batch 6, 7, and 8 data further revealed a trend toward degraded physical properties. An investigation of this problem indicated the probable cause to be inadequate stripping of the solvent from the polymer during processing. Processing methods were revised and tightened, and Batches 11, 12, 13, and 14 were mixed and tested. Average values for Stress, Strain, and Modulus for these batches are presented in Table 3-III, along with comparable values for the Propellant Characterization batches.

The latter values compare favorably with those for the propellant characterization batches. Based on these data, physical property control limits were established for the MMA motor propellant. Table 3-IV presents these limits along with other propellant processing control information.

TABLE 3-III
PROPELLANT PHYSICAL PROPERTIES

Batch Number	Maximum Stress, psi	Strain at Maximum Stress, %	Modulus, psi
1-1R	107	26	720
2-2R	108	25	750
3-3R	97	24	699
5A-5B	105	22	808
11	121	27	830
12	115	27	778
13	141	27	887
14	140	31	830

TABLE 3-IV
PROPELLANT CONTROL LIMITS

<u>Physical Properties Limits</u>		
	<u>Minimum</u>	<u>Maximum</u>
Maximum Stress, psi	80	
Strain at Maximum Stress, percent	20	
Tangent Modulus, psi		1250
Density, lb/cu in.	0.061	0.064

<u>Mix Composition</u>	<u>Weight Percentage</u>	
	<u>Nominal</u>	<u>Tolerance</u>
Ammonium Perchlorate	63.00	+0.10
Carbon Black	1.00	+0.01
Epoxy Resin	1.33	+0.10
Ethyl Acrylate	4.88	+0.02
Acrylic Acid	0.32	+0.01
TVOPA	29.47	+0.10

	<u>Minimum</u>	<u>Maximum</u>
Strand Burning Rate, in/sec at 10,000 psi	6.5	7.5
Ammonium Perchlorate Particle Size (micron)	6.5	7.1

3.2 IGNITER DEVELOPMENT

The basic igniter concept was demonstrated during feasibility tests prior to PDR. This unit was loaded with a bridgewire mix of 10 mg of KDNEF and a main output charge of 100 mg of "Bullseye" powder. The charge was housed in a guiding metal container, roll crimped at one end to a glass/metal header, and crimped at the output end with a 6-point star crimp.

Modifications to the feasibility demonstration igniter were required for compatibility with the specific MMA design requirements. A competitive procurement was conducted by ARC for igniter development and deliveries. Space Ordnance Systems (SOS) was selected as the igniter vendor, and go-ahead was authorized in March 1972.

3.2.1 Initial Development

The flight weight header/body configuration was defined and ordered. The header consisted of a glass to KOVAR seal using KOVAR wire 0.010 inch in diameter. The header was to be bonded to the aluminum housing/end plug using EC 1838 adhesive. The housing closely resembled the end plug used at the other end of the motor, modified to accept the header.

Concurrently, a development configuration was procured to begin testing of the pyrotechnic aspects of the design. The development version was similar to the flight weight except for the bridgewire. The flight weight design called for a 0.0001 inch diameter tungsten bridgewire. The development igniter used a 0.001 inch diameter Nichrome V bridgewire.

The initial two closed bomb firings of the development unit showed long rise times (time from current application to bomb peak pressure) in excess of 10 ms. Investigations revealed that, because of the configuration of the star crimping tool, the bullseye loading density was 0.78 grams/cc rather than the desired 0.70 grams/cc after crimping. Also, it was noted that

SOS had selected 1100 aluminum for the charge can in the initial two tests. A unit was subsequently manufactured using 7075 aluminum in the hope that a stronger can material would improve the retention capability of the star crimp. It was hypothesized that retention of the powder for a longer period prior to expulsion would enhance the ignition of the powder. Although the hypothesis proved to be correct in the long run, this particular test showed no measurable improvement over the previous two tests.

Two additional units were fired per the baseline configuration except with the KD NBF weight increased to 15 milligrams. Some improvement was noted in the rise time although this change alone was not sufficient to yield satisfactory results.

In order to test the theory that rise time was directly affected by loading density, a test series was conducted in which the bullseye charge weight was varied while the volume was held constant. The results of these tests clearly showed that as density increased, ignition delay increased.

It became apparent that the output charge density would have to be reduced to below the 0.7 gm/cc design level. It also seemed appropriate to increase the KD NBF weight to assist in providing a faster rise time.

To achieve the lower packing density, a longer can (.344 in. vs .315 in.) was adopted. Two firings with 10 mg of KD NBF showed 5.0 and 5.2 ms. rise times. A third unit with 15 mg KD NBF had a 3.4 ms. rise time to peak pressure.

Based on these tests, a configuration with a loading density of 0.60 gm/cc, containing 92 mg of bullseye and 18 mg of KD NBF, was established as the baseline design. As a check of this configuration, two units incorporating the flight weight header and bridgewire were tested. A pressure of 500 psi was reached in 0.6 ms and peak pressure occurred in approximately 4 ms.

3. 2. 2 Reliability Testing

3. 2. 2. 1 No Fire Testing

Four units of the baseline design configuration were subjected to 35 milliamps for 5 minutes. One of the units was given 50 milliamps for 5 minutes. No unit fired under these conditions. Subsequent ballistic testing of these units showed no apparent degradation.

3. 2. 2. 2 Random Vibration

To examine capability to survive the environments specified in the VSD procurement specification, 5 units were subjected to the test profile specified in Table II of Specification 3-371-04-O-10185. Units functioned nominally subsequent to this test.

3. 2. 3 Igniter Qualification

Twenty units of the flight weight configuration were delivered to ARC for closed bomb testing. The successful performance of these units was to prove the acceptability of the design. However, two of the units completely failed to fire, and six of the units exhibited rise times in excess of the desired 6 msec.

The failure investigation indicated that the probable cause of misfires was a poor weld between the tungsten bridge and the KOVAR pin. A 100 percent bridgewire pull test was therefore instituted to weed out bad welds. Also, it was decided to gold plate the pin ends to achieve a better welding medium. A similar procedure had been used by SOS previously with regard to the "microdot" squibs. This unit, in mass production, employed a similar tungsten bridge/KOVAR pin arrangement.

The failure analysis indicated that the long rise times were due to premature expulsion of bullseye powder from the squib can. Consequently, the following actions were taken to assure ignition of a larger percentage of powder prior to expulsion from the can.

- (a) The star crimp was improved to make the seal tighter.

- (b) The crimp lips were dip soldered closed.
- (c) The can material was changed to guiding metal to provide additional strength.
- (d) Adhesive was applied to the roll crimp joint to prevent can rotation and gas expulsion.

3.2.4 Igniter Requalification

A series of 20 units were manufactured to the improved design. Fifteen units were tested at SOS and five at ARC. Two of the units tested at SOS exhibited long delays, although the magnitude of the delay was considerably less than had been previously experienced. All other units functioned properly. Investigation by SOS identified the probable cause of the anomaly to lie in improper dip soldering of the can, thus yielding an unsatisfactory seal. A more rigorous soldering technique was instituted, including 100 percent high-intensity light inspection of the seal with no leakage permitted.

Based on incorporation of this corrective action, the design was frozen and released for production.

A production lot of 170 squibs was ordered from SOS. Thirteen units were bomb-tested by SOS for lot acceptance; no anomalies were noted. Sixty-three motors were tested with this squib lot during the prototype program with no ignition anomalies noted.

3.3 MOTOR DEVELOPMENT TESTS

The testing described herein is basically presented in chronological order, beginning with the initial design evaluation tests and ending with the Prototype Array Tests. It will be found that some test sequences were interrupted due to failures, and resumed after diagnostic tests and corrective design changes were implemented. For example, thrust alignment tests were initiated in July 1972, (Section 3.3.1.2), suspended due to motor failures, and resumed in June 1973 (Section 3.3.5.2).

3.3.1 Initial Tests

3.3.1.1 Design Evaluation Tests

In June 1972, two static firings were conducted to evaluate the SOS development igniter, the cellulose nitrate case liner, and a port to throat ratio of 1.0. These tests utilized heavywall titanium motor cases which conformed internally to flight weight dimensions. Both motors operated successfully but the first motor exhibited a long ignition delay of 0.0061 second. As discussed under section 3.2, the delay was attributed to the high loading density of the igniter charge. In the second test, the loading density of the main charge was reduced and the primer charge of the squib was increased. The ignition delay of the second motor was reduced to 0.0011 second which met the specification limit of 0.0015 second maximum.

In July, a small quantity of overwrapped flight weight motor cases were received, and two tests were conducted to evaluate the cases. Each motor performed normally and produced acceptable ballistic data. Pressure data were lost on the second firing due to an ignition spike that unsettled the transducer. SOS development squibs were used in the test motors and yielded acceptable ignition delays.

3.3.1.2 Thrust Alignment Tests

Four motors were fired during July 1972 to perform a preliminary evaluation of thrust alignment. Three of the motors with heavywall

titanium alloy motor cases performed as expected, but the fourth with flight weight cases failed shortly after ignition. Examination of the ballistic trace showed the thrust rose sharply during ignition, experienced a slight change at 600 pounds and continued to rise rapidly until case failure. The forward (igniter side) case was left intact but the aft (plug side) case ruptured severely. Failure analysis determined the primary cause of the failure to be unbonded areas between the carbon phenolic motor case insulator and the propellant grain. Other factors that were suspected to have contributed to the failures included damage to the propellant from igniter blast and overstress of the propellant. The analysis of the motor failure disclosed the fact that the cellulose nitrate liner, introduced in the preceding five motors tested, was extremely moisture-sensitive. Consequently, it was removed from the design.

All of the motors used interim flight weight igniters, and heavywall nozzles machined to extremely close tolerances to minimize geometric misalignment. The internal configuration of the first two motors conformed to the flight weight configuration established in the VSD-ARC design review held in late May 1972. Thrust misalignment measured in the pitch axis for these two motors was approximately 0.1 degree (pitch up) as compared to the 0.25 degree limit specified by VSD. It was hypothesized that the pitch-up thrust misalignment obtained in the two tests could be due to the unequal length of the propellant grains in the two motor cases. The third motor tested had both grains the same length as the igniter side grain; however, thrust misalignment was consistent with the first two motors. The exit cone of the fourth motor nozzle was purposely canted. If it could be shown that thrust misalignment of the short nozzle cone was not affected by this slight cant, the nozzle cone tolerances could be relaxed at significant cost savings. The failure of this motor prevented any conclusions to be drawn.

All of the tests were conducted on the thrust stand described

in the Test Plan (Appendix 3). The stand employed a multi-component load cell which measured side components of thrust as well as axial thrust.

3.3.1.3 Adjacent Tube Interaction (ATI) Tests

While ways to improve the propellant case bond were studied, two additional tests were conducted in late August 1972 to study the effects of adjacent motor tube (case) interaction. As shown in Figure 3-1, a thirteen motor nozzle segment was assembled with seven live motors in the center. All motors were bonded together with inter-tube spacers and beryllium ring segments using EA 943 adhesive. Before static firing, the unit was subjected to low-level tensile testing to verify bond quality. The end plug and igniter were detorqued from the centermost motor and an adjacent motor so that tensile testing fixtures could be threaded into the unit. During detorquing, the bond joint between two of the tubes was damaged and was subsequently repaired.

As a precaution against possible grain unbond as suspected in the fourth thrust misalignment motor, the nozzle ends of the grains of the motors to be fired were inhibited with EA 943. The adhesive was applied through the nozzle as the bonded ATI test segment could not be disassembled. The assembly had been completed before the thrust alignment motor failure and contained the moisture sensitive nitrocellulose liner.

The first unit fired was the centermost motor. The motor operated successfully but the initial slope of the ballistic trace was slightly higher due to the end inhibiting. The second motor, adjacent to the first, failed at 10.4 milliseconds after ignition. Before failure the unit appeared to be performing normally. At failure the thrust suddenly dropped to zero.

High speed movies of the tests showed substantial plume impingement on the motor cases as the plume reflected off simulated battery and telemetry packs attached to the mounting ring segments. The failed hardware showed evidence of significant thread leakage and burn through at the nozzle-motor case thread joints for the aft (plug side) tube.

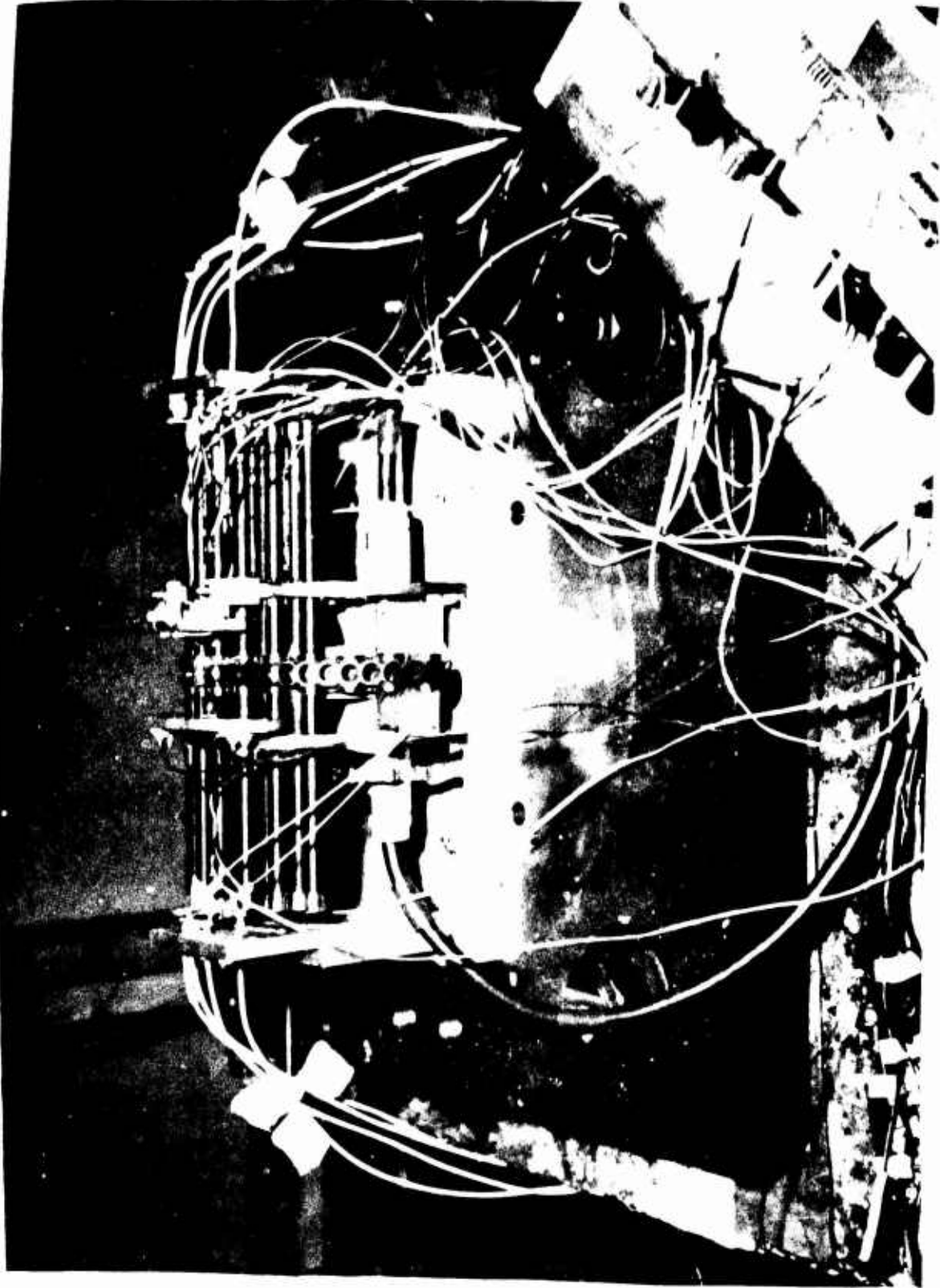


FIGURE 3-1 ATI Test Set-Up

The forward (igniter side) tube was left intact. Examination of unfired motor cases from the test assembly revealed cracked insulators.

The investigation of the second ATI test motor failure concluded that the most probable cause of failure was cracking of the carbon phenolic insulator, followed by eroding away of the steel nozzle land and titanium tube end, leading to thread leakage and rupture of the tube. A postulated secondary failure mode was insufficient margin of safety in the motor tube.

3.3.2 Failure Diagnosis Tests

A joint VSD-ARC meeting was held in early September 1972, to discuss changes in motor design and to develop a test plan for a series of single motor tests that would permit diagnosis and elimination of the deficiencies in the MMA motor design. Consequently, the following design changes were implemented: (1) increase tube titanium wall thickness from 8.0 to 10.0 mils; (2) increase the nominal nozzle land thickness from 14.5 to 29.5 mils; (3) change the carbon phenolic motor case insulator to normalized 4130 steel; (4) increase tube overwrap thickness from 10.0 to 14.5 mils; and (5) utilize loctite sealant in tube-to-nozzle threads.

The test plan that was developed included tests to evaluate the effects of: (1) igniter impingement on the propellant grain; (2) unbonded areas at different locations in the propellant to motor case interface; (3) softened ignition; (4) lengthening the nozzle cone to reduce plume impingement; and (5) grain voids.

3.3.2.1 Igniter Impingement Tests

In early October 1972 six test motors were fired at a simulated altitude of 100,000 feet with the mylar nozzle closure removed. The intent was to preclude motor ignition and examine grains for damage caused by igniter discharge. The propellant grains in three of the motors had square ends except for the 30° taper at the igniter end. Propellant grains in the other three motors were tapered at a 30° angle on all ends.

Five of the igniters discharged as planned; one igniter did not function. One motor ignited and burned normally to completion. The remaining motors were disassembled and examined. It was noted that the igniter tended to round off the grain corners. On the tapered grain ends, the rounding was barely noticeable. On square ended grains, the rounding was severe. The square end of the grain at the nozzle of the aft (plug side) motor was rounded to a radius of about 0.040 inch. The square ends of the grains at the nozzle of the forward (igniter side) motor and at the end plug of the aft motor showed much less effect.

The five motors were then retrofitted with new igniters and nozzle closures and static fired. Each motor operated without any catastrophic effect from the initial igniter blast. A seventh test motor, fired as a control unit, also functioned normally. All motors utilized interim lightweight igniters, heavywall titanium motor cases, thickened nozzle lands, and steel insulators.

3.3.2.2 Unbonded Grain Tests

Seven motors were tested to determine the effects of unbonded areas between case and propellant at different locations within the motor. Unbonds were induced at the igniter end taper of the grain on two units, and at the forward (igniter side) motor case insulator on two units. Unbonds were induced at the aft (plug side) motor case insulator on three units. Failures occurred in all three units with unbonds at the aft side insulator, and in one of the units with unbonds at the forward side insulator. In each motor failure, the motor case burned through directly behind the aft motor case insulator at times ranging from 8.5 to 10.5 msec into the burn. The failure of the unit with an unbond at the forward insulator was attributed to an undetected unbond at the aft insulator existing either before, or as a function of, ignition.

All of the test motors utilized interim lightweight igniters, heavywall titanium motor cases, thickened nozzle lands, and steel

insulators. All grain ends were square except for the 30° taper at the igniter end.

It was concluded that unbonds at the propellant-to-insulator interface on the aft (plug side) tube were fatal, leading to failures very similar to that for the ATI motor.

3.3.2.3 Soft Ignition Tests

Four motors were tested to study the effects of softened ignition on motor performance. The test motors employed heavywall titanium motor cases, steel insulators, and square-ended grains except at the igniter end. One motor was ignited with an Atlas Match and 50 milligrams of Black Powder. The motor fired and performed nominally but exhibited an ignition delay of 0.0215 second. The second motor was ignited with nickel-chromium hot wire that laid against the grain at the igniter end. At approximately two seconds after ignition, the grain ignited and the motor performed nominally. The last two tests utilized bridge-wires containing 50 milligrams of Black Powder, and resulted in misfires. No basic differences were noted in these ballistic traces versus normally ignited motors. It was concluded that none of these methods could be used for satisfactory ignition performance.

3.3.2.4 Plume Impingement Tests

In October 1972, two motors were tested at sea level ambient pressure to evaluate the performance of nozzles having exit cones lengthened by 0.6 inch to prevent plume impingement on HIT external subsystems. Both motors performed satisfactorily. Evaluation of the exhaust plume expansion angle from high-speed movies indicated acceptable plume behavior. Subsequently four additional tests of the lengthened nozzles were conducted in conjunction with a shroud device that simulated the battery and telemetry mountings of the HIT vehicle relative to the nozzle exit plane. The test set-up consisted of an individual motor with a modified nozzle, a shroud simulating the exterior of the array, and simulated

battery and telemetry packs (Figure 3-2). High speed camera coverage and heat sensing equipment were used to record any plume impingement on the HIT components.

The test results showed that the sea level plume impingement problem was eliminated by the lengthened nozzle. The third test motor, however, failed at 4.1 msec after ignition. Post-firing examination and review of the high speed motion pictures showed that the motor case burned through at the pressure-monitoring end plug. This failure mode occurred again during subsequent tests; the cause and resolution is discussed in Section 3.2.2.6. The three other test motors operated normally. The shroud test motors contained propellant grains with tapers at all ends.

The test results also confirmed that specific impulse increased about 20 sec, as predicted, due to increased nozzle expansion ratio and decreased nozzle half angle.

3.3.2.5 Grain Void Tests

Four motors were tested with propellant grains having scattered voids on the surface and ends to assess whether these imperfections affected ballistic trace shapes. Two of the motors had tapered grains, one had a tapered and a square grain, and one unit had no tapers except at the igniter end. Two of the motors functioned normally, one resulted in a failure and another misfired. The motor that failed had a 1/8 inch void near the end of the igniter tube insulator and burned through at that location. It was concluded that (a) voids produced no noticeable effect on trace shape, but (b) the presence of voids near the motor case insulator end can lead to case burnthroughs and is therefore unacceptable. The grain X-ray accept/reject criteria was modified accordingly.

3.3.2.6 Longer Insulator Tests

Based on the results of the failure diagnosis test series, the following changes were incorporated into the MMA motor design: (1) lengthen the insulator from 0.171 to 0.432 inch and roughened the insulator



FIGURE 3-2 Plume Impingement Test Setup

ID and OD to enhance bonding to the motor case and propellant grain, (2) taper all ends of the propellant grains at a 30° angle, and (3) protect the nozzle end of the aft (plug side) motor propellant grain with a conical extension of the nozzle closure. At ignition, the flap would be pressed against the nozzle end of the grain to protect it from the igniter blast.

In December 1972, five motors incorporating these design changes were static fired. All five motors operated normally. Post-test examination of the motor cases and insulators revealed no indication of excessive erosion which previously had caused hot spots or case burn through.

One other motor was tested in this series to measure the temperature versus time profile of the titanium motor case at the area outside the insulator. The shorter (0.171 inch) insulators were used in the motor cases. At approximately 9.5 milliseconds after ignition, the motor failed at the pressure-monitoring plug-motor case joint. The failure was similar to the one experienced in the plume impingement tests (see section 3.3.2.4). Further investigation of these two failures led to an analysis of the titanium alloy pressure plug (used for test purposes only) which showed that the plug face reached 1600° F during a firing. At that temperature the loctite sealant fails, permitting direct exposure of the case-end plug threads to combustion gases. Use of aluminum reduces the temperature-time profile significantly, thus confirming the adequacy of the standard aluminum end plug and the aluminum igniter plug used on the other end of the motor.

3.3.2.7 Aluminum End Plug Tests

In January 1973, three motors were static fired to check for thread burning damage with the aluminum end plug. As a further precaution, a small amount of A-2 adhesive was added to the plug threads as a gas barrier. Two of the units contained short motor case insulators and one employed the longer insulators. All the grains were tapered. Each

motor operated without incident. Post-test examination of the sectioned titanium motor cases showed no evidence of thread leakage or degradation at the plug end. It was decided to discontinue use of titanium pressure adapter plugs, and to extend the forward face of the flight weight aluminum end plug slightly inboard of the threads to form a barrier for the A-2 thread sealant.

3.3.3 Heavywall Confirmatory Tests

The limited number of tests conducted to date was not statistically sufficient to conclude that the marginal failure modes had been eliminated by the design changes developed from the failure diagnosis tests. Thus, VSD directed ARC to conduct an additional 15 static firings of the modified design. The test motors incorporated heavywall titanium motor cases, 0.432 inch long steel insulators, tapered grains, conical nozzle closures, long exit cone nozzles, and aluminum end plugs. The motors were ignited with interim flightweight igniters. The nominal nozzle throat diameter was increased from 0.305 to 0.3115 inch because higher operating pressures had been experienced in the five preceding tests. The threaded joints were sealed with Loctite HV except at the end plug where A-2 adhesive was used.

The first four tests were conducted in February 1973. Thrust-time traces were obtained in all firings. Pressure was recorded in two of the tests. Each of the motors operated normally and produced acceptable ballistic performance. Action times were longer and pressures were lower due to the enlarged throat diameter.

In March 1973, nine more motors of the same design configuration were successfully static fired. Again, all motors operated normally. The ballistic data were very reproducible and agreed with the previous four motors with propellant from a different batch.

To complete the heavywall confirmation tests, an additional two units were successfully tested in conjunction with the pressure

oscillation tests conducted in May 1973 and discussed later in this report. Nozzle throat diameter was adjusted downward to 0.3085 inch for these and subsequent tests. Ballistic data from the heavywall confirmatory tests are presented in Table 3-V. Typical traces are shown in Section 1 of Appendix 2.

3.3.4 Pressure Oscillation Phenomena Tests

Beginning in October, 1972, a new phenomena was observed to occur in individual motor tests. This phenomena involved a rapid oscillation (approximately 7100 CPS) superimposed upon the normal motor pressure-time trace. Examples of this phenomena may be seen in the following pressure-time traces from Appendix 2.

<u>Test Series</u>	<u>Section of Appendix 2</u>	<u>Firing Numbers</u>
Heavywall Confirmatory	1	39063, 39064, 39314
Flightweight	2	39574
Pressure Oscillation	4	39787, 39902

The phenomena did not occur in all firings, nor was the duration or amplitude constant across all firings. In many firings the amplitude appeared to increase toward the center on the trace and subside later in the firing. The anomaly was observed only on the pressure trace and not on the thrust trace.

Although some concern existed relative to this oscillation, no extensive analysis of the event was undertaken at that time since no adverse motor effect had been noted and it was believed that the oscillation was not the destructive unstable burning phenomena but rather an "organ pipe" mode harmonic.

In the spring of 1973, discussions relative to this phenomena were conducted with ABMDA propulsion consultants. Although the consultants supported the harmless "organ pipe" theory, it was decided to conduct a series of firings to (a) measure the case strain response relative to the pressure oscillation, and (b) examine the data obtained utilizing a more

TABLE 3-V
HEAVYWALL CONFIRMATORY TEST BALLISTIC DATA SUMMARY

Test No.	Test Date	Prop. Batch	t _a , msec	t _b , msec	t _d , msec	\bar{v}_b , in/sec	F ^{max} , lb	I _T , lb-sec	I _{sp} , sec	P ^{max} , psi	\bar{P}_b , psi
38820	2-9	19	13.1	11.9	0.7	6.13	774	7.93	233.0	8099	7167
38821	2-9	19	13.1	11.7	0.5	6.24	779	7.98	234.6	N/A	N/A
38822	2-9	19	13.2	11.9	0.5	6.13	774	7.96	233.6	N/A	N/A
38823	2-9	19	13.8	12.6	0.7	5.79	752	7.99	234.4	7848	6889
39064	3-26	21	14.0	12.8	0.7	5.70	709	7.99	233.8	7872	6895
39068	3-26	21	14.4	12.9	0.8	5.66	707	8.00	234.1	7560	6774
39069	3-27	21	13.8	12.0	0.6	6.08	740	7.98	233.2	7961	6992
39061	3-26	22	13.6	12.3	0.4	5.93	735	7.95	232.9	N/A	N/A
39062	3-26	22	14.0	12.6	0.5	5.79	707	7.97	233.5	7560	6861
39063	3-26	22	13.6	12.0	0.6	6.08	732	8.05	235.4	7783	7143
39065	3-26	22	13.5	11.9	0.7	6.13	742	8.00	234.4	N/A	N/A
39066	3-27	22	13.9	12.3	2.0	5.93	737	8.00	234.3	N/A	N/A
39067	3-27	22	13.6	12.3	0.6	5.93	735	7.93	232.1	N/A	N/A
39313	5-3	23	12.7	11.5	0.4	6.35	797	7.89	235.7	8616	7667
39314	5-3	23	12.6	11.4	0.3	6.40	797	7.85	234.2	8616	7831

NOTES: (1) Interim-Design Igniters Utilized

(2) Tests 39313 & 39314 had .3085 in. nozzle throats

(3) Other tests had .3115 in. nozzle throats

sensitive pressure gage. Both investigations were aimed at determining whether the oscillation was real and was imparting some effect to the motor case, or whether the oscillation might be a pressure transducer response phenomena.

In May 1973, four heavywall titanium motors were ballistically tested to investigate this phenomena. The final two heavywall confirmatory units were instrumented with a strain gage pressure transducer of the type previously used. The other two units were fitted with high frequency piezo-electric pressure transducers capable of accurately responding to signals as high as 100,000 CPS. All four units were instrumented with strain gages, two axially oriented and two hoop oriented. The strain gages were placed at the tube center on each side of the nozzle. Based on the results of these test firings, the following observations were made:

- (a) Both the strain gage transducer and the piezo-electric transducer yielded some indication of the oscillatory behavior although the piezo-electric response was assumed to be more accurate.
- (b) Some oscillatory response was noted in the strain gages with the most severe response noted in the longitudinal direction. The longitudinal oscillation frequency and amplitude could not be correlated with the frequency of the pressure oscillation.

As part of the initial investigation of pressure oscillations, an attempt was made to determine the frequency of occurrence and the maximum amplitude of the pressure oscillation. Slow-speed data tape playbacks indicated that the pressure oscillations indeed had major excursions from the nominal, a situation masked when the trace was played at normal speed. Additionally, it was observed that:

- (a) High frequency oscillations were present to some extent in all firing series.

- (b) Amplitude increases began, as noted previously, with the firings of October 1973. The only geometric change that coincided with onset of high-amplitude oscillations involved the thickening of the nozzle throat land, a move made to prevent thread erosion.

In order to more fully explore these observations, a second series of tests were conducted. In one subseries, the nozzle throat was chamfered to simulate the thin land situation. In another subseries, a previously-fired nozzle was used to again simulate the thin land. In both cases the thesis was advanced that the sharp nozzle entrance corner coupled with the thickened land was causing the organ pipe mode oscillation. However, neither series conclusively demonstrated this to be the case.

Relative to amplitude, a third series of tests were conducted and the data analyzed using a "transient analyzer", a digital oscilloscope capable of displaying in great detail the highs and lows of the oscillations. The results of these investigations and the subsequent investigations of previous tests, using the transient analyzer, indicates the amplitude to be no greater than $\pm 30\%$ of the mean in the worst case.

Based on the analytical and empirical investigations, it was concluded that the severity of the amplitude was not sufficient to warrant further work to either (1) eliminate the occurrence, or (2) further strengthen the motor to provide additional compensation for the phenomena. VSD structural/dynamic analyses, accounting for known case mechanical properties and burst test results, verified the structural adequacy of the individual motors and the array under these pressure oscillation conditions.

Ballistic data from the pressure oscillation test motors is summarized in Table 3-VI, and typical traces are shown in Section 4 of Appendix 2.

3.3.5 Design Verification Tests

With the confidence gained from the heavywall confirmatory tests, VSD released ARC to begin a series of design verification tests which included seven flightweight motor vibration and spin tests, ten thrust alignment tests and

TABLE 3-VI
PRESSURE OSCILLATION TEST BALLISTIC DATA SUMMARY

Test No.	Test Date	Prop. Batch	t _a , msec	t _b , msec	t _d , msec	\bar{F}_b , in/sec	F _{max} , lb	I _T , lb-sec	I _{sp} , sec	P _{max} , psi	\bar{P}_b , psi
39315	5-3	23	12.4	11.3	0.3	6.46	809	7.96	237.0	8563	7764
39316	5-3	23	12.6	11.5	0.5	6.35	788	7.92	236.2	8301	7783
39753	6-28	23	12.5	11.4	0.5	6.40	805	7.91	234.1	8415	7556
39786	7-2	23	12.4	11.1	0.7	6.58	803	7.98	237.1	8706	7087*
39792	7-3	23	13.1	11.8	0.5	6.19	754	7.93	234.5	N/A	N/A
39816	7-11	23	13.3	12.0	0.5	6.08	754	7.95	235.8	8226	6501*
39787	7-3	24	13.8	12.2	0.8	5.98	716	7.91	234.2	7595	7299
39788	7-3	24	14.1	12.7	0.3	5.75	707	7.83	231.3	N/A	N/A
39899	7-20	25	13.4	12.0	0.6	6.08	786	7.82	233.1	8168	5814*
39900	7-20	25	13.3	12.1	0.8	6.03	777	7.93	235.9	8055	6520*
39901	7-20	25	12.6	11.5	1.0	6.35	770	7.81	237.3	8424	7721
39902	7-20	25	13.5	12.6	0.6	5.79	763	7.91	236.0	7913	6781
39903	7-20	25	13.2	11.8	0.6	6.19	784	7.90	235.3	8140	7290

NOTES: (1) Flightweight Igniters
(2) 0.3085 in. nozzle throat
(3) * - Suspect Data

the firing of a complete prototype array. These tests spanned the period from May through November 1973.

3.3.5.1 Flightweight Motor Tests

The seven flightweight motors were tested in May 1973. The motors utilized titanium alloy motor cases with a nominal wall thickness of 10.0 mils and overwrapped with carbon filament. The units employed the final-design flightweight igniters with a main charge of 92 milligrams of "bullseye" smokeless powder. As in previous tests, the motors contained tapered propellant grains, long insulators, and conical nozzle closures.

Prior to firing, six of the units were subjected to shock and vibration testing by General Environment Corporation under contract to ARC. The shock and vibration schedule shown below was utilized.

<u>Frequency (Hz)</u>	<u>Amplitude, g's (rms)</u>
10 - 400	1.4
400 - 600	11.0
600 - 2000	3.0

Two sweeps were made from 10 to 2000 to 10 Hz at 1/2 octave per minute.

Each of the six units were then subjected to 28 shocks applied in each of the two transverse axes for a total of 56 shocks. The shock pulse was a half-sine, with 70 g's magnitude and four milliseconds duration. There was no apparent damage as a result of the tests except that fine delaminations occurred between adjacent filaments in the wrap of the motor cases after the vibration test.

After the environmental tests, three of the motors were fired under static conditions and three under a simulated spin rate of 25 RPS. An additional unit which had been included as a spare was also static fired. The ballistic data from the tests are represented in Table 3-VII and traces are shown in Section 2 of Appendix 2. All of the motors performed normally, and there was no significant difference in ballistic performance between the motors fired under static or spin conditions or as a result of the environmental testing.

TABLE 3-VII

FLIGHT WEIGHT TEST BALLISTIC DATA SUMMARY

Test No.	Test Date	Prop. Batch	Test Mode	t _a , msec	t _b , msec	t _d , msec	T _b , in/sec	F _{max} , lb.	I _T , lb-sec	I _{sp} , sec	P _{max} , psi	P _b , psi
39568	5-30	24	Static	12.1	10.7	0.5	6.82	855	7.94	235.5	N/A	N/A
39569	5-30	24	Static	12.3	11.0	0.4	6.64	841	7.92	234.4	N/A	N/A
39576	5-31	24	Static	12.8	11.5	0.5	6.35	800	7.97	234.9	8584	7611
39577	5-31	24	Static	12.5	11.4	0.3	6.40	811	7.88	233.6	N/A	N/A
39573	5-31	24	Spin	13.1	11.6	0.5	6.29	777	7.90	234.2	8403	7451
39574	5-31	24	Spin	13.1	11.7	0.5	6.24	790	7.81	231.4	8541	7425
39575	5-31	24	Spin	13.2	11.6	0.5	6.29	801	7.89	233.2	8541	7489

NOTES: (1) Flightweight igniters

(2) Spin tests conducted at simulated 25 rps

(3) 0.3085 in. nozzle throat

(4) All except 39576 environmentally tested prior to firing

3.3.5.2 Thrust Alignment Tests

In June 1973, ten additional flightweight test motors were static fired to measure any pitch and roll moments generated due to thrust misalignment. The motors employed geometrically precise nozzles that duplicated outer and inner segments of the MMA nozzle ring. A three-component load cell was used as in the initial development tests discussed in Section 3.3.1.2. The load cell was instrumented to measure axial thrust and two orthogonal moment components. The nozzle body was positioned on the test apparatus so that the nozzle throat was fixed at a location of 3.62 inches above the null plane of the transducer. In this position, a vector misalignment of a quarter of a degree would produce an average moment of 8.36 in-lbs.

All ten test motors operated normally. The data from the tests yielded the following values for misalignment:

<u>Direction</u>	<u>Average, deg.</u>	<u>1 σ, deg.</u>
Roll	+ 0.009	0.044
Pitch	- 0.003	0.040

The VSD specification allowed a misalignment of 0.25° at 3σ , inclusive of array nozzle ring geometry errors. It was calculated that in the nozzle ring configuration, geometric tolerances contribute no more than 0.125° (3σ) of possible misalignment. Thus, the root-sum-square of geometric and ballistic misalignment sources produced three sigma values of 0.183° (pitch) and 0.174° (roll), which falls within the three sigma maximum allowable value of 0.25° .

The data did not show any significant difference in performance between long and short (inner and outer row) exit cone nozzles. Ballistic data from the thrust alignment tests are presented in Table 3-VIII and typical traces are shown in Section 3 of Appendix 2. A detailed discussion of the tests can be found in Atlantic Research Report TR-PL-10135.

TABLE 3-VIII

THRUST ALIGNMENT TEST BALLISTIC DATA SUMMARY

Test No.	Test Date	Prop. Batch	t _a , msec	t _b , msec	t _d , msec	\bar{t}_b , msec	F _{max} lb.	IT, lb-sec	I _{sp} , sec	Roll θ , deg.	Pitch θ , deg.
39645	6-12	23	12.2	10.9	0.5	6.70	827	7.96	235.9	+0.021	-0.027
39664	6-15	23	11.8	10.4	0.7	7.02	866	7.94	235.3	-0.054	-0.051
39670	6-15	23	12.1	10.7	0.7	6.82	864	8.01	235.9	-0.009	-0.006
39684	6-18	23	12.0	10.8	0.5	6.76	852	7.99	236.6	-0.024	+0.030
39695	6-19	24	12.0	10.8	0.5	6.76	872	7.99	236.7	-0.021	+0.003
39698	6-20	24	12.4	11.2	0.4	6.52	840	7.96	235.9	+0.057	-0.015
39705	6-21	24	13.4	12.1	0.6	6.08	773	7.97	235.8	-0.003	+0.036
39721	6-21	24	13.4	11.7	0.5	6.24	774	7.97	235.9	+0.009	-0.203
39736	6-25	24	13.4	11.9	0.5	6.13	768	7.94	235.5	+0.075	+0.060
39730	6-25	24	13.2	11.7	0.5	6.24	791	7.95	235.7	+0.039	-0.060

NOTES: (1) Flightweight Igniters

(2) 0.3085 in. nozzle throat

(3) θ = thrust misalignment angle

3.3.5.3 Array Batch Check Tests

Fourteen batch check motors cast from propellant Batch 2285H (Prototype Array batch) were fired for ballistic evaluation. The motors employed flightweight components except that heavywall test nozzles were utilized. The ballistic results from the batch tests are presented in Table 3-IX, and typical traces are shown in Section 5 of Appendix 2. The data from these tests compare well with the data obtained from the array static tests. Only eleven of the motors were tested. The remaining three motors were placed in controlled storage to evaluate aging effects. Four of the batch check motors tested utilized propellant that had been frozen for about 2 weeks prior to casting and cure. This was done to demonstrate feasibility of replacing a defective grain in a given motor tube with propellant from the same batch. Ballistic data were normal.

3.3.5.4 Prototype Array Tests

The development of the Maneuver Motor Array was concluded with the successful static firing of all 56 motors from a single array in November 1973. The testing of the array was divided into three parts. First, 12 motors were fired with the array suspended from a pendulum. These motors were fired in six groups of two. Within a group, motors were fired at 0.25 second apart and in opposing directions. To duplicate the structural loading during flight, representative structural model HIT subsystems were installed onto the MMA for the Pendulum tests. Next, 24 motors were fired, with the array mounted on a spin stand, at a spin rate of 25 rps. The motors were fired in groups of 12, 4, 4, and 4. Within a group, motors were fired at 0.25 second intervals. Product of inertia measurements were obtained on the array after each group of motors was fired. To conclude the tests, the last 20 motors were fired statically with the array mounted on a thrust stand. The tests were conducted in accordance with Atlantic Research Test Plans TS-0183, TS-0184, and TS-0185 (Appendices 4, 5, and 6, respectively). The

TABLE 3-IX
ARRAY BATCH CHECK TEST BALLISTIC DATA SUMMARY

Test No.	Test Date	t_a , msec	t_b , msec	t_d , msec	\bar{v}_b , in/sec	F_{max} , lb.	I_T , lb-sec	I_{sp} , sec	P_{max} , psi	\bar{P}_b , psi
40218	9-21	12.0	10.5	0.6	6.95	847	7.97	236.3	8860	7832
40219	9-21	12.0	10.9	0.5	6.70	817	7.88	233.8	8575	7873
40220	9-21	12.1	10.9	0.6	6.70	847	7.91	234.2	8860	7526
40221	9-21	11.9	10.8	0.6	6.76	850	7.89	233.7	8947	7725
40222	9-21	12.0	10.8	0.6	6.76	852	7.90	233.9	9013	7651
40223	9-21	11.6	10.5	0.6	6.95	854	7.91	234.4	9079	7870
40224	9-21	11.7	10.5	0.6	6.95	866	7.90	233.9	9211	8249
40272	10-4	12.2	11.0	0.4	6.64	836	7.96	235.7	8695	7728
40273	10-4	12.0	11.0	0.6	6.64	846	7.87	233.9	N/A	N/A
40274	10-4	12.1	10.7	0.7	6.82	859	7.90	234.1	8924	7834
40275	10-4	12.1	10.5	0.9	6.95	853	7.90	234.7	N/A	N/A

- NOTES: (1) Flightweight Igniters
(2) 0.3085 in. nozzle throat
(3) Propellant batch 2285H
(4) Tests 40272 - 40275 utilized frozen propellant

Prototype Maneuver Motor Firing Circuit was installed onto the MMA and utilized for all 56 motor firings.

VSD personnel installed the MMFC and all structural model components onto the Prototype MMA prior to the pendulum test. VSD personnel also attached accelerometers to the MMA and structural model sensor to monitor shock and vibration levels. These operations are illustrated in Figure 3-3.

The pendulum test apparatus (Figure 3-4) consisted of a thin hollow tube suspended from a ball bearing support which allowed the tube to swing in only one vertical plane in response to a motor fired horizontally (#1 in Figure 3-4). An opposing motor (#2) is fired after approximately 45° of pendulum motion to limit excursions. A bracket on the lower end of the tube permitted the MMA to be attached at the outside diameter of the nozzle ring (Figure 3-5). The tube was sized to prevent the MMA from rotating significantly between firings and yet not be so stiff that it would weigh down or damp out the response of the MMA. In the first four 2-motor pendulum tests, the movement of the MMA was tracked by a FASTRAC system supplied and operated by VSD. These tests were conducted in darkness with the tracking equipment set up 60 feet from the test unit and focused on the structural model sensor located inside the MMA cylinder. Tests 1, 5 and 6 were recorded with high speed cameras. Accelerometers attached to the MMA and structural model sensor during the pendulum tests monitored self-induced shock both in the thrust axis and in a perpendicular direction to it. The accelerometer data indicated that the overall structural response of the vehicle was as expected. No transient response outside predicted bounds was seen. The motors were fired in the following sequence.

<u>Test No.</u>	<u>Motor Numbers</u>
1	6 - 34
2	20 - 48
3	8 - 36
4	22 - 50
5	7 - 35
6	21 - 49

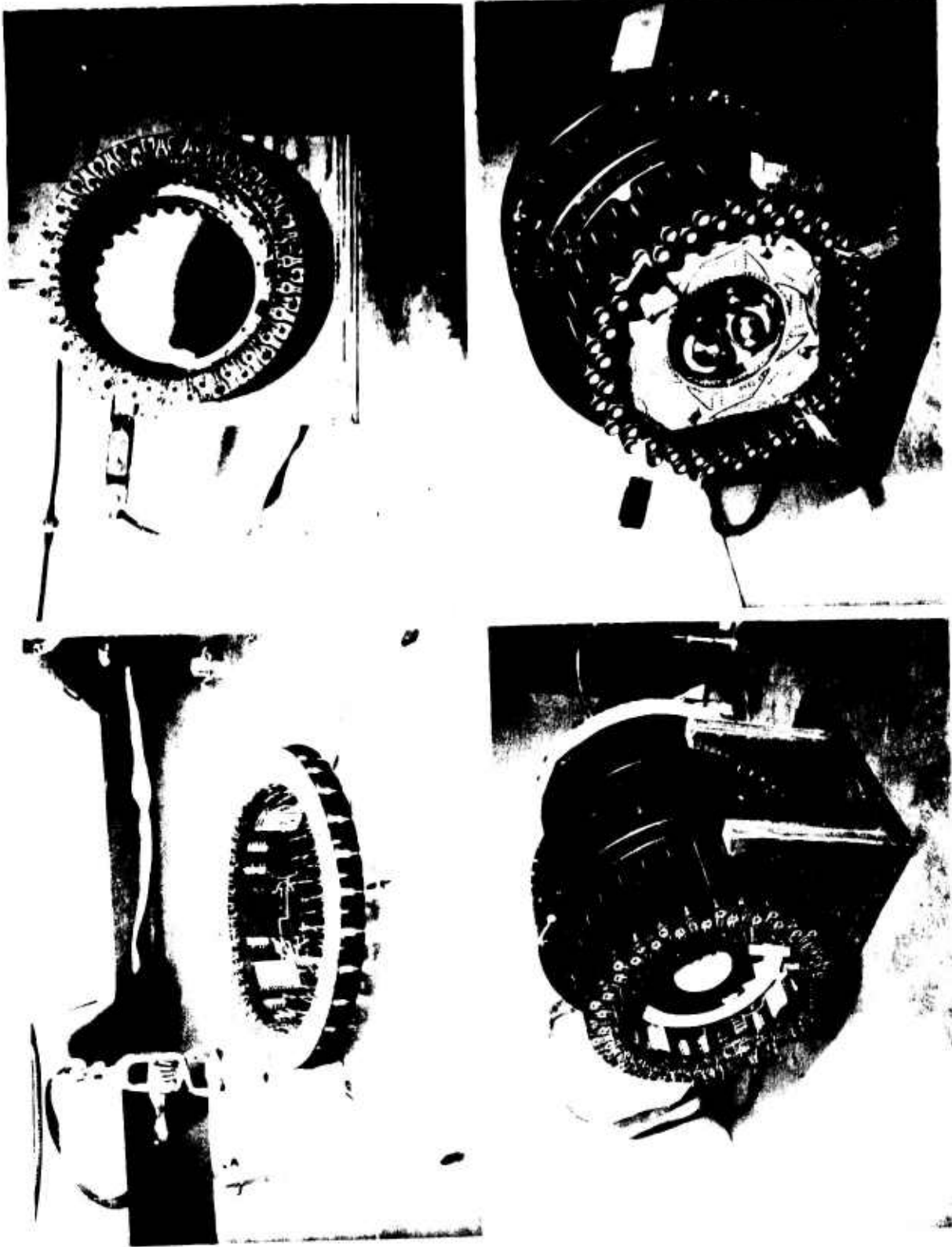


FIGURE 3-3 MMFC and Structural Model Subsystem Installation

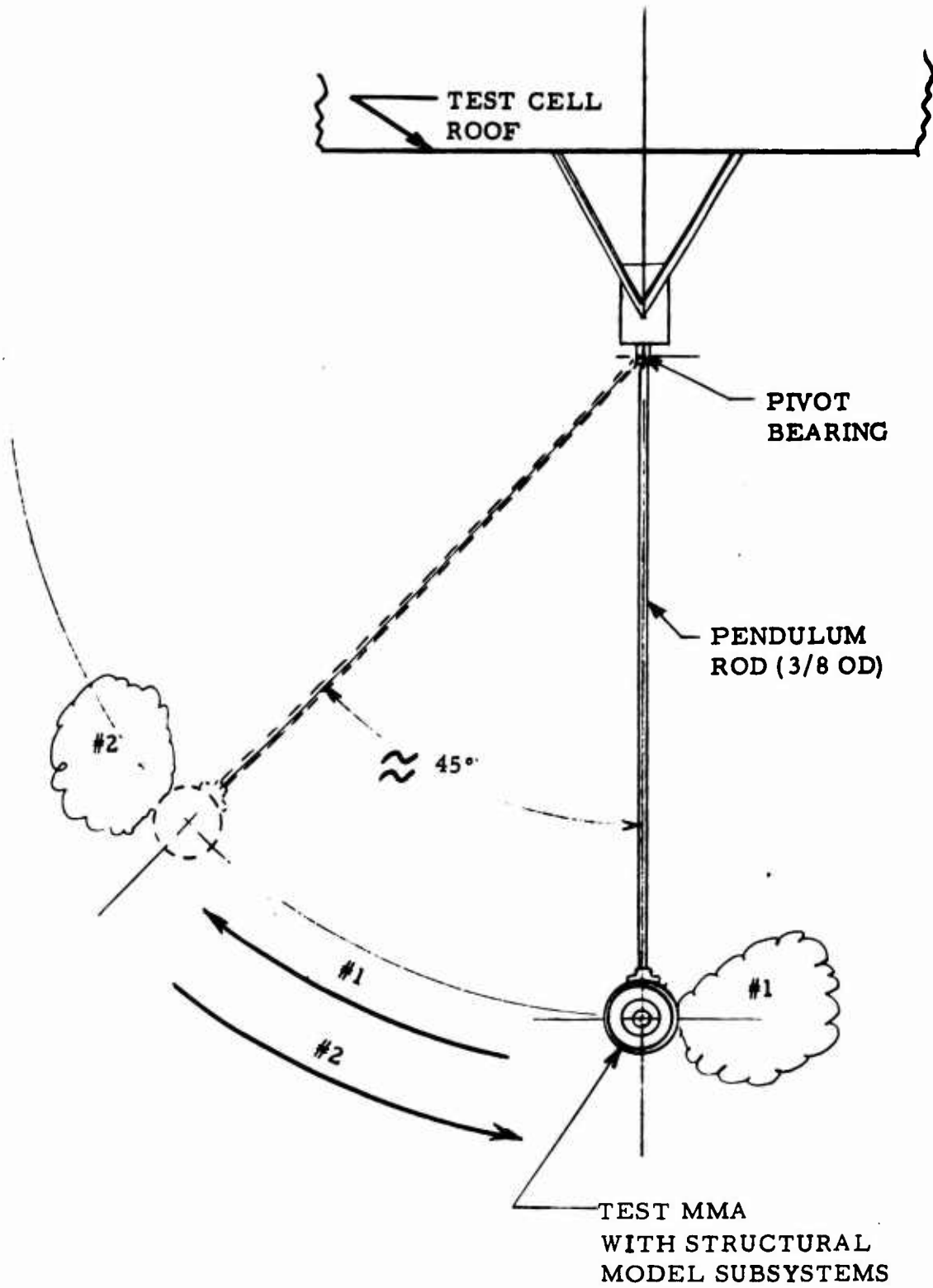


FIGURE 3-4 Pendulum Test Fixture



FIGURE 3- 5 Pendulum Test Set-Up

Following these tests the structural model components were removed from the MMA and a post-test inspection of the MMA bond joints was performed under a microscope. No damage was detected.

The spin tests were conducted with the array mounted on a spinning thrust stand (Figure 3-6). The stand consisted of a two-inch diameter shaft supported at two points by a pair of high precision bearings. The shaft was coupled to a 1/2 hp motor on one end and held a 22-channel slip ring assembly on the other. A speed control on the drive system allowed fine adjustment of spin rate. The array was held on the shaft by three removable clamps which interfaced with the inside diameter of the nozzle ring. During the tests, spin rate and firing times were recorded and two high speed cameras were used. The motors were fired in four groups; motors within each group were fired at 0.25 second intervals in the sequence shown below.

<u>Motor Numbers</u>			
<u>Group 1</u>	<u>Group 2</u>	<u>Group 3</u>	<u>Group 4</u>
15	02	11	10
29	30	39	38
01	16	25	24
43	44	53	52
09			
41			
37			
23			
31			
17			
45			
03			

MMA product of inertia was measured after each of the four test sequences, and post-test inspections were performed under a microscope. No damage was detected.

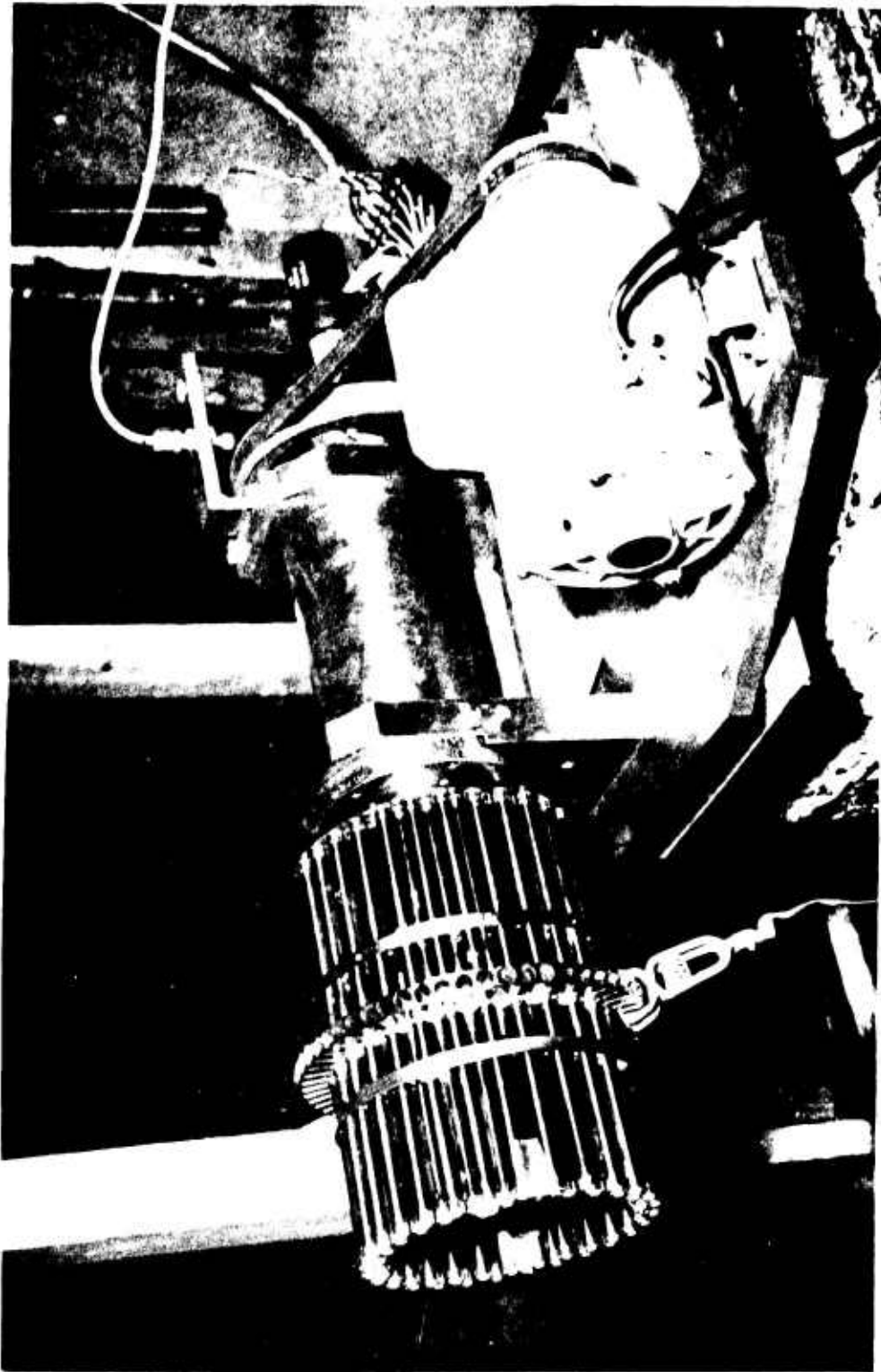


FIGURE 3- 6 Spin Test Set-Up

The static tests were conducted with the array clamped in a mounting bracket that attached directly to the load cell (Figure 3-7). The mounting bracket used the exit cone of the motor 180° away from the one to be fired to align the array. A clamp on both sides of the bracket utilized the "lightening cutouts" in the nozzle ring to hold the array against the bracket. An internally mounted clamp inside the bore of the array stiffened the nozzle ring and improved the frequency response of the thrust measurements. In the first test three adjacent motors were to be fired at 0.25 second intervals. Thus, two of the motors would be fired at an angle 6.4° away from the thrust axis of the load cell. This did not prevent the load cell from accurately measuring the vertical component of thrust. In firing the first three units, however, two motors (12 and 14) fired at the same time due to a malfunction of the ARC firing control unit. Consequently, the test was repeated with adjacent motors 40, 41, and 42. Motors 40 and 42 were fired 0.25 second apart, and Motor 40 was fired one minute later. During the tests, the array was instrumented with thermocouples at 24 different locations, to record temperature versus time.

The 15 remaining motors were statically fired one at a time in the sequence shown below.

<u>Firing Order</u>	<u>Motor Number</u>
1	47
2	46
3	55
4	54
5	56
6	5
7	4
8	13

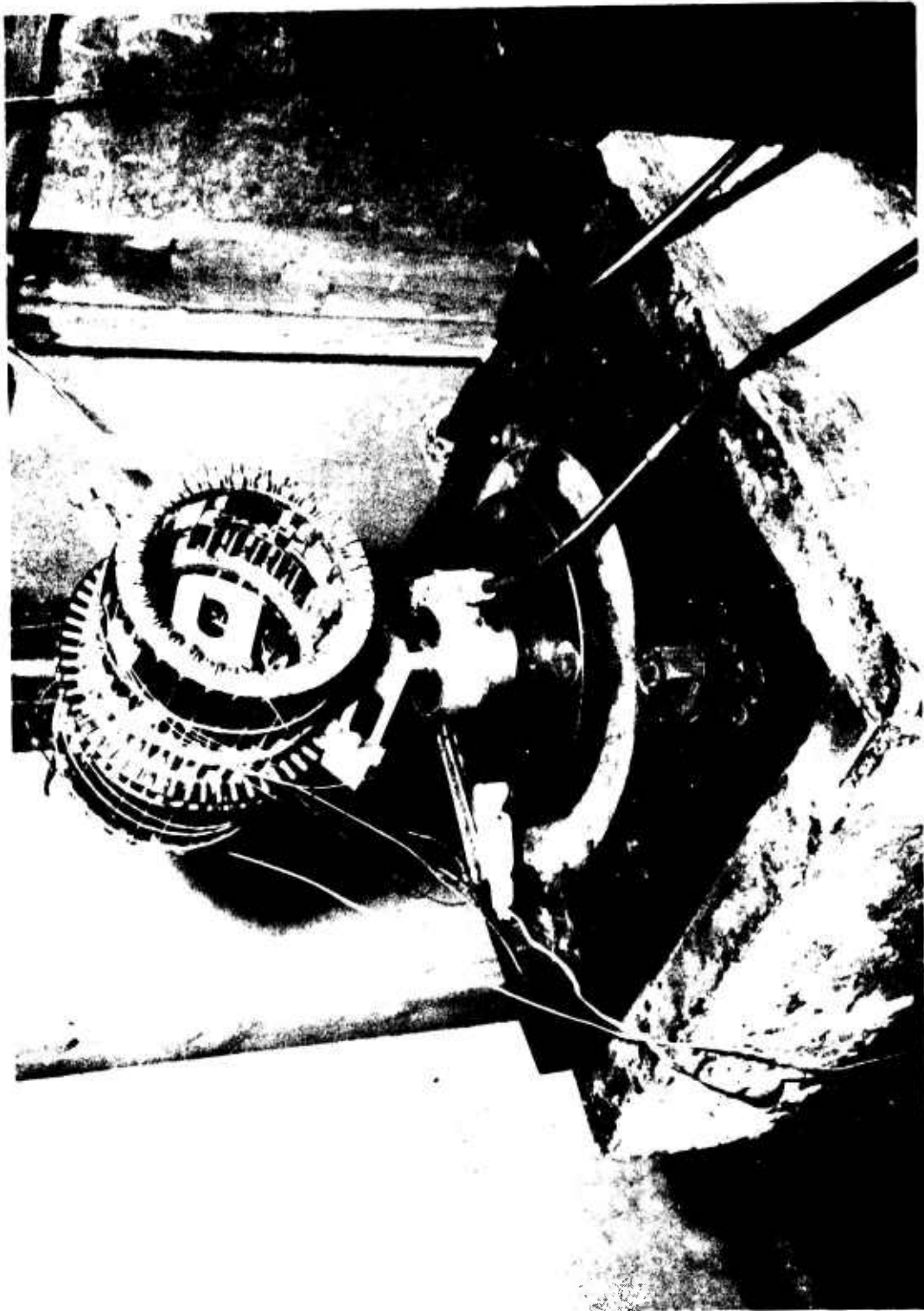


FIGURE 3-7 MMA Static Test Set-Up

<u>Firing Order</u>	<u>Motor Number</u>
9	18
10	19
11	27
12	26
13	28
14	32
15	33

The array was again visually examined under a microscope after completion of the static tests. No indication of bond damage or other structural degradation was seen.

Ballistic data from the static array firings are presented in Table 3-X, and typical traces are shown in Section 6 of Appendix 2. All ballistic data met the performance requirements of Specification 3-371-04-O-10185D. A summary of the thermocouple data is given in Table 3-XI. Thermocouple locations are shown in Figure 3-8.

3.4 MOTOR CASE TESTS

3.4.1 Burst Tests

Seventeen cases of the PDR configuration (0.00075 ± 0.0005 in. titanium thickness) were tested. Burst pressure ranged from 15,000 to 19,500 psi for 13 of these cases. The remaining cases withstood the maximum facility pressure of 20,000 psi without bursting.

Twenty-seven cases of the final configuration (0.0010 ± 0.0005 in. titanium thickness) were tested. Burst pressure ranged from 17,250 to 22,250 psi. Since MMA motor maximum operating pressure is 10,000 psi, the demonstrated burst capability exceeds the 1.3 safety factor requirement by a substantial margin.

3.4.2 Tube/Overwrap Bond Tests

During receiving inspection of overwrapped tubes at ARC in May 1973 it was noted that the entire overwrap could be rotated as a unit

TABLE 3-X

PROTOTYPE ARRAY TEST BALLISTIC DATA SUMMARY

Test No.	t_a , msec	t_b , msec	t_d , msec	\bar{F}_b , in/sec	F_{max} , lb.	I_T , lb-sec	I_{sp} , sec	P_{max} , psi	\bar{P}_b , psi
40704	11.7	10.4	0.3	7.02	966	8.12	240.2	9170	7950
40705	11.4	10.3	0.3	7.09	981	8.04	238.3	9606	8844
40706	11.6	10.3	0.5	7.09	964	8.04	238.0	9426	8659
40707	12.0	10.8	0.3	6.76	919	7.93	235.3	8938	7779
40708	11.6	10.4	0.3	7.02	974	8.08	239.0	9426	8288
40709	11.7	10.6	0.2	6.89	924	8.13	241.1	9015	8293
40710	12.5	11.1	0.3	6.58	892	8.04	238.3	8579	7696
40711	11.8	10.5	0.4	6.95	971	8.20	241.7	9169	8334
40712	11.7	10.4	0.3	7.02	954	8.05	238.7	9221	8159
40713	11.7	10.5	0.4	6.95	942	8.10	239.6	9247	8605
40714	11.9	10.6	0.2	6.89	942	7.88	233.1	9015	7884
40715	12.1	10.9	0.4	6.70	917	8.06	239.4	8861	7939
40716	12.0	10.5	0.3	6.95	942	8.06	238.7	8861	8106
40717	11.5	10.3	0.3	7.09	966	7.93	234.3	9092	8467
40718	11.4	10.1	0.2	7.23	961	7.93	235.9	9477	8509

NOTES:

- (1) Fired 11-20-73
- (2) Propellant Batch 2285H
- (3) Flight weight igniters
- (4) 0.3085 inch nozzle throat
- (5) Times measured from pressure traces due to ringing thrust stand
- (6) F_{max} values approximately 10% high due to ringing thrust stand

TABLE 3-XI

ARRAY THERMOCOUPLE DATA SUMMARY

Thermocouple No.	Motors 40, 42		Motor 41	
	Max. Temp. °F	^a Time, sec.	Max. Temp. °F	^b Time, sec.
1	147	17	100	5
2	147	26	192	6
3	97	18	107	7
4	93	26	103	245
5	107	26	147	16
6	186	22	328	4
7	90	26	153	21
8	163	13	160	29
9	183	12	160	22
10	80	26	137	21
11	222	14	370	3
12	90	26	137	22
13	91	15	103	252
14	153	20	113	58
15	96	15	110	5
16	93	14	137	5
17	123	26	206	6
18	87	26	90	166
19	140	26	192	9
20	140	26	150	28
21	206	10	199	10
22	163	13	166	20
23	189	26	232	5
24	93	23	133	24

(a) From ignition of Motor No. 40

(b) From ignition of Motor No. 41

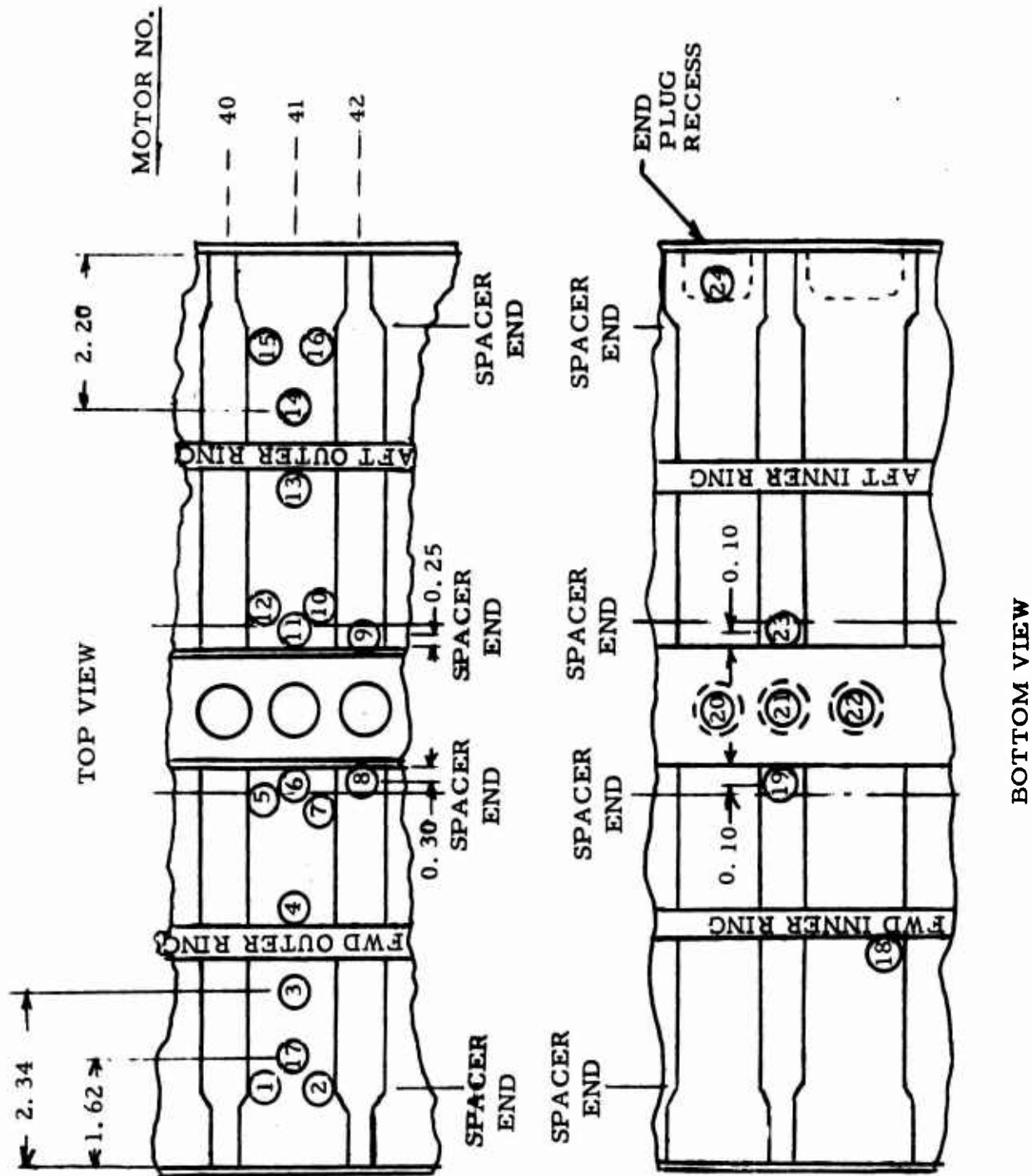


FIGURE 3-8 Prototype MMA Thermocouple Locations

with respect to the titanium on some tubes. Subsequent shear tests in which the overwrap was pulled off the tube in the axial direction revealed bond shear strengths of 63 - 202 psi for that tube lot. Similar tests using tubes from the structural model (SM) MMA (for which acceptable structural stiffness had been measured by tests at VSD) established bond strengths of 115 - 298 psi for those tubes. It was considered mandatory that the prototype MMA to be fired for structural integrity verification should utilize tubes having tube/overwrap bond strengths equal to the best structural model tubes. Therefore, a test quantity of tubes were manufactured and tested utilizing one coat of NARMCO 2021-10 primer applied to the titanium tube OD prior to wrapping. This particular primer had been previously recommended by ABMDA as a candidate to enhance tube/overwrap bond strength. These tubes produced bond strengths of 236 - 430 psi - significantly improved, but still not better than the best SM tubes. At this time it was noted by qualitative peel tests that the overwrap bond was stronger on one end of the tube than the other end, and that due to the dipping method used to apply the primer, the primer was thicker at the "strong" end due to flowing of the primer during cure. It was therefore decided to fabricate and test a second experimental quantity of tubes which had been "double-dipped" prior to wrapping - that is, the tube was dipped in the primer and allowed to drain and cure with one end down, then dipped, drained and cured with the opposite end down. These tubes produced bond strengths of 520 - 665 psi, which was considered acceptable. Figures 3-9 and 3-10 depict the test specimen assembly and representative samples of the motor cases resulting from the VSD shear test program. Figure 3-11 indicates the shear specimen test setup which was utilized by VSD, ARC, and USP to validate the process. Tubes manufactured to this process were utilized in the Prototype MMA.

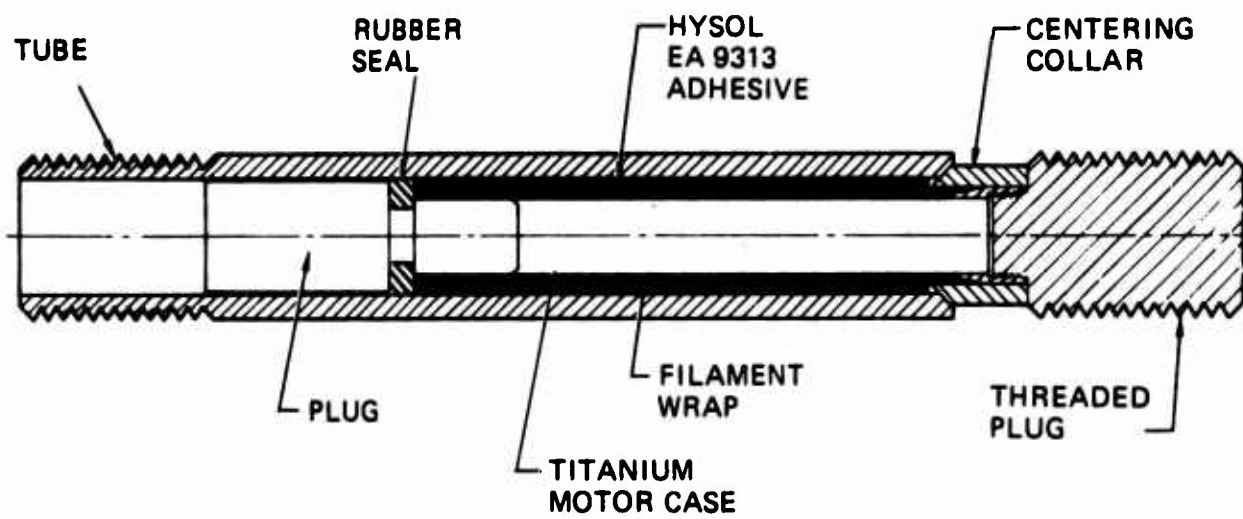
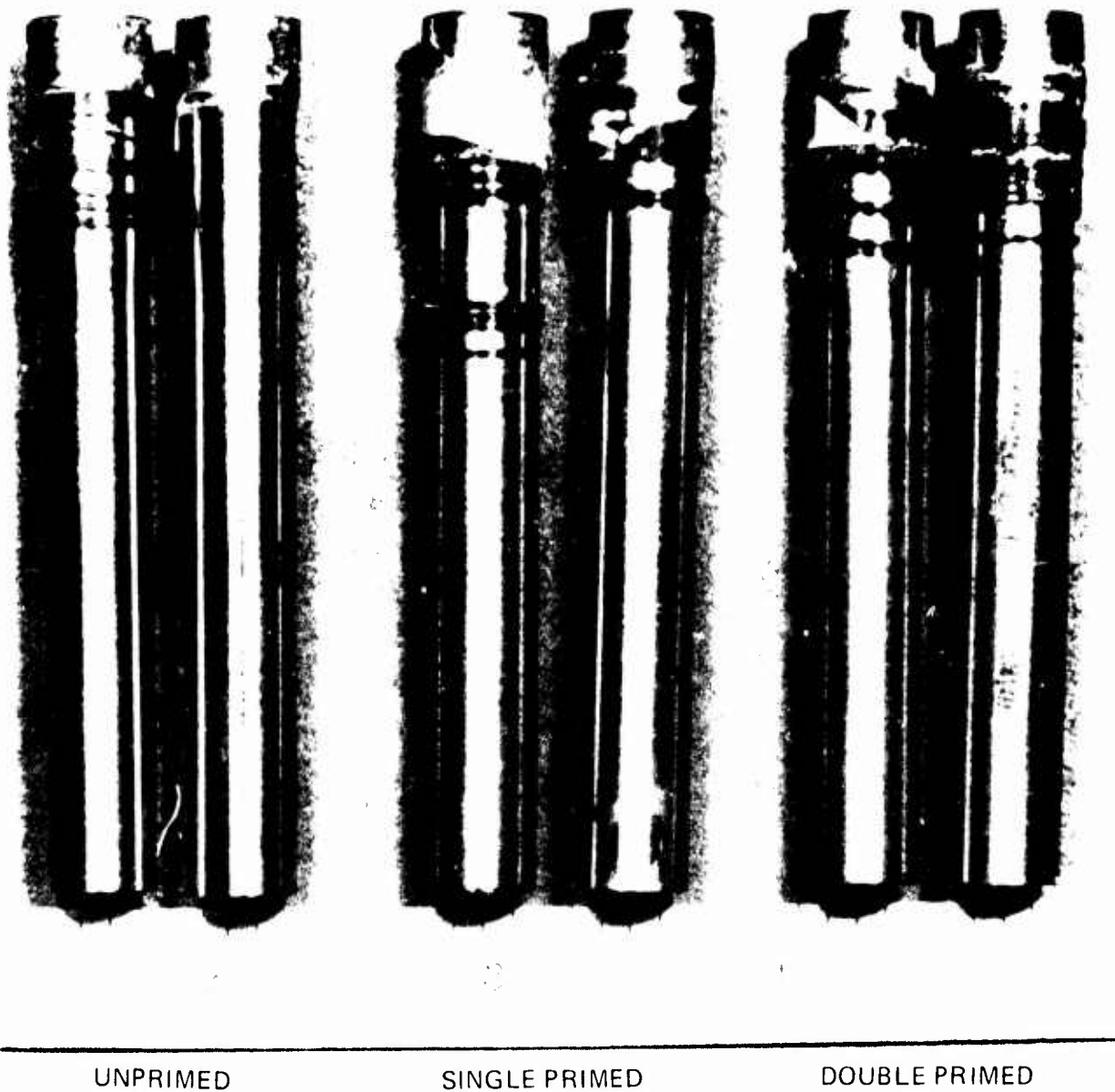


FIGURE 3-9 Tube/Overwrap Bond Test Specimen Assembly



UNPRIMED

SINGLE PRIMED

DOUBLE PRIMED

FIGURE 3-10 Typical Failure Modes - Tube/Overwrap Bond Tests

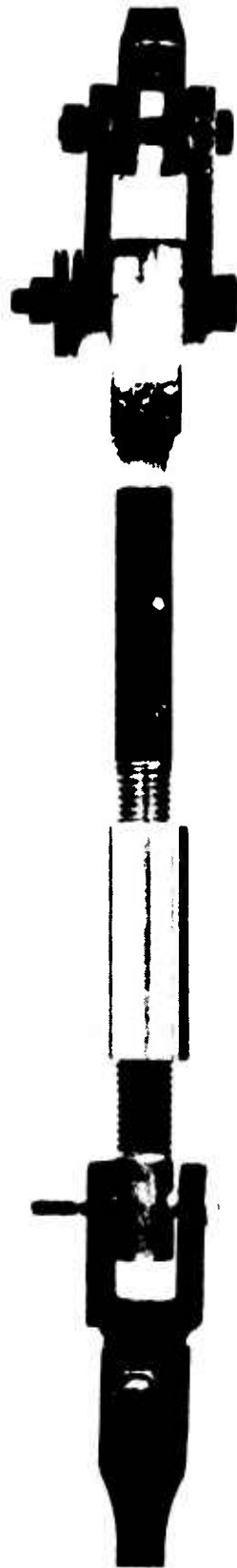


FIGURE 3-11 Tube/Overwrap Bond Test Setup

3.5 ANALYTICAL SUPPORT PROGRAMS

Concurrent with the motor and igniter development efforts, Atlantic Research conducted several comprehensive programs of design analysis. These efforts provided basic MMA sizing trade-offs, information on the expected structural behavior of materials and components of the rocket motor, and predicted structural adequacy, characteristics, and performance of the MMA assembly. The greatest efforts were concentrated in the areas of structure and mass properties studies. The analyses were extremely useful in supporting the decisions made under the motor development program and in prediction of properties and performance of the final MMA assembly. This section of the development report reviews and summarizes the work performed under these programs.

3.5.1 MMA Sizing Analysis

As part of the initial design effort toward definition of a baseline design, a computer sizing program was developed to parametrically evaluate all the required design parameters. The design baseline required a system capable of imparting 970 fps ΔV to the MMA and a 6.608 lb payload. The computer program produced trade-offs of weight, dimensions and ΔV toward optimization of the design. A description of the computer program is presented below.

- (a) The computer program starts by reading the input data. It then initializes grain inner radius equal to 0.07 inch (this value is known to be too small and is selected since minimum grain inner radius is known to give minimum MMA weight).
- (b) The total combined length of one inner row and one outer row propellant grain is now calculated to provide the surface area necessary at the specified burning rate to give initial mass flow consistent with specified initial pressure.

- (c) The required outer propellant grain radius is next calculated to give a volume, hence weight, equal to 1/28 of specified propellant weight.
- (d) The nozzle throat area may then be calculated knowing grain inner radius and the specified grain port area to nozzle throat area ratio.
- (e) Further MMA geometric dimensions are calculated next, such as motor case thickness from case ultimate strength MEOP, ultimate design safety factor, etc.
- (f) Inner and outer motor row radii can now be calculated knowing the minimum nozzle ring inner diameter, motor case O.D., and minimum nozzle ring web between motors.
- (g) Center of gravity and moment of inertia of consumable components is calculated next. The objectives of the calculations are threefold. First is to assure equal c. g. location for both inner and outer row motors.
- (h) The solution to this problem is started by assuming equal length grains in both motor rows. (This is known to be wrong initially but the direction of iteration is known.) The c. g. location of the outer row motors is solved for using the input distance between the igniter case and grain end. The same c. g. location is forced for the inner row motors using the linear distance between igniter and grain end as the variable.
- (i) Moment of inertia calculation of consumables are made next in both pitch (equals yaw) and roll planes for motors in each motor row.
- (j) Inertia ratios for the two motor circles (pitch/roll) are then calculated and tested to determine if they are equal. Since they cannot be initially equal (because both grain

lengths are assumed the same but lie on different motor circle radii), they can be made equal by lengthening outer row grains and shortening (by the same amount) inner row grains. This iterative lengthening-shortening process is carried out until equality of inertia ratios (within an allowable tolerance) is obtained.

- (k) Inertia ratios are next tested for magnitude. If they fall in the acceptable band of $1.07 \pm .01$, they are accepted; if not, the inner grain radius is increased by a small increment and the entire iteration process is repeated from the top as many times as is necessary to obtain acceptable values.
- (l) Inert weight of each element of the MMA is calculated next. For instance the nozzle ring weight is calculated by starting with a solid ring of known material of a given inner diameter and width. The ring outer radius is further calculated to maintain input values for throat L/D, nozzle half-angle, and minimum web between nozzle exit planes. Calculated weights for exit cones, motor holes, and lightening cutouts are subtracted from the solid ring weights to obtain net ring weight.
- (m) The end rings are handled in a like manner except that ring width is solved for based on allowable strengths of ring material (bending) to provide the required structural safety factors. Shear length as required for adhesive is also calculated and used where applicable.
- (n) Straightforward calculations of case, spacer, insulation igniter case and nozzle insert and epoxy weights follow. Total MMA inert weight is then summed and the payload weight is added.

- (o) Final ballistics are calculated next where reference ISP is corrected by ratio of thrust coefficients made up by the new value (found by table lookup of CF versus expansion ratio) ratioed to the reference input value CF. Thus, $ISP = ISPO (CF/CFO)$. The propellant burn rate is then calculated from the average pressure, and the burn time is calculated by dividing the propellant web by the average burning rate. The smear factor is calculated based on motor burn time and MMA spin rate of 25 rps. Smear factor follows by multiplying I_{sp} by the smear factor. System ΔV is finally calculated by:

$$\Delta V = ISPS \times g \times \log_e \left(\frac{\text{Total Weight}}{\text{Total Weight-Propellant Weight}} \right)$$

All desirable quantities are then printed as output.

- (p) Propellant weight is incremented up and the next case is run. This is repeated until the desired range of propellant weights has been completed.

This routine was used to establish the PDR Baseline MMA design configuration, which represented the departure point for subsequent detailed design and analysis efforts.

3.5.2 Performance Variability Analysis

Variability of individual MMA motor performance parameters was calculated by means of a statistical analysis of static test data obtained from final-design motors. These data encompass 56 motor firings and 7 propellant batches, and include all tests beginning with the Heavywall Confirmatory series and ending with the Prototype Batch Check series. Data from the Prototype Array itself was not included in this analysis. Applicable data from motors using non-standard nozzle throat diameters were corrected to a nozzle throat diameter of 0.3085 inch prior to statistical analysis. Average and standard deviation values computed for selected performance parameters are summarized in Table 3-XII.

TABLE 3-XII

INDIVIDUAL MOTOR PERFORMANCE VARIABILITY

Parameter	No. Of Samples	Average	Standard Deviation
Action Time, msec	56	12.76	0.64
Ignition Delay Time, msec ⁽¹⁾	41	0.56	0.15
Time to Impulse Centroid, msec ⁽²⁾	35	6.72	0.38
Maximum Thrust, lb	56	802	41
Maximum Pressure, psi	33	8453	358
Total Impulse, lb-sec	56	7.932	0.052
Specific Impulse, sec	56	234.68	1.352
Propellant Weight, lb	56	0.03380	0.00023
Smear Factor ⁽²⁾	35	0.86926	0.01325

(1) Includes only those firings utilizing final design igniter.

(2) Includes only thrust alignment and subsequent firings.

A separate analysis was required to determine variability of MMA ΔV since this parameter cannot be measured in static tests. The nominal ΔV was calculated as follows:

$$\Delta V = g \times I_{sp} \times S \times \log_e \left(\frac{W_i + W_p + W_{pl}}{W_i + W_{pl}} \right)$$

$$\begin{aligned} \Delta V &= 32.174 \times 234.68 \times .86929 \times \log_e \left(\frac{4.783 + 1.8928 + 6.608}{4.783 + 6.608} \right) \\ &= 1008.94 \text{ ft/sec} \end{aligned}$$

To calculate variability of ΔV , an equation of the following form was utilized:

$$\sigma_y^2 = \left(\frac{\partial y}{\partial x_1} \right)^2 (\sigma_{x_1})^2 + \left(\frac{\partial y}{\partial x_2} \right)^2 (\sigma_{x_2})^2 + \dots + \left(\frac{\partial y}{\partial x_n} \right)^2 (\sigma_{x_n})^2$$

where $y = f(x_1, x_2, \dots, x_n)$

and x_1, x_2, \dots, x_n are independent variables. Therefore,

$$\begin{aligned} (\sigma_{\Delta V})^2 &= \left(\frac{\partial \Delta V}{\partial I_{sp}} \right)^2 (\sigma_{I_{sp}})^2 + \left(\frac{\partial \Delta V}{\partial s} \right)^2 (\sigma_s)^2 \\ &\quad + \left(\frac{\partial \Delta V}{\partial W_i} \right)^2 (\sigma_{W_i})^2 + \left(\frac{\partial \Delta V}{\partial W_p} \right)^2 (\sigma_{W_p})^2 \end{aligned}$$

MMA standard deviation values for I_{sp} , s , and W_p must be calculated from the individual motor values given in Table 3-XII. For I_{sp} , this can be calculated as follows:

$$I_{sp_{mma}} = \frac{I_{sp_1} + I_{sp_2} + \dots + I_{sp_{56}}}{56}$$

$$(\sigma_{I_{sp_{mma}}})^2 = \left(\frac{1}{56} \right)^2 (\sigma_{I_{sp_1}})^2 + \left(\frac{1}{56} \right)^2 (\sigma_{I_{sp_2}})^2 + \dots + \left(\frac{1}{56} \right)^2 (\sigma_{I_{sp_{56}}})^2$$

since $I_{sp_1} = I_{sp_2} = \dots = I_{sp_{56}} = I_{sp}$, then

$$\sigma_{I_{sp_{mma}}} = \frac{\sigma_{I_{sp}}}{\sqrt{56}} = 0.13363 \times 1.352 = 0.18067$$

Similarly,

$$\sigma_{W_{p_{mma}}} = \sqrt{56} \quad \sigma_{W_p} = 7.4833 \times .00023 = 0.00172$$

$$\sigma_{s_{mma}} = \frac{\sigma_s}{\sqrt{56}} = 0.13363 \times .01325 = 0.00177$$

Now taking partial derivatives:

$$\frac{\partial \Delta V}{\partial I_{sp}} = \frac{\Delta V}{I_{sp}} = \frac{1008.94}{234.68} = 4.2992$$

$$\frac{\partial \Delta V}{\partial s} = \frac{\Delta V}{s} = \frac{1008.94}{.86926} = 1160.7$$

$$\frac{\partial \Delta V}{\partial W_i} = - \frac{g \times I_{sp} \times s \times W_p}{(W_i + W_p + W_{pl})(W_i + W_{pl})}$$

$$= - \frac{32.174 \times 234.68 \times .86926 \times 1.8928}{13.2838 \times 11.391} = -82.102$$

$$\frac{\partial \Delta V}{\partial W_p} = \frac{g \times I_{sp} \times s}{(W_i + W_p + W_{pl})} = \frac{32.174 \times 234.68 \times .86926}{13.2838} = 494.09$$

Insufficient data exists to calculate a standard deviation value for MMA inert weight. However, it is conservatively estimated that inert weight will vary no more than ± 0.1 lb (3σ). Therefore,

$$\sigma_{W_i} = \frac{0.1}{3} = 0.033333$$

Standard deviation of MMA ΔV may now be calculated as:

$$\left(\sigma_{\Delta V}\right)^2 = (4.2992)^2 (.18067)^2 + (1160.7)^2 (.00177)^2$$

$$+ (-82.102)^2 (.033333)^2 + (494.09)^2 (.00172)^2$$

$$\sigma_{\Delta V} = 3.6 \text{ ft/sec}$$

$$3\sigma_{\Delta V} = \pm 10.8 \text{ ft/sec}$$

Therefore, the minimum (-3σ) ΔV expected from the MMA is $1008.9 - 10.8 = 998.1$ ft/sec. This is comfortably higher than the specification minimum requirement of 970 fps (-3σ).

3.5.3 Thermal Analysis

The MMA structure was subjected to a thorough thermal analysis to describe the thermal properties of specific areas and to provide degraded material strengths for use in the structural analysis. A detailed description of this effort can be found in the ARC Thermal Analysis Report submitted to VSD in July 1972.

In the course of the thermal investigations, specific areas were analyzed as shown below:

<u>Area</u>	<u>Analyses Performed</u>
Nozzle Ring	Determination of local and average temperatures.
Motor Case	
Insulation	Material selection, erosion and thermal gradients.
Interior	Internal heating, thermal gradients.
Spacer, propellant and mounting ring bonds	Conduction from internal gradients, nozzle ring, head end and adjacent motors.
Head End of Motor	Head end heating failure analysis and redesign.

Maximum temperatures were predicted for these areas at two time intervals, as shown in Table 3-XIII. The first time interval was less than 10 seconds after motor firing when thin wall temperature gradients had equalized and negligible conduction had occurred. The second interval, 120 seconds after ignition, was the maximum time specified from first to last motor firing of the array. Thus, it represented the maximum period when conduction between all components could occur.

The following assessments were made with regard to the maximum temperature predictions.

- (a) The highest temperatures will occur at the nozzle ring, the nozzle end of the motor case, and the igniter end of the motor.

TABLE 3-XIII

MAXIMUM PREDICTED MMA TEMPERATURES (1)

Area	Short-Time (<10 Sec) Temperatures (F)	Long-Time (120 Sec) Temperatures (F) (2)
Nozzle Ring	430 (2)	360
Motor Case (Fired Motor)		
At nozzle ring edge	212	350
0.8 in. from nozzle ring edge	195	175
1.9 in. from nozzle ring edge	170	135
3.1 in. from nozzle ring edge	138	157
Spacer (Fired Motor)		
0.8 in. from nozzle ring edge	160	175
1.9 in. from nozzle ring edge	-	135
3.1 in. from nozzle ring edge	-	157
Beryllium Rings	90	135
Head End		
Igniter	295	250
Plug	270	-
Propellant (Unfired Motor)		
At nozzle ring edge	-	260
3.1 in. from nozzle ring edge	135(4)	-

NOTES

- (1) Initial temperature for MMA is 90°F.
- (2) Temperatures calculated after all 56 motors have fired.
- (3) Temperature of case not contacting spacer.
- (4) Heat conducted from a fired motor adjacent to an unfired motor.

- (b) Motor case temperatures generally will remain under 200°F as required by VSD specification 3-371-04-O-10185, but will be exceeded at the nozzle and head ends of the motor.
- (c) The beryllium mounting ring temperature, however, will remain substantially under 200°F.
- (d) The adhesive bonds at the rings will remain at the ring temperature. Low enough temperatures should occur along the length of the motor case so that the intertube spacer bonds will not be damaged.
- (e) Conduction from a fired motor to an unfired motor should not cause a propellant bond failure or pre-ignition of the propellant.

3.5.3.1 General Approach

The investigation of the MMA thermal properties was based on analysis of internal convective heating from the propellant gases to the motor case and nozzle ring and the subsurface effects of transient conduction to the other components of the MMA structure. The thermal properties of the gases were calculated from an ARC modification of the Thermo-chemical Equilibrium analysis and from empirical calculations. The convective heating of the motor case and nozzle ring interior was calculated from the pipe flow correlation:

$$h = 0.023 c_p G/RE^{0.2} Pr^{2/3}$$

The transient conduction calculations were made with computerized finite difference solutions of the general conduction equation for one, two and three dimensional nodal networks. These techniques provided the basis for the temperature predictions and were also used in the analyses as described below.

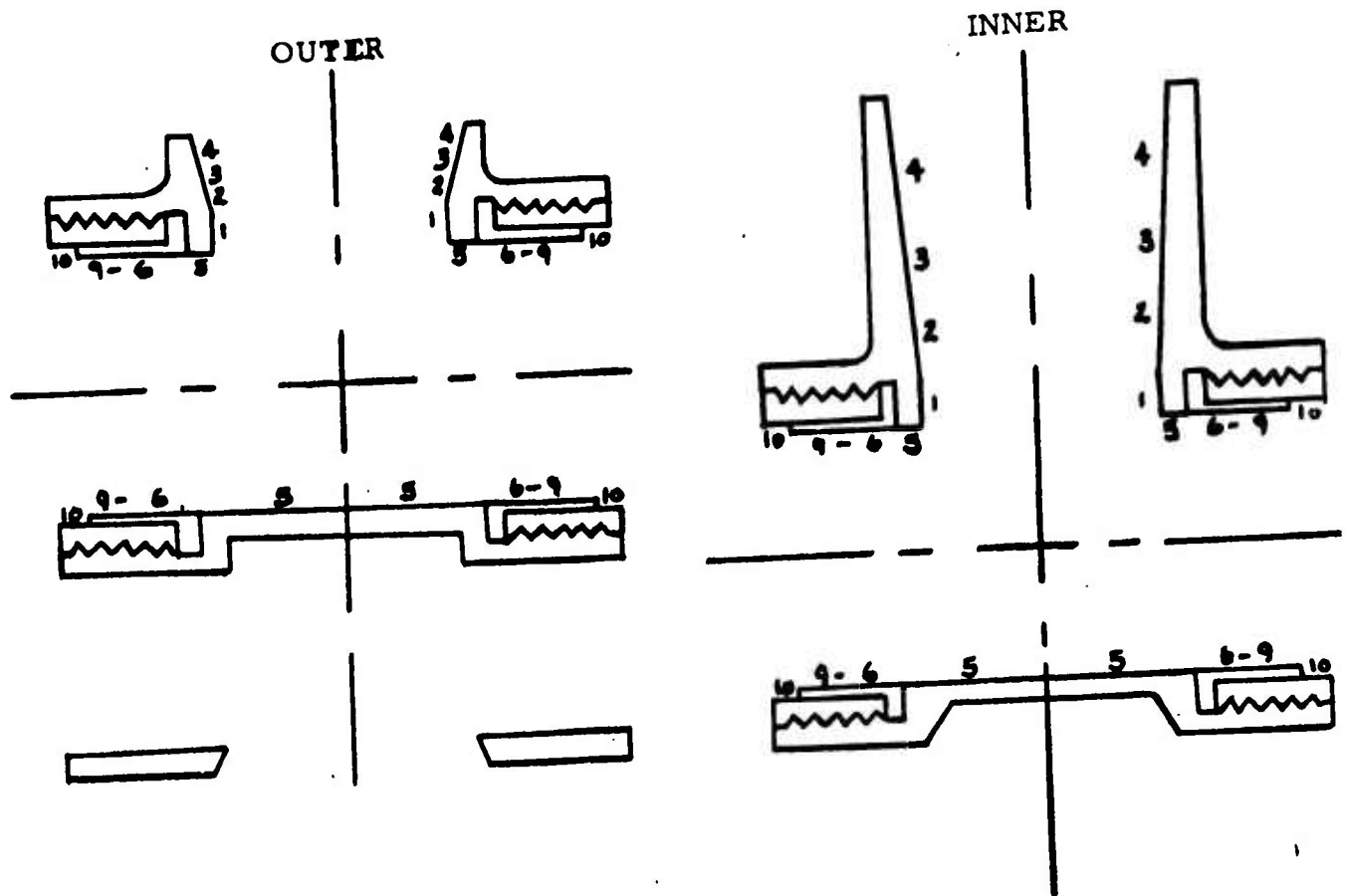
3. 5. 3. 2 Nozzle Ring Analysis

Because there is no insulation in the nozzle ring, a sufficient heat sink wall thickness had to be assured. One purpose of the thermal analysis was to predict the thermal gradients in each section of the ring in support of the structural analysis. In addition, the analyses were used to calculate the bulk temperatures of the ring for use in transient conduction predictions of heat flow to unfired propellant and bonds in the vicinity of the nozzle ring. As shown in Figure 3-12, nine different ring stations were analyzed. The maximum surface temperature in the interior of the nozzle ring was predicted to be 2550°F and the highest bulk temperature to be 725°F. As would be expected, both temperatures occurred at the nozzle throat where the gases turn to exit the nozzle. The throat surface was expected to approach the melting point of steel and post-test motor throat measurements confirm that 0.003 to 0.005 inch of material is lost.

3. 5. 3. 3 Motor Case Analysis

Thermal analyses of the motor case were made to define the gas heating effects and the protection required for internal motor case surfaces. The effects investigated were surface convective heating, which could lead to surface erosion, and subsurface heat conduction, which could produce a reduction in structural properties.

The analyses showed that the wall thickness of the case and the low thermal conductivity of the propellant would protect the majority of the motor case from overheating during motor operations. During the firing, the propellant would absorb the heat generated and the short duration of pressure blowdown at propellant burnout would not be detrimental. At the nozzle end of the case the attachment threads needed protection in the form of an internal insulator. By means of the thermal analysis program, carbon phenolic was selected as the most suitable material to provide protection from erosion because of its lightweight and excellent thermal properties. The carbon phenolic was later found to be unsatisfactory because it cracked under adjacent motor operation and/or assembly



AREA	MAX. SURFACE TEMPERATURE °F	LOCAL BULK TEMPERATURE °F	
		Outer	Inner
1	2550	530	825
2	2450	465	820
3	2355	745	610
4	2260	825	510
5	1720	725	
6	2250	150	
7	2070	140	
8	1725	125	
9	1200	110	
10	1250	115	

NOTE: Temperatures are for an initial temperature of 70°F.

FIGURE 3-12. Nozzle Ring-Local Temperature Predictions

torquing. The insulator was subsequently changed to 4130 steel. Although the steel is heavier, it satisfied all of the other requirements of the MMA motor design.

The head end of the motor case (igniter or plug end) is not protected by insulation or propellant during the firing. Prior to PDR, failures occurred in this area due to heat transfer. Through motor data interpretation, a combined thermal and structural analysis was performed to establish the heating rate that would degrade material properties during the firing period. This heating rate was used to determine the increase in local wall thickness needed to prevent overheating. Based on the analysis, the local wall thickness was increased from a nominal of 0.008 to 0.013 inch. The local wall thickness was further increased to 0.015 inch nominal as a result of the change in safety factors directed by VSD.

3.5.3.4 Motor Case Conduction Heating

Four different evaluations were made to determine the effects of heat conduction from adjacent motor firings. These were:

- (a) Maximum heat conduction along the motor case.
- (b) Maximum heat conduction from nozzle ring to an unfired motor.
- (c) Maximum heat conduction from a fired motor to an unfired motor.
- (d) Conduction between adjacent fired motors.

In addition to those previously stated, the following conclusions were reached from the conduction heating evaluations.

- (a) Spacer bond line temperatures will remain below 120°F near the center of the motor case. At the ends of the cases, the bond line temperatures will be significantly higher.
- (b) The first 0.6 inch of the propellant at the nozzle end must be capable of withstanding temperatures up to

200°F. (The auto ignition temperature of the propellant is 375°F.)

- (c) When two adjacent motors have fired, the spacer bond line must withstand temperatures up to 160°F.

3.5.3.5 Thermocouple Data Comparisons

During the development program, temperature data were obtained for the array static firings as shown in Table 3-XI. These data are plotted in Figure 3-13 and compared to the temperature profile predicted by the thermal analysis at 30 seconds after firing. It should be noted that the temperatures recorded by thermocouples on the motor cases compare favorably with the predictions made under the thermal analysis.

3.5.4 Mass Properties Analysis and Measurements

The HIT vehicle has a "strap down" guidance system which provides its own inertia reference system. Coning motion of the spinning vehicle will result in apparent line-of-sight errors which degrade the vehicles performance. The vehicle mass properties must be controlled through the entire operating period. It is necessary to establish specific mass properties requirements for the MMA consumables (propellant, igniter and nozzle closure). Table 3-XIV presents the primary mass properties specified and the errors that are minimized by controlling these properties.

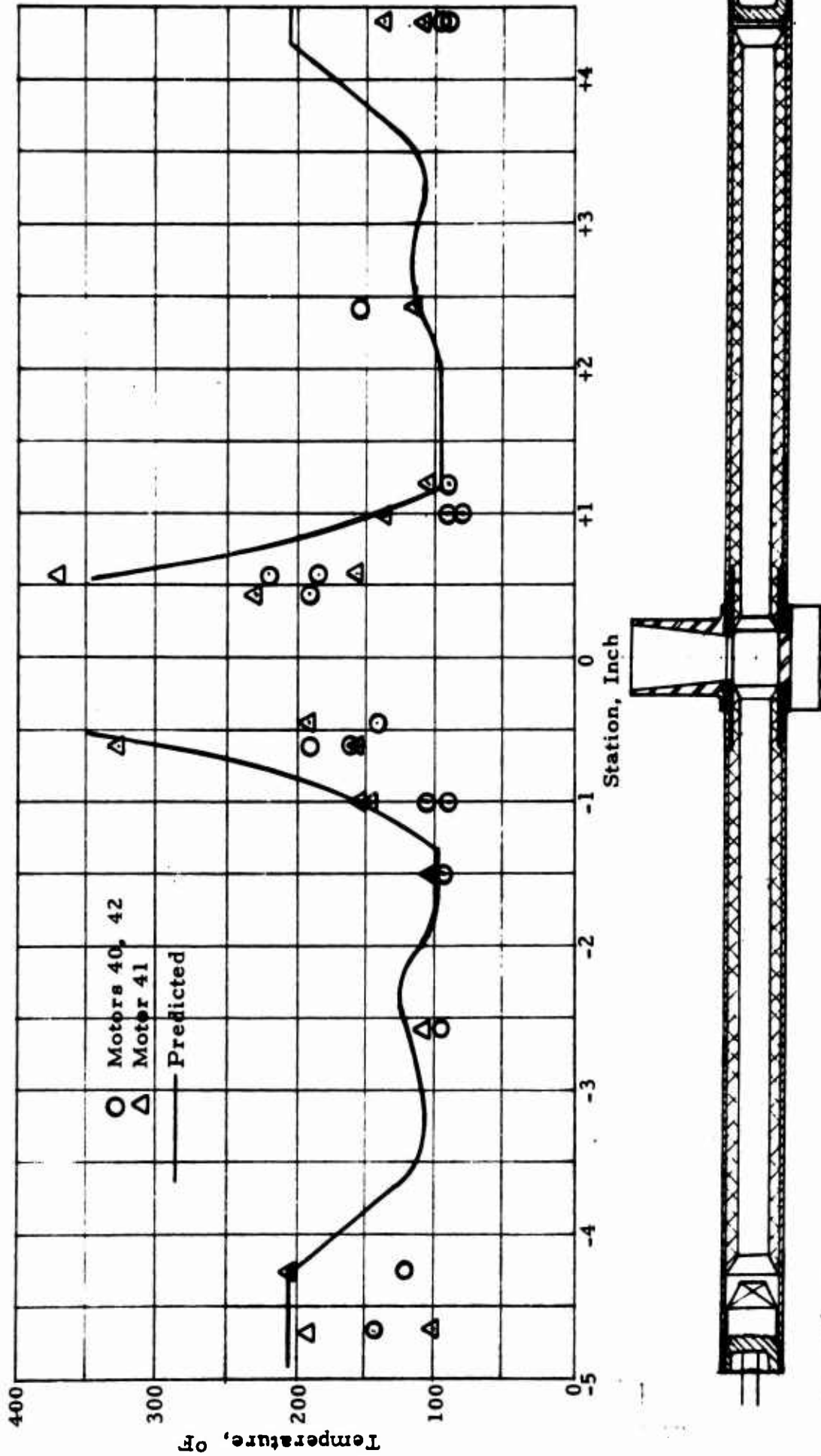


FIGURE 3-13 Thermocouple Data Comparisons

TABLE 3-XIV

MASS PROPERTIES CONTROLS

Controlled Mass Properties	Errors Minimized
Longitudinal Center of Gravity	Transverse moment produced by Maneuver Motor Pulse which results in coning motion.
Moment of Inertia Ratio	Variation in phase rate which results in coning computational errors.
Products of Inertia	Principle axis shifts relative to the optical axis resulting in guidance computational errors.

The specific mass properties requirements for the MMA are presented in VSD Procurement Specification 3-371-04-O-10185D, dated 28 August 1973. A summary of the consumable mass properties requirements is shown in Table 3-XVIII. The MMA inert CG was specified to be within 0.25 inch of the nozzle exit plane along the longitudinal axis. After locating this center of gravity position, it must not vary more than ± 0.001 inch. The inert radial center of gravity position was required to be within 0.010 inch of the longitudinal axis.

In order to meet these mass properties requirements a mass properties control plan was developed. The fundamental design approach for the MMA was to develop a configuration that would achieve the required mass properties without balancing (i. e., mass properties measurements and adjustments, if required). The design approach established was to meet the mass properties requirements through dimensional controls, manufacturing process and assembly methods of the MMA. The dimensional tolerances were established and based on these values the nominal mass properties and standard deviations were determined. The results of this analytical study, reported in the ARC Mass Properties Control Plan, indicated the MMA consumable mass properties could be controlled within the required limits.

In order to verify that the dimensional controls would satisfy the required mass properties, a mass properties measurement program for the prototype array was established. This program included the check-out of precision mass properties measuring equipment, measurements during build-up of the array and measurements before and after motor firings. A description of this measurement test program was also presented in the Mass Properties Control Plan. The measurement program included measurements of consumable weights, center of gravity location, moments of inertia and products of inertia. The errors associated with measurement instrument accuracy and fixture/instrument/test part interface repeatability were initially evaluated. Table 3-XV presents a summary of the measurement errors for the various mass properties measured. These measurement accuracies are acceptable to confirm the measured mass properties.

The mass properties measurement instruments are shown in Figure 3-14. The CG/MOI fixture and dynamic balance fixture which interface the test part to the instrument are shown in Figure 3-15.

TABLE 3-XV

MASS PROPERTIES MEASUREMENT ERRORS

Mass Properties	Measurement Instrument	Measurement Errors
Weight	Balance	
Individual propellant		± 0.01 mg
Total propellant		± 0.04 mg
Center of Gravity		
Longitudinal	Static CG Locator	± 0.0005 inch
Radial	Dynamic Balance	± 0.000005 inch
Products of Inertia		
Dual motors	Dynamic Balance	$\pm 4 \times 10^{-7}$ in-lb-sec ²
"Fire Down"	Dynamic Balance	$\pm 13.6 \times 10^{-7}$ in-lb-sec ²
Moments of Inertia Ratios		
Four Motor Sets	Torsional Pendulum	± 0.017
Total (inner and outer) rings	Torsional Pendulum	± 0.010

The weights of the 128 individual motor tube propellant was measured and recorded. The average and standard deviation of the igniter and plug side tube weights is presented in Table 3-XVI. These measured weights were coupled with assumed nominal center of gravity locations to estimate the various mass properties for comparison with the measured mass properties data. The mass properties estimates based on these data appear in Table 3-XVIII. These results compare vary favorably with the measured mass properties. Therefore, the measured consumable



CG
Instrument



Spin Balance
Instrument



CG
Instrument

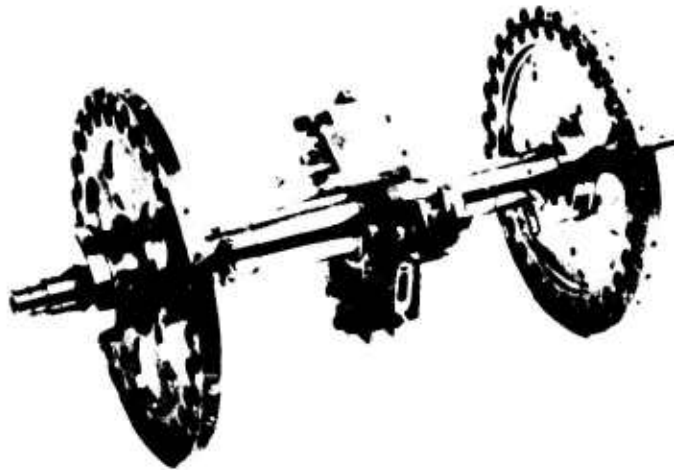


MOI Instrument

FIGURE 3 -14 Mass Property Measurement Instruments



CG/MOI Fixture



Spin Balance Fixture

FIGURE 3-15 Mass Property Measurement Fixtures

weights, results in the capability of estimating the consumable mass properties. This also provides a simple method of gaining confidence that subsequent MMA's will meet the specified mass properties requirements. A procedure of ordering the motor tubes by weight and installing them in a specific sequence in the array could be developed and easily incorporated in the assembly procedure.

TABLE 3-XVI

INDIVIDUAL MOTOR PROPELLANT WEIGHTS

Statistics	Igniter Side	Plug Side	Total
Average Weight (grams)	7.5427	7.6609	15.204
Standard Deviation	0.0177	0.0170	0.280

The inert MMA longitudinal center of gravity was analytically predicted to be 0.245 inch forward of the nozzle exit plane, which is within the required limit of 0.250 inch. The inert radial center of gravity was predicted to be displaced from the array centerline by 0.0006 inch, which is within the limit of ± 0.010 inch.

The longitudinal center of gravity of the consumables was measured with the static CG instrument to be 0.0007 inch aft of the nozzle exit plane. This result is within the specified requirement of ± 0.001 . The predicted value based on dimensional tolerances was 0.0004 inch ± 0.003 inch. The radial center of gravity of the array was measured on the dynamic balance machine and determined to be within 0.0008 inch of the array centerline, which is less than the required limit of ± 0.005 inch. This measured radial center of gravity is within the predicted

tolerance of 0.0019 inch. A summary of the consumable center of gravity analytical and test results are presented in Table 3-XVIII.

The products of inertia (POI) of the consumables was measured on the dynamic balance machine. The POI with respect to the array center-line were measured on 28 sets of motor pairs (each motor installed 180° apart in nozzle ring). This data provided an estimate of the standard deviation of POI for each motor during buildup. This standard deviation of POI due to consumables of each motor was 12×10^{-7} in-lb-sec², which is less than the required 22×10^{-7} in-lb-sec² (1σ). The measured POI of the total array consumables was also determined to be 87×10^{-7} in-lb-sec², which is less than the required 165×10^{-7} in-lb-sec². The measured single motor and total array POI are also within the predicted POI which are based on the dimensional tolerances. These measured results confirm that the dimensional tolerances are controlling the POI during the buildup and assembly process. The POI were also measured between a sequence of four motor firing tests. The array was spun at 25 rps during these firing tests. The POI change from these tests is presented in Table 3-XVII. Based on these 24 motor firings the mean POI change is 14.25×10^{-7} in-lb-sec². This non-zero average change in POI/motor indicates the possibility of POI/motor bias, since the population mean was assumed to be zero. An investigation and conclusion regarding this possible POI bias is dependent on the measured variability of the Δ POI/motor.

Only the most general conclusions can be drawn regarding the observed variation in Δ POI on a per motor basis from the limited available data. The approach used in estimating the per motor POI variation is predicated on the following property of the sample mean: this variability of the sample mean of a population ($\sigma_{\bar{x}}$) is related to the population variable σ_x by the relation:

$$\sigma_{\bar{x}} = \frac{\sigma_x}{\sqrt{n}}, \text{ where } n \text{ is the sample size.}$$

TABLE 3-XVII
ARRAY FIRE DOWN POI MEASUREMENTS

Sample Set Number	Number of Motors	Total POI Change (x 10 ⁻⁷ in-lb-sec ²)	Average Per Motor Change (x 10 ⁻⁷ in-lb-sec ²)
1	12	179	14.917
2	4	88	22
3	4	14	3.5
4	4	61	15.25
Total	24	342	14.25

When applied to the problem under consideration, this result asserts that a measure of $\sigma_{\Delta POI}$ (the per motor POI variation) can be estimated from the observed variability in the single mean. According to the data in Table 3-XVIII, the variation in the sample mean determined from the 4 sample data set measurement is:

$$\begin{aligned} \sigma_{\Delta POI} &= \left\{ \frac{1}{3} \left[(14.917 - 14.25)^2 + (22 - 14.25)^2 \right. \right. \\ &\quad \left. \left. + (3.5 - 14.25)^2 + (15.25 - 14.25)^2 \right] \right\}^{1/2} \times 10^{-7} \\ &= 7.683 \times 10^{-7} \text{ in-lb-sec}^2 \end{aligned}$$

Hence

$$\sigma_{\Delta POI} = \sqrt{4} \times 7.683 \times 10^{-7} = 15.37 \times 10^{-7} \text{ in-lb-sec}^2$$

Since the data is based on a small sample, it is imperative that not too much significance be attached to this number. Perhaps a more useful measure of the per motor variability in ΔPOI is the upper limit of a 95% confidence interval determined from the above data. Hence, assuming that the observed variation in the sample mean (based on 4 measurement)

is 7.683×10^{-7} in-lb-sec², the upper limit of a 95% confidence interval is 22.43×10^{-7} in-lb-sec²; i. e., we are 95% confident that the true variation of the sample mean is less than 22.43×10^{-7} in-lb-sec². Equivalently, we are 95% confident that the per motor POI variation is less than 44.9×10^{-7} in-lb-sec².

Based on these observations, one concludes that it is not statistically significant that the sample average per motor POI change is 14.25 in-lb-sec². The assumption that the population mean is zero is still valid. Similarly, the data support the hypothesis that the variability of the per motor POI change is 22×10^{-7} in-lb-sec². The conclusion of the preceding analysis is that the limited available test data does not provide information which contradicts the specified population distribution parameters.

If the variability of the per motor POI change was assumed to be 44.9×10^{-7} in-lb-sec² rather than 22×10^{-7} in-lb-sec², the estimated total vehicle POI change would become 1308×10^{-7} in-lb-sec² (3σ) instead of 969×10^{-7} in-lb-sec² (3σ). However, the change in guidance mechanization from cone damp to the optical axis to cone damp to the principal axis desensitized the HIT guidance to products such that this 30% POI increase has an insignificant influence on the vehicles performance. These POI change test results will be combined with additional results from the battery and balancing tests to revise the POI change estimates.

The torsional pendulum was used to measure the moment of inertia (MOI) ratio of the inner and outer rows of the consumables. These measurements included groups of four orthogonal motors and the entire inner or outer motor rows. The mean inertia ratio for the inner row sets of four motors was 1.215. The total inner row inertia ratio as measured was 1.206. The mean inertia ratio for the outer row sets of four motors was 1.101 and the total outer row was determined to be 1.096. These results are in good agreement with the predicted MOI ratios (based on

dimensional tolerances). The predicted results are higher than the specified range for the MOI ratio. These predicted values have been reviewed as to their influence of the HIT vehicle mass properties and resulting vehicle performance and determined to be satisfactory. Therefore, the MMA array specifications should be revised to the predicted MOI ratios. A summary of these results is shown in Table 3-XVIII.

In general, the dimensional controls used in the manufacture and assembly of the prototype array did result in the mass properties being controlled within the design limits. The mass properties control has been demonstrated on the prototype array and it is not necessary to require additional mass properties measurement tests during the assembly of the MMA's for the IST. Since the calculated mass properties from the measured weight data were in good agreement with the measured and predicted mass properties, the measured weights of the consumables can be used as an assembly guide with high confidence in meeting the required mass properties.

3.5.5 Structural Analysis

3.5.5.1 Development of Computer Programs

A series of computer programs was developed by ARC to aid in the analysis of the MMA structure and its components. These programs which were used to determine the static and dynamic properties of the array and components are described below. A completely detailed discussion of the computer programs and the greater part of the stress analysis effort may be found in the ARC Structural Analyses Report, submitted to VSD on 25 August 1972.

TABLE 3 -XVIII
CONSUMABLES MASS PROPERTIES SUMMARY

Mass Properties	Requirement	Predicted Based on Dimensional Control	Measured Mass Property	Calculated from Measured Consumable Weight	Remarks
<ul style="list-style-type: none"> • <u>Center of Gravity</u> • Longitudinal (inch) • Radial (inch) • <u>Products of Inertia</u> • Per Motor • Build Up (x 10⁻⁷in-lb-sec²) • Fire Down (x 10⁻⁷in-lb-sec²) • Total Array • Build Up (x 10⁻⁷in-lb-sec²) • <u>Moments of Inertia</u> • 4 Motor Sets • Outer Row • Inner Row • Total Row of Motors • Outer Row • Inner Row 	<ul style="list-style-type: none"> ±0.001 ±0.005 ±22.0 ±22.0 ±165.0 1.05-1.07 1.15-1.17 1.05-1.07 1.15-1.17 	<ul style="list-style-type: none"> -0.00004 0.0019 ±19.9 ±19.9 ±149.0 1.10065 1.20478 1.10065 1.20478 	<ul style="list-style-type: none"> -0.0007 0.0008 ±12.0 ±22.0 ±87.0 1.101 1.215 1.096 1.206 	<ul style="list-style-type: none"> -0.0002 0.001 ±9.0 ±65.0 1.093 1.196 	<ul style="list-style-type: none"> Measured on static CG Locator Measured on Dynamic Balance Machine Measured on torsional pendulum

Atlantic Research Computer programs D-9033 and D-9049 were modifications of computer programs AMG-033 and AMG-049, respectively, developed by the Rohm and Haas Company. Program D-0933 uses a finite element direct stiffness method to perform a small deformation stress analysis of linear isotropic planar bodies optionally encased by an orthotropic shell and subjected to loads from surface tractions, body forces, point loads, and temperature distribution. Program D-9049 is a similar program that analyzes anisotropic axisymmetric bodies in the same manner.

The MRI/STARDYNE Analysis System consists of a series of compatible digital computer programs designed to analyze the full range of static and dynamic properties for linear elastic structural models. The programs were developed by and are proprietary to Mechanics Research, Inc. The system is operated by Control Data Corporation through its 6600 digital computer. The STARDYNE System uses finite modeling elements to perform static load analysis and eigen value/eigen vector extraction. The static analysis and nodal extraction phases are based on the "stiffness" or "displacement" method.

To analyze the MMA structure for static and dynamic properties with the STARDYNE System, a model was developed to represent as closely as possible the real structure which has a complex geometry and is comprised of a variety of materials. Certain elements of the structure were idealized without losing their original physical identity, for example, the supporting rings were idealized as triangular plate elements with a zig-zag geometric pattern that approximates the actual geometry, average cross section and moment of inertia. Another example was the motor cases, whose stretching and bending properties and spatial locations are represented by beam elements. The modeling followed a series of steps discussed below:

- (a) A global cartesian coordinate system was defined with nodal points having a position or location in the global reference system to define the overall structure.
- (b) A motor tube array nodal connectivity system was developed which defined corresponding geometric, mechanical and physical properties.
- (c) A triangular plate nodal connectivity and numbering system was developed to define the thickness and materials properties of the support rings.
- (d) A similar system was developed to define the support rings.
- (e) The connectivity of the motor tube spacers, idealized as beam elements, was defined.
- (f) Boundary conditions, including symmetry, restraints, inter-connectivity and degrees of freedom were defined.
- (g) The information developed above was coded and punched into data cards to form the STARDYNE geometry deck setup.
- (h) The geometry deck setup was run into the CDC 6600 computer to check all input parameters and to check time estimates.
- (i) Corrections and modifications of the input parameters were incorporated and the deck setup was rerun.
- (j) The static and dynamic analyses were run in the 6600 computer.

Computer Program D-6180 was written specifically to calculate moment of inertia and area and centroid of irregularly shaped plane areas. The program also allowed use of different material properties so that the moment of inertia and area became representative of the reference material. Cross sectional property data for the nozzle and mounting rings were evaluated with this program.

Computer program D-9341 was developed to compute the shear, tension and bending moments at various angular locations on the nozzle ring and mounting rings. As mentioned above, the rings were idealized for the STARDYNE program as triangular plate elements of constant thickness. The STARDYNE computer output gave among other results, the element joint and corner force of each triangular plate in the ring. By appropriate summation of these joint forces, the local shear, tension and bending moment in the ring was calculated to determine actual ring stresses. The D-9341 program was developed to automate this process and reduce the joint forces into local transverse shear, tangential tension and bending moment at 30 circumferential locations for each ring analyzed.

Computer program D-7790 was used to calculate the composite laminate elastic constants from basis filament and matrix properties. The cylindrical fiber model theory of Greszazuk was selected from four available theories and used to determine the properties of the motor case overwrap.

An analytical expression was needed to represent experimental relaxation data for viscoelastic materials. Computer program D-2790 was used to find:

- (a) A Prony series representation of relaxation modulus.
- (b) A Prony series approximation of creep compliance.
- (c) Complex modulus and loss tangent for dynamic loading conditions.

All of the above employed an experimental relaxation modulus versus reduced time curve.

3.5.5.2 Component Static Analysis

With the aid of the computer programs, each of the MMA components was subjected to a thorough stress analysis under static conditions. The analyses included the motor case, the nozzle ring, the mounting rings, the end plug, the igniter, the adhesive areas, the spacers, and the propellant

grain. A summary of the maximum stresses and minimum safety factors for these components is presented in Table 3-XIX. The locations of these areas are shown in Figure 3-16. For the purposes of the static analyses, the primary loading condition was that of one motor firing during MMA free flight. This condition includes a thrust load radial to the nozzle ring structure, internal pressure acting on the fired motor, and a 25 rps constant spin velocity. The thrust load was assumed to be reacted by a g field corresponding to an 11 pound array and payload. Time and spatial varying temperature gradients were taken into account as appropriate. Material properties were taken from established sources when available. Propellant and spacer mechanical properties were obtained primarily by testing at ARC.

Results of the stress analysis showed that most areas of the MMA design had safety factors that fell above the specified minimums. One area that did not was along the thin walled section of the motor case. The hoop and axial stresses for this area showed that an excellent balance of filament overwrap to titanium thickness had been achieved. The possible heat soak from adjacent motors, however, caused the stresses in the titanium to fall below a yield safety factor of 1.1 and an ultimate safety factor of 1.2. Similarly, the thickened case region at the igniter end of the motor case had a safety factor slightly lower than 1.1 for yield stress. Atlantic Research recommended a 6 and 10% increase in thickness in each of these areas, respectively. As a result of the ATI test failure and subsequent failure analysis discussed earlier, VSD increased the safety factors from 1.1 to 1.2 for yield tensile strength, and from 1.21 to 1.32 for ultimate tensile strength. VSD also directed that the motor case be thickened by 2 mils along the entire case except for the threaded ends to meet these levels.

TABLE 3-XIX

MMA STRUCTURAL SAFETY FACTOR SUMMARY

Location on Figure 3-9	Type of Stress	Stress (ksi)	Temperature ^a (°F)	Yield Strength (ksi)	Ultimate Strength (ksi)	S. F. y	S. F. u
			<u>MOTOR CASE</u>				
			180	N/A	216	N/A	1.91
1. End of taper	Hoop stress in filaments	113	531	106.5	123	1.057	1.22
2. Thickened igniter end	Axial in titanium	100.8					
	Hoop in titanium	130.6	135	140	152	1.072	1.16
3. Nominal case wall	Axial in titanium*	134	135	140	152	1.042	1.135
			<u>NOZZLE RING</u>				
4. End of threads	Hoop in steel	15.6	430	114	139	7.3	8.9
5. Outer radius section near exit cone	Ring bending and tangential	-12.0	430	114	139	9.5	11.6
			<u>END PLUG</u>				
6. Center of cap	Hoop in aluminum - inside surface	-30.0	470	18.0	21.0	Yields 1.68	N/A
	- outside surface	37.6	165	63.2	74.5		1.98
			<u>IGNITER</u>				
7. Igniter	Hoop at surface of aluminum cap	-15.1	470	18.0	21.0	1.19	1.39
	Hoop at surface of Kovar plate	-26.7	350	40.0	80.0	1.50	3.0
	Hoop at surface of glass plate	-20.2	350	N/A	80.0	N/A	3.96
	Triaxial in epoxy potting	-13.4	350	N/A	20.0	N/A	1.44
			<u>MOUNTING RINGS</u>				
8. Outer edge surface	Ring bending and tangential	31.3	135	39.0	48.0	1.25	1.53
9. Outer edge surface	Ring bending and tangential	-16.8	135	39.0	48.0	2.32	2.86
			<u>ADHESIVE</u>				
10. Near tube spacer ends	Shear stress	2.28	70	N/A	2.42	N/A	1.06
	Shear stress, upper temperature limit	54 psi	220	N/A	490 psi	N/A	9.1
11. Under mounting ring spacer	Shear stress	2.38	70	N/A	2.42	N/A	1.02
12. Mounting ring spacer	Maximum principal	7.0	70	N/A	18.5	N/A	2.64
			<u>PROPELLANT GRAIN</u>				
13. Grain bore surface	Hoop stress and strain	28 psi and 3.0%	50	Max. stress 380 psi	Strain at max. stress 39 percent	13.0	N/A
14. Grain-to-case end terminations	Shear stress	66 psi	200	Max. stress 229 psi	N/A	3.47	N/A

^a Temperature values were re-evaluated in this table to insure that safety factor calculations reflect the best interpretation of available thermal data. Temperature values in most areas have been conservatively increased over those reported elsewhere in this report.

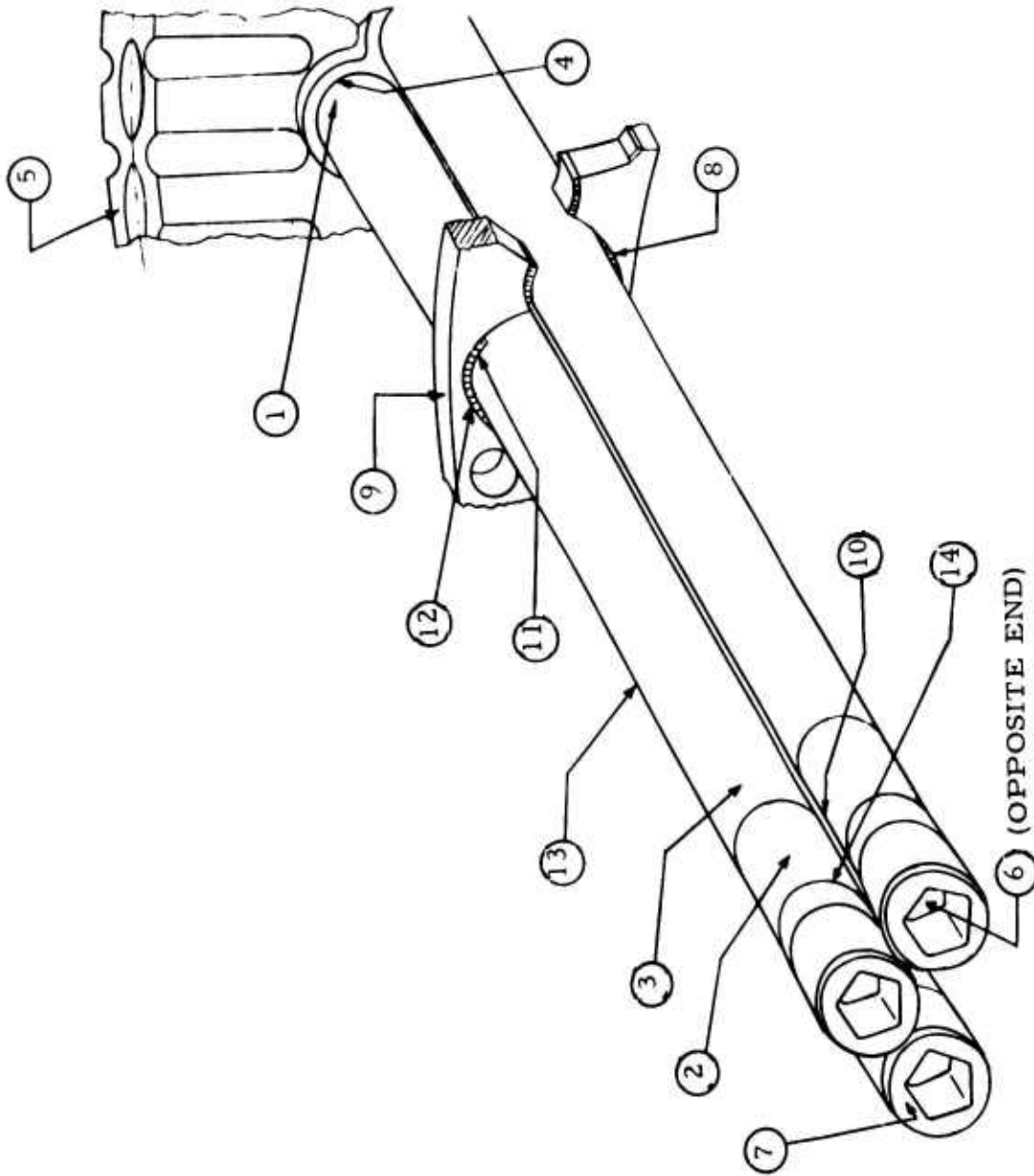


FIGURE 3-16 MMA Stress Analysis Locations

Two other areas showed safety factors below the required levels. These were the adhesive bonds between the carbon phenolic mounting ring spacers and the motor cases and the bonds between the carbon phenolic intertube spacers and the motor cases. The tendency of the motor case to grow axially and circumferentially caused relatively high shear stresses in both areas. However, subsequent thickening of the motor case caused a reduction of the equipment ring web thickness which was compensated for by an increase in ring (and spacer) width. The increased bond surface area caused the bond stress levels between tubes and ring spacers to be diminished to acceptable levels. The high stress levels in the bonds between the motor case and intertube spacers were likewise reduced to acceptable levels by changing to the dual spacer design.

A region near the inner surface of the aluminum end plug showed local yielding due to pressurization. Because this condition was a surface bending stress which did not extend significantly into the plug, it was judged that no appreciable permanent deformation of the plug would occur and was therefore acceptable.

3.5.5.3 Dynamic Analysis

The initial STARDYNE analysis was conducted on three versions of the MMA model. In the first version, the MMA model was analyzed by itself. In the second, the analysis included the effect of the VSD - supplied MMFC bonded to the igniter ends of the motor cases. The third version included the MMFC bonded not only at the igniters but also at four places at the end of the board. For the computer analysis, the shell-flange of the MMFC was idealized as triangular plate elements connected at the outer motor tube row at every other igniter.

Free-free beam frequencies were determined for each model version. The model without a MMFC yielded a nominal frequency of 1843 cps. In the model with the MMFC bonded only at the end, the frequency

was determined to be 1710 cps. For the model with the additional bond, the frequency value was 1622 cps. Independent calculations by VSD gave values of 1164 cps without the MMFC and 1710 cps with the MMFC included. Although the same Et and Gt values were used by both companies, the hoop stiffness of the tube bundle was calculated to be higher by ARC's discrete finite element method versus the four coupon approach employed by VSD. This contributed to the higher values calculated by ARC. Although inclusion of the MMFC lowered the ARC values and raised the VSD values, agreement was reached that the frequency of the total structure was in the order of 1710 cps.

The design goal of the MMA program was to achieve a free-free beam frequency of 2800 cps. The only effective way to increase the frequency was to increase the equivalent Gt value of the structure. The Gt value in turn was a function of the tube spacer design and the rigidity of the tube wall. A dual spacer design was therefore designed and incorporated. Additional improvement in frequency, although of lesser degree, was expected from thickening the motor case wall. These changes produced a final calculated free-free beam frequency value of 2260 cps. The 2260 cps value was subsequently demonstrated to be adequate based on structural tests of the Target Sensor and the MMA Structural Model.

3.5.5.4 Structural Effect of Pressure Oscillations

High frequency pressure oscillations were first measured during single motor fire tests in October of 1972. The phenomenon was evident in pressure-time histories for the majority of fire tests conducted thereafter, but with varying degrees of severity. VSD undertook an analytical program to evaluate the phenomenon and determine if corrective action was required.

A severe example of pressure oscillations is illustrated in Figure 3-17. Oscillation frequencies were estimated from the graphical data to range from 4000 to 12000 cps. Since the pressure rates greatly exceed reasonable changes in propellant burn rate, the origin is associated

FREQUENCIES OBSERVED (CPS): 4000 7330 12230 14630 14890

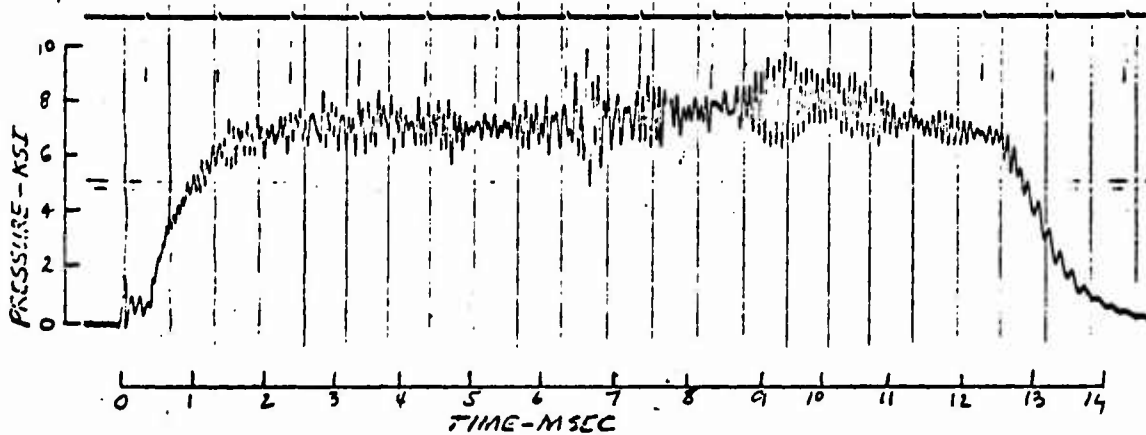


FIGURE 3-17 Pressure vs Time-Firing No. 39900

with gas dynamics rather than combustion instability. Several possible gas flow disturbances were introduced during the October period in the form of minor design changes to protect the grain ends. These changes were necessary to reduce stress levels in the propellant-to-case adhesive bonds and to improve thermal protection of the titanium motor cases. A chronological review of design changes and the test data was made in an attempt to pinpoint the cause. The results of this review were inconclusive unless additional fire tests could be made which re-introduced the changes in singular order. It was evident that such a program entailed a lengthy schedule of diagnostic trials. Further, if the cause could be pinpointed, there was no assurance of correction without compromising demonstrated benefits derived from the design changes. Therefore, it became necessary to take a hard look at living with the oscillation phenomenon. Preliminary analyses had indicated that oscillation pressures could degrade structural reliability. However, it was recognized that these analyses contained conservative assumptions to bridge incomplete statistics

on pressure oscillations. The purpose of this study was to develop better information on oscillating loads, to evaluate structural dynamic response, to predict induced stress levels for the MMA, and to evaluate possibility of low cycle fatigue failure. The tests of section 3.3.4.2 provided statistical data for input to this study.

This study indicates significant stress levels will be produced by the pressure oscillations but all stress levels are within acceptable limits. Analysis of possible failure due to fatigue indicated a maximum of 21% of the expected fatigue life will be expended on pressure oscillations.

3.6 HIT STRUCTURAL MODEL ANALYSIS AND TEST

As part of a VSD development of methodology for predicting shock induced timing error of the HIT target sensor, an analytical structural model of the HIT was developed. This model included a model of the MMA. Also, a HIT structural model was assembled using the structural model MMA supplied by ARC, along with a structural model target sensor and dummy subsystems representing the other elements. This model was tested at VSD. The analytical and structural models are described in the following paragraphs along with test results. Figure 3 - 18 shows the relative orientation of the HIT Structural Model subsystems.

3.6.1 HIT Structural Model Analysis

The complex geometry of the HIT subsystems and the highly redundant load paths which exist in the integrated vehicle dictated the use of finite element techniques to generate the analytical models of the structures. Each of the subsystems was represented analytically by a stiffness matrix and a mass matrix. The repertoire of basic elements used to generate the matrices included beam, rod, and isotropic and orthotropic shear and bending plates, both triangular and quadrilateral. Stiffness and mass matrices were generally consistent in that the displacement field used to define stiffness coefficients was also used to define the velocity field in the evaluation of kinetic energy to obtain collocated masses. However, point masses were used where small concentrated masses occurred in the structure. The effective sizes of the matrices were commensurate with the complexity and structural function of the particular subsystem. The generation of these matrices was accomplished with a VSD developed finite element structural analysis routine STRAF. Supporting matrix algebra, eigen frequency/eigen function computations and transient response computations were accomplished with a VSD developed software package PASS. STRAF is included in this package. Computations were executed via a remote terminal to the Huntsville ARC CDC 7600 digital computer. NASTRAN was also used but to a much lesser extent, on an IBM 370 computer.

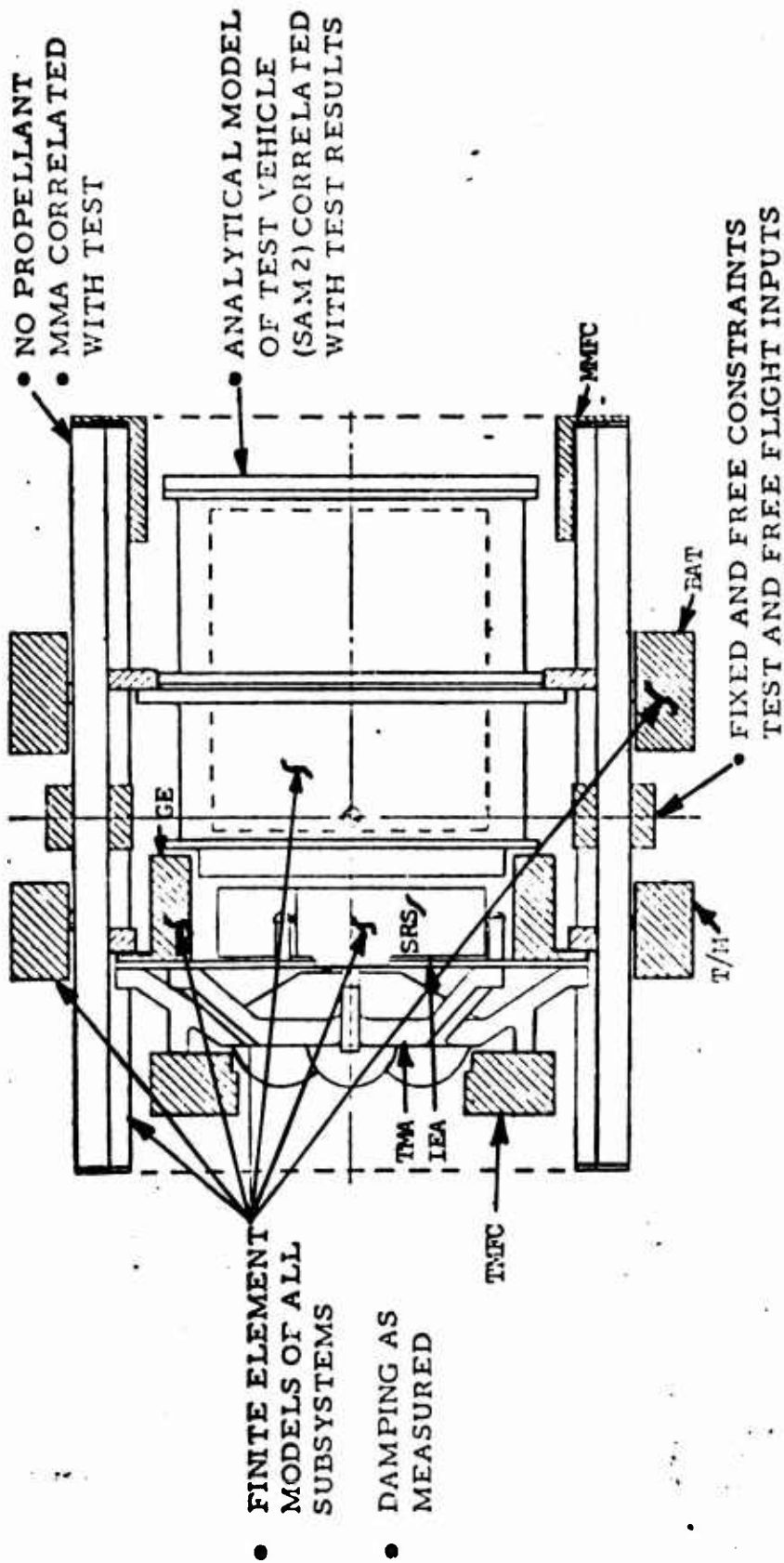


FIGURE 3-18 HIT Structural Model

Because of the axisymmetry of HIT, half models were used in conjunction with symmetry constraints in a plane containing the vehicle axis. In essence, this allows more structural detail to be accounted for within the routine/computer size limitations. As the analytical model of each structural subsystem was generated, the matrices were retained on a computer file to be recalled as they were required either to form a larger subassembly or for determining structural dynamic parameters of a particular subsystem such as the target sensor.

To evaluate the accuracy of the analytical models, analysis and test correlations were performed in the following buildup:

- (a) Natural frequencies and mode shapes for the empty MMA as constrained at a single point on the nozzle ring.
- (b) Natural frequencies and mode shapes of the target sensor structural model for the sensor constrained at the interface ring and tabs in a rigid fixture. Both transverse and axial motions are considered.
- (c) Transient response of the target sensor resulting from a transverse acceleration input with the structure constrained as in (b).
- (d) Natural frequencies and mode shapes of the HIT structural model constrained at a single point on the nozzle ring.
- (e) Transient response of the HIT structural model when shocked transversely by a laboratory generated pulse.

A study was made to determine if synergistic effects of significance would occur as a consequence of the spin of the vehicle coupling with transient elastic motions. Because of the wide separation of the structural frequencies from the spin frequency, the effects were determined to be negligible and are not considered in these analyses.

The MMA analytical model was generated following a procedure that had proven successful for an earlier Vibration Validation Model (VVM)

program. Each motor tube in the MMA structural model is a titanium cylinder overwrapped with carbon filament. Tubes are joined together in a stagger pattern by an epoxy bonded carbon phenolic strip. A finite element analytical model of an array coupon was first generated in which geometries and materials were faithfully accounted for. The coupon consisted of four tubes across its width and was of an equal length. NASTRAN was used to generate the structural representation which contained 1800 degrees of freedom. Edge loads were analytically applied to this model to determine stiffnesses which were then assigned to an orthotropic plate element. The MMA was subsequently modeled with the orthotropic plate elements equivalent to the joined tubes and structural rings were modeled with beam elements. The VVM program also served to show that a good model of the nozzle ring by analysis alone was difficult to achieve. However, by using measured ring stiffness from a static test, the analytical model could be satisfactorily modified. This was done in the case of the structural model nozzle ring.

A vibration survey of the MMA structure was made to obtain data for comparison with mode shapes and frequencies predicted by analysis. The particular configuration corresponded to a constraint at the nozzle ring in the plane of symmetry. The correlation of results was quite good and is indicated below.

Frequencies (Hz)		Comments
Analysis	Measured	
553	525	Mode shapes correlate
569	600	
1133	940	Detail interpretation of test data not possible
1181	1050	
1338	1200	

3.6.2 HIT Structural Model Test

As a first step in determining that accuracies achieved at a sub-system level would persist upon assembly into the integrated system, comparisons were made between vehicle measured and calculated mode shapes and frequencies. Excitation was input to the structural model through a sting clamped in a nozzle port. The analytical model was correspondingly clamped at a single point of the nozzle ring at the plane of symmetry. Excellent correlation of analytical to measured vibration modes was obtained.

The shock test of the HIT structural model had two objectives:

- (a) To provide data about the elastic motions of the subsystems when the structure was shocked in an essentially free condition.
- (b) To demonstrate the structural integrity of the vehicle when shocked by a pulse which had a damage potential close to, but not less than, an MMA pulse.

Shocks of 100 "g" nominal level were applied by a pneumatic ram at a nozzle port with the structural model free to respond as a pendulum, Figure 3-19. The pulse shape used was a consequence of the constraints implicit in these objectives. This force function was applied to the analytical model and accelerations and displacements were calculated at stations throughout the vehicle for a period of time of 10 msec past the end of the pulse. The acceleration levels predicted were compared with measured values to determine analytical accuracy.

In the range of values that are judged to be significant, relative to Target Sensor timing error, calculated frequencies were within 5% of measured values at the Target Sensor. Vehicle structural model frequencies calculated were within 10% of measured values. Mode shape agreement was excellent.

A total of 56 shock pulses were applied to the structural model HIT, each at least as severe as the motor fire pulse. No structural failures were induced in the structural model MMA and no evidence of incipient failures could be detected (i. e., cracked bond lines, etc).

A detailed report of the structural model test results is presented in VSD report 3-371-TIR-E-30054 dated 14 September 1973.

The conclusion was that the Structural Model MMA was structurally adequate and sufficiently stiff for the HIT application. Subsequent MMA development activity resulted in increasing motor wall thickness, improving intertube bonding, and increasing the nozzle ring O.D. All three changes increased the natural frequency and the structural integrity of the MMA thereby providing additional margin over the Structural Model results.

3.7 PROCESSING AND ASSEMBLY

MMA process and assembly operations are depicted in Figure 3-20 and described in the following paragraphs. These operations were developed and used to fabricate the Structural Model and Prototype MMA's.

3.7.1 Component Part Manufacture

ARC subcontracts the manufacture of most of the MMA inert components. A list of component parts and Manufacturers utilized during the MMA Development Program is shown in Table 3-XX.

3.7.2 Motor Case Preparation

The first processing step performed by ARC is preparation of the motor cases for casting. Insulators are bonded into the nozzle ring end of the tubes using EPON 917 adhesive. After adhesive cure, the internal surfaces of the tube and insulator are dry-honed to a 22-32 microinch finish and cleaned with MEK.

3.7.3 Propellant/Grain Manufacture

The propellant used in the MMA is an NF type, ARCEF 143B. The polymer used in ARCEF 143B is produced at ARC by the reaction of benzoyl peroxide, ethyl acrylate and acrylic acid. The TVOPA, an energetic plasticizer, is stored as a solution desensitized with an inert solvent. The solvent is removed when the TVOPA solvent and polymer are mixed and heated in a vacuum to form the binder. ARCEF 143B contains ultrafine ammonium perchlorate (AP) as the oxidizer. This material is obtained using a fluid energy mill which reduces stock 200-micron AP to 6.5 - 7.1 microns. The binder, AP, carbon black, and curative is mixed in a small Baker-Perkins vertical mixer to form the propellant slurry.

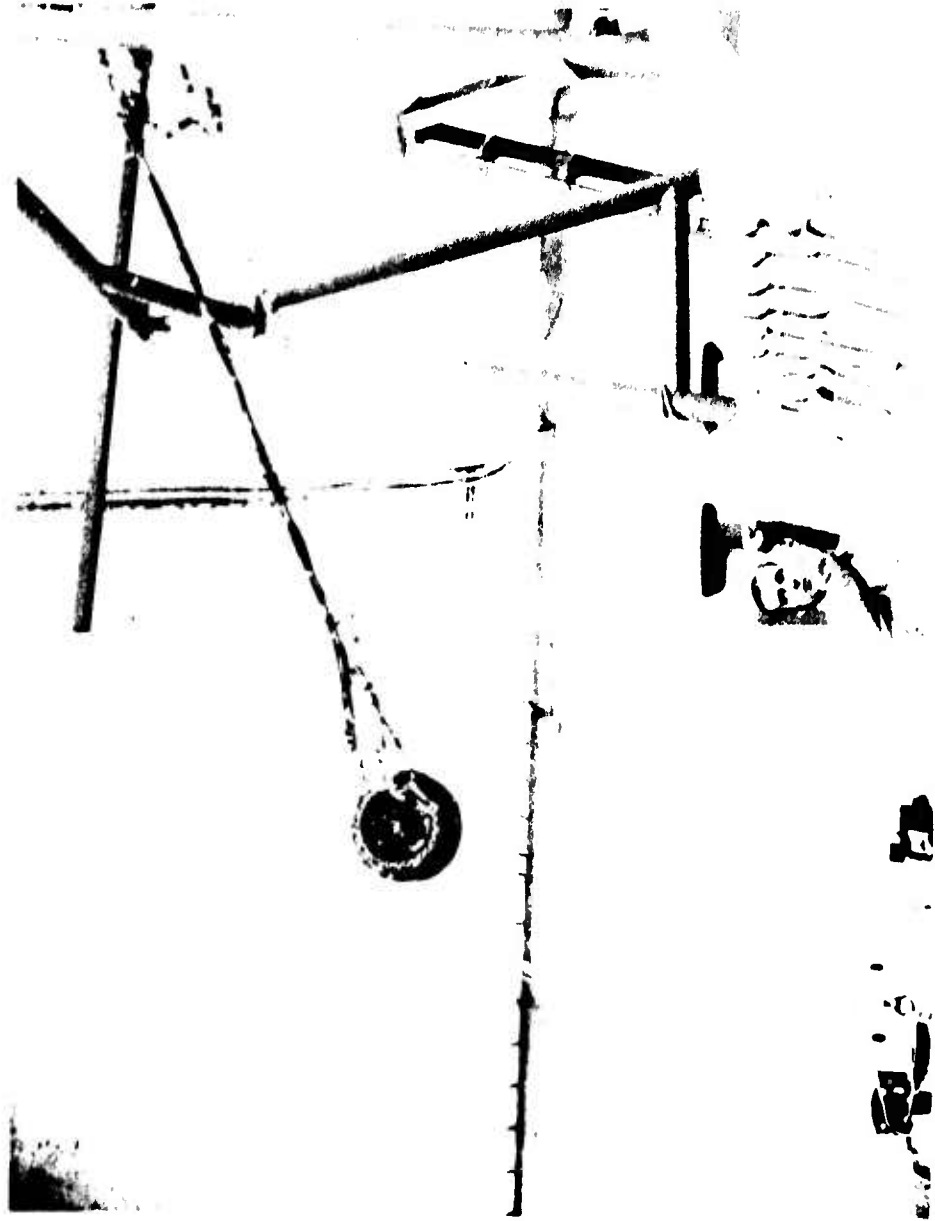


FIGURE 3-19 Typical Structural Model Shock Test

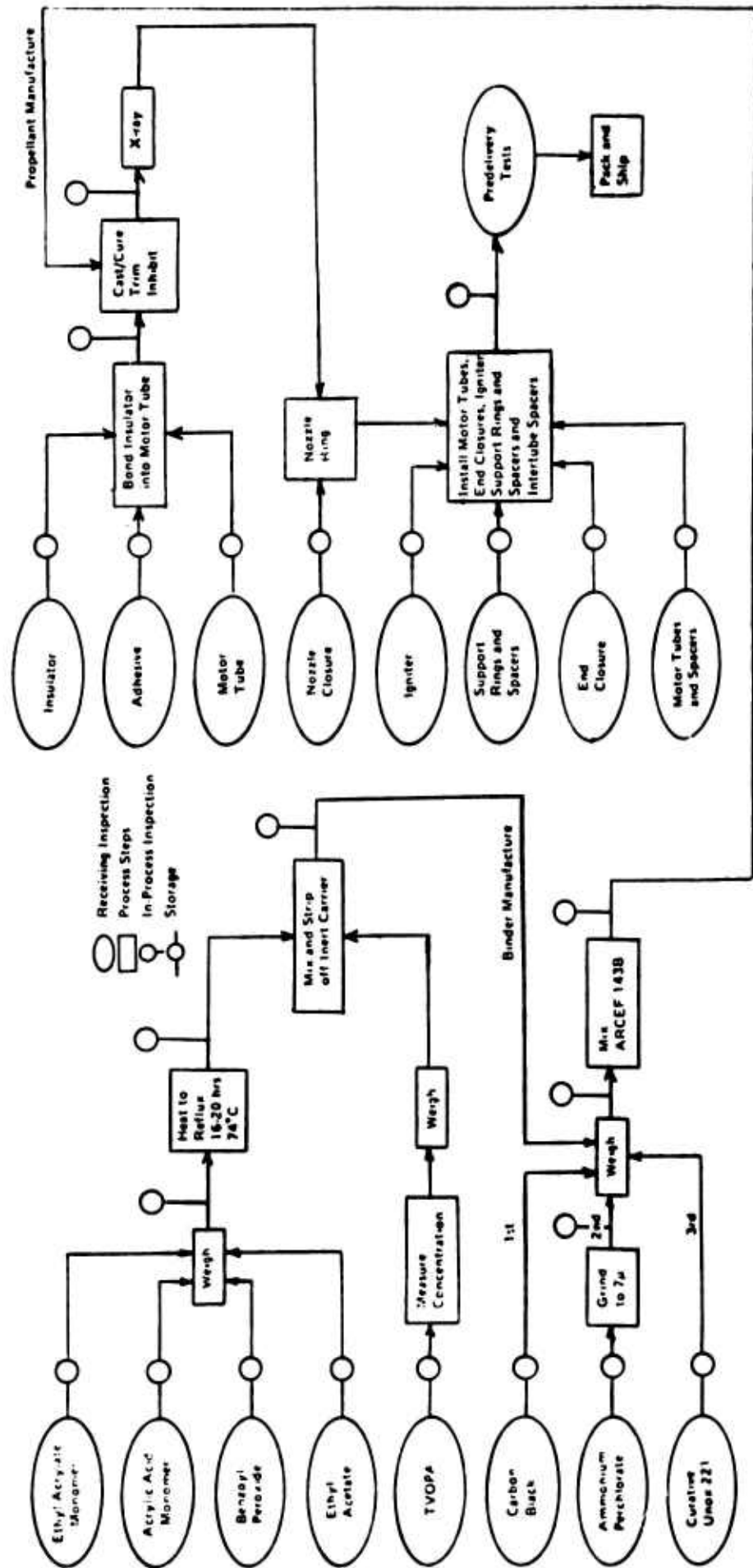


FIGURE 3-20 MMA Processing and Assembly Flow Chart

TABLE 3-XX

MMA COMPONENT PARTS

COMPONENT	MANUFACTURER
Nozzle Ring	American Beryllium Corp., Sarasota, Florida Pioneer-Astro Industries, Chicago, Illinois Winslow, Div. of G.E., Cleveland, Ohio
Titanium Motor Case	Thermo Electron, Inc., Boston Massachusetts Middlestadt Machine Co., Baltimore, Maryland
Case Overwrap	U. S. Polymeric, Inc., Santa Anna, California
Overwrap Machining	Middlestadt Machine Co., Baltimore, Maryland
End Plug	Thermo Electron, Inc., Boston, Massachusetts
Igniter	Space Ordnance Systems, Inc., Sunnyvale, Calif.
Intertube Spacers	Haveg Industries, Santa Fe Springs, California ARC
Ring Spacers	ARC
Support Rings	American Beryllium Corp., Sarasota, Florida
Nozzle Closure	Universal Plastics, Rockville, Maryland
Insulator	Rayloid, Inc., Riestertown, Maryland ARC

To cast, each tube is filled from the bottom until it is about half full of propellant. This propellant is very fluid and has a pot life in excess of 16 hours at the mixing and casting temperature of 135°F. Once the tubes have been filled to the prescribed height and plugged on the bottom, a mandrel is plunged into the propellant from the top. The propellant rises as the mandrel is installed, forming the propellant grain. The tubes are then cured for 5 days at 135°F. When cure is complete, the casting tooling is removed and a 100% radiographic inspection performed to ensure acceptable grain quality.

3.7.4 Assembly

Assembly of the MMA begins with the bonding of the carbon phenolic spacers to the beryllium mounting support rings. These spacers are positioned and bonded to the rings with EA-943 adhesive. A bonding and alignment fixture clamps the spacers to the rings to ensure intimate contact between spacer, ring and adhesive.

Next, the 56 nylon nozzle closures are bonded into the nozzle ring with EP-12 adhesive. The seals are checked for leakage by pressuring each seal to 10 psi for one minute minimum.

3.7.4.1 Nozzle Ring - Motor Assembly

The nozzle ring is clamped into the spin balance fixture. The aft motor tubes are placed upright, plug end down, into two end support rings with holes that locate the tubes in the same position they will have when attached to the array. The inner and outer aft mounting ring assemblies are then placed over the tubes from the nozzle end. The spin balance fixture, containing the nozzle ring, is placed on top of the tubes and the case threads are barely started into the nozzle ring. The forward tubes are placed upright, igniter end down, in the other end support ring and the forward mounting rings are placed over the tubes. The spin balance fixture

with nozzle ring and forward tubes is then placed over the aft tubes, and the aft tube threads are started as before. The entire assembly is rotated to the horizontal position and supported by V-blocks under the spin balance fixture arms. Loctite HV adhesive is applied to the threads at the nozzle, to the internal threads of the igniter end of the motor tube, and to the igniter threads. A-2 adhesive is applied to the end plug threads and to the thread relief of the internal plug end motor tube threads. The motor tubes are threaded into the nozzle ring and the end plugs and igniters are threaded into the tube ends. The tubes, plugs and igniters are then torqued to 35-45 in/lbs.

3.7.4.2 Spacer and Mounting Ring Assembly

The outer spacers are applied first and the inner spacers second. The mounting rings are slid toward the nozzle and a thin coating of EA-943 adhesive is applied to the spacer and tube bonding surfaces. The spacers are installed 0.62 to 0.68 inch from the nozzle and adhesive is blended over the radius between the tube and spacer. A bonding fixture is used to install the mounting rings. EA-943 is applied to the rings and the tube bonding surface. The rings are positioned with the bonding fixture and clamped in place.

3.7.4.3 Inspection

After curing the bonds, the assembly is inspected for the following:

- (a) Location and concentricity of mounting rings and tubes with respect to the nozzle ring.
- (b) Location of inner tube spacers.
- (c) Location of scribe lines and mounting holes.
- (d) Overall length.
- (e) Identification.
- (f) Igniter resistance.
- (g) Bond joint integrity (under magnification)

3.8 DESIGN EVOLUTION SUMMARY

During the course of the MMA development program, the components of the array underwent varying degrees of change. This section describes the chronological design evolution of each of the MMA components.

3.8.1 Nozzle Ring

The first major change to the nozzle ring occurred after the adjacent tube interaction tests in late August 1972, when a motor failed at the nozzle-motor case joint. To prevent erosion of the thin nozzle throat section during motor operation, ARC concluded by analysis that the minimum thickness of the nozzle land should be increased by 15 mils from 0.0145 to 0.0295 inch. This change was effected by reducing thread depths (for motor case attachment) from 0.180 - 0.185 in. to 0.165-0.170 in.

Observation of the plume impingement from the motor during the ATI tests resulted in a second change of more considerable magnitude. In October 1972, LTV directed that ARC increase the nominal length of the inner and outer nozzles by 0.6 inch. This change was required to prevent plume impingement on external HIT subsystems.

During assembly of the structural model, the nozzle ring was cleaned with MEK solvent. Subsequent examination of this ring (coated with black oxide) showed significant corrosion. An investigation of several alternative coatings led to the selection of electroless nickel as a replacement. To verify this choice, samples of 4130 normalized steel were coated with electroless nickel at a thickness of less than 0.0001 inch, bathed in tap water, and subjected to an ambient atmosphere for two weeks. Only minor corrosion was noted. For added protection, a nominal thickness of 0.0002 inch of electroless nickel was specified for the nozzle ring. It should be noted that a very thin coating was dictated in order to prevent any significant effect on dimensional and mass properties of the array. Otherwise, corrosion resistance could have been easily achieved by utilizing a relatively thick plating.

3.8.2 Motor Case

The first change to the motor case design involved local thickening of the titanium near the case ends to prevent burn throughs. A discussion of the relevant analysis is given in section 3.5.3. In light of the analysis, the motor cases were locally thickened near the igniter and plug ends by 6 mils.

At the same time, the internal thread diameter at the igniter and plug ends was increased so that the threads no longer protruded into the inside diameter of the case. This change was made to facilitate manufacture and therefore reduce costs at a slight increase in weight. Also, the motor case inside diameter was reduced from a nominal of 0.373 inch to 0.362 inch. This change was based on initial mass properties/ ΔV analysis. Finally, the inner row motor tubes were lengthened equal to outer row motor lengths to provide commonality.

The next changes to the motor case design were incorporated after the thrust alignment and ATI motor failures discussed in section 3.3.1. Because it appeared that the case design was marginal, VSD increased the safety factors on the motor case from 1.1 to 1.2 on yield tensile strength, and from 1.21 to 1.32 on ultimate tensile strength. These safety factors were achieved by increasing the nominal wall thickness of the heat treated titanium alloy case from 0.008 to 0.010 inch, and by increasing the nominal overwrap thickness from 0.010 to 0.014 inch.

As a consequence of thickening the nozzle ring land to prevent erosion, the external motor case threads were shortened from 0.185 - 0.180 to 0.170 to 0.165 inch. Because of the large margin of safety in thread length and the use of thread sealant, this minor decrease did not produce any loss of integrity.

One other change of significance was incorporated into the MMA motor case design. Originally, the epoxy impregnated graphite overwrap was applied directly to the bare case. When it was discovered that some of the wraps rotated on the case, VSD and ARC conducted a joint test program to evaluate the use of a nitrile phenolic primer, Narmco 2021-10, prior to overwrapping the case. These tests are discussed in section 3.4.2. As a

result, a requirement to double prime the case with Narmco 2021-10 was incorporated into the design.

3.8.3 Igniter

Under the igniter development effort described in Section 3.2 of this report, one of the first tasks was to design a lightweight igniter body that would serve as an end closure for the motor, house the glass to metal header, and provide a lip to attach the roll-crimped charge can. While the igniter bodies were being fabricated, testing to verify the pyrotechnic aspects of the design was initiated with development version of the igniter body. For the tests, ARC specified that main charge weight should be 100 milligrams, the bridgewire charge should be 10 milligrams, and that the packing density of the main charge should be 0.7 gm/cc. In addition to these features, the initial design as tested included an 1100 aluminum charge can.

Unsatisfactory test results led to the following changes: (1) the bridgewire charge was increased first to 15 and then 18 milligrams; (2) the main charge was reduced to 92 milligrams; (3) the 1100 aluminum charge can was changed to 7075 aluminum and lengthened from 0.315 to 0.344 inch nominal.

Twenty igniters with flightweight igniter bodies and the above changes were subjected to qualification testing. In the bomb tests, some of the units failed to fire and other units exhibited long functioning times.

The following design changes were incorporated to eliminate these problems: (1) the ends of the Kovar lead pins were gold plated to enhance welding of the bridge wire; (2) the star crimp was improved to create a tighter seal; (3) the crimp lips were closed by dip soldering; (4) the can material was changed to gilding metal, and (5) adhesive was applied to the roll crimp joint. The design was subsequently requalified and further proven in the flight weight motor tests and the full array firing.

3.8.4 End Plug

As discussed in section 3.3.2.7 of this report, it was discovered that the titanium alloy end plug used to monitor pressure during motor static

firings caused the motor case threads to overheat, leak, and sometimes fail. Although the flight weight aluminum end plug has a lower temperature-time profile, changes were made to ensure that the seal is maintained between the end plug and the motor case threads. A small bead of A-2 adhesive is applied to the motor case at the internal thread relief. The threads of the end plug are also coated with A-2 adhesive before installation. To retain the A-2 adhesive bead against the case during cure, the internal side of the end plug was extended past the threads to form a supporting platform.

3.8.5 Support Rings and Spacers

The MMA structure is supported by four beryllium rings which provide attachment points for the HIT subsystems. Two different carbon phenolic spacers are bonded to the internal radii of the rings with EA-943 adhesive to minimize strain incompatibility between the motor tubes and rings. The only major change to the support rings and spacers occurred when the motor case wall thickness was increased as a result of the thrust alignment and ATI test failures early in the development program. To compensate for the reduced ring web thickness caused by the larger diameter of the case, the ring (and spacer) width was increased from 0.25 to 0.35 inch.

3.8.6 Intertube Spacers

Longitudinal carbon phenolic spacers are bonded between the motor cases to stiffen the MMA. The spacers are molded to fit the tube O.D. contour. Originally, the spacer was a one-piece design which was installed from the O.D. of the MMA. A dual spacer was subsequently designed and incorporated wherein segments were installed both from the OD and ID of the MMA. This was done to: (1) increase the free-free beam and ring mode natural frequencies; (2) lower adhesive shear stresses, and (3) facilitate improved bonding and assembly.

3.8.7 Insulator

Initially, the insulator was fabricated from carbon phenolic. One of the corrective actions resulting from the ATI test failure (see section

3.3.1.3) was to change the insulator to 4130 steel because of cracking caused by adjacent motor operation. At this point, the insulator was 0.171 inch in nominal length as was the carbon phenolic insulator.

During subsequent failure diagnosis tests, it was observed that despite improvement with the change in material, motor case burn through sometimes occurred ahead of the insulator. The insulator was subsequently lengthened to 0.432 inch nominal which eliminated the burn through problem.

3.8.8 Nozzle Seal

In the early development tests, the nozzle closure was a thin cylinder of mylar, 0.005-0.008-inch thick. As a result of the failure diagnosis tests, it was determined that the igniter pressure shock wave tended to erode the grain and break the propellant to motor case bond at the nozzle end of the aft motor. A tapered section was added to protect this grain end. The material was changed to nylon at this time since the tapered cylinder could not be fabricated from mylar.

3.8.9 Propellant Grain

The PDR flight weight design demonstration motors were characterized by cylindrical propellant grains cast into and bonded directly to the case. The ends of the grains at the igniter and end plug were tapered at a 30° angle.

During the initial development tests, the same grain configuration as above was employed except that a cellulose nitrate liner was applied to the dry-honed motor case prior to casting and only the igniter end of the grain was tapered.

As a result of the ATI motor failure investigation and the subsequent failure diagnosis tests, the cellulose nitrate liner was deleted, the grains were cast directly against and bonded directly to the dry-honed case, and all ends were tapered at a 30° angle to the bore.

4.0 CONCLUSIONS AND RECOMMENDATIONS

A summary of the more critical MMA design requirements, with the corresponding values demonstrated or projected for the prototype design, is given in Table 4-1. It is seen that the prototype MMA meets all ballistic requirements of the VSD specification. It does not meet all specified requirements in the areas of structure, mass properties, and thermal characteristics. The non compliance areas are discussed below:

Structure

FFB Frequency - Although lower than the specification requirement, the actual 2260 cps value has been subsequently shown to be adequate for the HIT system by VSD tests and analyses and will be reflected in future specifications.

Mass Properties

- (a) Total Weight - The actual weight of 6.779 pounds exceeds the 4.8 pounds maximum specification value, due mainly to the lengthened nozzle exit cones and thickened motor tubes required to resolve development problems. This added weight is not detrimental to the terminal HIT performance since the minimum ΔV requirement was achieved.
- (b) MOI Ratios - The design nominal consumables MOI ratios of 1.101 (Outer Row) and 1.205 (Inner row) are slightly higher than the allowable specification requirements. VSD has ascertained by analysis that these values are acceptable.
- (c) Consumables c.g. Location - The measured c.g. location for the prototype array was .0007 inch in the longitudinal direction. Dimensional analysis indicates that $\pm .003$ inch is the achievable tolerance. VSD analysis indicates that this range is acceptable.

TABLE 4-1
MMA DESIGN REQUIREMENTS COMPLIANCE SUMMARY

PARAMETER	REQUIREMENTS (TARGET)	ACTUAL
<u>BALLISTIC</u>		
Total ΔV , ft/sec	970 min	998 (-3 σ)
Action Time, msec	15.0 max	14.68 (+3 σ)
Impulse Centroid Repeatability, msec	± 1.25 max	± 1.14 (3 σ)
Total Impulse Repeatability, %	± 5 max	± 1.97 (3 σ)
Peak Thrust, lbs	1330 max	925 (+3 σ)
Peak Pressure, psi	10,000 max	9,527 (+3 σ)
Thrust Misalignment, Degrees	± 0.25 max	± 0.18 (3 σ)
<u>STRUCTURAL</u>		
Array FFB Frequency, cps	2800 min	2260
<u>MASS PROPERTIES</u>		
Total Weight, lbs	4.80 max	6.779 (+3 σ)
Nominal Consumables MOI Ratio		
Outer Row	1.05-1.07	1.101
Inner Row	1.15-1.17	1.205
Repeatability of Consumables MOI Ratio	± 0.01 max	± 0.01 max
Single Motor Consumables POI, lb-in-sec ²	22×10^{-7} max (1 σ)	22×10^{-7}
Repeatability of Consumables cg location	± 0.001 max	$\pm .003$ max
<u>THERMAL</u>		
Motor Case External Temp, ^o F	200 max	370 max

Thermal

Motor Case External Temperature - As indicated in section 3.5.3, motor case external temperature exceeds the 200°F maximum requirement near the nozzle ring and at the igniter end. The tube OD remains under 200°F for the majority of its length. These locally "hot" areas are not expected to be detrimental to HIT performance in any way.

Note that all of the above specification deviations are acceptable as-is for the IST HIT and for possible application to a Phase III exoatmospheric HIT.

4.1 CONCLUSIONS

Dramatic proof of the structural integrity and reliability of the prototype MMA design was demonstrated by the final 112 sequentially successful motor firings conducted during the development program.

The measured c.g., POI, and MOI of the prototype MMA consumables were in good agreement with the specified and design values. The dimensional tolerances and assembly techniques were adequate in achieving the mass properties controls. No additional mass properties measurements, except individual component weights, are required on subsequent MMA assemblies.

All ballistic performance requirements are achieved by the prototype MMA design, as demonstrated by the final 112 motors fired during the development program.

Finally, all mechanical and electrical interface requirements have been achieved by the prototype MMA design, and verified by fit and functional checks with other HIT subsystems.

Based on these accomplishments, it is concluded that the MMA development has been successfully completed and that the existing prototype MMA design is suitable for use in HIT Integrated Systems Tests.

Use of the current MMA design during the Phase III exoatmospheric flight-test program will require performance certification at the

anticipated temperature extremes (50^o - 90^oF) and vacuum testing to determine the extent of plume impingement on the array and other sub-systems.

4.2 FUTURE ACTIVITY

During the MMA development program a number of procedures were evolved which will be incorporated in future MMA production. Also, the MMA test fire control was not sufficiently reliable. The planned activities to implement these procedures and improve the test fire control system is detailed below:

- (a) Burst tests will be included during the ARC nozzle closure acceptance tests.
- (b) ARC acceptance tests of interface spacers will include validation of material physical properties.
- (c) MMA igniter leads will be twisted and soldered after the MMFC is installed on the MMA and will remain in this "safe" condition until the leads must be diked off for system level tests.
- (d) ARC will implement a procedure to selectively locate igniter and plug-end tubes within the array to assure that specified mass properties are achieved. The propellant weight data is the basis for achieving this control. Array measurements of CG, POI, and MOI are not planned or required.
- (e) VSD will verify the integrity of the Protective Torodial Plenum (PTP) handling device by firing live motors in the device without firing other nearby live motors.
- (f) A detailed inspection and quality verification plan will be prepared and implemented during MMA materials and parts procurement, subassembly processing, and array assembly and inspection.

- (g) The ARC Fire Control System will be redesigned to incorporate a solid state switching device in place of the mechanical stepper switch used in prototype MMA tests, to minimize the possibility of inadvertently firing the wrong motor.

4.3 RECOMMENDATIONS

It is recommended that the prototype MMA design developed and validated as reported herein be employed for the Integrated Systems Test.

5.0 BIBLIOGRAPHY

5.1 VSD DOCUMENTS

- (a) VSD Control Drawing for the Maneuver Motor Array, 371B000010, Rev. M.
- (b) Procurement Specification for the Maneuver Motor Array, 3-371-04-O-10185, Rev. D.
- (c) Statement of Requirements for the Maneuver Motor Array, 3-371-13-O-10186, Rev. D.
- (d) PDR Report 3-371-3R-Y-20023

5.2 ARC DRAWINGS

- (a) A0070074 MMA Top Drawing
- (b) A0070077 Nozzle Ring
- (c) A0070047 Motor Case (bare titanium)
- (d) A0070048 Motor Case, Filament Wrapped
- (e) A0070072 Motor Case, Insulated
- (f) A0070049 Motor Case, Loaded
- (g) A0070118 End Plug
- (h) A0070051 Insulation (motor tube insulator)
- (i) A0070052 Igniter Assembly
- (j) A0070075 Spacer, Tube (spacer between tubes)
- (k) A0070166 Spacer, Tube (spacer between tubes)
- (l) A0070054 Package Drawing
- (m) A0070055 Nozzle Seal
- (n) A0070056 Structural Model (top assembly)
- (o) A0070067 Mounting Rings, Aft (bare beryllium ring)
- (p) A0070068 Mounting Ring Aft Assembly (ring with ring/tube spacers bonded on)
- (q) A0070069 Mounting Rings, Forward (bare beryllium ring)

- (r) A0070070 Mounting Ring Forward Assembly (ring with ring/tube spacers bonded on)
- (s) A0070071 Insulation, Spacer (spacer used between rings and tubes)

5.3

ARC SPECIFICATIONS

- (a) SP10066 Propellant, ARCEF 143B
- (b) PP50010 Filament Winding Procedure, HIT Rocket Motor Case
- (c) PP50011 Specification for Heat Treatment of Titanium and Titanium Alloys
- (d) PP50012 Dry Blasting of HIT Insulated Motor Case
- (e) SP10062 Igniter Assembly, Smokeless, 30 milli-amperes, No-Fire

5.4

ARC REPORTS AND RELATED DOCUMENTS

- (a) Progress Reports Nos 1-11
- (b) Structural Analysis Report
- (c) System Description and Performance Report, July 1972.
- (d) Updated System Description and Performance Report, TR-PL-10153
- (e) Thermal Analysis Report
- (f) Mass Properties Report
- (g) Reliability Analysis Report
- (h) Hazard Analysis Report
- (i) Failure Mode and Effect Analysis Report
- (j) Development Plan
- (k) Propellant Bond Aging Report (to be submitted)
- (l) Static Measurement of Thrust Vector Misalignment in an Individual Motor from the MMA, TR-PL-10135.
- (m) Test Plan for Static Interaction Test of MMA Segment, TS-0155.
- (n) Test Plan for Shock and Vibration Testing of the MMA Motor, TS-0171A.

- (o) Test Plan for Functional Test of MMA Suspended from a Pendulum, TS-0183.
- (p) Test Plan for Functional Spin Test of MMA, TS-0184.
- (q) Test Plan for Functional Static Test of Individual MMA Motors, TS-0185.
- (r) MMA Functional Test Report, TR-PL-10152.
- (s) MMA Development Final Report, TR-PL-10147.

LIST OF APPENDICES

1. Propellant Characterization Motor Test Data
2. Typical Traces
3. Thrust Alignment Test Plan
4. Array Pendulum Test Plan
5. Array Spin Test Plan
6. Array Static Test Plan
7. Key Personnel
8. DD Form 1473

APPENDIX 1

PROPELLANT CHARACTERIZATION
MOTOR TEST DATA

Contained herein are detailed ballistic data and typical pressure and thrust/time traces derived during the propellant characterization testing, discussed in section 3.1.1 of this report.

L. 1 V-HIT.

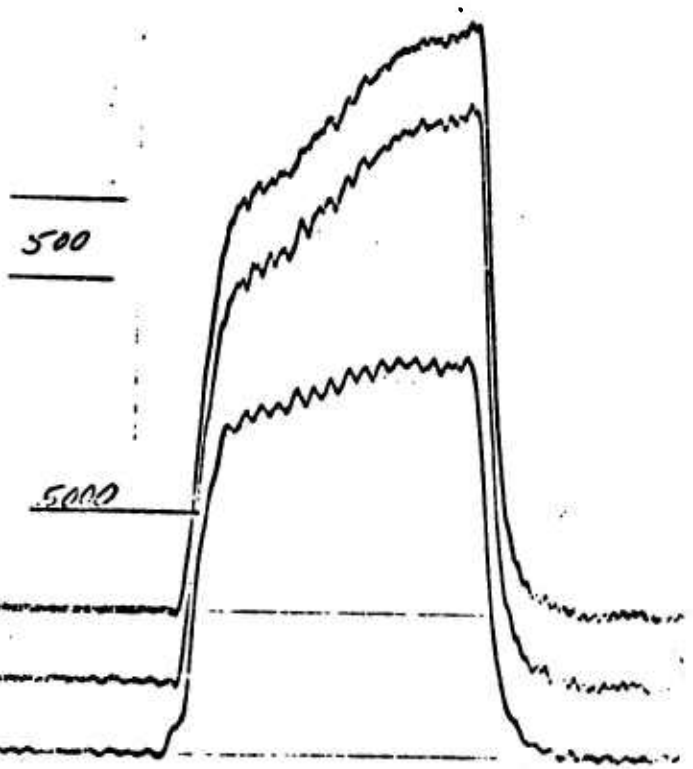
Firing No.	37417	37418	37419	37420	37421	37422	37423
Motor No.	17	18	19	21	22	23	24
Date	1972 4-25						4-25
Grain No.	PHIT- 3-17	3-18	3-19	3R-21	3R-22	3R-23	3R-24
Propellant Weight (lbs.)	0.0282	0.0287	0.0282	0.0283	0.0285	0.0285	0.0277
Pre-fire Dt.	.294	.323	.312	.294	.294	.294	.294
Post-fire Dt.							
Action Time	.0138	.0133	.0163	.0131	.0137	.0133	.0136
Burn Time	.0121	.0111	.0143	.0113	.0112	.0120	.0116
Total Time	.0176	.0247	.0302	.0156	.0165	.0171	.0168
Ignition Delay (mill. sec.)	0.7	0.6	0.6	0.7	0.7	0.5	0.7
Burn Rate	5.45	4.68	4.62	5.64	5.07	5.50	5.69
Time to Centroid Impulse							
Max. Thrust	5415	4921.6	473.9	577.8	521.3	545.2	531.0
Initial Thrust	4647	3157.7	402.6	434.8	452.9	441.7	441.3
Avg. Action Thrust	431.6	313.6	369.1	454.7	442.1	426.5	426.2
Avg. Burn Thrust	1552.3	3111.3	346.9	476.6	477.3	452.9	456.5
Total Impulse	1.02	5.95	1.04	5.98	1.09	5.92	5.83
Specific Impulse	215.0	212.5	257	211.3	215.2	202.2	209.0
Centroid Impulse							
Max. Pressure	1.660	4.238	5.344	7.022	6.857	6.857	6.627
Initial Pressure	5.106	4.160	5.245	6.397	6.425	6.331	6.364
Avg. Burn Pressure	6.665	4.034	4.876	6.540	6.310	6.265	6.053
Pressure Time Integral	77.10	1.847	73.86	80.83	80.49	81.01	77.33
Temperature TEMP	60°F	60°F	60°F	60°F	60°F	90°F	90°F

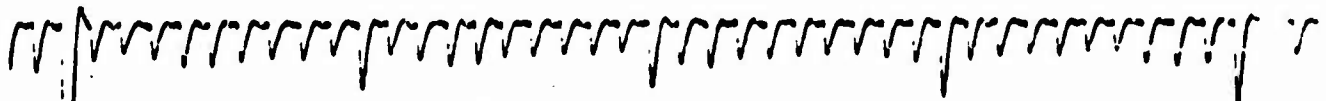
Firing No.	37424	37425	37426	37427	37428	37429
Motor No.	25	26	27	29	30	31
Date	1972	4-5				4-35
Train No.	4L-25	4L-26	4L-27	4H-29	4H-30	4H-31
Propellant Weight (lbs.)	0.0581	0.0550	0.0283	0.0291	0.0280	0.0282
Pre-fire Dt.	.094	.093	.095	.093	.094	.092
Post-fire Dt.						
Action Time	.043	.044	.041	.035	.030	.033
Burn Time	.0118	.0120	.0122	.0114	.0107	.0103
Total Time	.0176	.0173	.0186	.0168	.0159	.0171
Ignition Delay (mil/secs)	0.7	0.7	0.7	0.6	0.7	0.7
Burn Rate	559	520	468	579	617	641
Time to Centroid Impulse						
MAX. Thrust	526.0	525.3	541.5	526.8	623.5	637.3
Initial Thrust	427.4	400.3	425.1	450.9	430.2	395.7
Avg. Action Thrust	446.7	407.4	428.1	435.3	479.7	471.2
Avg. Burn Thrust	475.1	433.0	455.4	469.8	509.9	510.3
Total Impulse	6.35	6.50	6.06	5.90	6.26	6.30
Specific Impulse	226.0	210.7	211.0	210.0	223.6	223.4
Centroid Impulse						
MAX. Pressure	679.1	639.7	679.4	656.1	738.3	761.4
Initial Pressure	596.9	787.0	633.1	639.7	623.2	557.4
Avg. Burn Pressure	615.9	557.1	633.3	640.5	687.4	674.6
Pressure Time Integral	9103	7874	8422	8032	8797	8226
Case Temp.	410°F	60°F	60°F	60°F	60°F	60°F

L. T. III

Firing No.	37433	37434	37435	37436	37437	37438	37439	37440	37441	37442
Motor No.	33	34	37	38	35	39	39	39	38	38
Date	4-28	5-1	5-1	5-1	5-1	5-1	5-1	5-1	5-1	5-1
Grain No.	5/8 μ-33	5/8 μ-34	5/8 μ-37	5/8 μ-38	5/8 μ-35	5/8 μ-39				
Propellant Weight (lbs.)	0.0782	0.0780	0.0787	0.0780	0.0781	0.0783	0.0783	0.0783	0.0783	0.0783
Pre-fire Dt.	.294	.294	.294	.294	.294	.294	.294	.294	.294	.294
Post-fire Dt.										
Action Time	.0112	.0113	.0113	.0117	.0117	.0117	.0117	.0117	.0117	.0117
Burn Time	.0093	.0093	.0112	.0117	.0094	.0126	.0126	.0126	.0108	.0103
Total Time	.0142	.0147	.0172	.0185	.0148	.0186	.0186	.0186	.0158	.0158
Ignition Delay <i>mil/Sec</i>	0.5	0.6	0.6	0.6	0.6	0.4	0.4	0.4	0.7	0.6
Burn Rate	7.10	7.10	5.69	5.64	7.02	5.24	5.24	5.24	6.11	6.16
Time to Centroid Impulse										
Max. Thrust	659.7	636.7	566.7	578.4	682.5	516.1	516.1	516.1	613.0	697.6
Initial Thrust	607.7	658.4	315.9	467.8	578.8	474.4	474.4	474.4	345.2	317.5
Avg. Action Thrust	595.2	539.4	437.5	411.8	579.3	418.9	418.9	418.9	450.2	518.2
Avg. Burn Thrust	604.7	587.4	480.5	446.3	568.4	440.7	440.7	440.7	511.7	540.7
Total Impulse	6.20	6.13	6.30	6.18	6.11	6.22	6.22	6.22	6.33	6.33
Specific Impulse	219.9	218.9	233.4	220.7	217.4	219.8	219.8	219.8	215.3	226.1
Centroid Impulse										
Max. Pressure	8043	7515	6776	5966	7907	6107	6107	6107	7505	8295
Initial Pressure	8354	8112	5508	6217	7656	5578	5578	5578	6811	5927
Avg. Burn Pressure	7758	7474	6223	5779	7226	5863	5863	5863	6835	7018
Pressure Time Integral	79.62	77.31	80.55	78.80	76.64	77.40	77.40	77.40	76.09	81.96

37372
PROJECT 1.7M H11
MOTOR NO. 1
1-1
SERIAL NO. 1



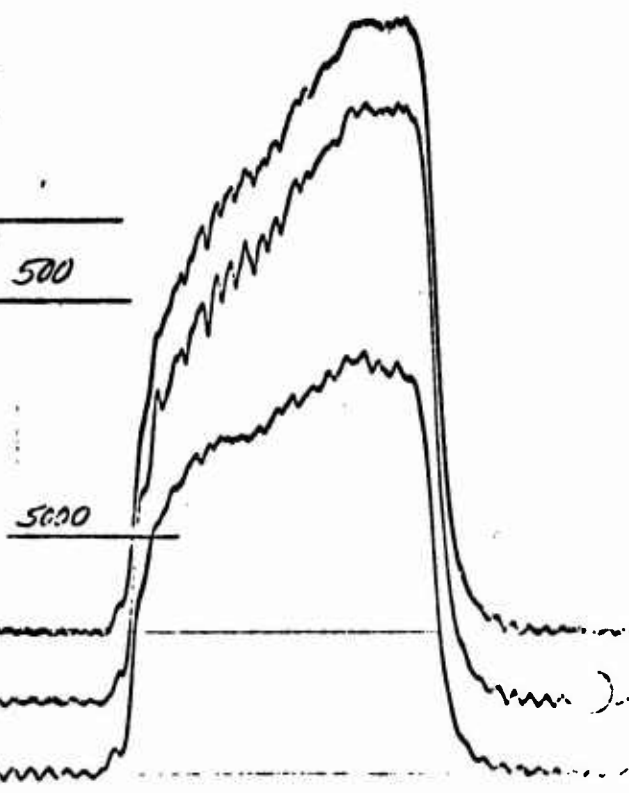


TESTING NO. 37374

DATE 1/1 PROJECT LTN 1117

COND. TEMP. 500 MOTOR NO. 7

CIRCUIT NO. 1R-7



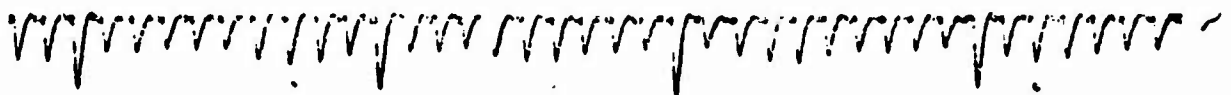
FIRING NO. 37417

DATE 4/4/57 PROJECT LTV HIT

COND. TEMP. 76.0 MOTOR NO. 17

GRAN. NO. 3-17

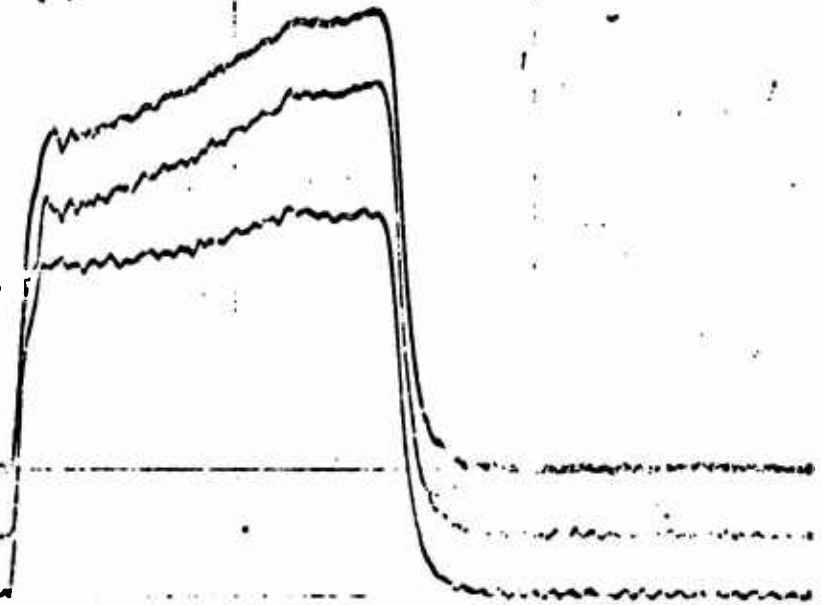
RECORD SPEED 1/10 IN/SEC (TIMING 100 / 01 SEC)



.13

750°F

5000 PSIG



FIRING NO. 37419

DATE: 1/21/50 PROJECT 1-1-11-T

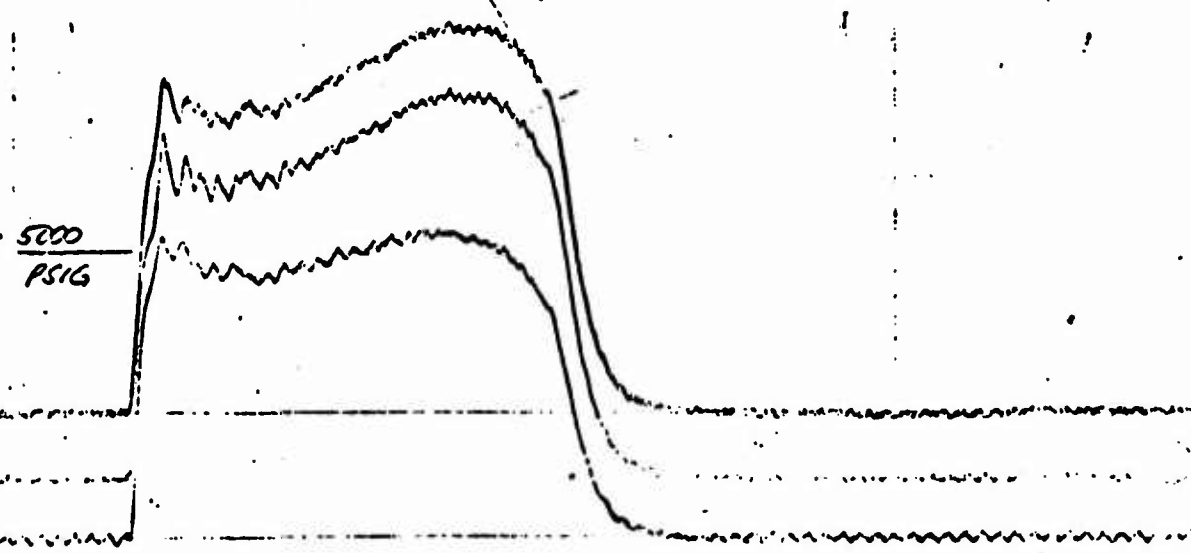
COND. TEMP. 200 MOTOR NO. 19

GRAN NO. 3-19

RECORD SPEED 200 IN/SEC TRIGG. 100 SEC.



750 F



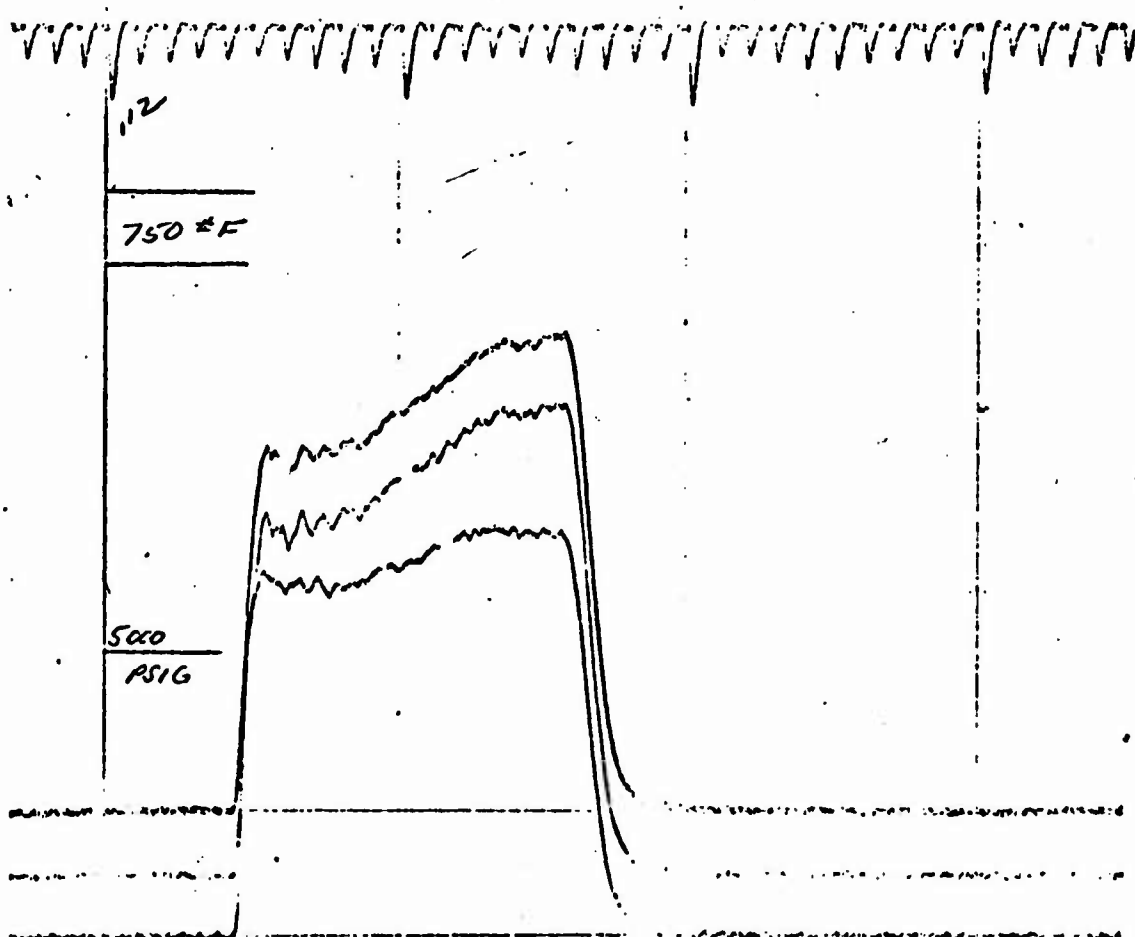
FIELD NO. 27420

DATE: 1-12-62 PROJECT L-V HIT

COND. TEMP. +60 MOTOR NO. 21

SCAN NO. 3R-21

RECORD SPEED 100 IN/SEC TRIGGER 100 SEC.



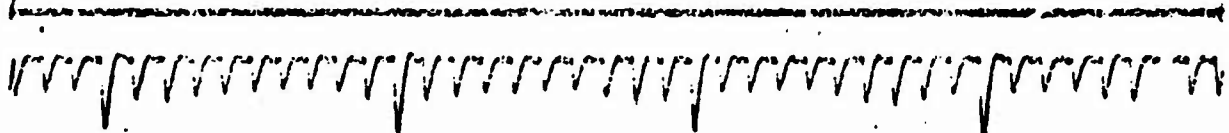
TRIAL NO. 37424

DATE 7/12/51 PROJECT LT-417

COND. TEMP. +10 MOTOR NO. 25

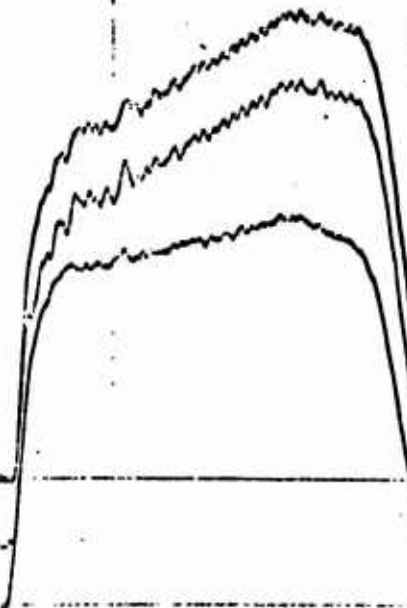
GRAN. NO. 4L-25

RECORD SPEED 1.20 IN/SEC TIMING 1.01 SEC.



750 #F

5000 psi



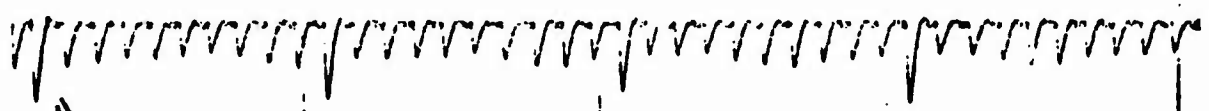
TRIPS NO. 37423

DATE: 1/11/57 PROJECT LTV #19

COND. TEMP. -40 MOTOR NO. 30

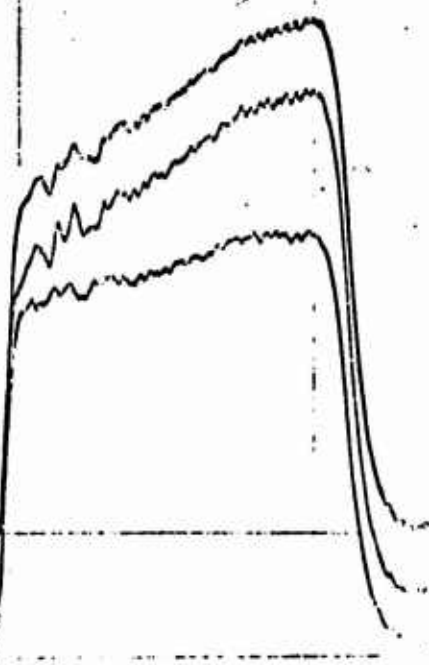
GRAPH NO. 44-50

RECORD SPEED 100 IN/SEC TIMING: 0.1 SEC.



750 #F

5000 psig

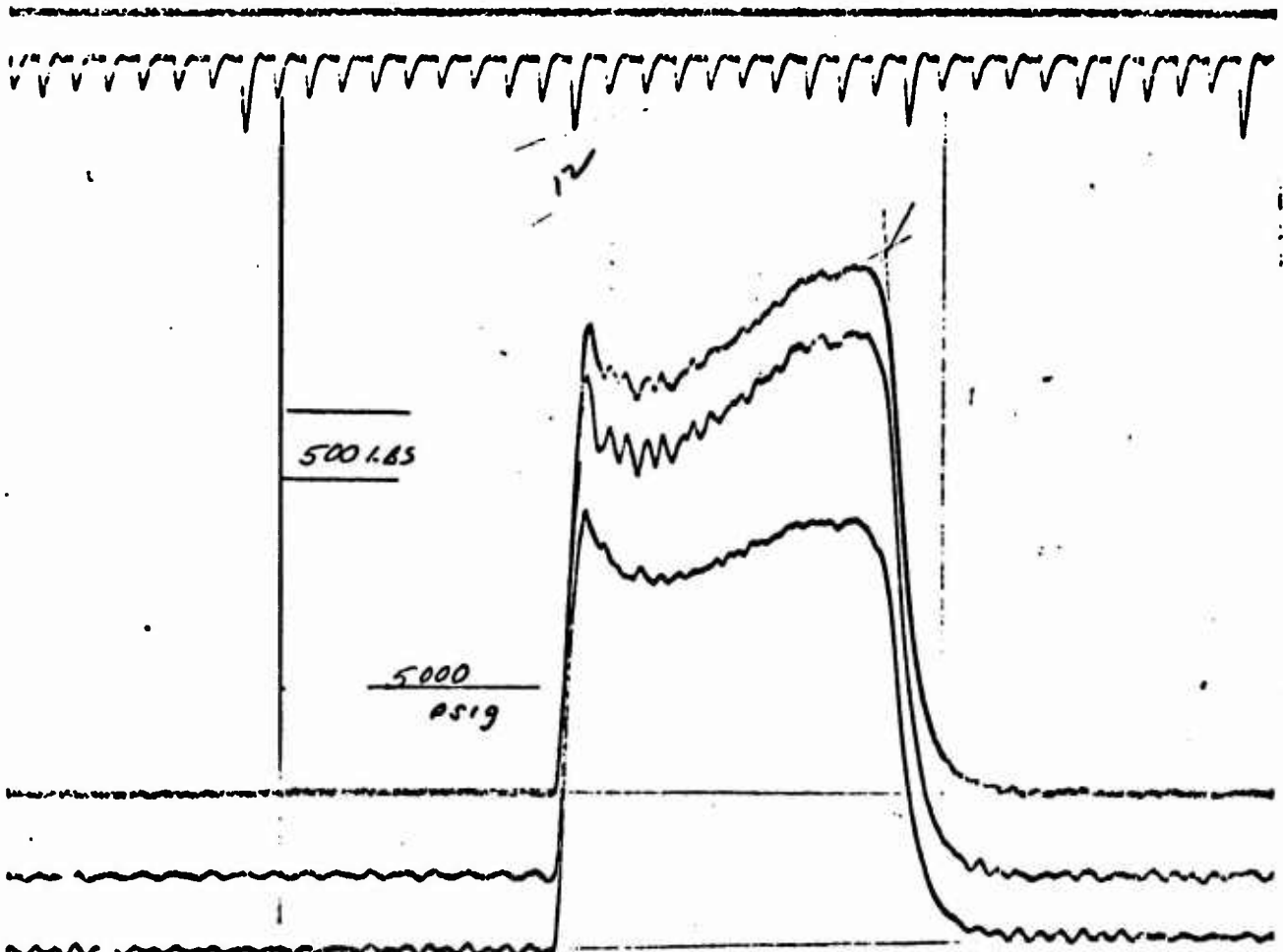


37433

46012 LTV Air

+60 33

160 100/100

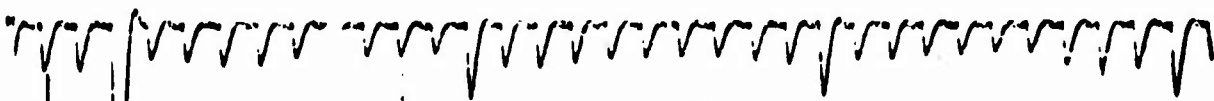


37436

42873 LTV HIT

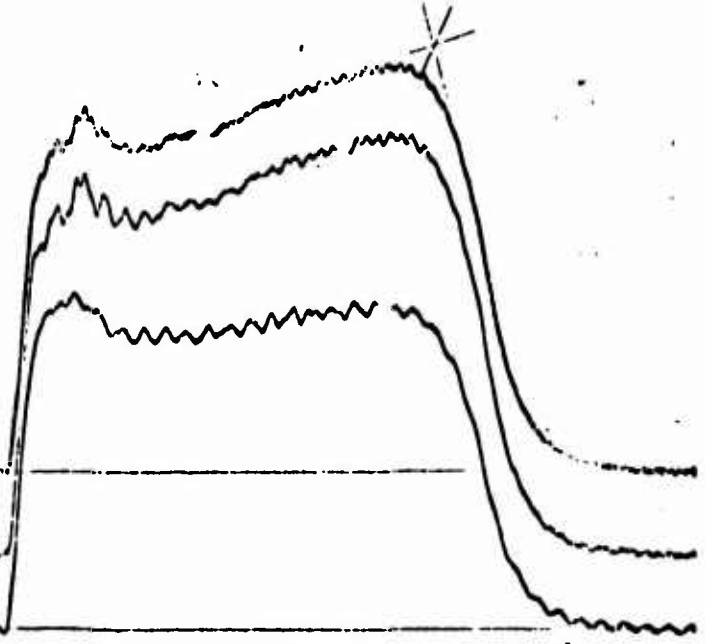
+60 34

160



500 LBS

5000 PSI

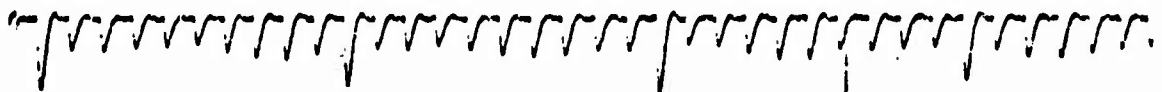


37564

5-26-72 LTV HIT

TEMP - +60 MOTOR NO 12

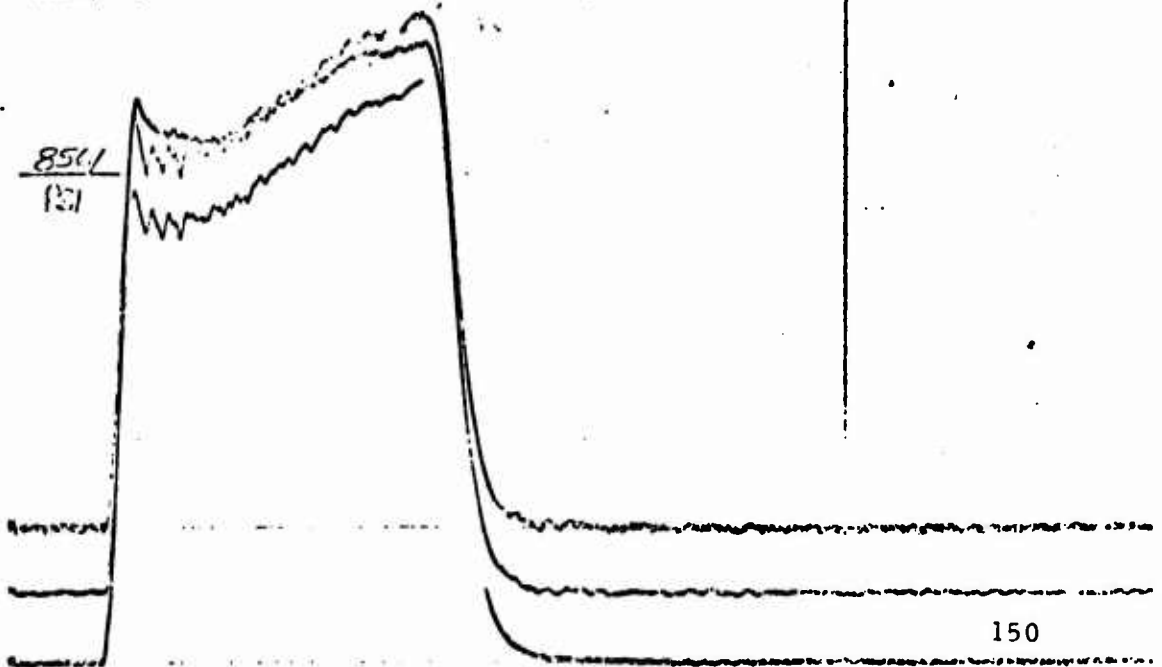
GRAIN NO PHIT - 2-12



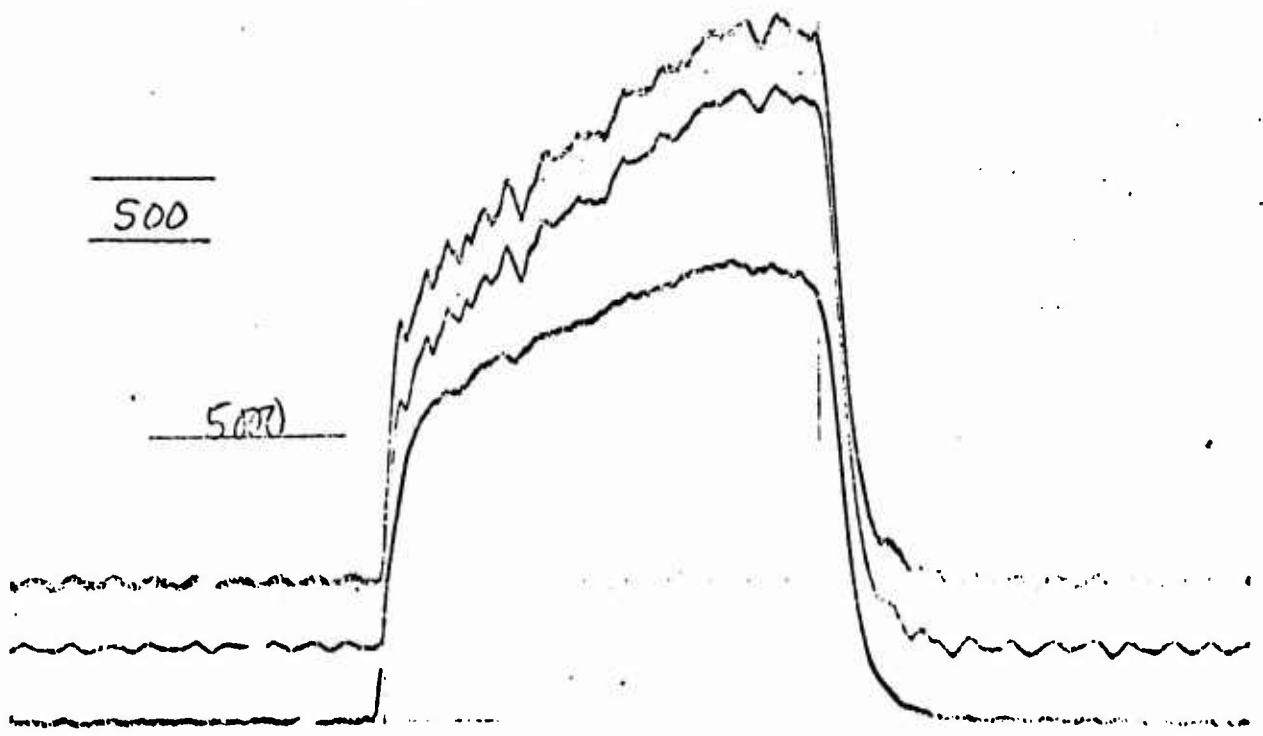
753.2 #F

750.4 #F

856.1
131



LTU Hit
Motor NO 32
FIRING NO 37612
DATE 6-1-72



APPENDIX 2

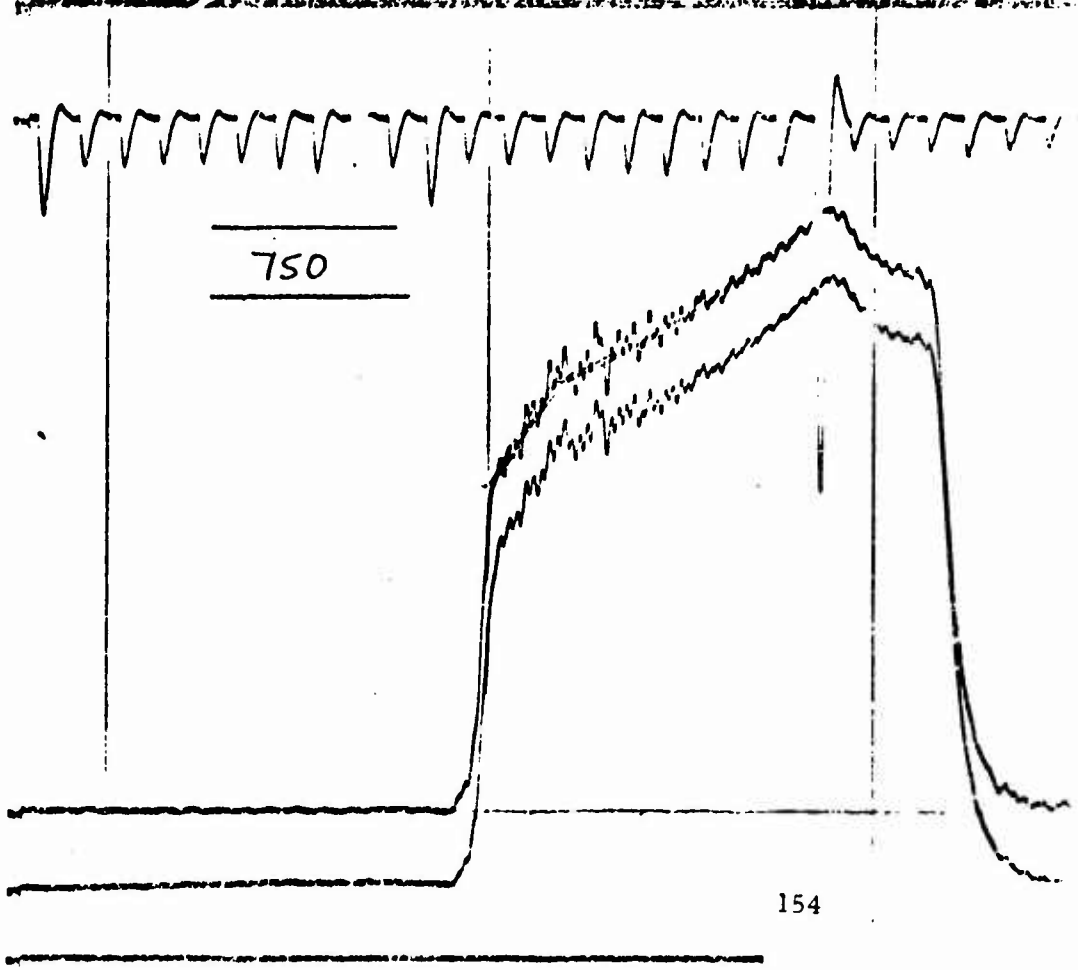
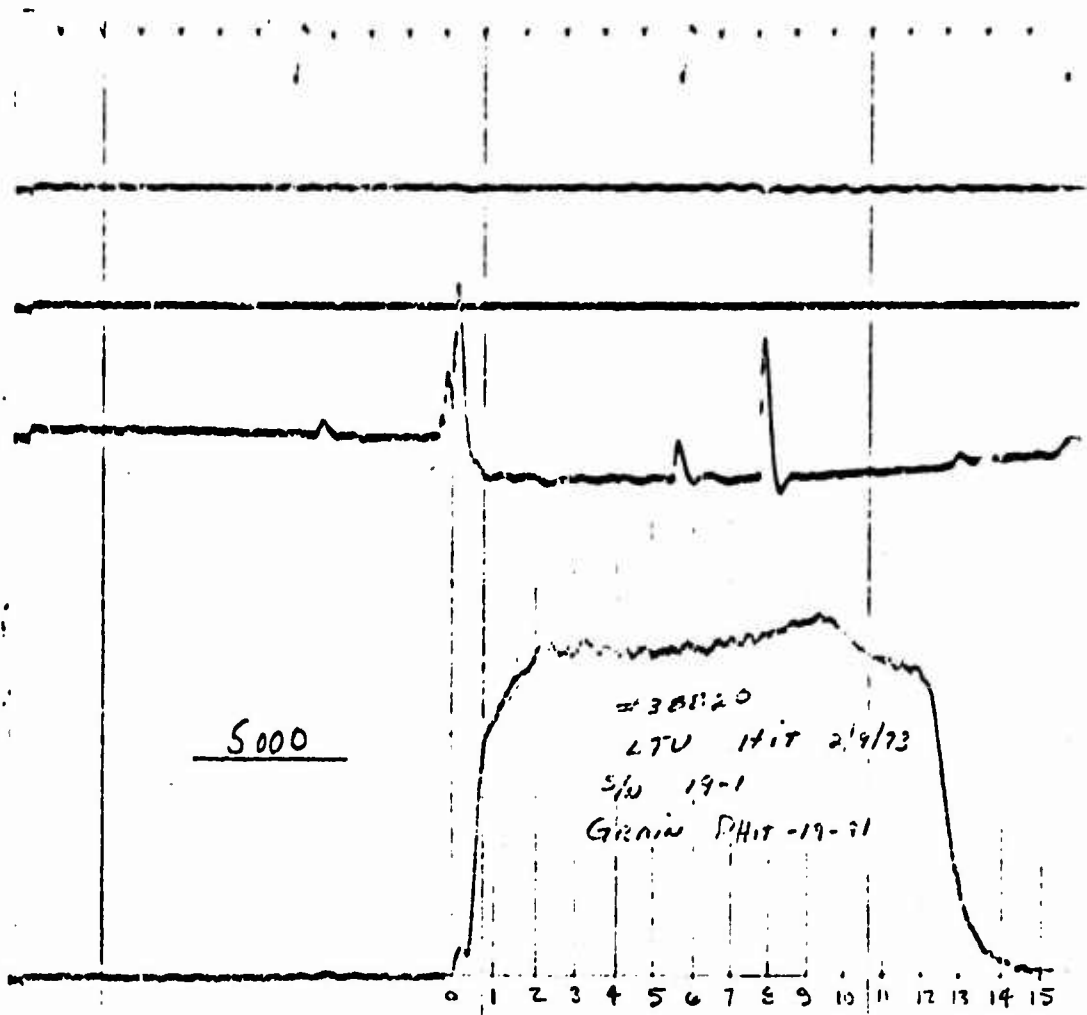
TYPICAL TRACES - HEAVYWALL CONFIRMATORY AND SUBSEQUENT MOTOR TESTS

This Appendix contains representative oscillograph records of thrust-time and pressure-time traces from certain of the development test motor firings. The records of this appendix are subdivided as follows:

<u>Section</u>	<u>Test Series</u>
1	Heavywall Confirmatory
2	Flightweight
3	Thrust Alignment
4	Pressure Oscillation
5	Array Batch Check
6	Prototype MMA

SECTION 1

HEAVYWALL CONFIRMATORY



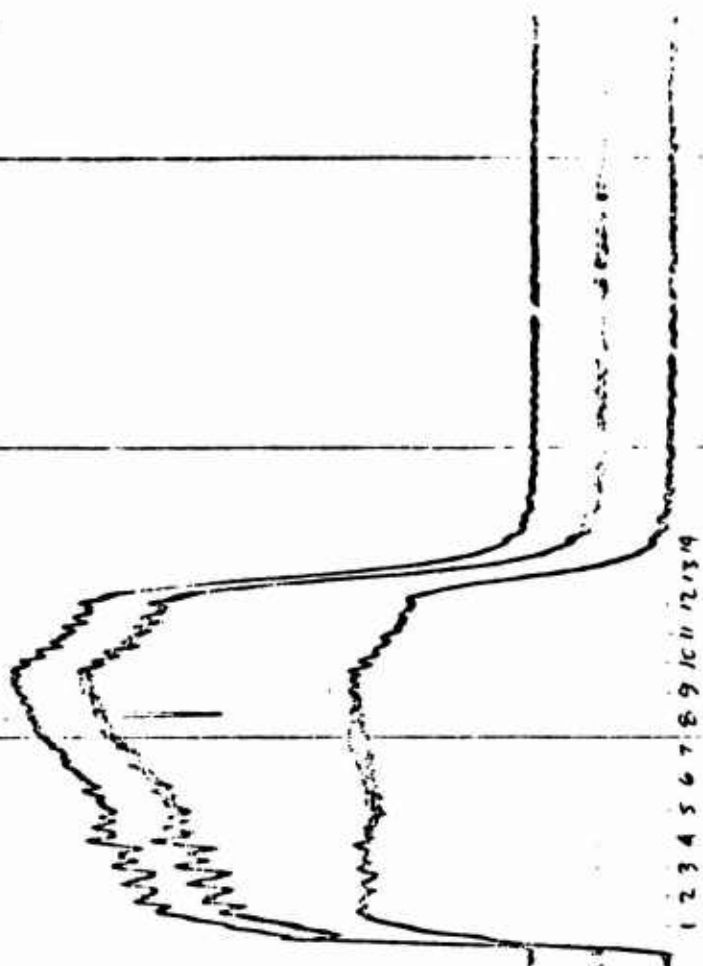
39063

LTV KIT

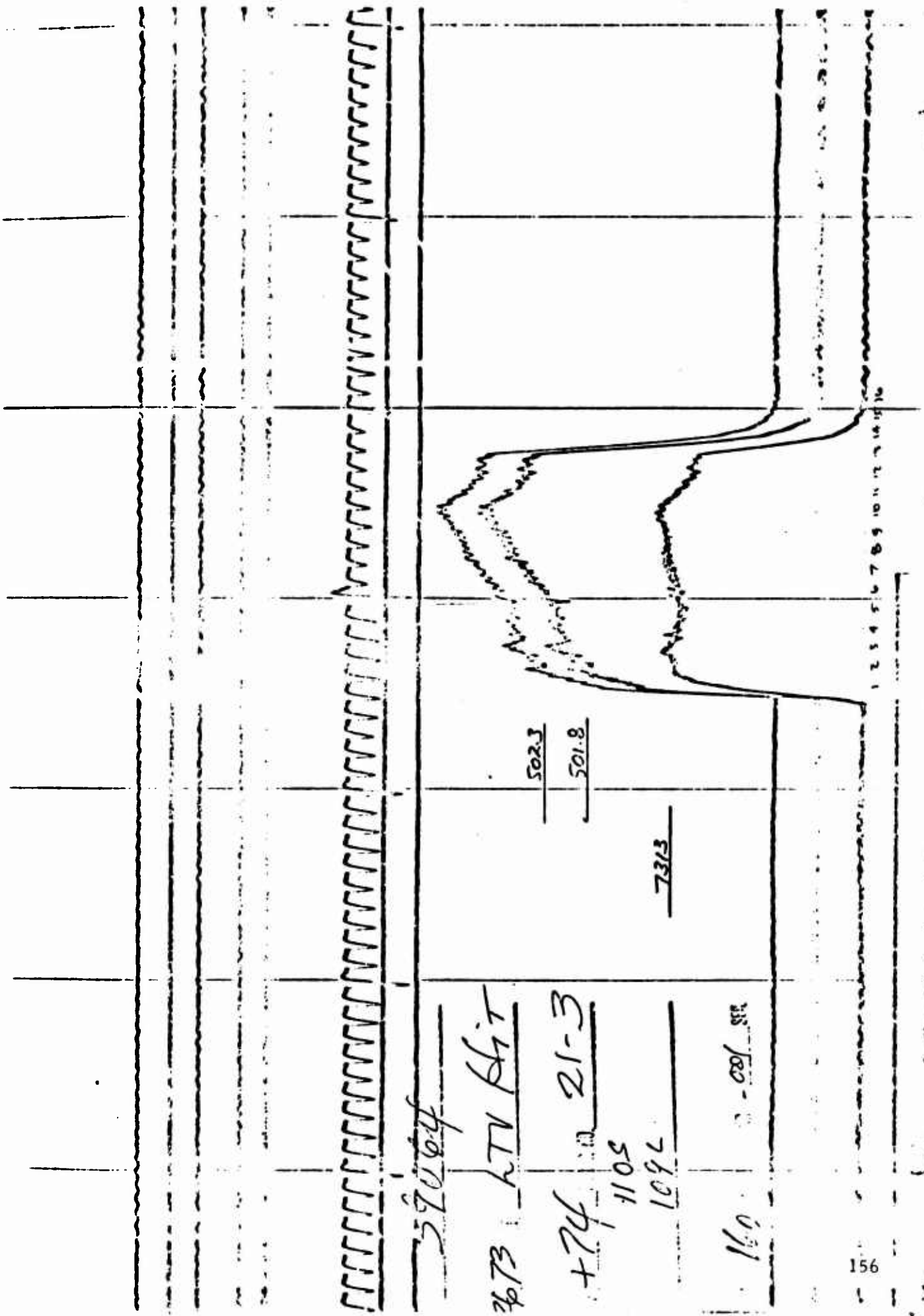
+74

1165
1166

160



7312



1000 (2)

1000 (4)

1000 (1)

2000 (2)

Hump 1

Hump 2

Hump 2

Hump 4

$$\frac{1.95}{5000} = \frac{2.18}{8480}$$

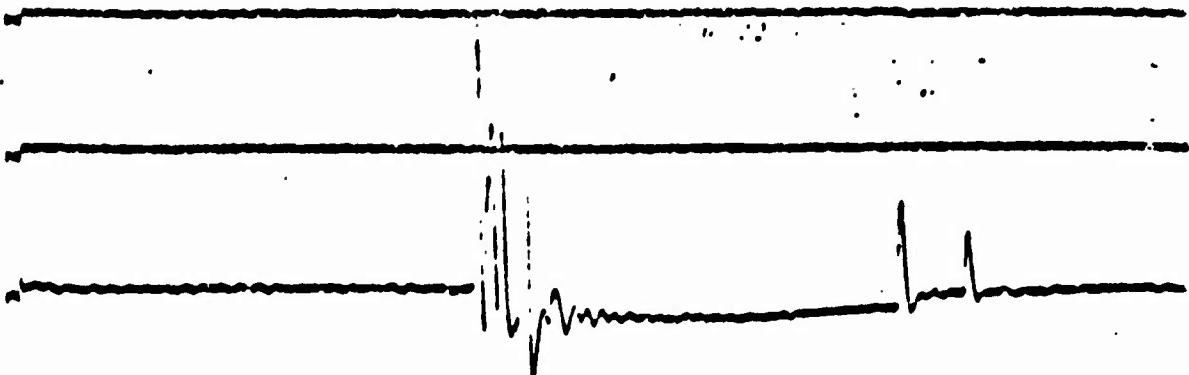
39314
S/N 23-125

500 #F

5000 psig

SECTION 2

FLIGHTWEIGHT

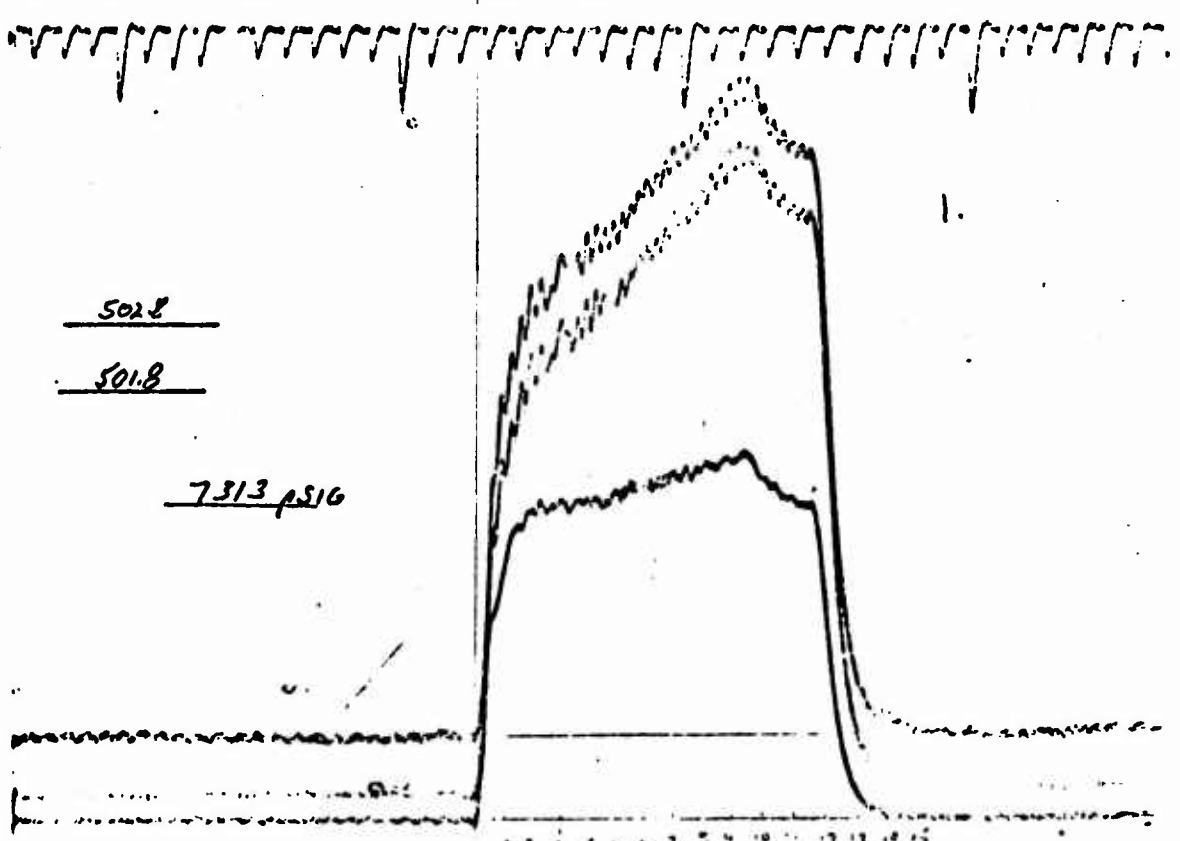
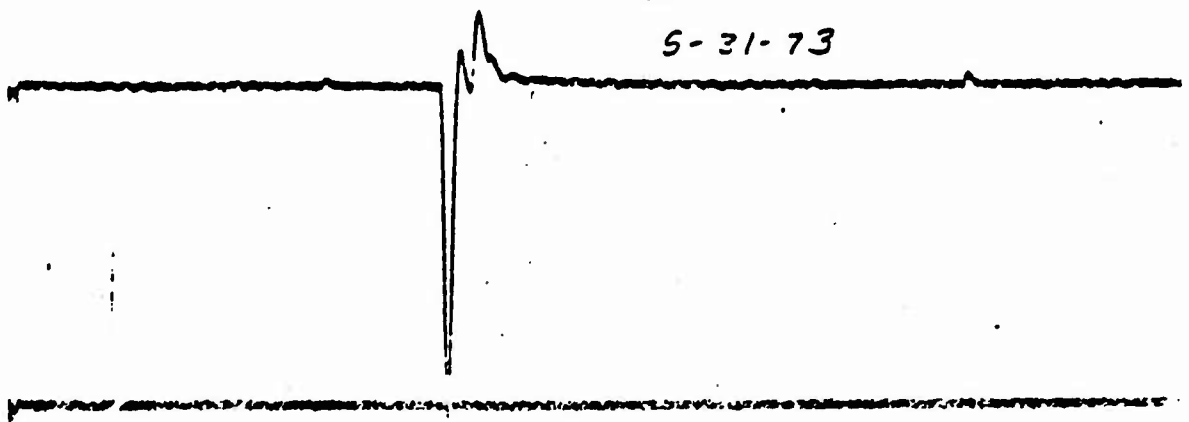


39573

LTU Hit

S/N 24-9

5-31-73

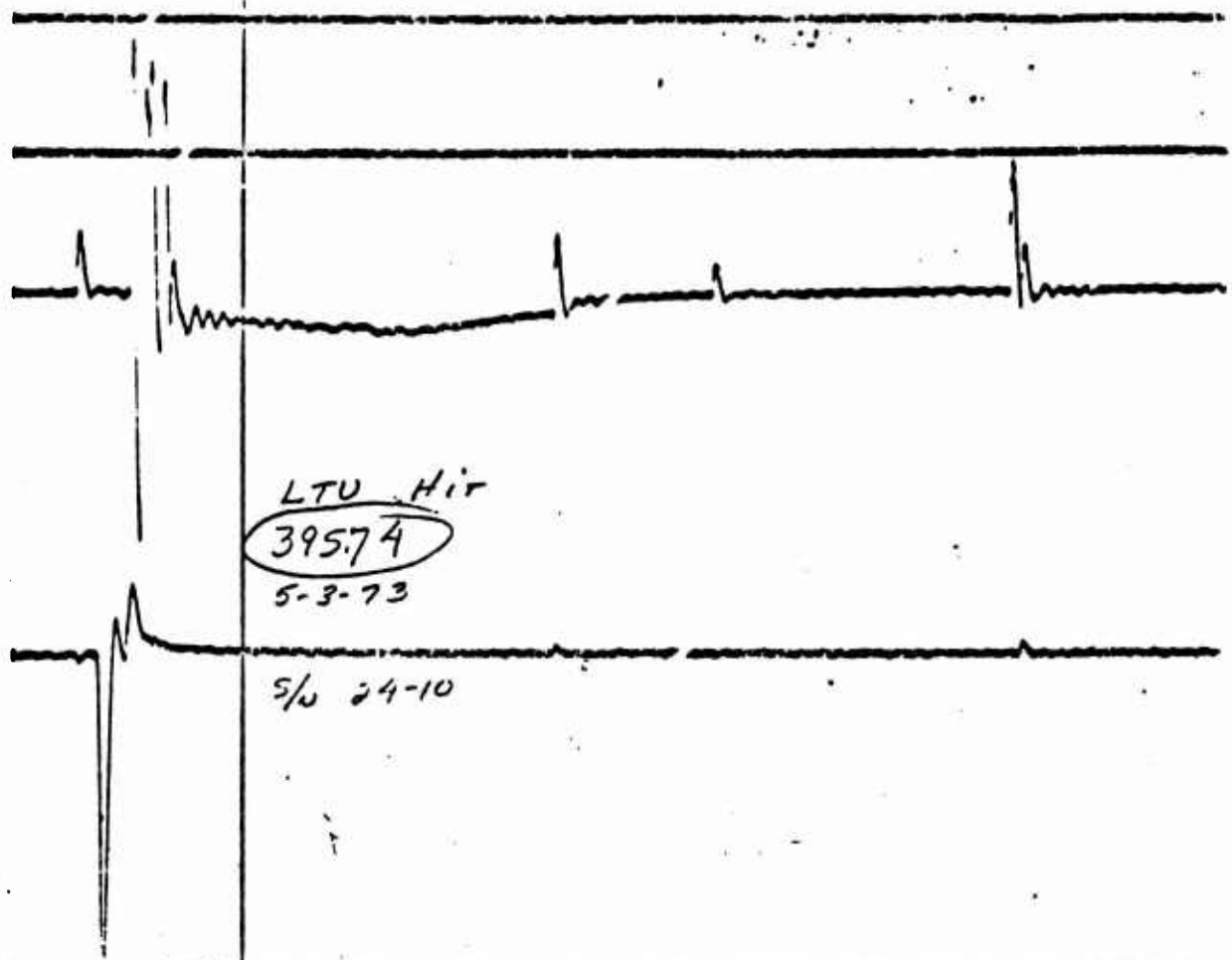


502.8

501.8

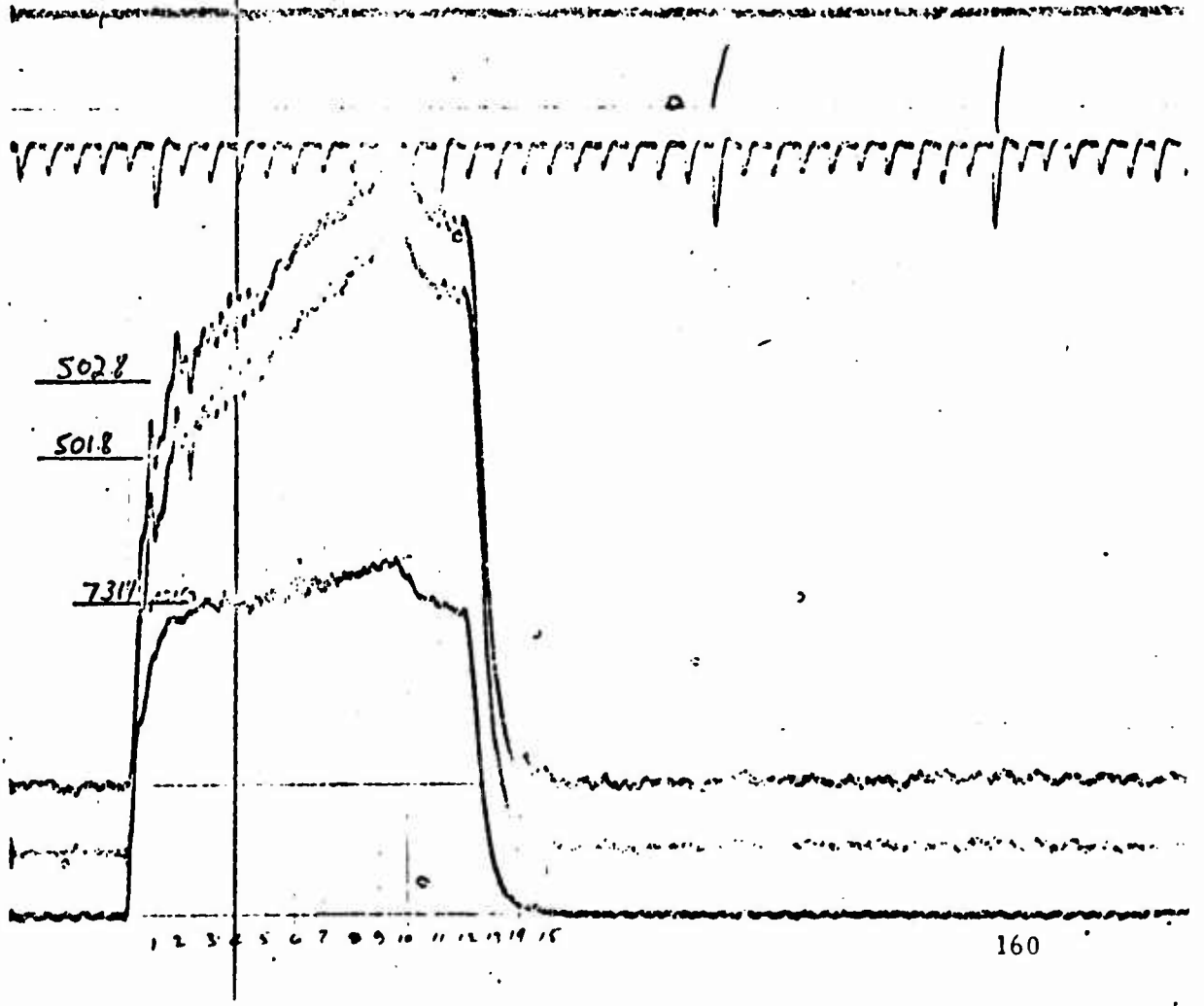
7313 PSIG

1 2 3 4 5 6 7 8 9 10 11 12



LTV Hit
395.74
5-3-73

S/O 24-10

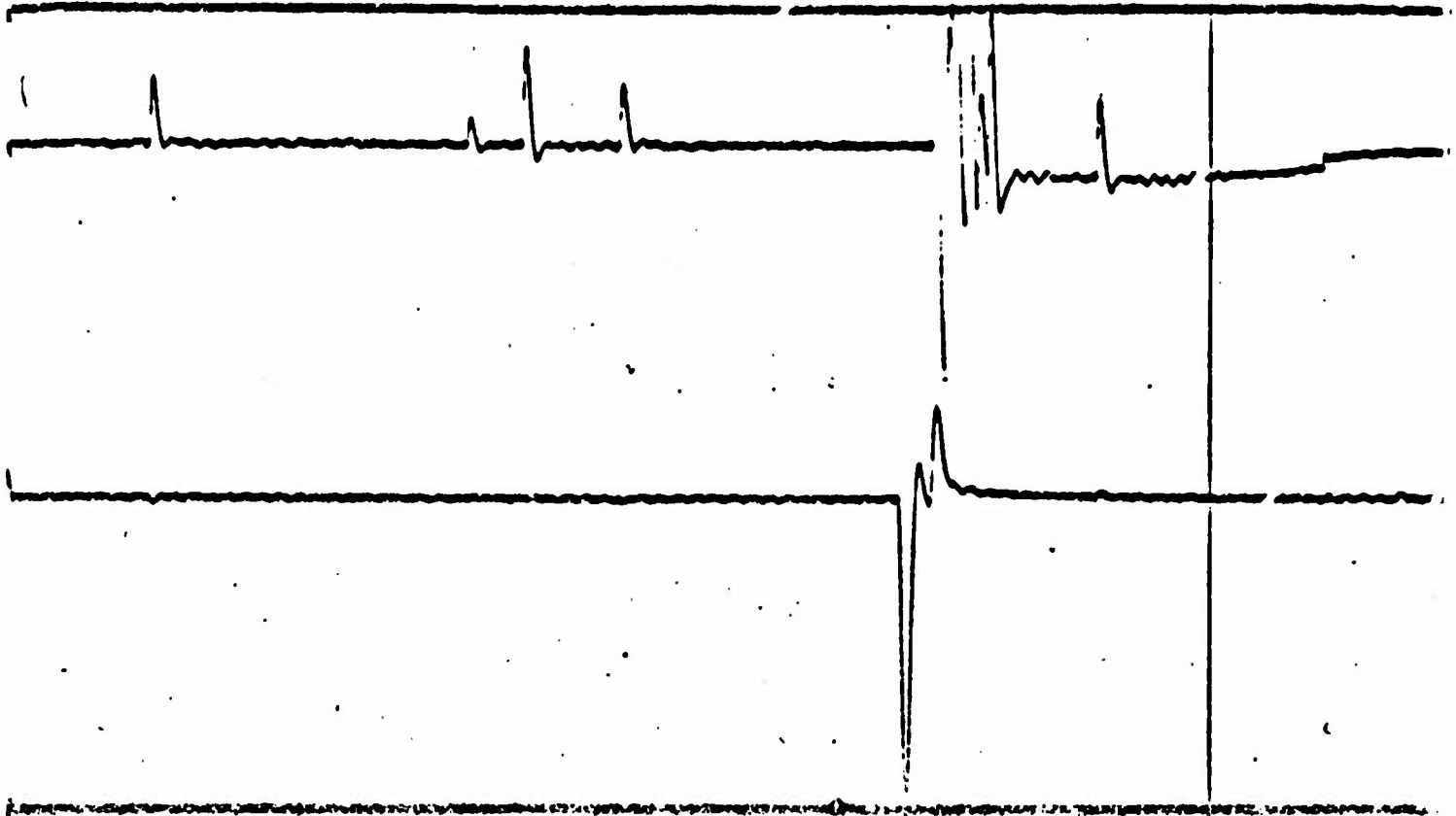


5028

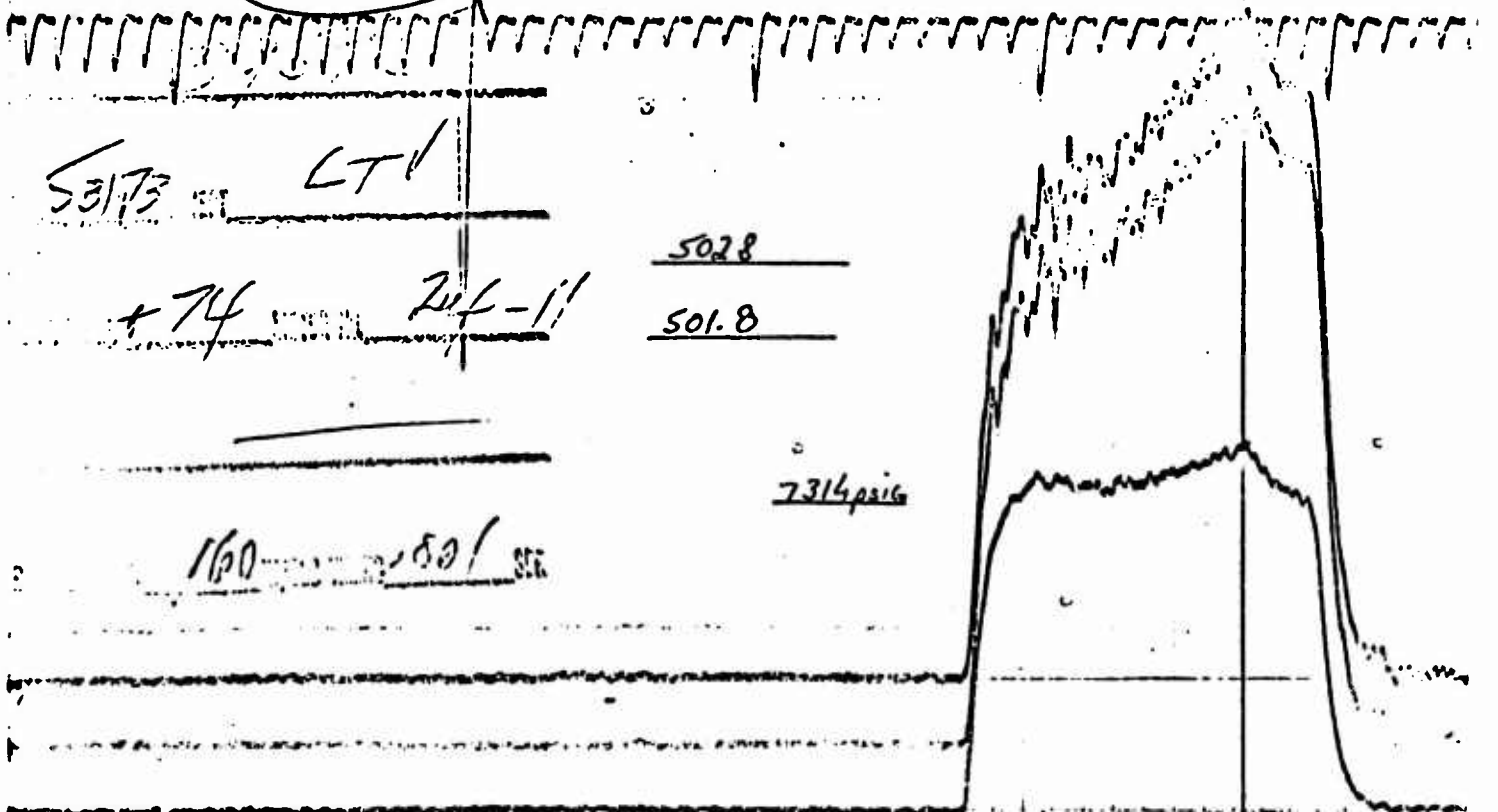
5018

7317

1 2 3 4 5 6 7 8 9 10 11 12 13 14 15



39575



53173 LT

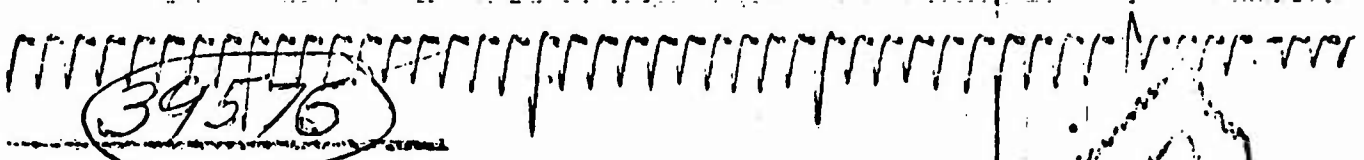
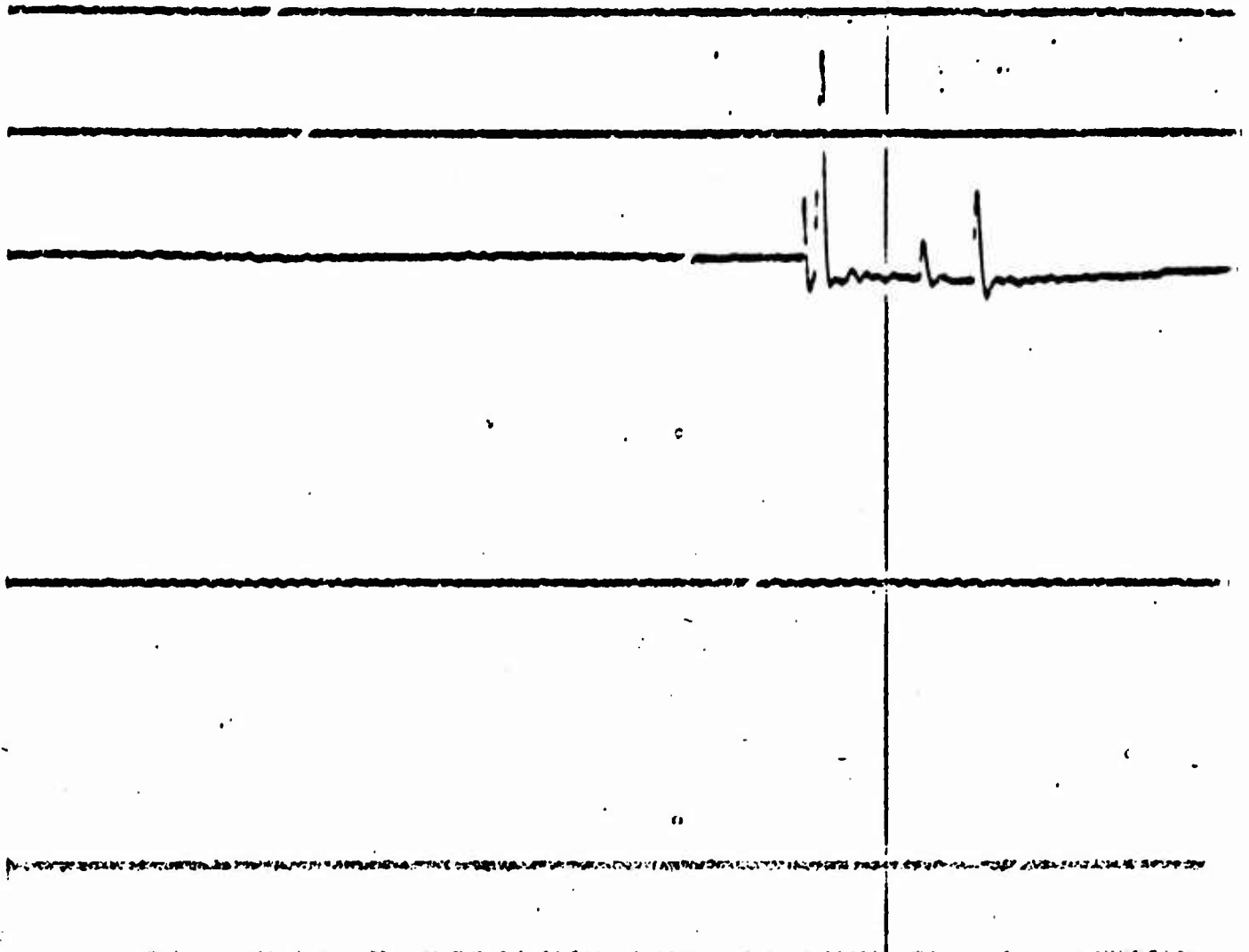
+74 Ref - 11

5028

501.8

7314 psig

160 501 SEC



LT/RT

474 24-12

502.8
501.8

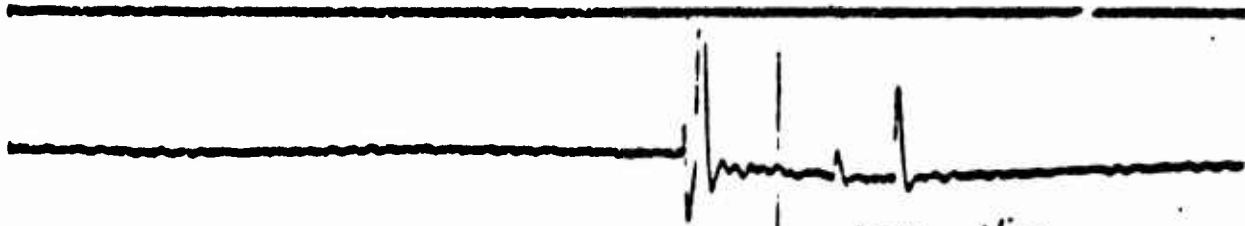
7314 psig

1/69



162

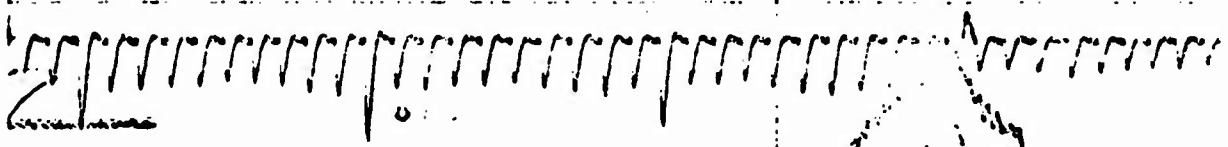
1 2 3 4 5 6 7 8 9 10 11 12 13



LTO KIT
39577

5-31-73

S/N - 24-8



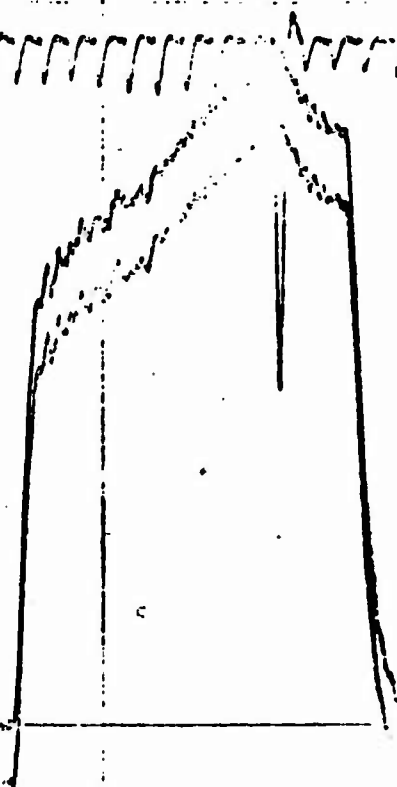
/

24-8

502.8

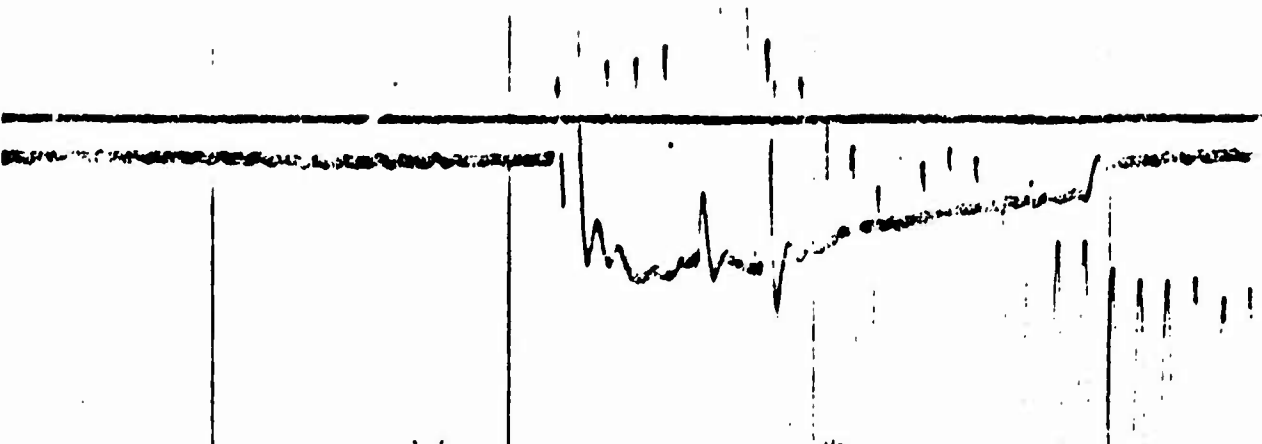
501.8

00/57



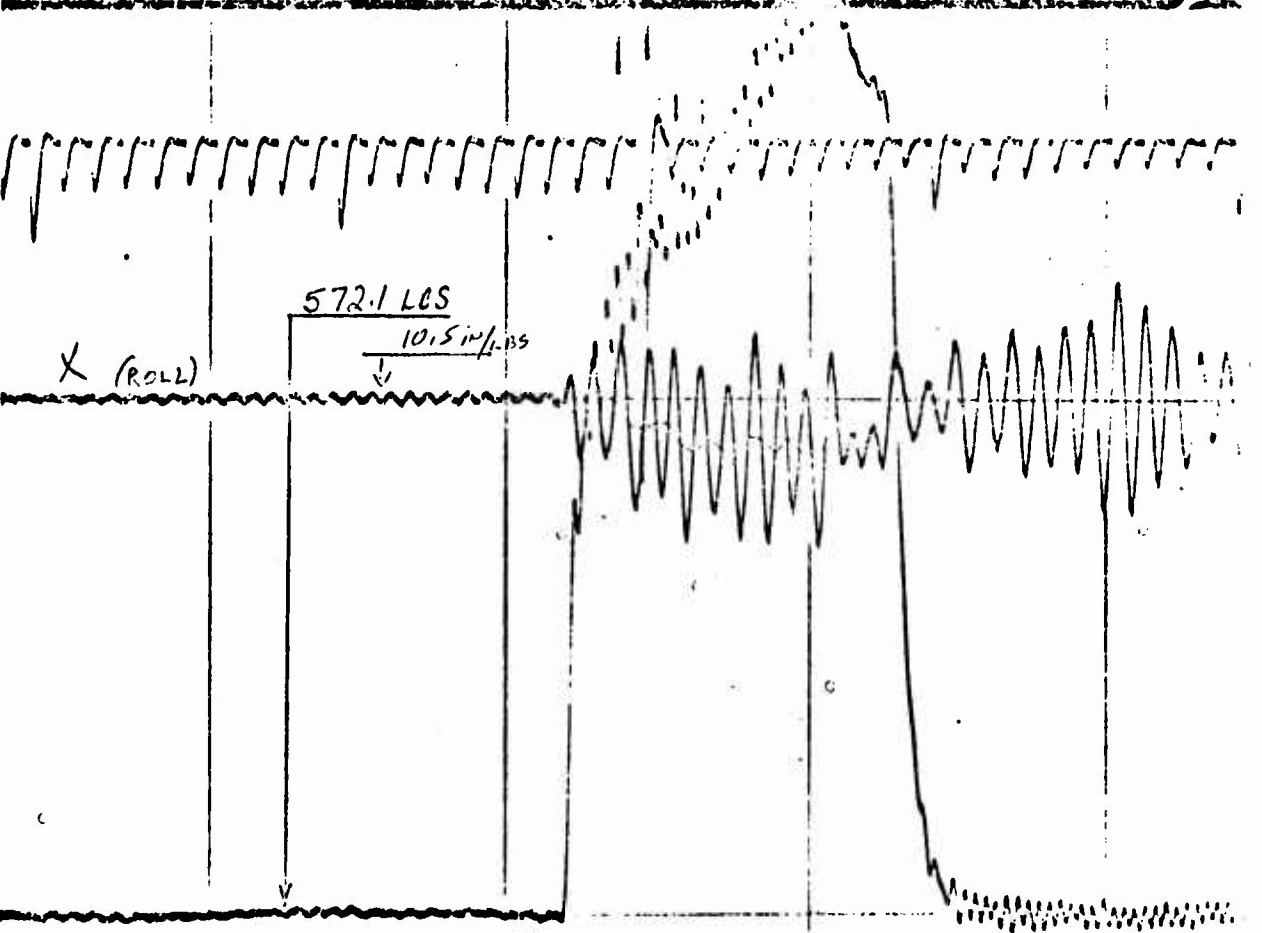
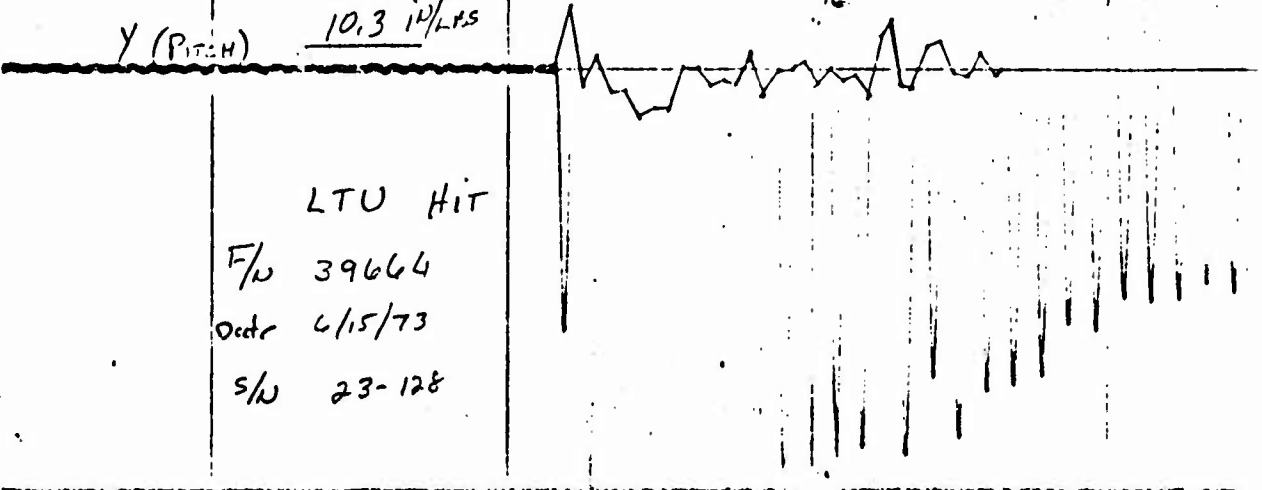
SECTION 3

THRUST ALIGNMENT



Y (PITCH) 10.3 in/LAS

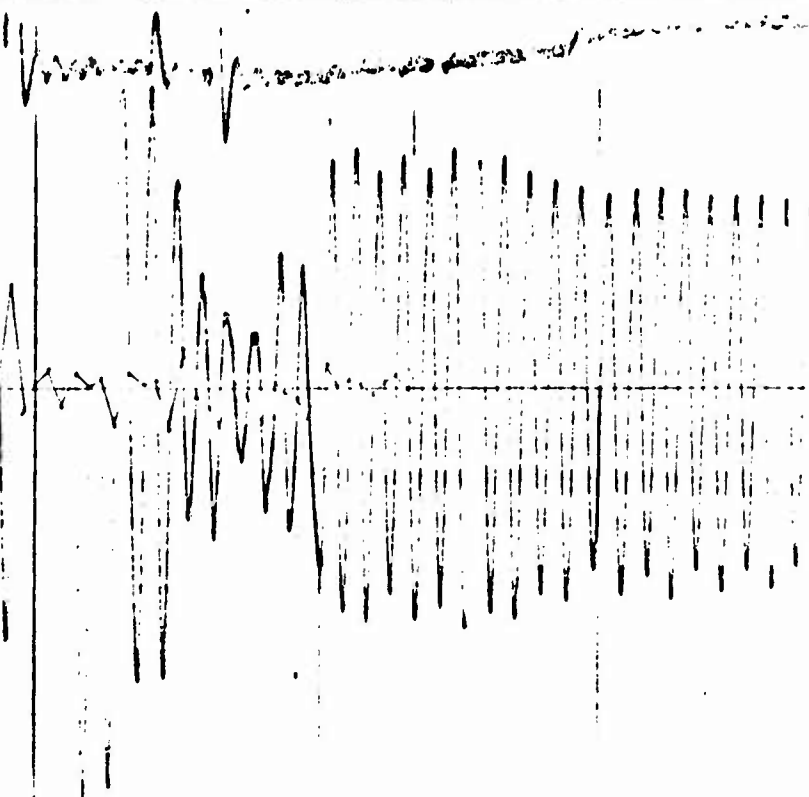
LTU HIT
 F/U 39664
 Date 6/15/73
 S/U 23-128



X (ROLL) 572.1 LCS
10.5 in/LAS

Y (mV) 10.3 uV

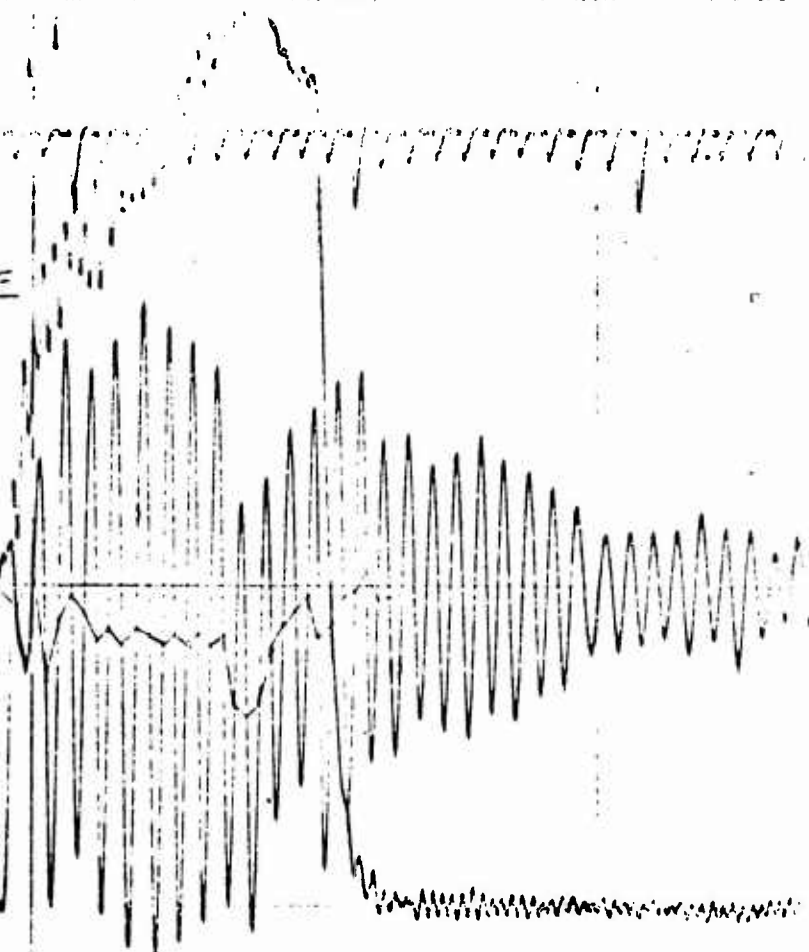
LTV Nit
Flu 39670
DATE 6-15-73
S/N 23-129

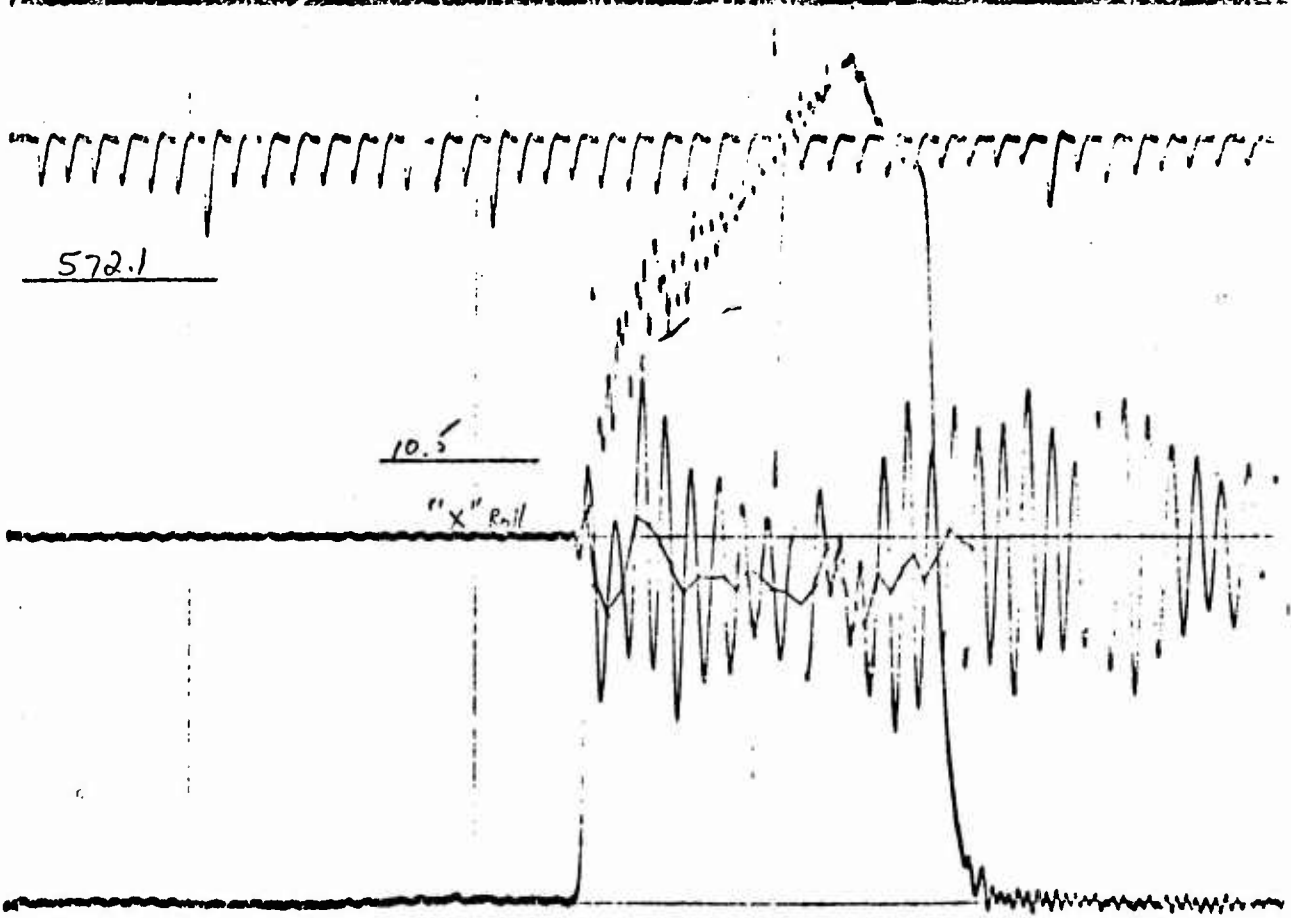
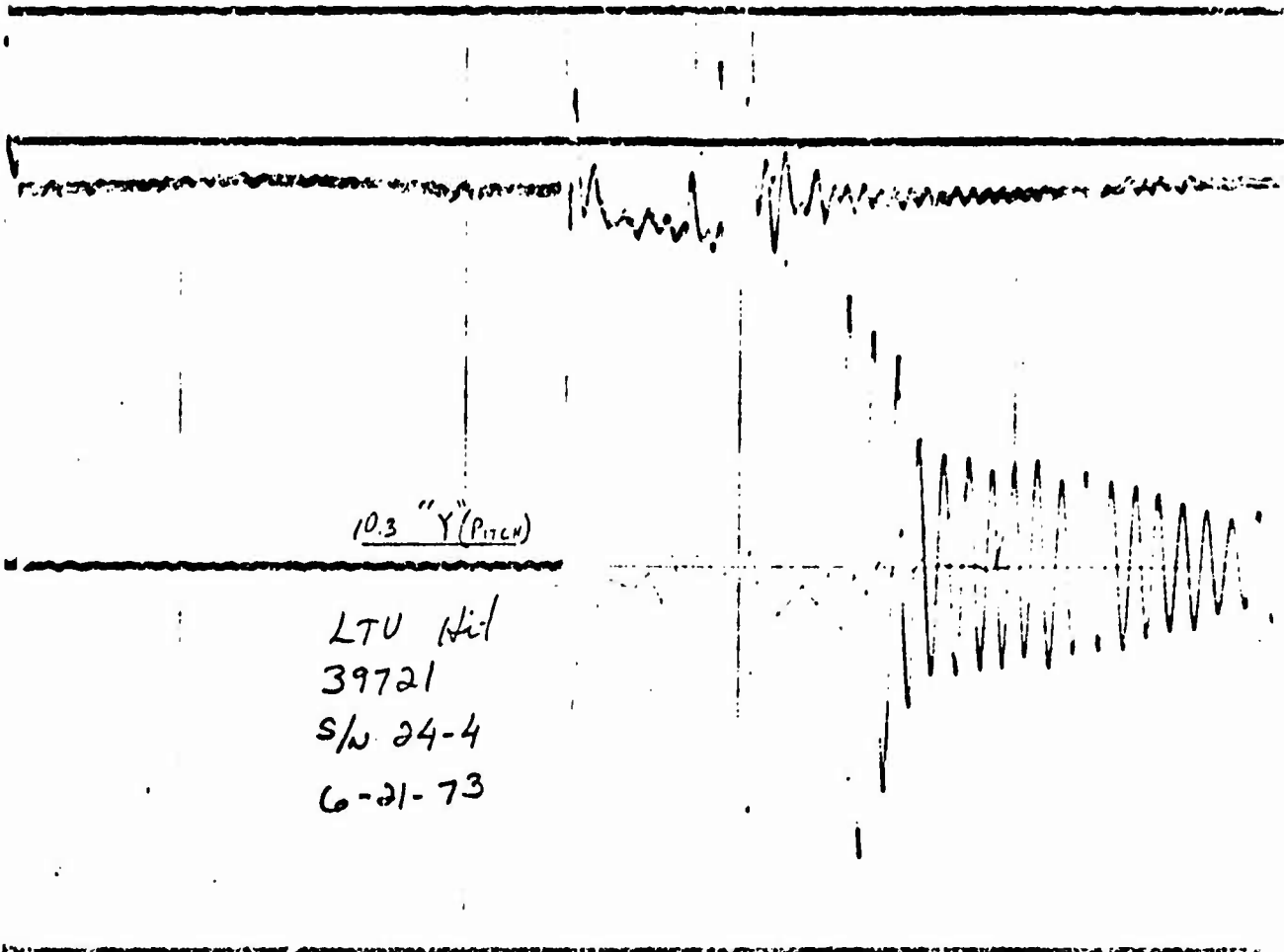


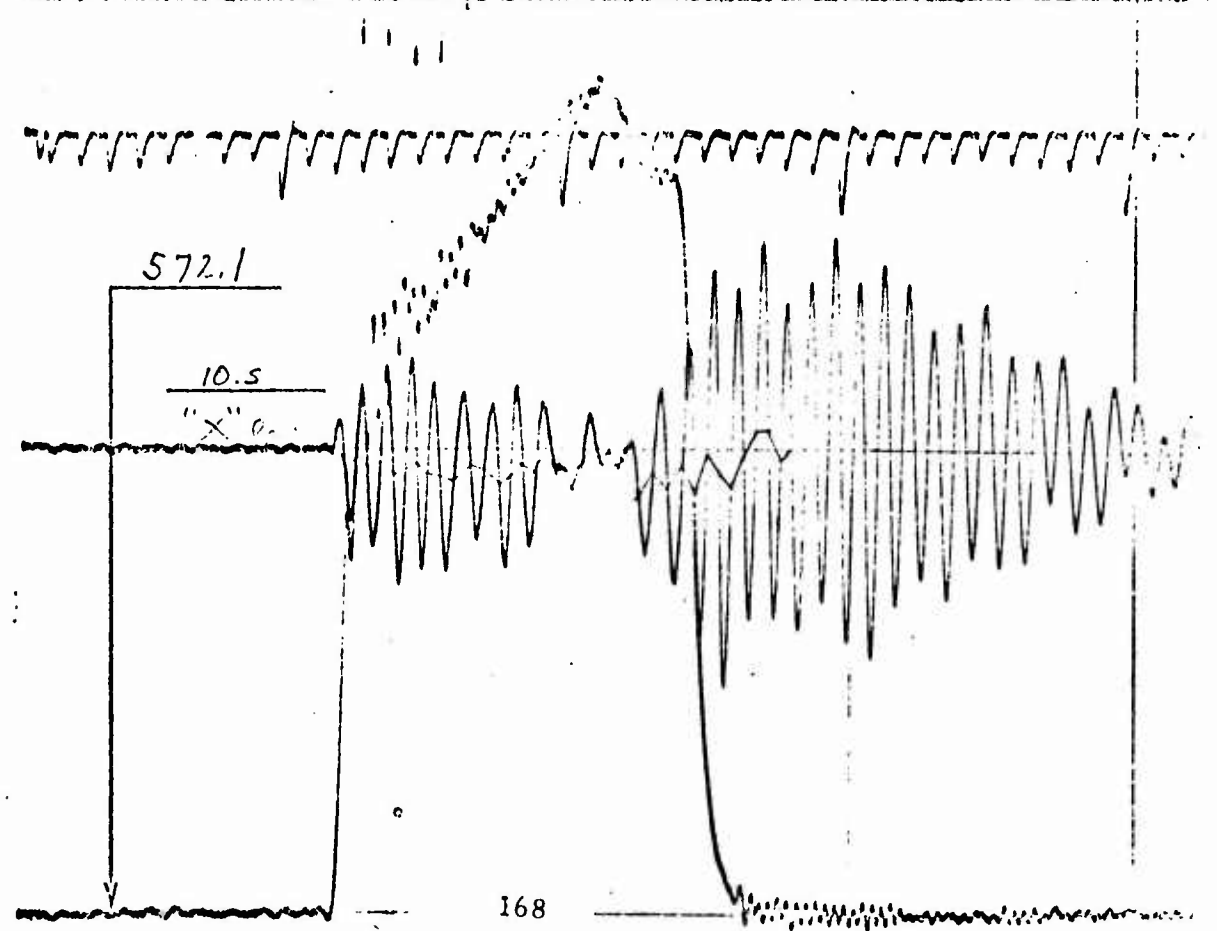
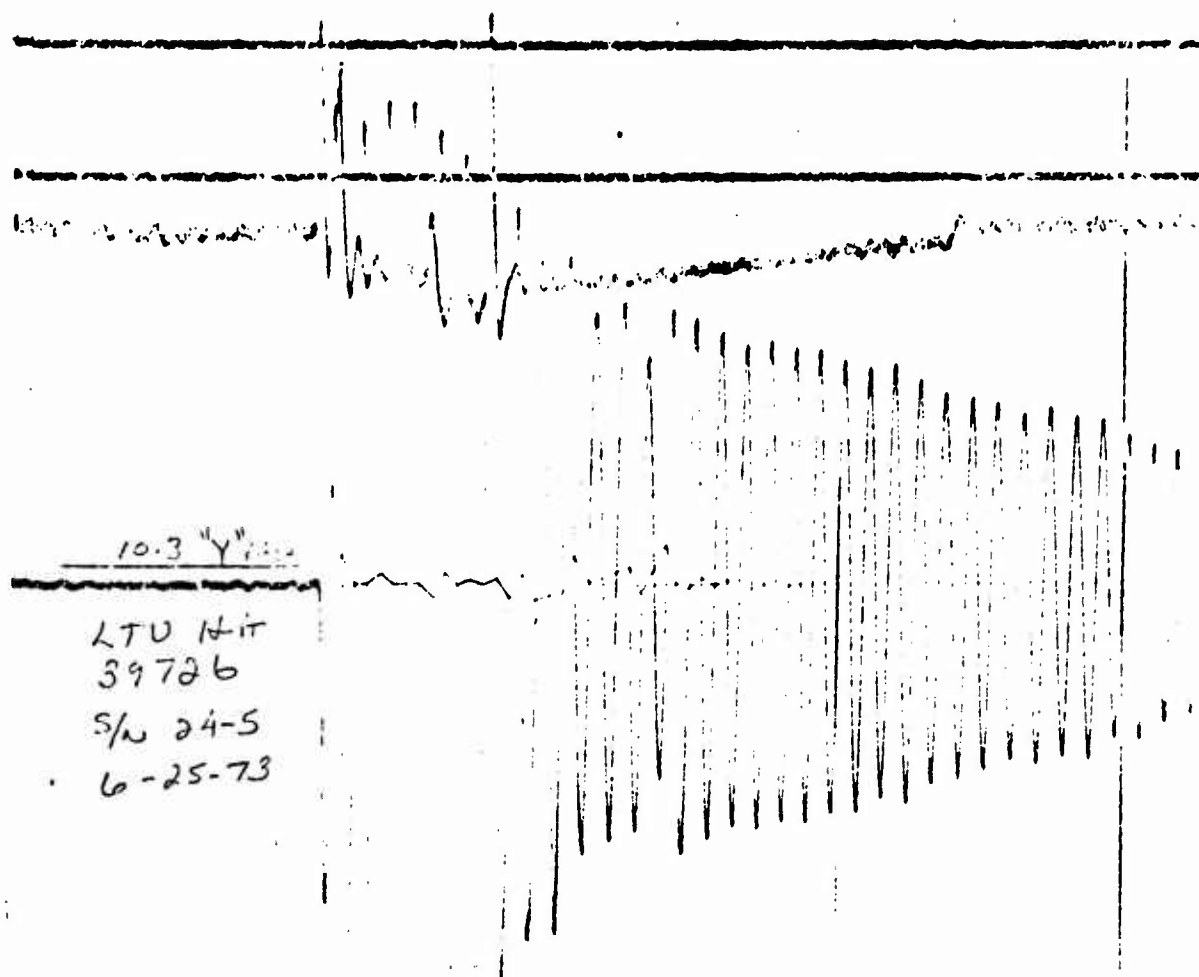
572.1°F

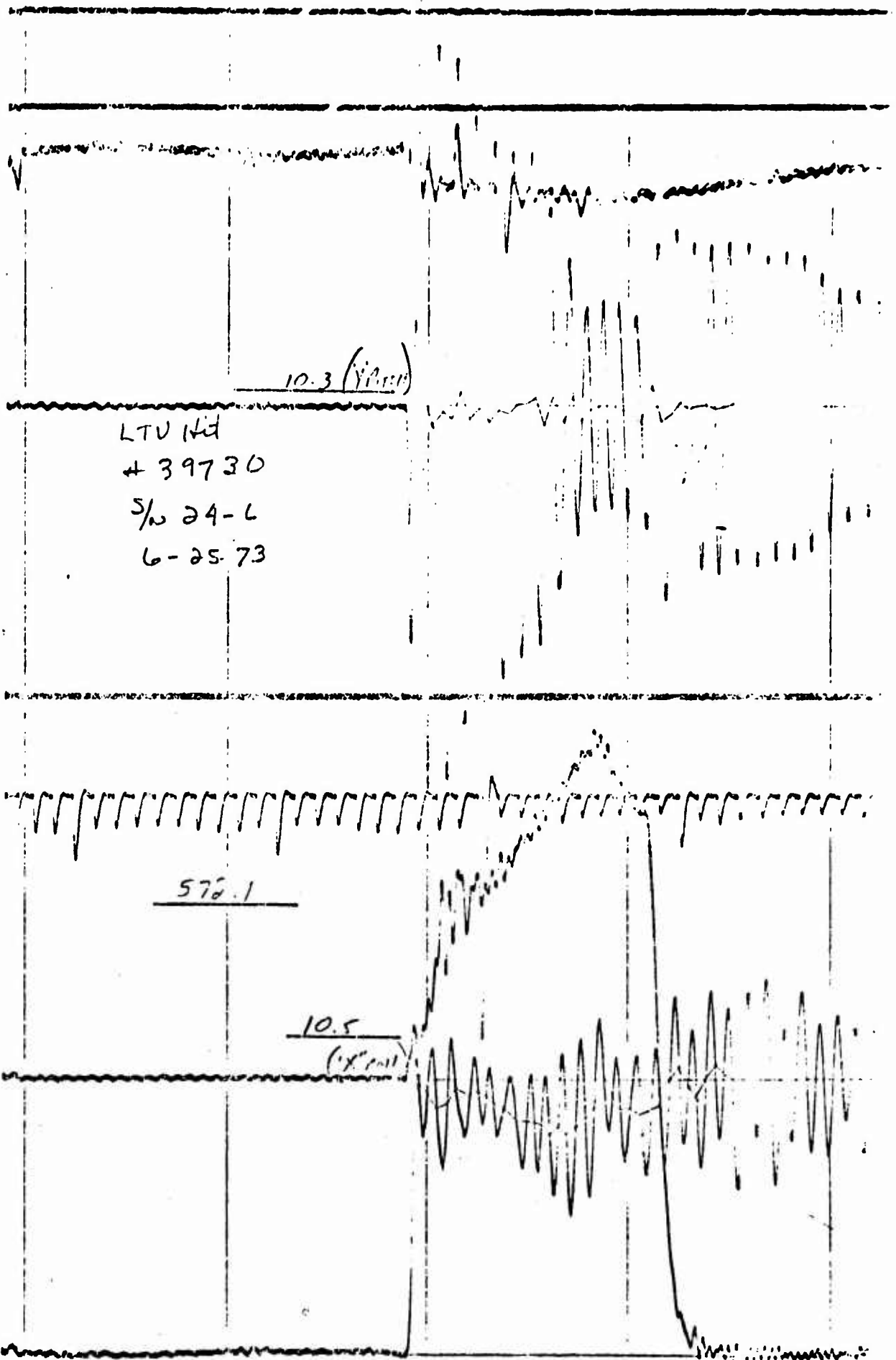
10.5 uV

Y (mV)









LTV Hd
+ 39730
S/N 24-6
6-25-73

10.3 (Y.P. 11)

572.1

10.5
(X.P. 11)

SECTION 4

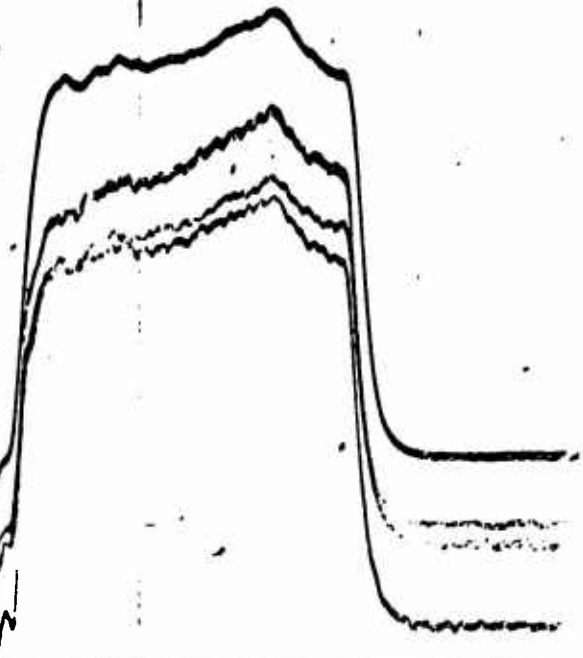
PRESSURE OSCILLATION

1000 μ

LTV Hit
(1-27-73)
39753
S/N 23-122

2000 μ
2000 μ

VSG 1
VSG 2
CL 4 9



1000 μ

1000 μ

750 LBS

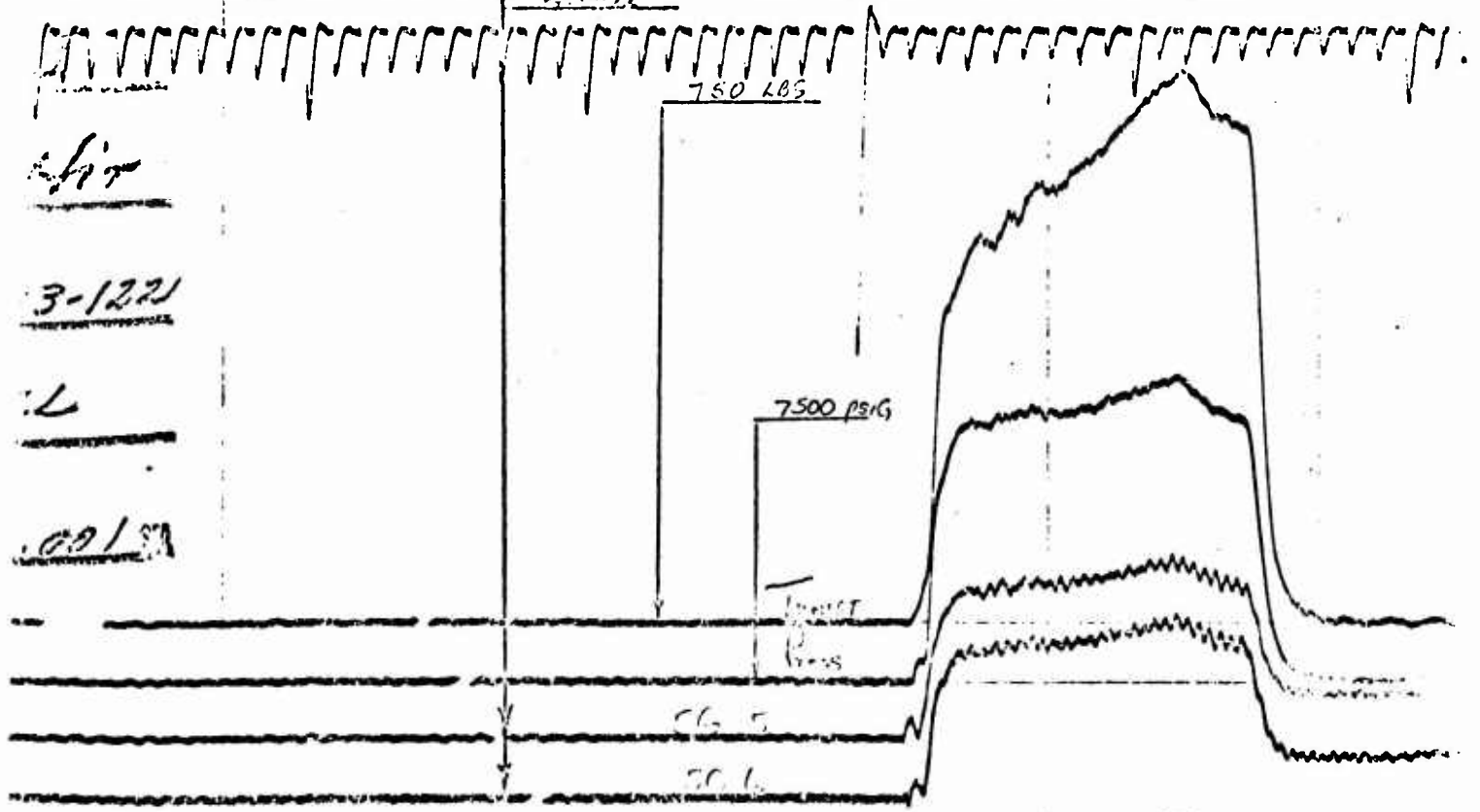
7500 PSI/G

Impact
Press

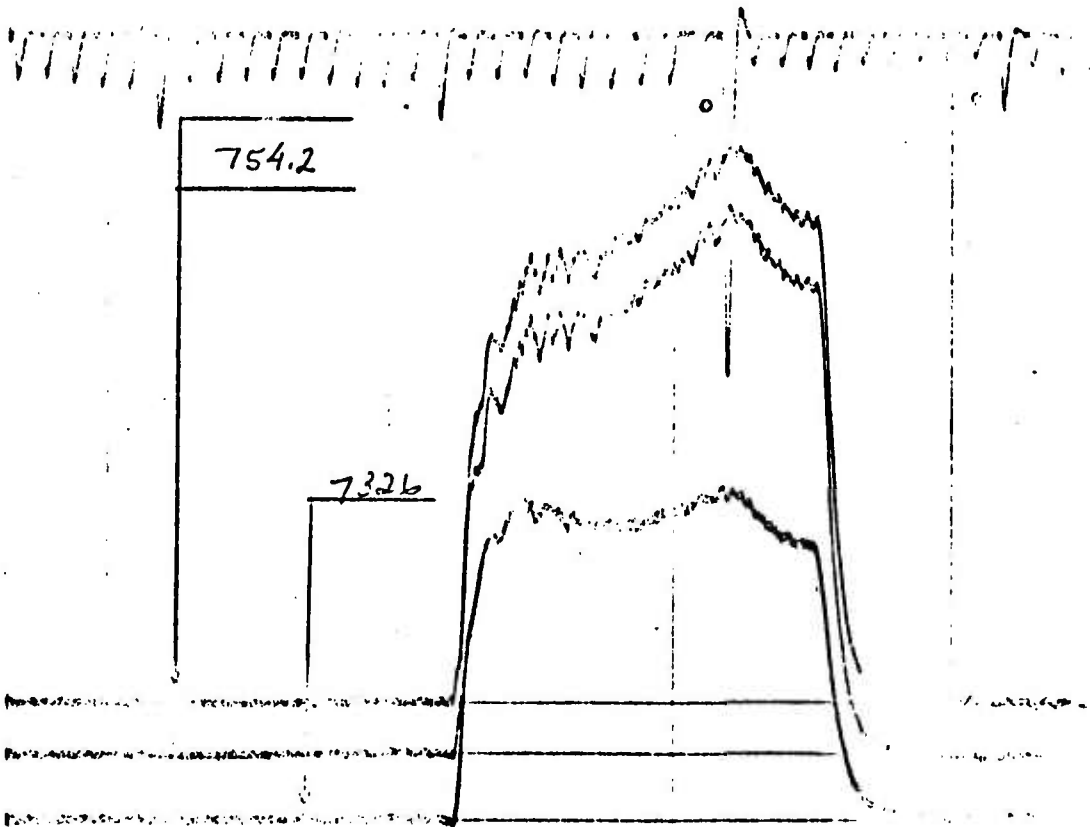
CL 5

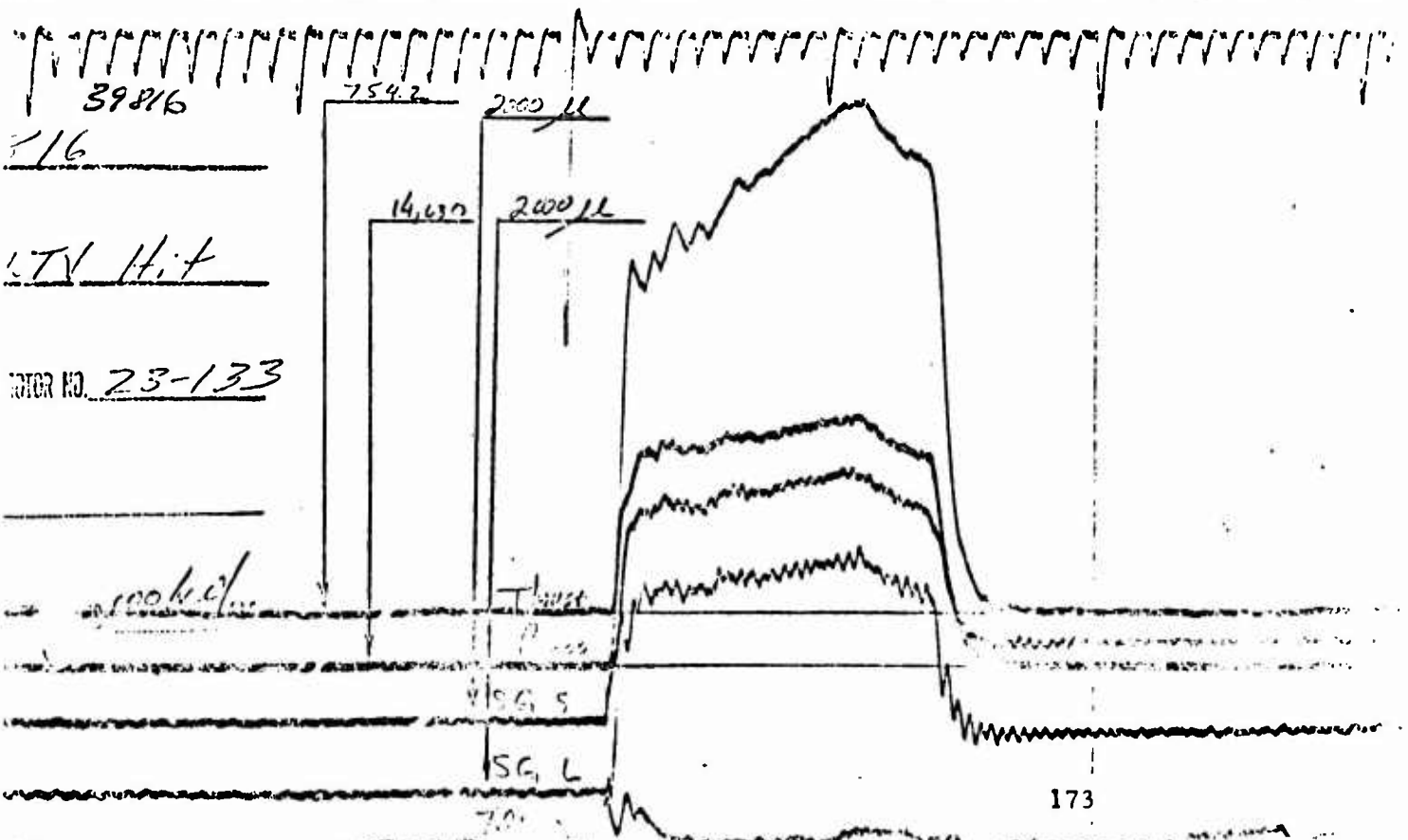
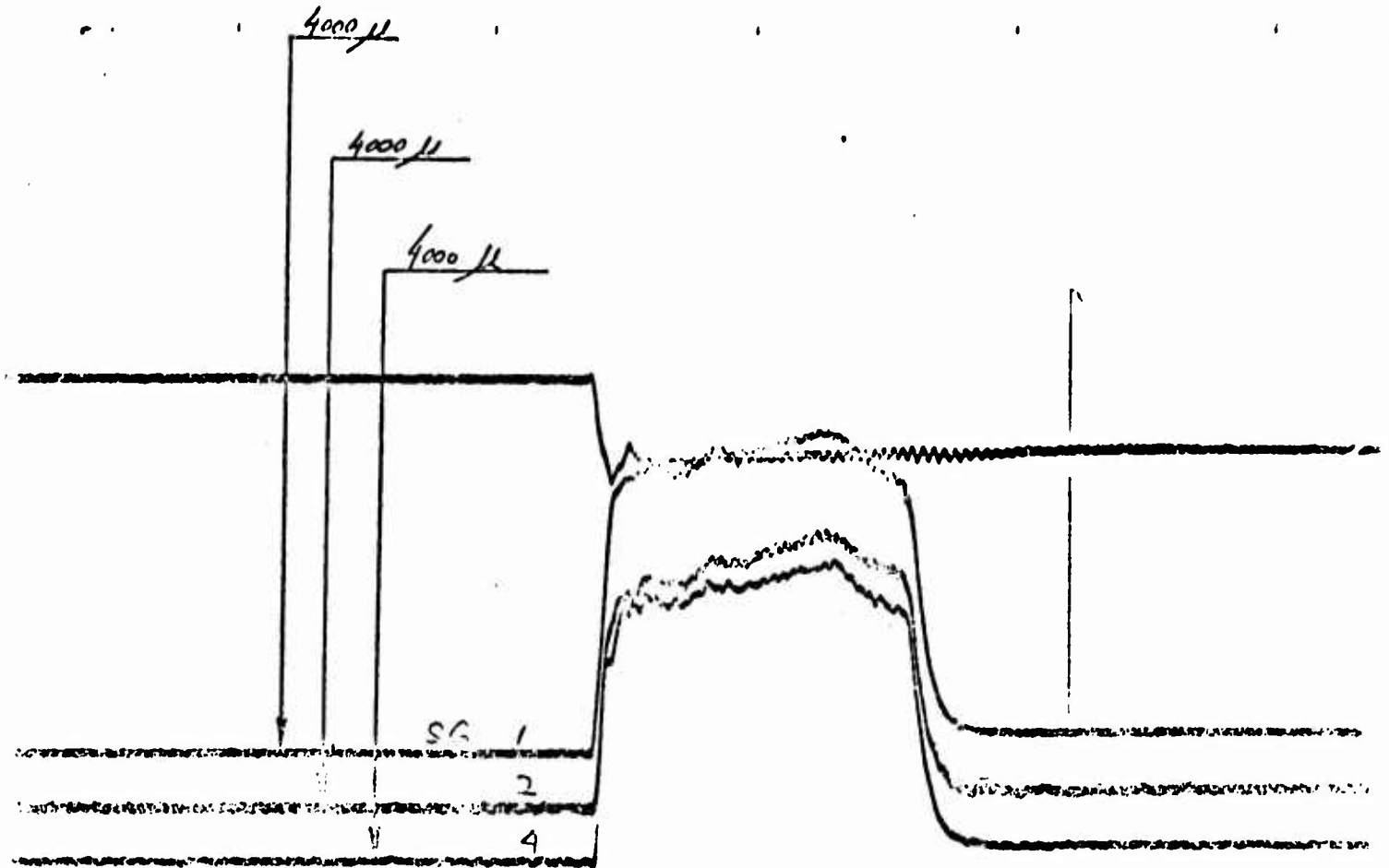
CL 6

Hit
3-122
L
001 SA



LTV Nit
7-3-72
39787
S/n 24-14





16

LTV Hit

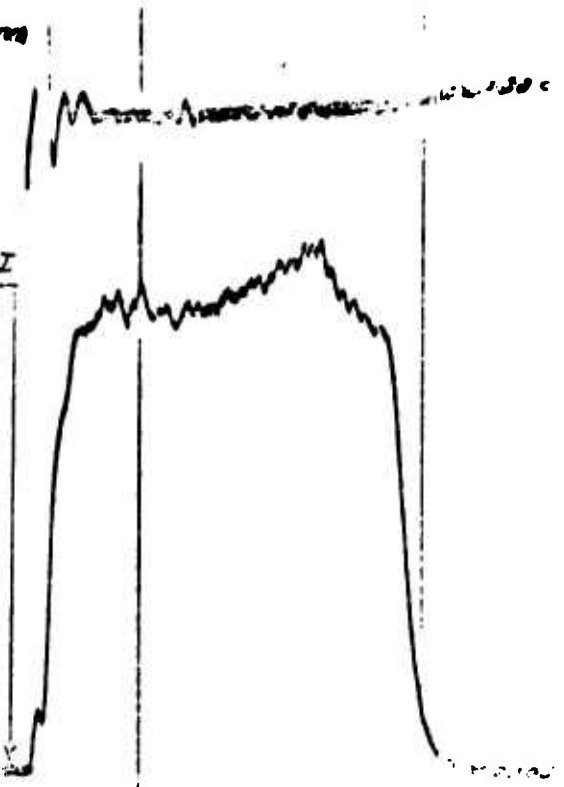
MOTOR NO. 23-133

100 k.c.

39900

7-20-73

7500 PSI



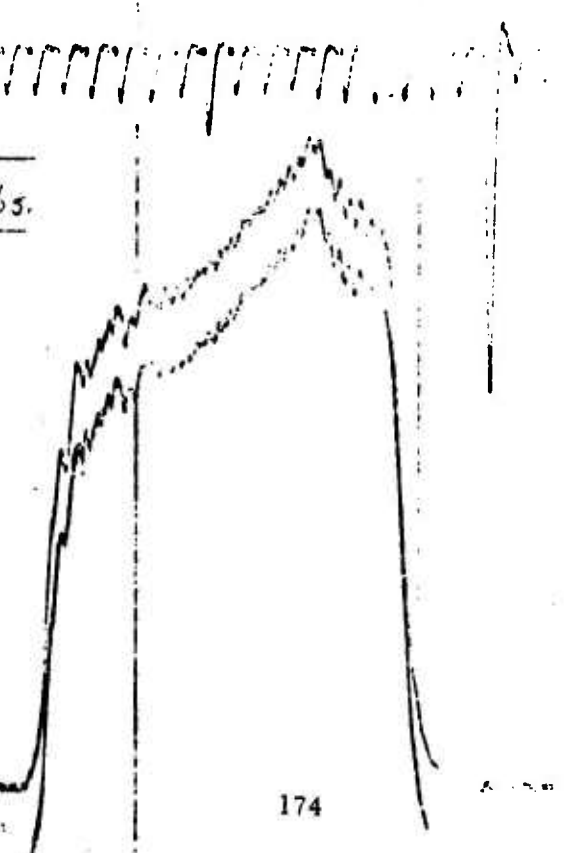
39900

3 - 27V Nit

+7K 25-2

100 1.00 1.53

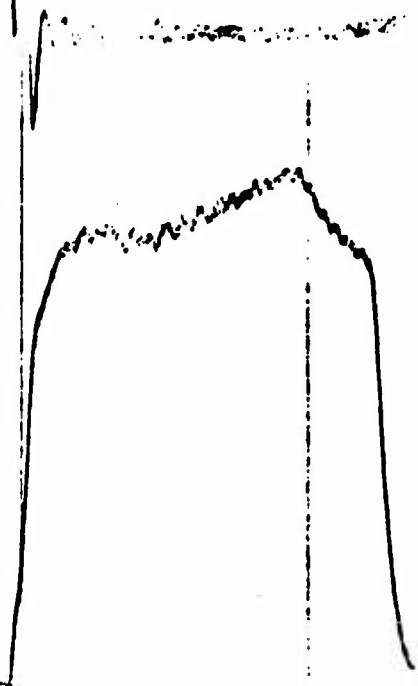
750 lbs.



39902

7-20-73

7500 PSI



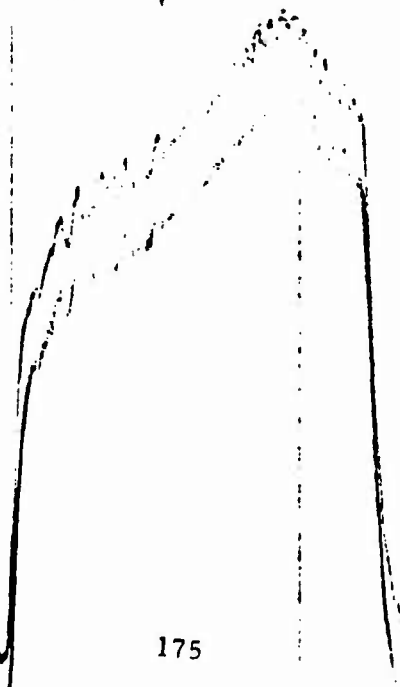
39902

7500 PSI

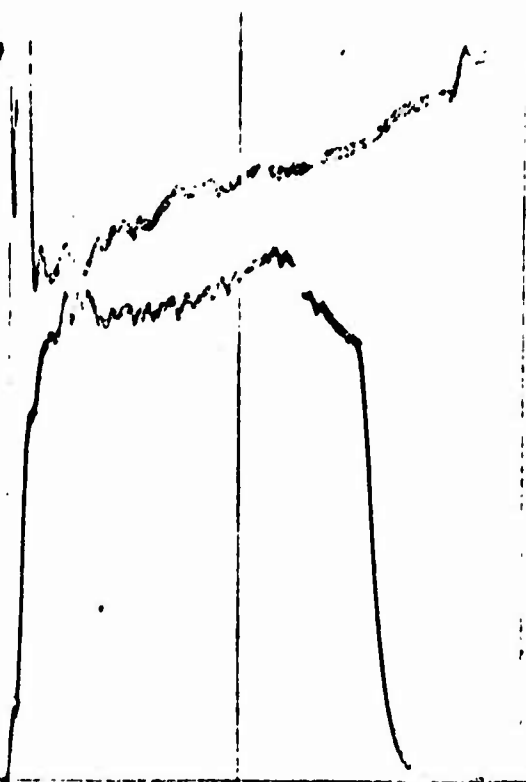
2073 11.7

24 25-4

100 100 100 SEE

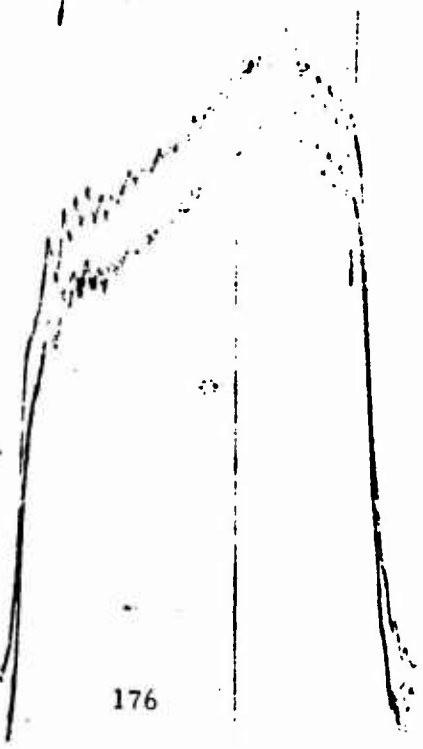


39903
7-20-75
7500 PSI



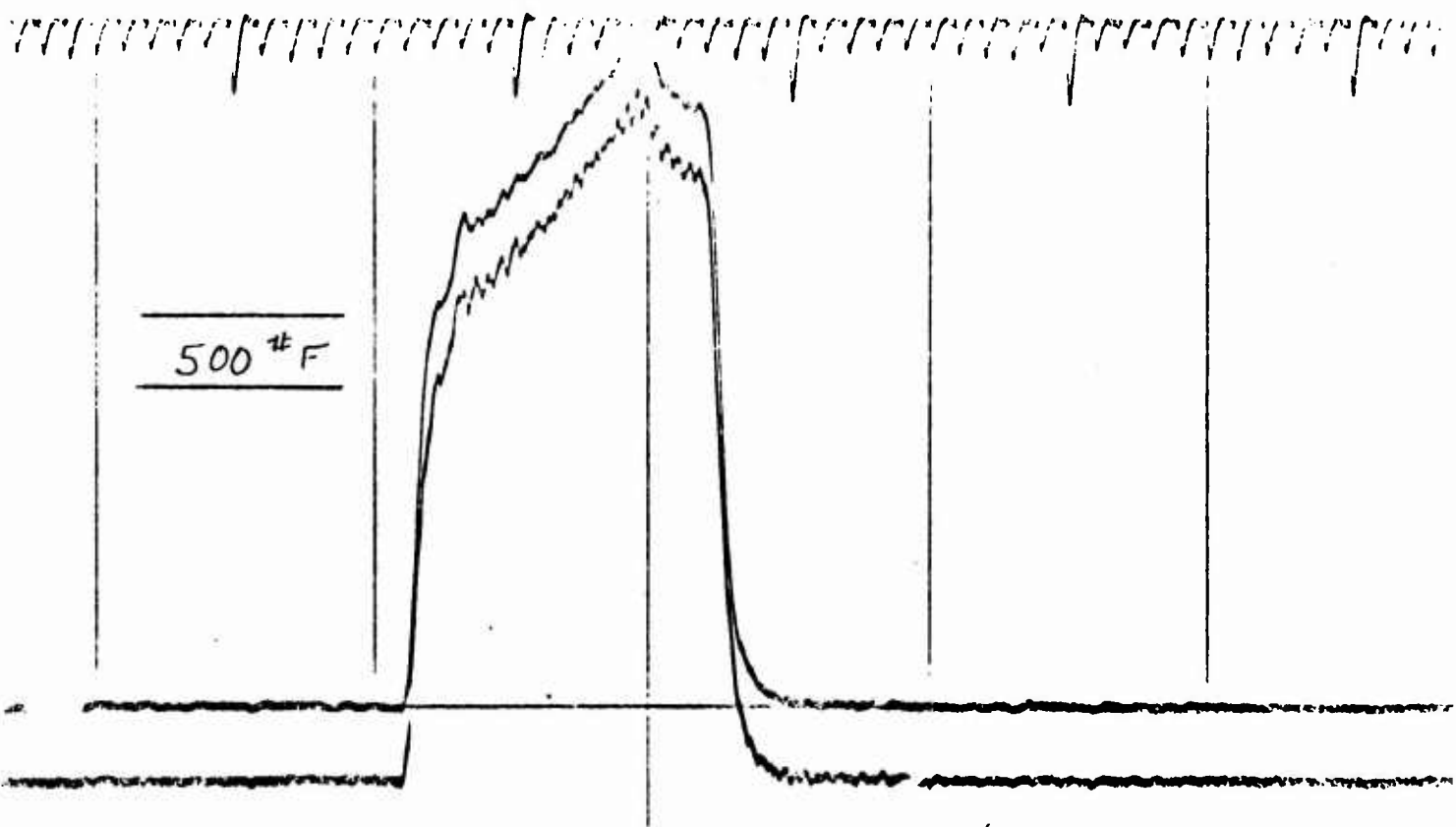
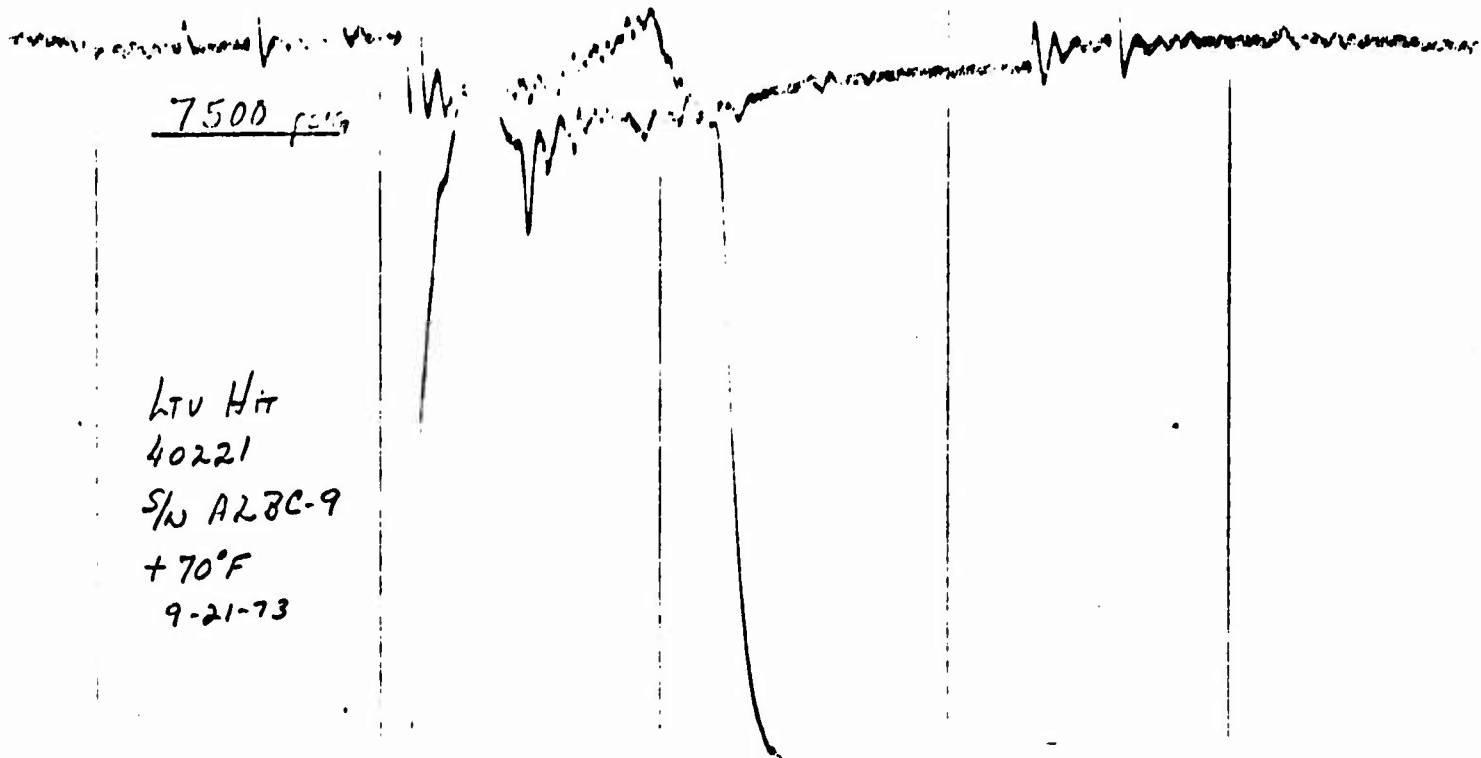
39903
7-20-75 TEST LTV N:7
TEMP 74 PRESSURE 25-5
SPEED 160

750 PSI



SECTION 5

ARRAY BATCH CHECK



7500 psig

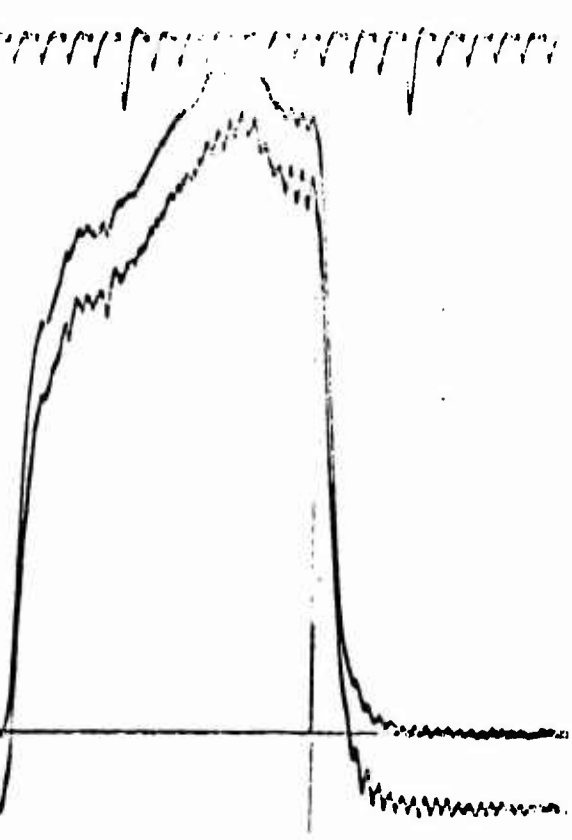


407221

9:17 LTV Plot

500°F

+70 AZ RC-10



160

7500(p.s.i.c.)

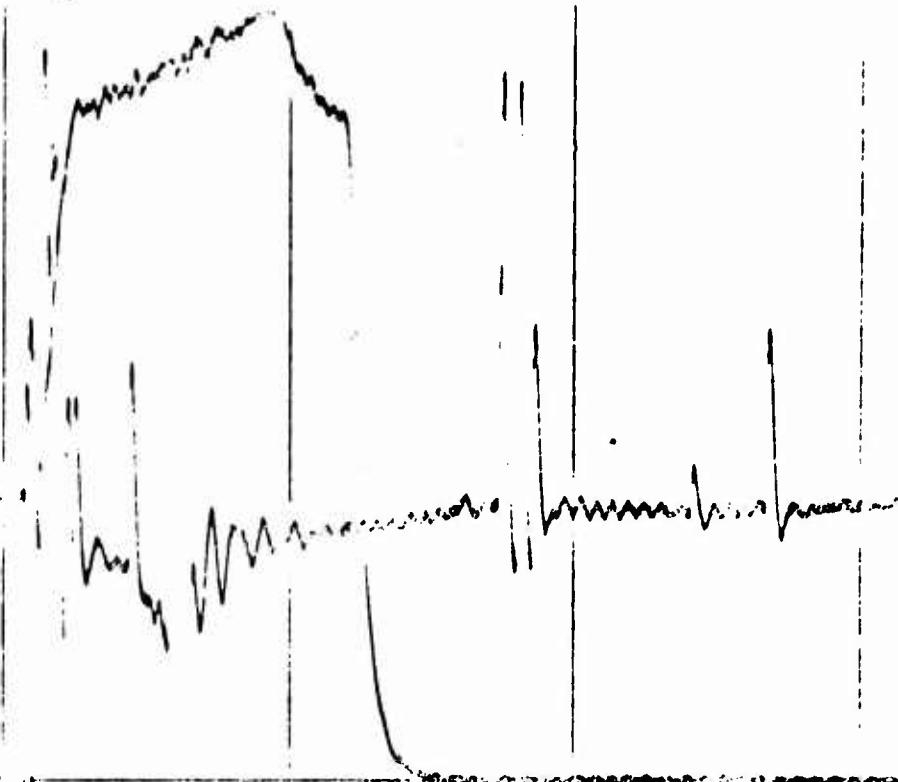
LTU Hit

40223

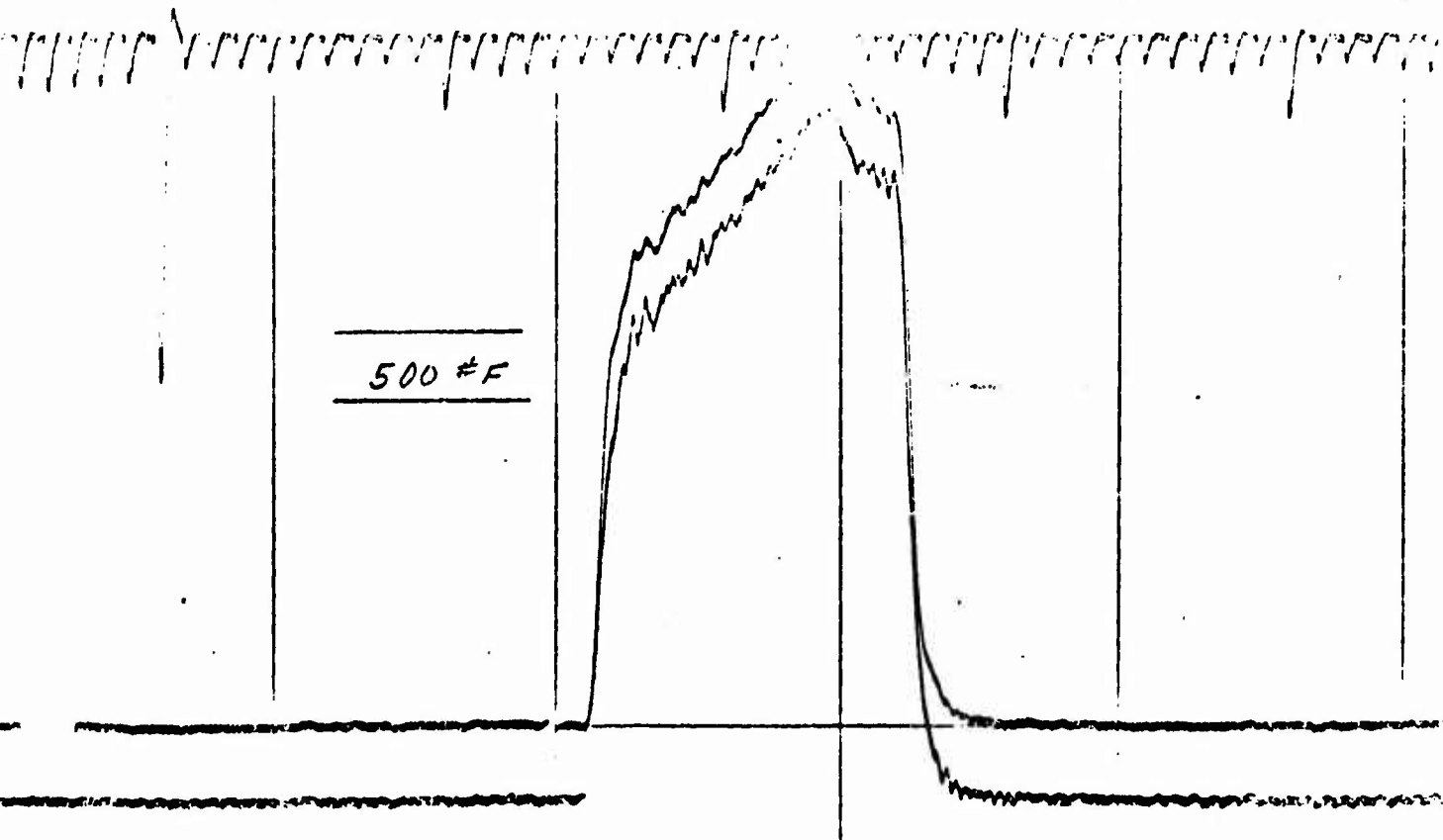
A2 BC-4

9-21-73

-70°F

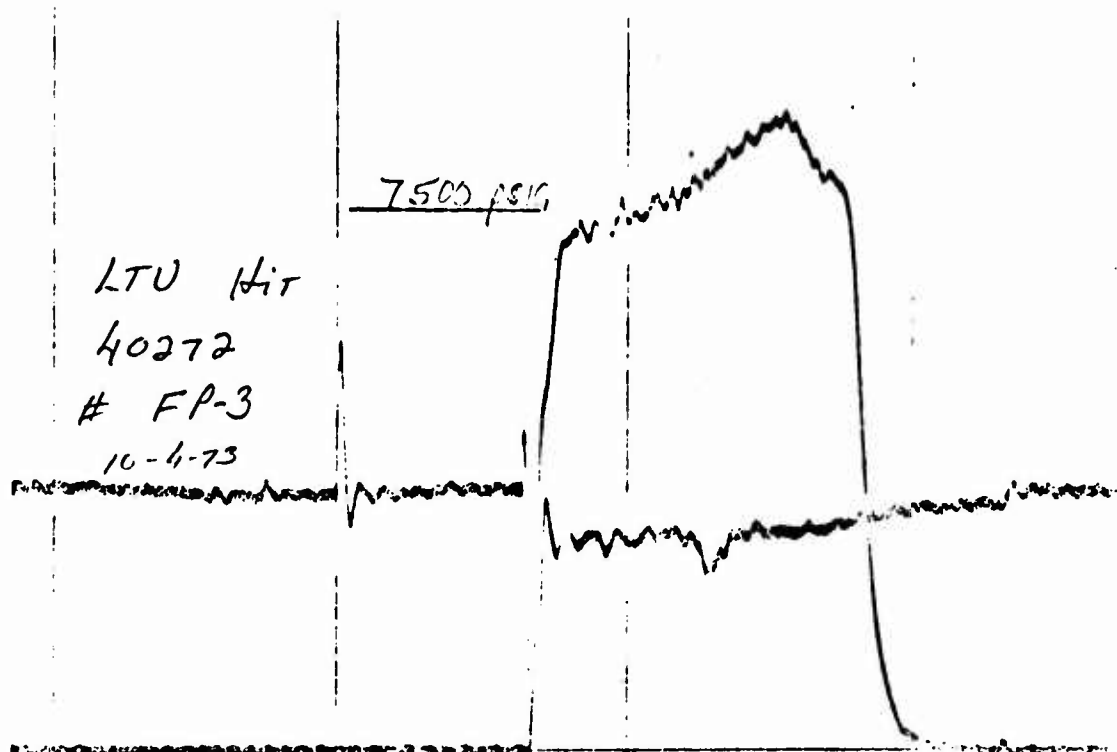


500 #F



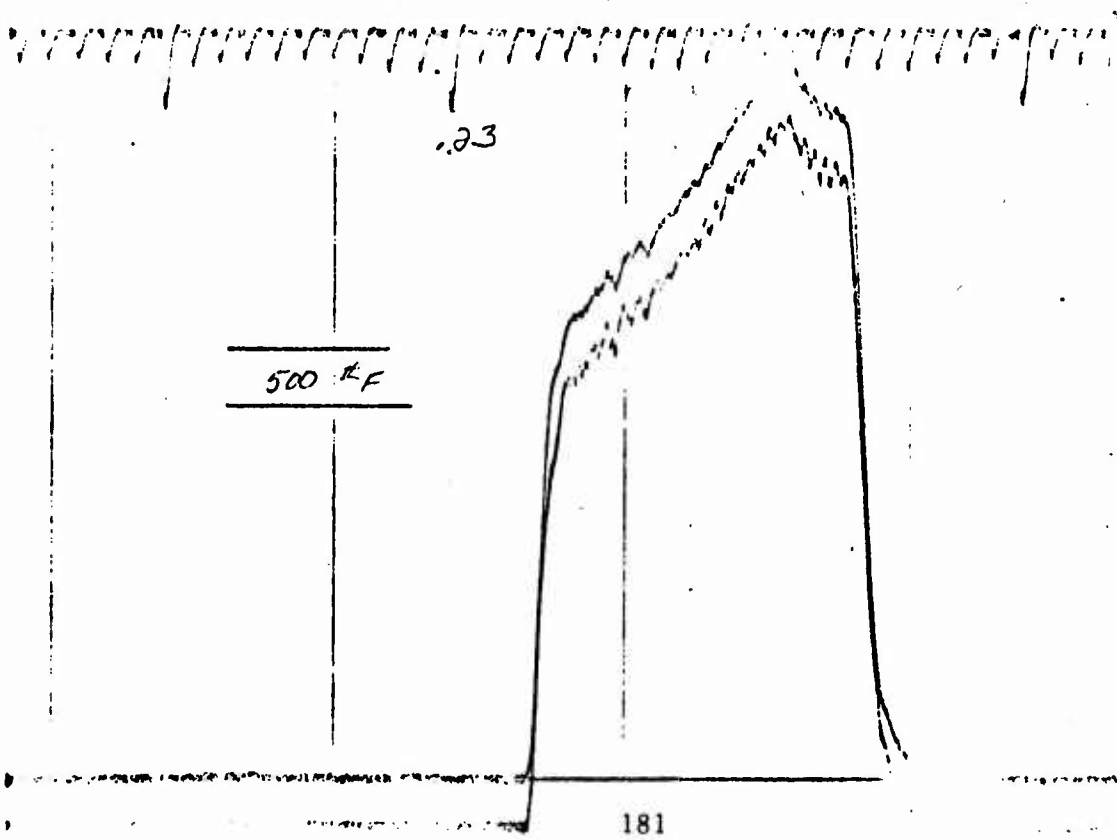
LTU Hit
40272
FP-3
10-4-73

7500 PSI



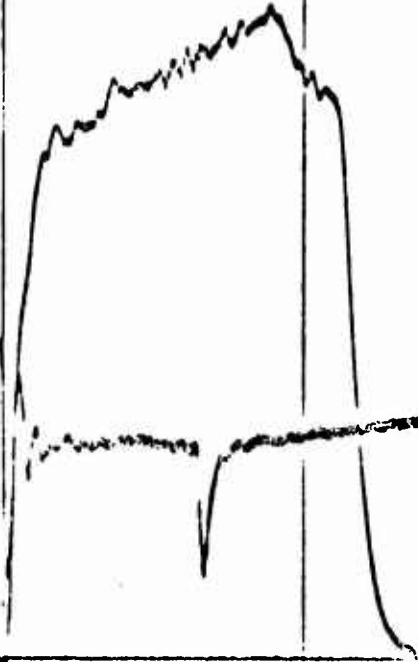
.23

500 KF



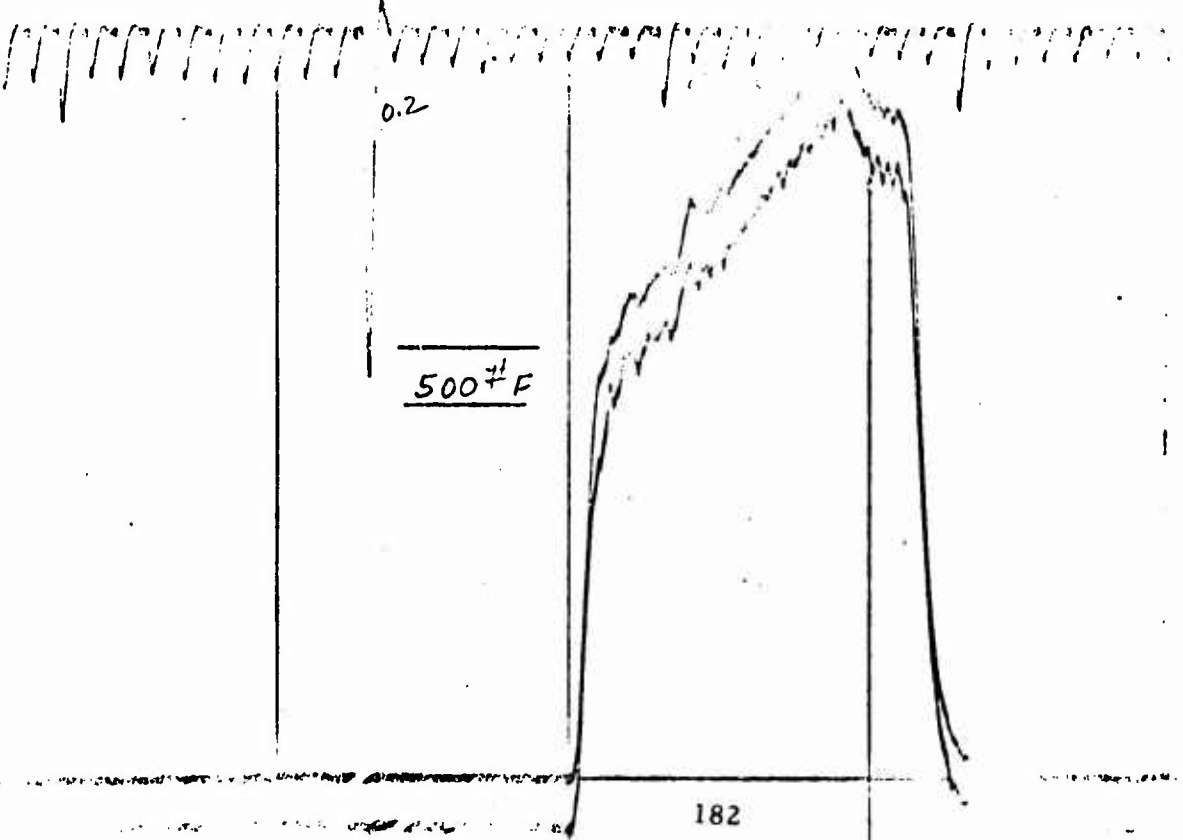
LTV Hit
40274
FP-2
10-4-73

7500 P.P.M.



0.2

500[#]F



SECTION 6

PROTOTYPE MMA

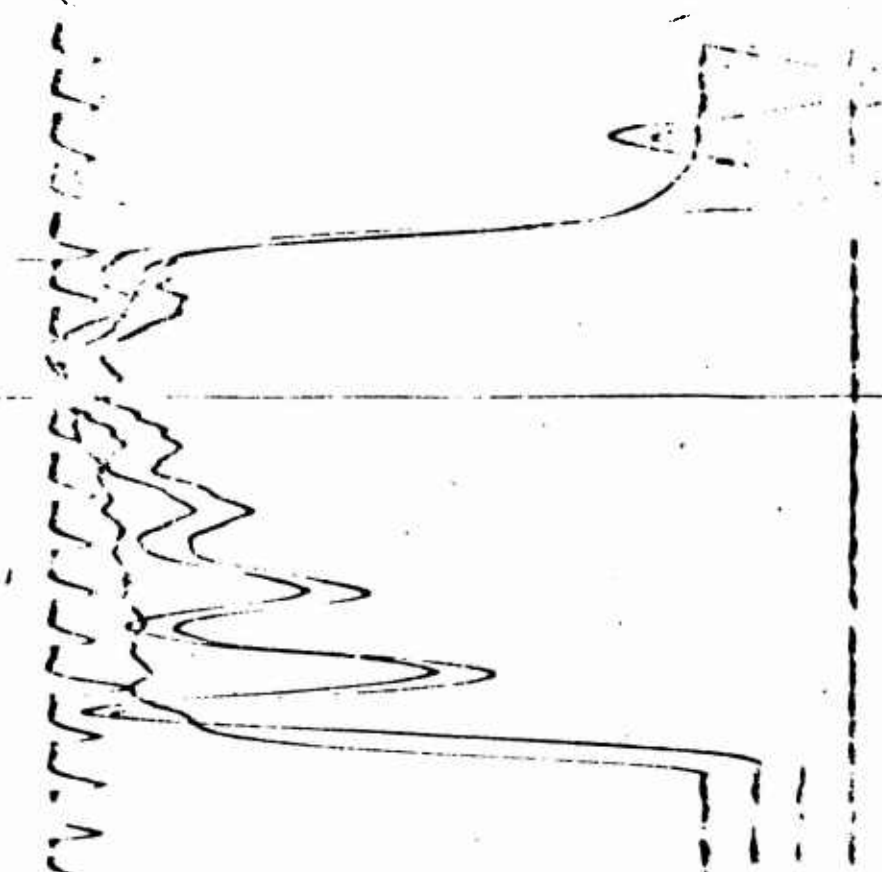
4107012

LTV 1417

+20

160

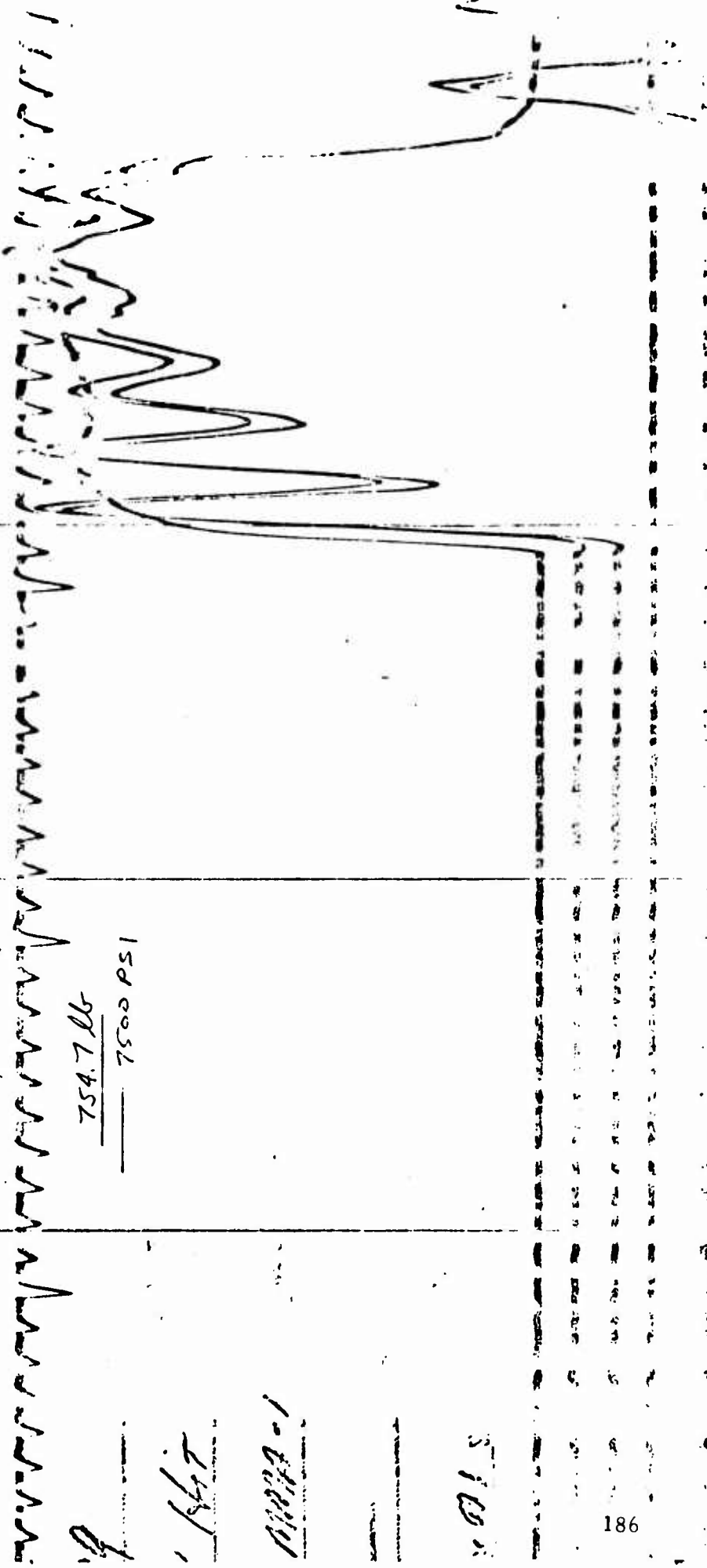
754.7 μ
7500 PSI



40709

754.7 ug

7500 PSI



1987

1867

1867

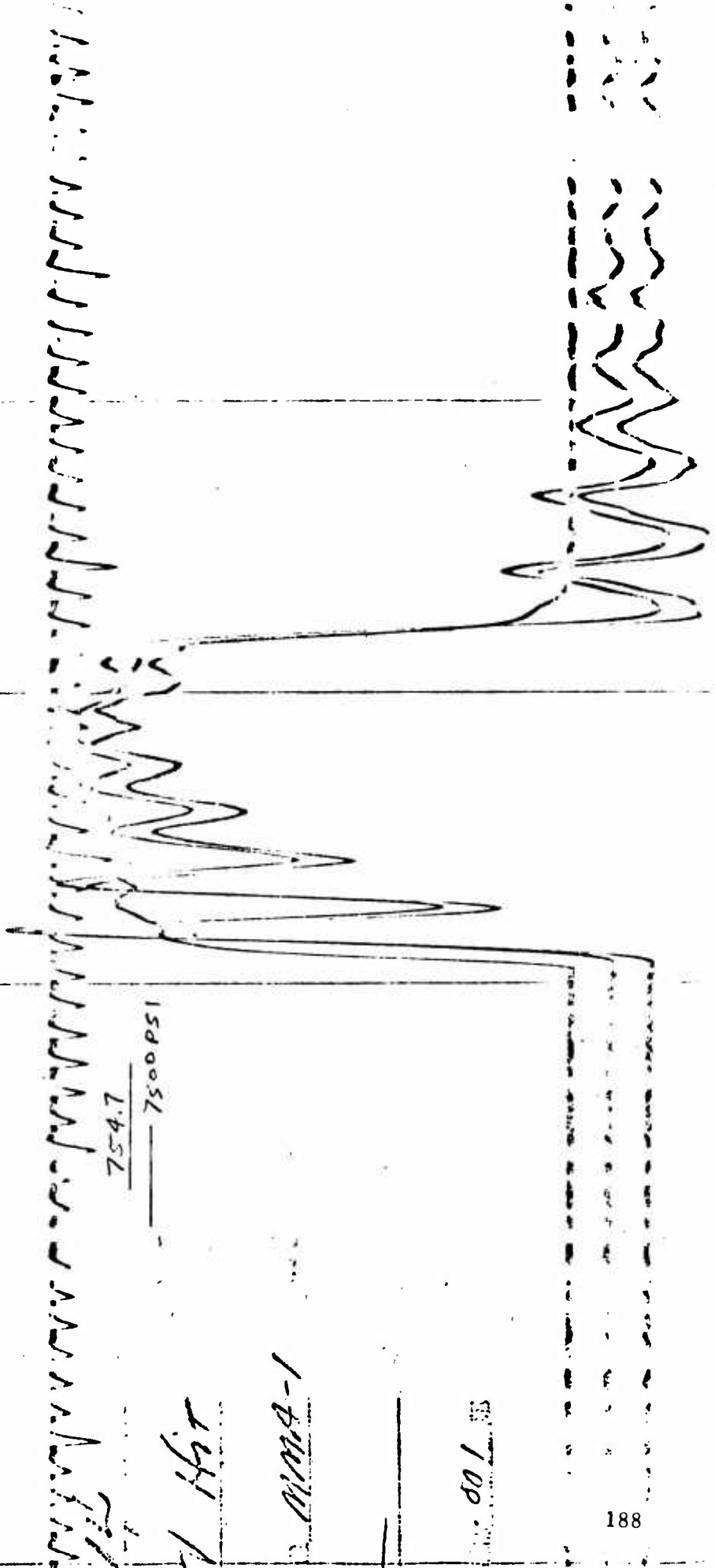
1867

40710

754.7 Mc

— 7500 PSI

40714



754.7
 ——— 7500 PSI

1 Hr

100A-1

100

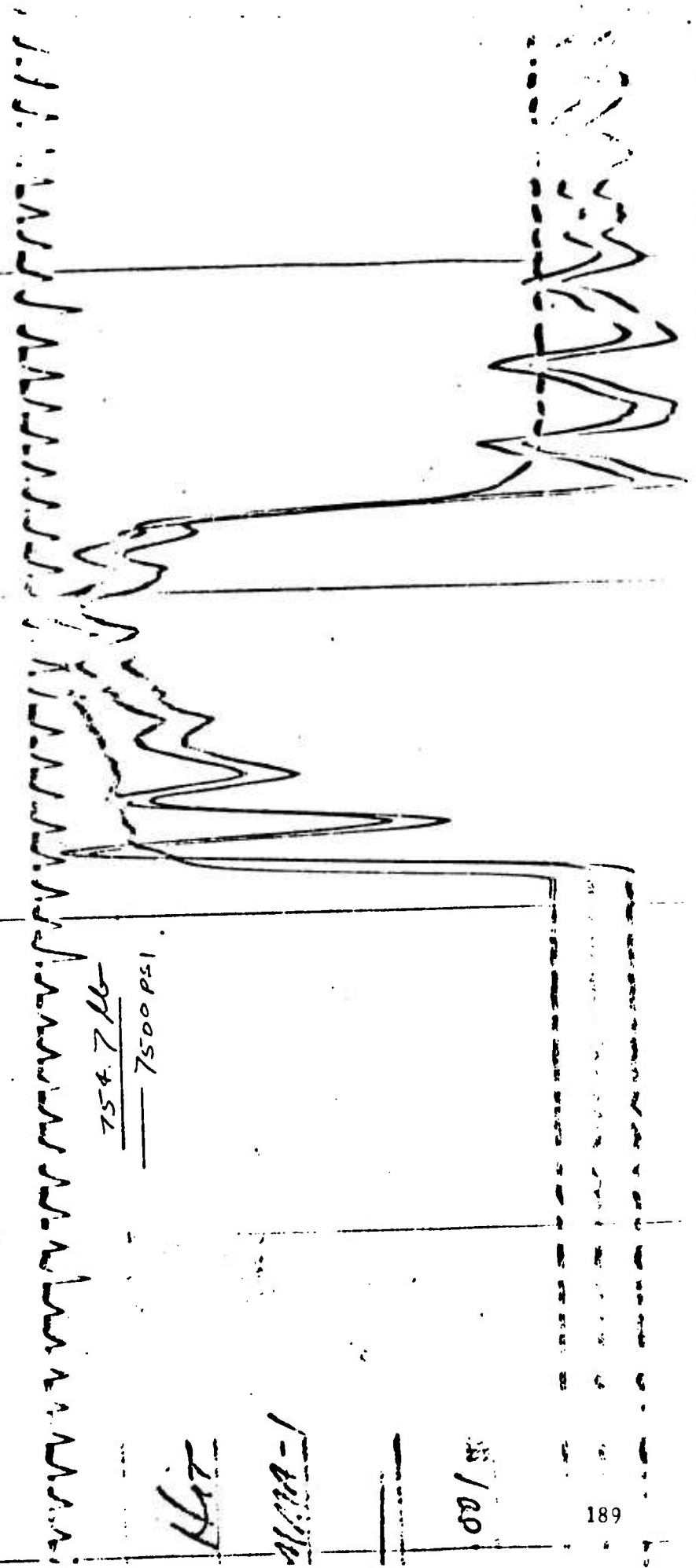
40715

754.7 μ
— 7500 PSI

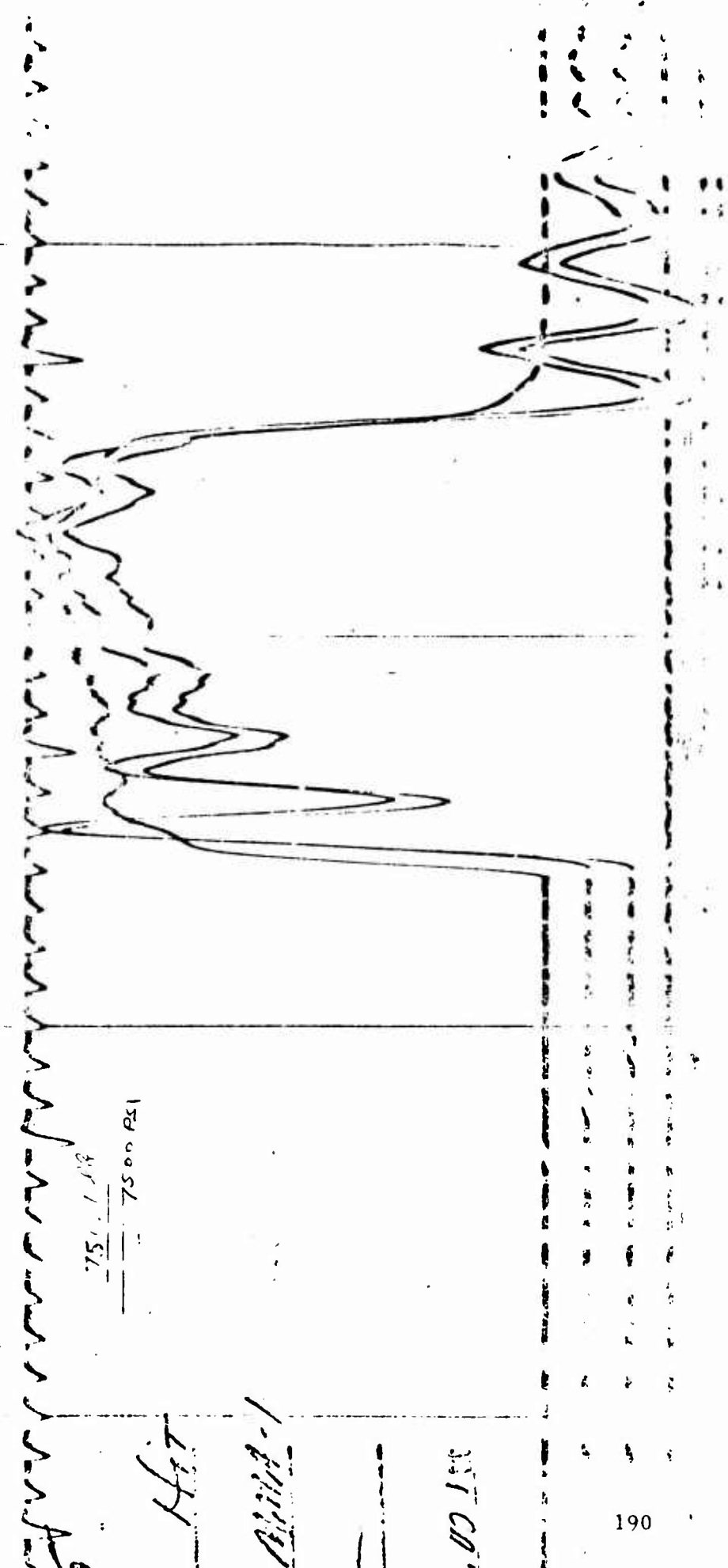
1617

1617-1

100 / 100



40716



75.128
 7500 PSI

40716-1

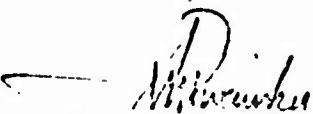
251 CM

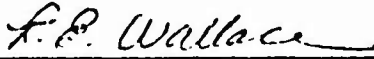
APPENDIX 3

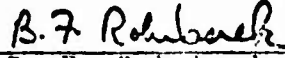
THRUST ALIGNMENT TEST PLAN

TEST PLAN AND PROCEDURE
FOR
THE STATIC MEASUREMENT OF
THE UST VECTOR MISALIGNMENT
IN AN
INDIVIDUAL MOTOR FROM THE
MANEUVER MOTOR ARRAY

PREPARED FOR
VOUGHT MISSILES AND SPACE CO.
Dallas, Texas

Prepared 
I. M. Procinsky
Test Engineer

Approved 
R. E. Wallace
Chief, Test Group

Approved 
B. F. Rohrback
Manager, Hit Project Office

Date 2 June 1972

1.0 SCOPE

This procedure describes the test apparatus, calibration procedures, and instrumentation to be utilized in the static test of individual MMA Motors. It is the purpose of these tests to measure the magnitude of the pitch and yaw moments due to gas-dynamic reactions.

2.0 APPLICABLE DOCUMENTS

VMSC Specifications

3-371-13-0-10186B	- Maneuver Motor Array, Statement of Requirements	20 March 72
3-371-04-0-10185C	- Maneuver Motor Array, Procurement Specification	20 March 72
3-371-TI-P-20021	- Maneuver Motor Firing Circuit	30 March 1972

Military Specifications

AMCR-385-100	AMC Safety Manual	
MIL-C-45662A	Calibration of Test Measuring Equipment	9 February 62

Military Standards

MIL-STD-453 Change Notice 1	Inspection, Radiographic	29 October 62 4 September 63
--------------------------------	--------------------------	---------------------------------

Atlantic Research Corporation Drawings

A0070051	Initiator, Single Squib
A0070057	Alignment Nozzle Body
A0070049-001	Motor Tube, Loaded
A0070049-002	Motor Tube, Loaded

3.0 TEST EQUIPMENT

Equipment to be used in the performance of the specified tests shall be as listed below, and shall exhibit evidence of calibration prior to use in any environmental or functional test.

3.1 Special Test Equipment

3.1.1 Thrust Alignment Fixture - A0070061

3.1.2 Static Calibration Fixture - A0070063

3.1.3 Electronic Level, Maryland Instrument Co. (Prototype)

3.1.4 Load Cell, Model 1810-TMM, Interface, Inc., three component, 1000 lb. axial, 10 in-lb in two orthogonal moment axes.

3.1.5 Firing Circuit Box, VMSC, 371T310004-1

3.1.6 Alignment Plate - A0070058

3.1.7 Load Cell Moment Calibration Fixture, A0070064, A0070065

3.2 Transducer Calibration Standards

3.2.1 Dead Weight Calibrator, accuracy 0.006 percent, Alinco, Model DW 12.5-125

3.3 Ballistic Recording and Computing Equipment

3.3.1 Dynamic Recording System; 12-inch width with record speeds to 160 inches/second; linearity, ± 1 percent full scale, Consolidated Electroynamics Corporation, 36-channel, Recording Oscillograph.

3.3.1.1 Recording Oscillograph, Consolidated Electroynamics Corporation, Model 5-119.

3.3.1.2 Galvanometers, Consolidated Electroynamics Corporation, Types 7-362, 7-363, 7-323, 7-319 and 7-348.

3.3.2 Dynamic Recording System, 12-channel measurement with 6-inch wide analog readout on oscillograph at record speeds up to 50 inches/second; linearity, ± 2 percent of full scale, Heiland Division of Minneapolis Honeywell, Visicorder.

3.3.2.1 Oscillograph, Heiland Division of Minneapolis Honeywell, Model 906C.

NOTE: Used for "quick-look" data.

3.3.2.2 Galvanometers, Heiland Division of Minneapolis Honeywell, Models M3300T, M400-120 and M1650.

3.3.3 Data Acquisition System, Atlantic Research Corporation

3.3.3.1 Electronic Counter, Beckman Corp., Model 7360C.

3.3.3.2 Voltage-to-Frequency Converter, Dymec Corporation, Model 2211BR-M28.

3.3.3.3 DC Amplifier, Redcor, Model 361.

3.3.3.4 Bridge Calibrator, Atlantic Research Corporation.

3.3.3.5 Frequency Standard, Hewlett Packard, Model 100ER.

3.3.3.6 Transducer Power Supply, Computer Engineering, Model PT-214.

3.3.3.7 Galvo Control Panel, Atlantic Research Corporation.

3.3.3.8. Automatic Firing Sequencer, Atlantic Research Corporation.

3.3.3.9 Tape Recorder System, Mincom 3M, Model G114.

4.0 TEST PROCEDURE

4.1 Test Specimen

Since it is the purpose of this test series to evaluate the existence of side components due to gas-dynamic reactions, the test motors duplicate a segment of the last available MMA design in every respect except the precision in locating and aiming the nozzle throat and exit cone.

In order to isolate the gas dynamic effects it was necessary to minimize the geometric errors inherent in the nozzle ring tolerances. A nozzle body was designed to gauge tolerances so that the nozzle throat and cone could be located very precisely on the three component load cell and that a static calibration could be performed.

The curvature of the nozzle ring on the surface adjacent to the exit cone as well as the interface with the motor tubes has not been changed.

The nozzle throat section and exit cone were machined to tolerances about an order of magnitude higher than what the nozzle ring requires.

To maximize gas dynamic effects the short exit cone, duplicating the geometry of the outer ring of motors, is being used.

4.2 Test Facility

The tests will be performed at the Pine Ridge Plant in Gainesville, Virginia. The test assembly will be mounted to a 24-inch cube of steel reinforced cement anchored to the foundation of Firing Bay #3.

A constant temperature of $70 \pm 1^{\circ}\text{F}$ will be maintained by a walled enclosure measuring 8 ft on the side and 7 ft high. This enclosure is insulated and maintained at the required temperature using an air conditioning or heating unit.

The temperature inside the enclosure will be measured and recorded on a strip chart.

4.3 Thrust Stand Description

The thrust stand consists of standoff to separate the nozzle body from the null point of the load cell by a distance equalling the radius of the MMA.

The standoff was made in two parts that can be moved relative to each other so that the nozzle body can be positioned exactly over the null point.

The 3.68 inch separation between the nozzle and null point is necessary because the load cell measures total moment and there would be no way of estimating how much of the resulting moment is due to side component and how much is due to thrust offset. Duplicating the moment arm of the MMA eliminates the need to make this distinction.

The standoff is being made out of beryllium to minimize weight.

ARC Drawing No. A0070061 defines the assembly. The top section can be moved by turning the set screws on the lower section. The two parts are held together with bolts that have a square segment to prevent transmittal of torque to the upper section during the tightening process (ARC Drawing No. A0070062).

5.0 TEST SETUP AND CALIBRATION

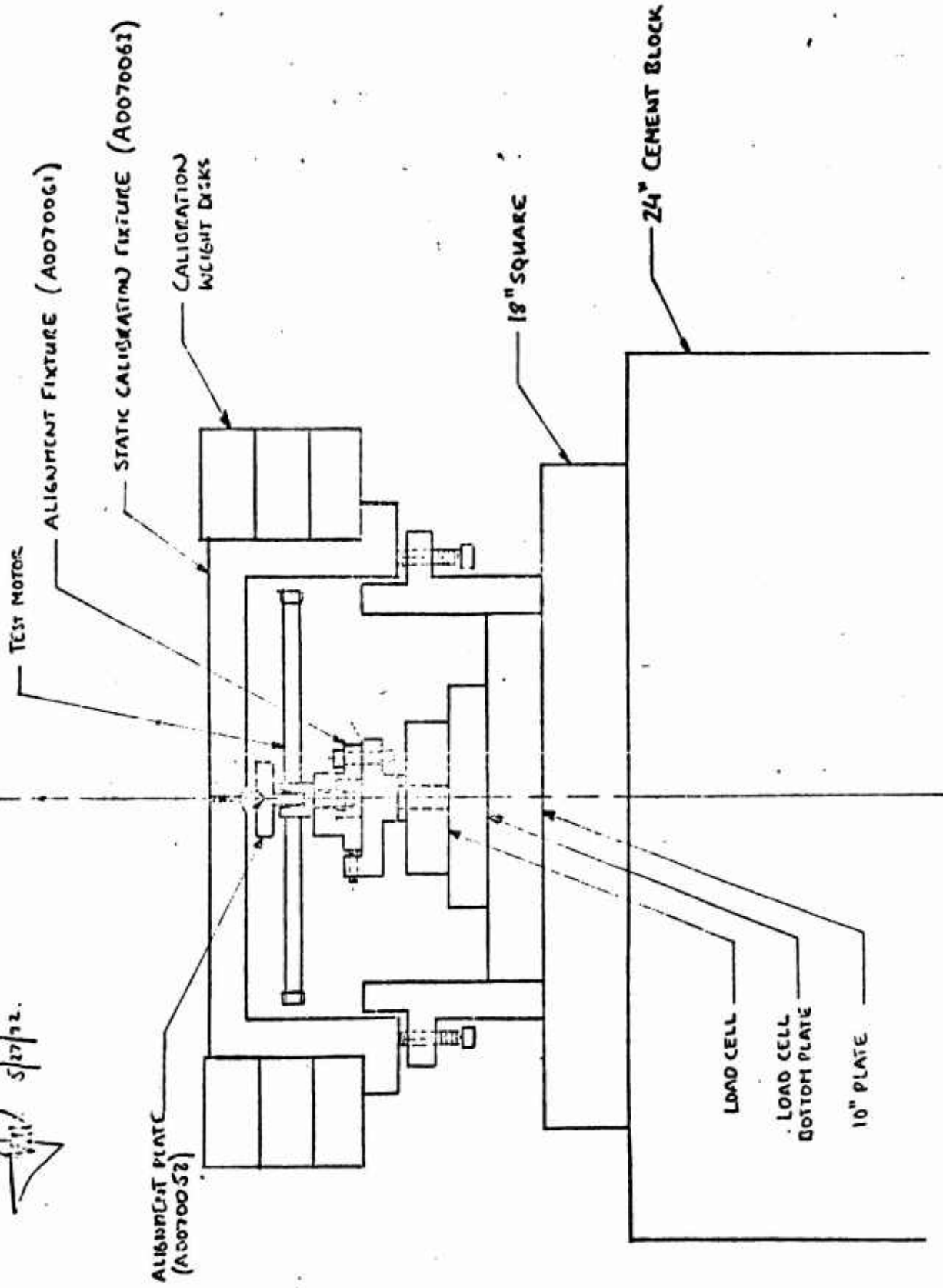
5.1 The test assembly begins with a 18-inch square, 2 1/4-inch high steel plate permanently attached to the cement block. This plate has a clean top surface, flat to .002 inches which will be levelled to whatever precision the irregularities of the surface allow. This serves as the foundation for the test apparatus. Figure 1 on page 6 is a schematic of the test assembly.

5.2 The next component is a 1.5 inch high plate, 10 inches square, which is bolted to the 18-inch square. This plate will have a 32 surface finish. The load cell bottom plate is mounted to the 10-inch plate and the load cell will go on top.

5.3 All attachment bolts will be torqued to constant values to assure repeatability.

Figure 1 : SCHEMATIC OF ALIGNMENT TEST ASSEMBLY

5/27/72



5.4 The top surface of the load cell will be levelled by shimming below the 10-inch square.

5.5 The device used to level the various surfaces is a metal cube with a cylindrical base about 2.50 inches in diameter containing an inverted pendulum. An electronic amplifier reads a signal which is proportional to the gap between the pendulum and an adjacent conductive surface to measure the tilt. The maximum sensitivity of the device is 1.0 seconds of arc per division. It is self-calibrating in that if the surface on which it rests is level, rotation of the base in the horizontal plane will yield a constant reading which can be taken for the level null point.

5.6 The thrust standoff threads into the load cell and the test motor nozzle body fits into a sleeve in the top section of the standoff.

The level of the nozzle body will be checked. Any tilt that is apparent will be corrected by shimming the surfaces between the upper and lower parts of the standoff.

5.7 The final measurement of nozzle axis alignment will be performed by inserting the alignment plate and plug into the nozzle throat until it bottoms. This plug will have been machined to be a match fit into the nozzle throat so that no appreciable movement between the two parts is possible. The top surface of the alignment plate is flat and perpendicular to the plug within .00005. This surface is the final reference in aligning the test motor. Once it has been levelled we know that the nozzle is vertical to within 5 seconds of arc. Any required shimming will be done between the two parts of the standoff.

5.8 At this point the test apparatus is level and symmetrical and all that remains is to adjust the position of the upper portion of the standoff laterally until the two moment bridges have been nulled indicating that the center of gravity is over the null point.

5.9 If necessary the levelling and lateral adjustments will be repeated until the structure is aligned.

5.10 As shown in Figure 1, four support posts, spaced 90° apart, are bolted to the 10-inch square plate. These supports provide a means for centering and gradually lowering the calibration weights onto the alignment plate.

5.11 The main calibration weights rest on a cradle. The cradle contains a conical depression at its center. The weight is transmitted to the alignment plate through a half-inch ball bearing which fits into the depression on the cradle and a matching depression in the alignment plate which is concentric with the plug to within .0001 inches.

5.12 Initially the cradle will be supported more than half an inch above the top of the alignment plate by set screws on the support posts. The cradle will be centered visually over the alignment plate through a hole concentric with the conical depression.

5.13 One of the weight disks (≈ 85.00 lbs) will be placed on the cradle, and the ball bearing inserted in the hole on the alignment plate.

5.14 The cradle will be gradually lowered until it rests on the ball bearing.

5.15 The ball bearing will allow the calibration weight to tilt until its center of gravity is directly below it so that any

asymmetry in the weight does not produce a moment on the load cell. Ideally the calibrating mass will settle with its center below the support point so that the gravity vector is being applied to the nozzle axis and the position of the nozzle can be adjusted laterally until the moment bridges have been nulled again. Within the limits of machining tolerances, this means that a perfectly vertical force vector has been nulled out and if the thrust output of the motor is parallel and concentric with the nozzle throat, the load cell moment bridges will read zero.

These tolerances translate into a possible uncertainty of .12 in-lb for misalignment and .60 in-lbs due to offset if a worst condition of 10 seconds of arc and .001 inch concentricity errors are assumed.

5.16 The ball will be lubricated but calculations show that the effective coefficient of friction may produce 0.5 to 1.0 in-lbs of friction load. However by allowing the weights to oscillate and by rotating them, several measurements can be taken to determine the variability and range of this effect. If necessary the weight will be positioned so that the moment bridge reads the mean value.

5.17 At this point the repeatability with which the weights are applied can be checked by removing the weight and reapplying it.

5.18 The precision of the alignment plate will also be checked by removing the weights and rotating the alignment plate before reapplying the weights.

5.19 To facilitate the removal of the plug and to prevent damaging the nozzle throat, liquid nitrogen will be poured down the center of the alignment plate before the plug is moved.

5.20 The position of the nozzle body will be adjusted to null out the moment bridges and the weight will be removed.

5.21 The level of the alignment plate will be rechecked.

5.22 Steps 5.12 through 5.21 will be repeated with first two and then three weight disks. This will show whether the additional load produces any asymmetrical deformation in the test apparatus.

5.23 By this process the total variability of the static calibration procedure will be defined.

5.24 The calibration of the axial load bridge will be performed on the Alinco Dead-Weight Machine. This bridge will be calibrated to 1000 lbs before and after each test series in accordance with our standard operating procedures.

5.25 During this calibration the two moment bridges will be monitored to ensure that they are not overloaded and to get a measurement of the cross-talk due to axial load.

5.26 The physical calibration of the moment arms will be performed by applying a dead weight of one, two and five pounds to a horizontal beam inserted into the sleeve on top of the standoff. (See Drawing A0070065.) The beam will have a span of 20 inches so that moments of 10, 20 and 50 in-lbs on either side of the null point can be produced.

5.27 Interface will define the two orthogonal moment planes on the load cell. ARC will perform the calibration in these two planes and two additional planes at thirty and sixty degrees from the moment bridges as a further check on their accuracy.

5.28 The vertical position of the null point will be defined by applying a horizontal load of known magnitude through a dead weight suspended by a string through a pulley (see Dwg. A0070065). This will confirm the value supplied by Interface.

5.29 The top of the nozzle body will be struck gently with a rubber mallet and the resulting bridge output recorded to measure the natural frequency of the system and to get an idea of magnitude of the oscillations.

5.30 The entire calibration process will be repeated before each test.

6.0 DATA ACQUISITION SYSTEM

6.1 Transducer

The only transducer used in this test will be an Interface Inc., Model 1810-TMM Load Cell. This unit contains one metal strain-gauge sensing bridge for axial thrust, rated at 1000 lbs and two orthogonal semiconductor bridges for moments, rated at 10 in-lbs. The signal level out of all three bridges is 2MV at rated capacity, but both moment bridges have a linear output up to 100 in-lbs and can take an overload to 500 in-lbs. Excitation voltage is 10V. All three bridges are powered by independent high quality power supplies.

6.2 Recording Instrumentation

The signals are fed through individual shielded cables to the data system where they enter chopper-stabilized dc amplifiers. The amplifier output is then routed to the analog and semidigital recording systems. Figure 2 shows the basic instrumentation components.

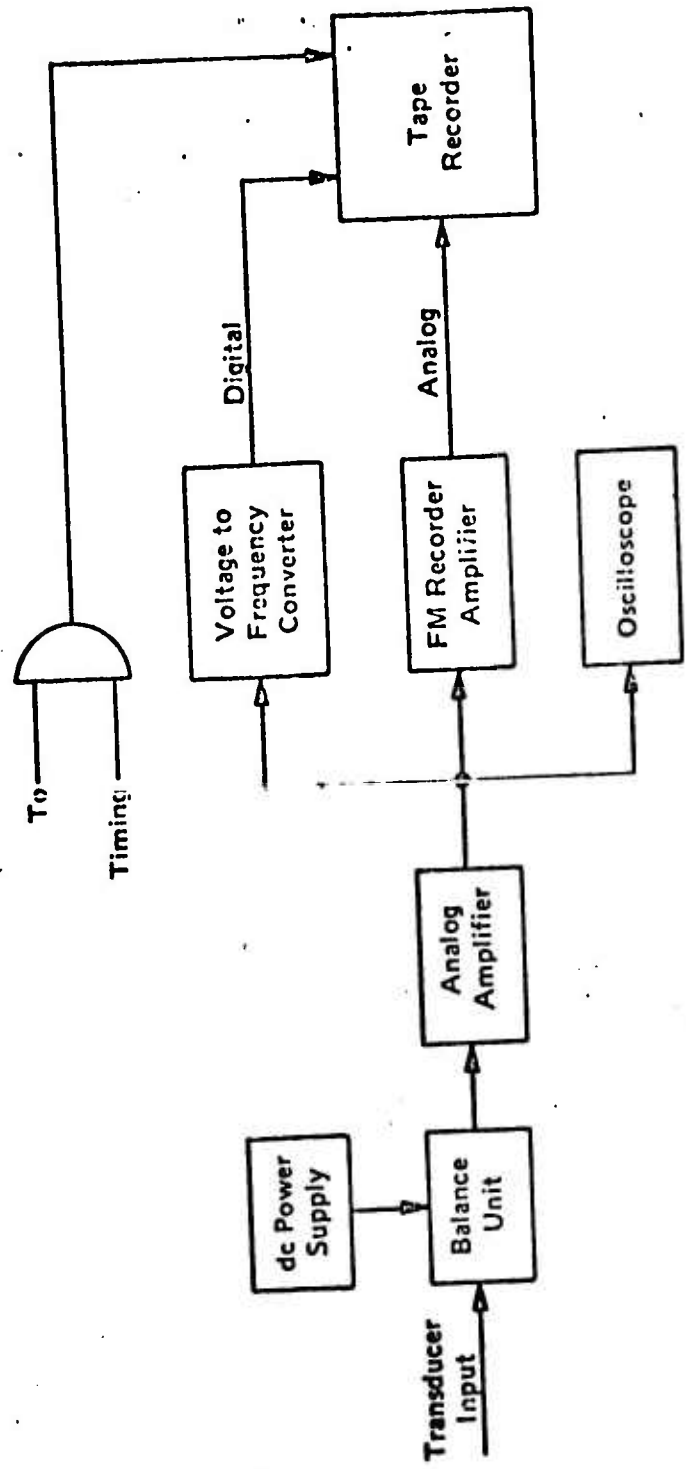


Figure 2 Record Instrumentation.

Because of the short functioning time two separate analog recording systems will be utilized for these firings. The signal will be recorded on CEC recording oscillographs operating at a speed of 160 inches a second. This will be utilized only for preliminary timing information because a 10-millisecond firing will yield only a 1.6-inch long record.

The second analog data recording uses a 3M MINCOM FM tape system. Analog signals will be recorded on this system at a magnetic tape speed of 60 in/sec. They will be played back onto recording oscillographs at a tape speed of 15 in/sec with the FM amplifiers adjusted and filtered accordingly. This difference in recording versus playback speeds will result in a 4/1 extension of the oscillograph recordings and will yield a 6.5-inch firing trace. By carefully recording calibration steps on the FM system immediately prior to firing, the data can be handled without any significant loss in accuracy. Calibrated timing will also be put on the tape so that it will appear on the expanded record at the proper intervals. A schematic of the data playback system is shown in Figure 3.

The semidigital data system is used primarily for the recording of the integral values which can be used to secure averages over selected time spans. In this system the data signal is converted into a series of pulses. These pulses range from 0 to 100,000 per second for full scale. This frequency converter is a true integrator in that it actually follows the input signal with no averaging or sampling. In terms of an analog curve, it follows the curve and emits pulses as equal area bits under the curve have been traversed. Thus, oscillations on a thrust-time curve do not affect the accuracy of the impulse measurement.

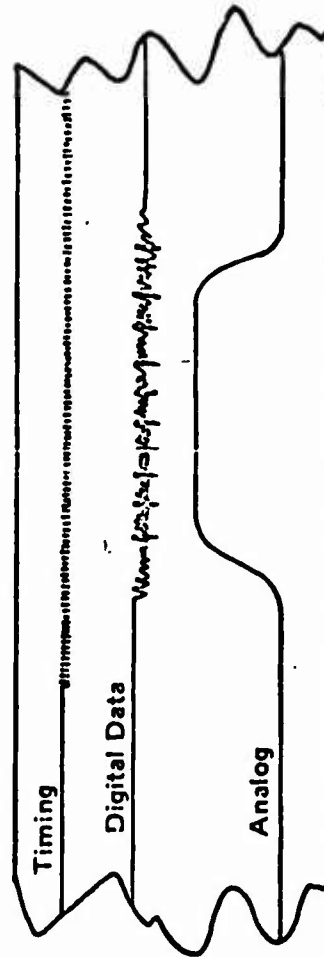
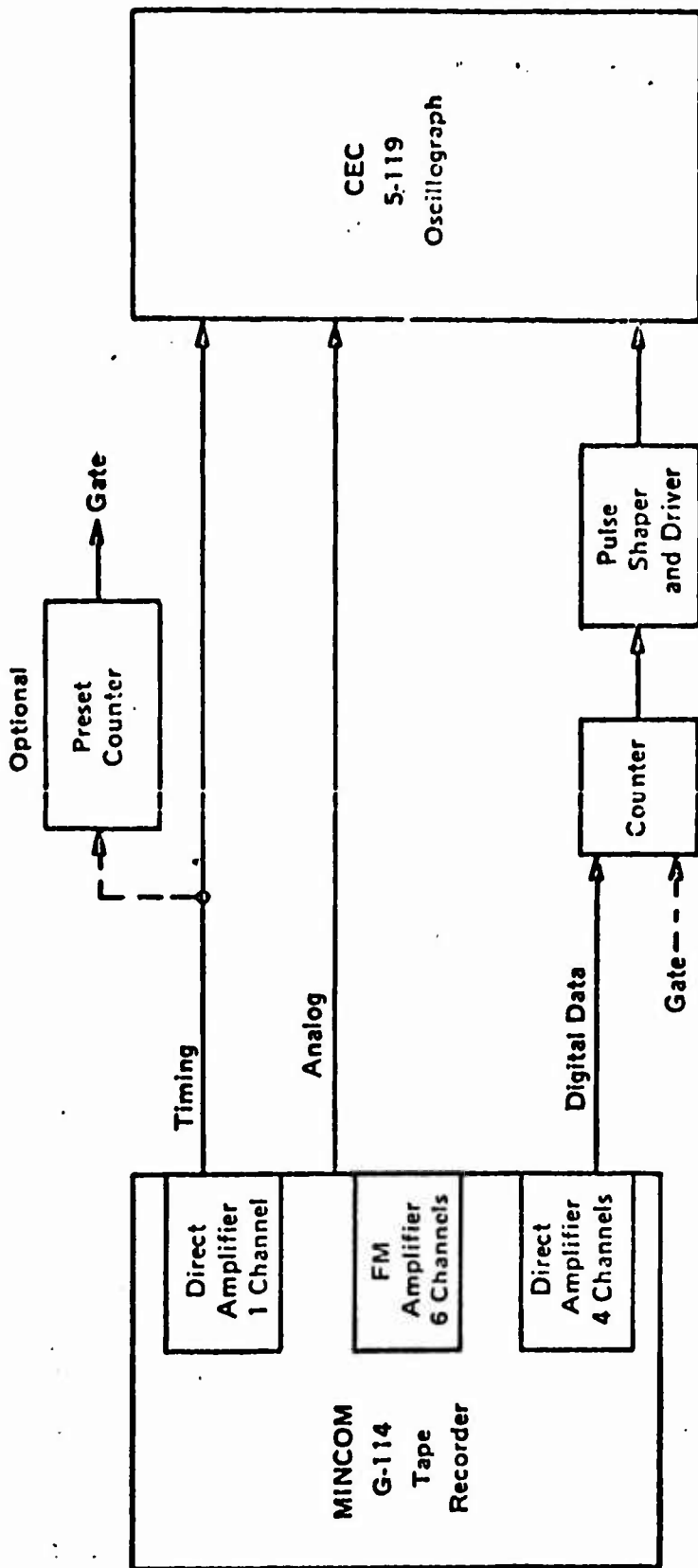


Figure 3 Oscilloscope Trace.

Integration of a curve requires only selection of the desired time interval and the playback of the semidigital tape over that interval. Calibration values are used to convert the pulses into an impulse integral.

6.3 Calibration Accuracy

All transducers will be calibrated physically and electrically. The physical calibration of the axial load will be performed with NBS certified weights which are accurate to 0.006 percent. Timing signals are generated by a secondary frequency standard which is accurate to at least one part in 10^8 .

The electrical calibration system is an 8-wire, double-shunt hookup in which a series of 0.005 percent resistors is shunted across two arms of the bridge. This makes errors due to changes in line resistance, transducer temperature, and contact resistance negligible.

Assuming we can control the weights to .005 lb and the moment arm to .01 inch, the moment applied will be accurate to 0.6 percent.

The total accuracy of the axial thrust impulse and moment impulse data will be ± 0.5 percent and ± 6.2 percent respectively.

6.4 Noise Compensation

Dynamic analysis of the test assembly shows that the shock input from the motor firing will produce significant oscillations in all three of the sensor planes. This ringing is expected to be as much as 200 percent of the magnitude of the two moment signals at frequencies up to 3000 or 4000 Hz. As stated previously the instrumentation system will integrate the signal without error but only if no oscillations reach below base or zero signal level. Any negative

oscillations will be integrated and added to the positive signal resulting in an error. To prevent this the base signal must be offset in the positive direction so that no oscillations go below base.

The system is capable of a maximum count rate of 100,000 counts per second. The moment bridges yield an output of 20MV per 10 in-lbs and the misalignment specification allows a 3 sigma maximum of 10 in-lbs of pitch moment. If we setup an initial test firing for a maximum expected value of 20 in-lbs and a 40 MV signal level, we can offset the integrators by forty percent or 40,000 counts so that a zero transducer output results in a count rate of 40,000 and we can calibrate the system so that a 40 MV output produces a 20,000 increase in the count rate to 60,000 counts per second. This leaves 200 percent above the 40 MV (60,000 counts/second) peak output and 200 percent below base (40,000 counts/second) for oscillations.

A 200 percent oscillation therefore limits the usable count rate to 20,000. This means that the total number of pulses we can get will be less than 200 for all three bridges and the count resolution error will be on the order of .50 percent. If the first firing shows oscillations of less than 200 percent we will adjust accordingly. Oscillations of 100 percent would allow us to improve count resolution to .33 percent.

6.5 Cross-Talk Compensation

Interface will provide a plot of the cross-talk effect of the axial load on the moment sensing bridges. All moment data will be corrected accordingly.

7.0 TEST FIRING

After the in-place calibrations described in Section 5.0 have been performed, the motor will be functioned as follows:

7.1 Tape a thermocouple to the nozzle body. Do not fire the unit until the temperature of the nozzle body has stabilized within 2°F of the ambient temperature.

7.2 Hook up firing circuit, VMSC P/N 371T310004-1, in accordance with VMSC TIR No. 3-371-T1-P-20021 so that switch S-3 is paralleled with firing relay in the sequencer.

7.3 Select the position desired for S6, MW-Sec Selector.

7.4 Place the following switches in the position indicated:

<u>Switch</u>	<u>Position</u>
S1: ON/OFF	OFF
S2: ARMED/DISARMED	DISARMED
S3: FIRE (pushbotton)	UP
S4: TEST/OPERATE	OPERATE
S5: SHORT/FIRE	SHORT

7.5 Connect the squib bridgewire to the terminals indicated.

7.6 Place S1 in the ON position and S2 in the ARMED position and note that the ARMED indicator is illuminated.

7.7 Place S5 (SHORT/FIRE) in the FIRE position.

7.8 The table below shows for each position of switch S6 the energy stored in the capacitors and the energy that is supplied in 50 microseconds assuming +6 VDC supplied voltage and a 6 ohm bridgewire.

<u>S6 Position</u>	<u>Stored Energy</u>	<u>Energy Supplied</u>
1	1.224 MW-sec	0.150 MW-sec
2	1.800 MW-sec	0.28 MW-sec
3	2.016 MW-sec	0.51 MW-sec
4	2.808 MW-sec	0.57 MW-sec
5	3.600 MW-sec	0.63 MW-sec

- 7.9 When the temperature is stable, balance out the thrust and moment channels for a zero count rate.
- 7.10 Check the gain by setting the electrical calibration switch to position "4" and observe a count rate change of $20,000 \pm 1$. If it is out of tolerance, adjust integrator gain controls (coarse and fine) on the bridge calibrator until it is back to nominal.
- 7.11 Return the electrical calibrate switch to "0".
- 7.12 Set all recorders to a slow speed to record an analog electrical calibration. Turn on all recorders with the OSC switch on the bridge calibrator control panel.
- 7.13 With the recorders running, perform an electrical calibration.
- 7.14 Record the count rate for the top electrical calibration step.
- 7.15 Switch the OFFSET switch on all integrators to the "+" position. Observe a count of $40,000 \pm 10$ counts.
- 7.16 Set the switch on the automatic firing sequencer labeled COUNT to the "ON" position. (Under these conditions the off-base condition will be shown on the counters.)
- 7.17 Adjust the fine balance controls of the channels until a count of $40,000 \pm 5$ is obtained.
- 7.18 On the automatic firing sequencer set all control switches to the "AUTO" position except COUNT.
- 7.19 Set all the oscillographs for high speed.
- 7.20 Set CEC Timing Circuit control switch to the "MASTER" position. Ensure that the counter tubes are stepping.
- 7.21 Start the automatic firing sequencer by setting the FIRE switch to the "START" position.

- 7.22 While the sequencer is counting, make final balance adjustments on all channels.
- 7.23 At T minus 10 second, set the COUNT switch on the sequencer to the "AUTO" position.
- 7.24 At T minus 1 second, assure that the oscillographs and tape system have started and the counters have reset. If they have not, shut off the sequencer.
- 7.25 At T minus 0 second, assure that the rocket motor fires. In the event of a misfire, wait for a minimum of 20 minutes before reentering the designated hazard area and proceed in accordance with Part 7, Section 1, Pine Ridge Plant Safety Manual.
- 7.26 When the thrust level of the main motor has decreased to a zero level as observed on the Visicorder, turn the FIRE switch to the "STOP" position.
- 7.27 Depress the "RESET" button on the Sequencer.
- 7.28 Record the count registered on the three counters on the Rocket Test Work Sheet.
- 7.29 Record the time the rocket motor round fired on the Rocket Test Work Sheet.
- 7.30 Without rebalancing the thrust channels, set the Electrical Calibrate switch to "FOUR" and record the count rate on the Test Data Sheet.
- 7.31 Repeat the electrical calibration.
- 8.0 DATA PLAYBACK
- The primary data obtained will be the integral moments. These will be obtained by playing back the taped signal.

8.1 Axial Thrust Ballistics

The firing pulse will be played back at 15 IPS, a quarter of the speed at which it was recorded. The signal will be fed into the oscillograph running at 160 IPS. All the ballistic axial thrust parameters will be obtained from this expanded trace.

8.1.1 Filtering

If the oscillations in the axial thrust signal are of sufficient magnitude and frequency to obscure the shape of the curve it will be necessary to filter the signal before it is played back. A comparison of the unfiltered and filtered signal integrals will show whether the filtering process has biased the data.

APPENDIX 4

ARRAY PENDULUM TEST PLAN



ATLANTIC RESEARCH CORPORATION
PROPULSION

DOCUMENT NO. TS 0183
DOCUMENT DATE 9-12-73

DOCUMENT APPROVAL SHEET
FOR
TEST PLAN AND PROCEDURE FOR
THE FUNCTIONAL TEST OF A MANEUVER MOTOR ARRAY
SUSPENDED FROM A PENDULUM

AUTHORIZED ACTIVITIES		ACTIVITY APPROVALS		
REQUIRED APPROVAL	ACTIVITY	NAME	SIGNATURE	DATE
X	PREPARING	I. M. PROCINSKY	<i>I. M. Procinsky</i>	9-11-73
X	PROGRAM MANAGEMENT	R. BROWN	<i>R. Brown</i>	9-17-73
	QUALITY ASSURANCE			
	RELIABILITY			
	DESIGN			
X	TEST	R. E. WALLACE	<i>R. E. Wallace</i>	9-12-73
	DEVELOPMENT			
	PRODUCTION			

CHANGE HISTORY		
AMENDMENT OR REVISION	DATE OF CHANGE	AUTHORIZATION

TEST PLAN AND PROCEDURE
FOR
THE FUNCTIONAL TEST
OF A
MANEUVER MOTOR ARRAY
SUSPENDED FROM A PENDULUM

PREPARED FOR
VOUGHT MISSILES AND SPACE CO.
DALLAS, TEXAS

SEPTEMBER 1973

1.0 SCOPE

This plan describes the procedures, apparatus and instrumentation that will be utilized in the functional tests of twelve motors from a Maneuver Motor Array suspended from a pendulum. It is the purpose of the suspension to allow the MMA to respond to the self-induced shock forces generated by the motor firings.

2.0 APPLICABLE DOCUMENTS

VMSC Specifications

3-371-13-0-10186B	- Maneuver Motor Array, Statement of Requirements	20 March 72
3-371-04-0-10185C	- Maneuver Motor Array, Procurement Specification	20 March 72
3-371-TI-P-20021	- Maneuver Motor Firing	30 March 72
2-84500/3L-379	- MMA Dev. Test Program Requirements	3 August 73

Military Specifications

AMCR-385-100	- AMC Safety Manual	
MIL-C-45662A	- Calibration of Test Measurement Equipment	9 February 62

Military Standards

MIL-STD-453 Change Notice 1	- Inspection, Radiographic	26 October 62 4 September 63
--------------------------------	----------------------------	---------------------------------

Atlantic Research Corporation Drawings

A0070051	- Initiator, Single Squib	
A0070049-001	- Motor Tube, Loaded	
A0070049-002	- Motor Tube, Loaded	
A0070074	- Maneuver Motor Array Ref VMSC-T-371B100010, Rev. M.	2 November 72 Rev. A

3.0 TEST EQUIPMENT

Equipment to be used in the performance of the specified tests shall be as listed below, and shall exhibit evidence of calibration prior to use in any environmental or functional test.

3.1 Special Test Equipment

3.1.1 Shock Pendulum, ARC Dwg. No. A0070126

3.1.2 Accelerometer, Endevco, Model 2220C

3.1.3 Charge Amplifier, Kistler, Model 504A

3.1.4 MMFC Control - ARC Prototype

3.2 Ballistic Recording and Computing Equipment

3.2.1 Dynamic Recording System; 12-inch width with record speeds to 160 inches/second; linearity, ± 1 percent full scale, Consolidated Electroynamics Corporation, 36-channel, Recording Oscillograph.

3.2.1.1 Recording Oscillograph, Consolidated Electroynamics Corporation, Model 5-119.

3.2.1.2 Galvanometers, Consolidated Electroynamics Corporation, Types 7-362, 7-363, 7-319 and 7-348.

3.2.2 Dynamic Recording System, 12-channel measurement with 6-inch wide analog readout on oscillograph at record speeds up to 50 inches/second; linearity, ± 2 percent of full scale, Heiland Division of Minneapolis Honeywell, Visicorder.

3.2.2.1 Oscillograph, Heiland Division of Minneapolis Honeywell, Model 906C.

NOTE: Used for "quick-look" data.

3.2.2.2 Galvanometers, Heiland Division of Minneapolis Honeywell, Model M3300T, M400-120 and M1650.

3.2.3 Data Acquisition System, Atlantic Research Corporation

3.2.3.1 Electronic Counter, Beckman Corp., Model 7360C.

3.2.3.2 Voltage-to-Frequency Converter, Dymec Corporation, Model 2211BR-M28.

3.2.3.3 DC Amplifier, Neff, Model 119

3.2.3.4 Bridge Calibrator, Atlantic Research Corporation.

3.2.3.5 Frequency Standard, Hewlett Packard, Model 100ER.

3.2.3.6 Transducer Power Supply, Computer Engineering, Model PT-214.

3.2.3.7 Galvo Control Panel, Atlantic Research Corporation.

3.2.3.8 Automatic Firing Sequencer, Atlantic Research Corporation.

3.2.3.9 Tape Recorder System, Mincom 3M, Model G114.

3.2.3.10 Digital Storage Oscilloscope - Nicolet Instrument Corp., Model 1090 with Model 92 Dual Channel Plug-In.

4.0 TEST PROCEDURE

4.1 Test Specimen

The test specimen will consist of a fully loaded flight weight configuration Maneuver Motor Array (ARC Dwg. No. A0070074) wired with the Maneuver Motor Firing Circuit Assembly (VMSC Dwg. 371-A-310011) and incorporating all accessories necessary to duplicate the structural loading of a free-flying array.

4.2 Test Facility

The tests will be performed at the Pine Ridge Plant in Gainesville, Virginia. The test assembly will be mounted to the ceiling of Firing Bay #2.

This bay is open to ambient air so that the functional tests will be conducted at ambient conditions.

4.3 Test Stand Description

The test apparatus consists of a thin hollow tube pendulum suspended from a ball bearing support which allows it to swing in one vertical plane. The pendulum ends in a bracket which attaches to the outside diameter of the MMA nozzle ring. The tube was sized to yield a torsional frequency of about 2.5 Hz and a longitudinal frequency of about 20 Hz so that the tube would be just stiff enough to prevent the MMA from rotating significantly between successive firings and not stiff enough to weigh down or damp out the response of the MMA. The idea being to allow the MMA to respond to the shocks of successive motor firings, while maintaining minimal control of any tendency to rotate or move in any mode other than translation in the plane of the pendulum.

5.0 TEST SET-UP

The pendulum support plate will be bolted to the ceiling of Firing Bay #2 so that when the MMA is attached to the bottom of the pendulum it will be about three feet above the floor of the bay. The vertical displacement between the array and the

bearing support point will be seven feet so that if only one motor fires the array will not swing up past the support point or make contact with the ceiling.

6.0 DATA ACQUISITION SYSTEM

6.1 Transducers

A small accelerometer will be attached to motor # 7 and 21 for the last two sets of firings. These accelerometers will be glued to the tube over-wrap as close to the igniter end as possible to monitor the self induced shock both in the axis of thrust and in a direction perpendicular to it.

They will be calibrated to 5000 g's and will be mounted to the outside of the motor tube with their axis of sensitivity facing the center of the MMA cylinder.

6.2 Tracking System

For the first two series of firings VMSC will provide a FASTRAC tracking apparatus which will be set up 60 ft. from the test specimen and facing down the axis of the MMA cylinder.

These tests will be conducted after sundown so that the FASTRAC system can track the movement of the pendulum. VMSC will operate the FASTRAC system.

6.3 Photographic Coverage

Two HY-CAM film cameras will be used to record all firings except the first two series, which will be conducted in darkness.

The cameras will be set to run at about 1500 frames per second.

6.4 Recording Instrumentation

The signals are fed through individual shielded cables to the data system where they enter chopper-stabilized dc amplifiers. The amplifier output is then routed to the analog and semidigital recording systems. Figure 1 shows the basic instrumentation components.

Because of the short functioning time two separate analog recording systems will be utilized for these firings. The signal will be recorded on CEC recording oscillographs operating at a speed of 160 inches a second. This will be utilized only for preliminary timing information because a 10-millisecond firing will yield only a 1.6-inch long record.

The second analog data recording uses a 3M MINCOM FM tape system. Analog signals will be recorded on this system at a magnetic tape speed of 60 in/sec. They will be played back onto recording oscillographs at a tape speed of 15 in/sec with the FM amplifiers adjusted and filtered accordingly. This difference in recording versus playback speeds will result in a 4/1 extension of the oscillograph recordings and will yield a 6.5 inch firing trace. By carefully recording calibration steps on the FM system immediately prior to firing, the data can be handled without any significant loss in accuracy. Calibrated timing will also be put on the tape so that it will appear on the expanded record at the proper intervals. A schematic of the data playback system is shown in Figure 2.

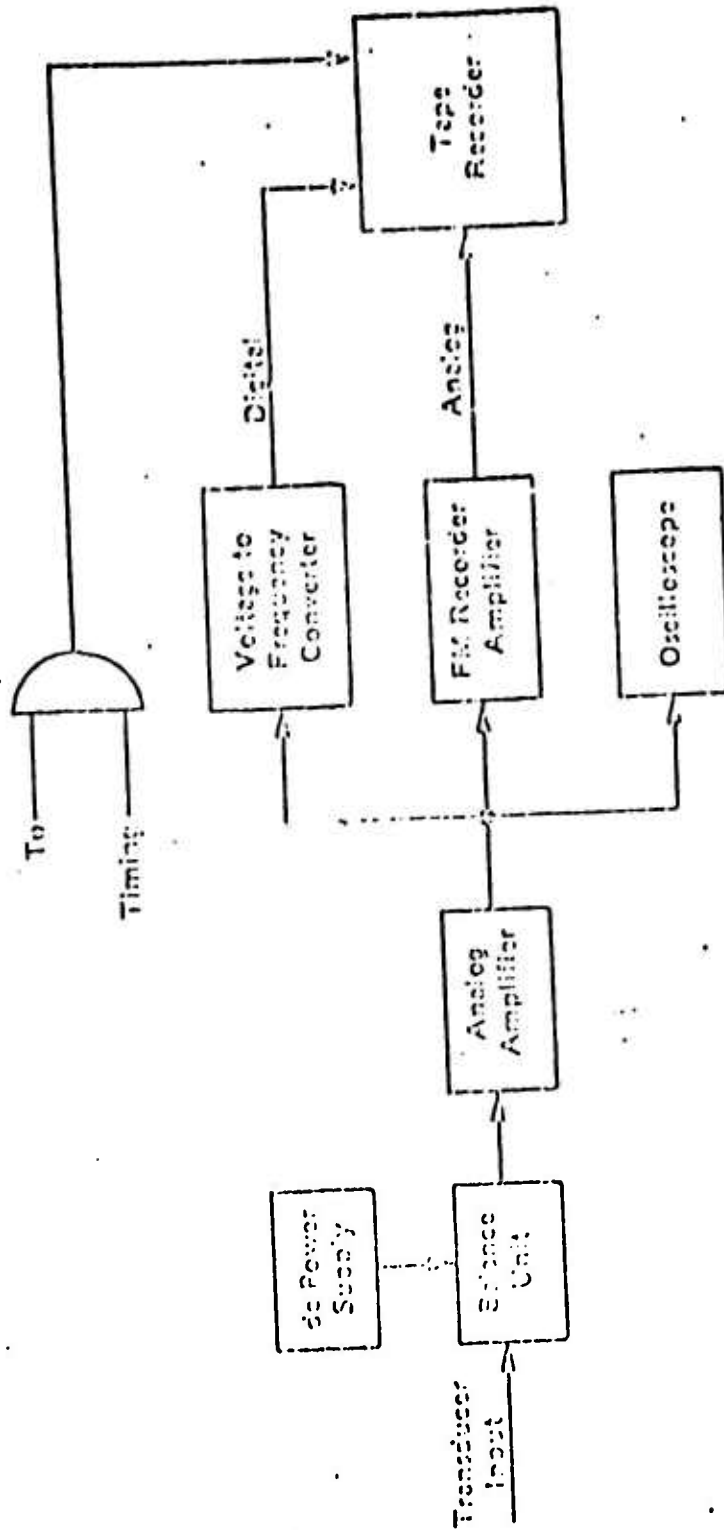


Figure 1 Record Instrumentation.

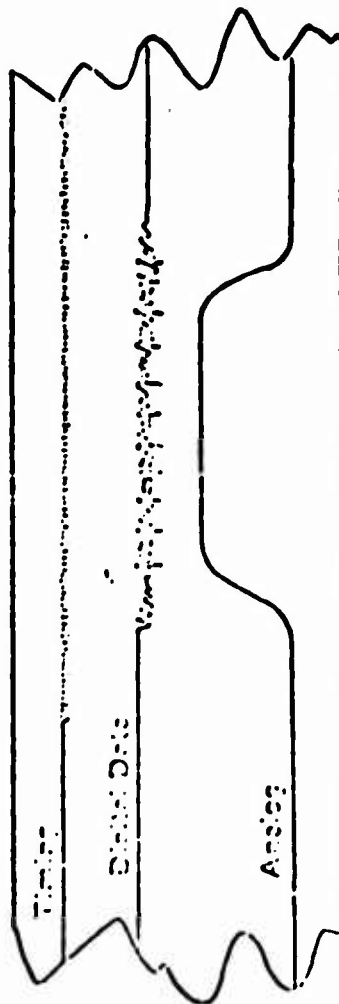
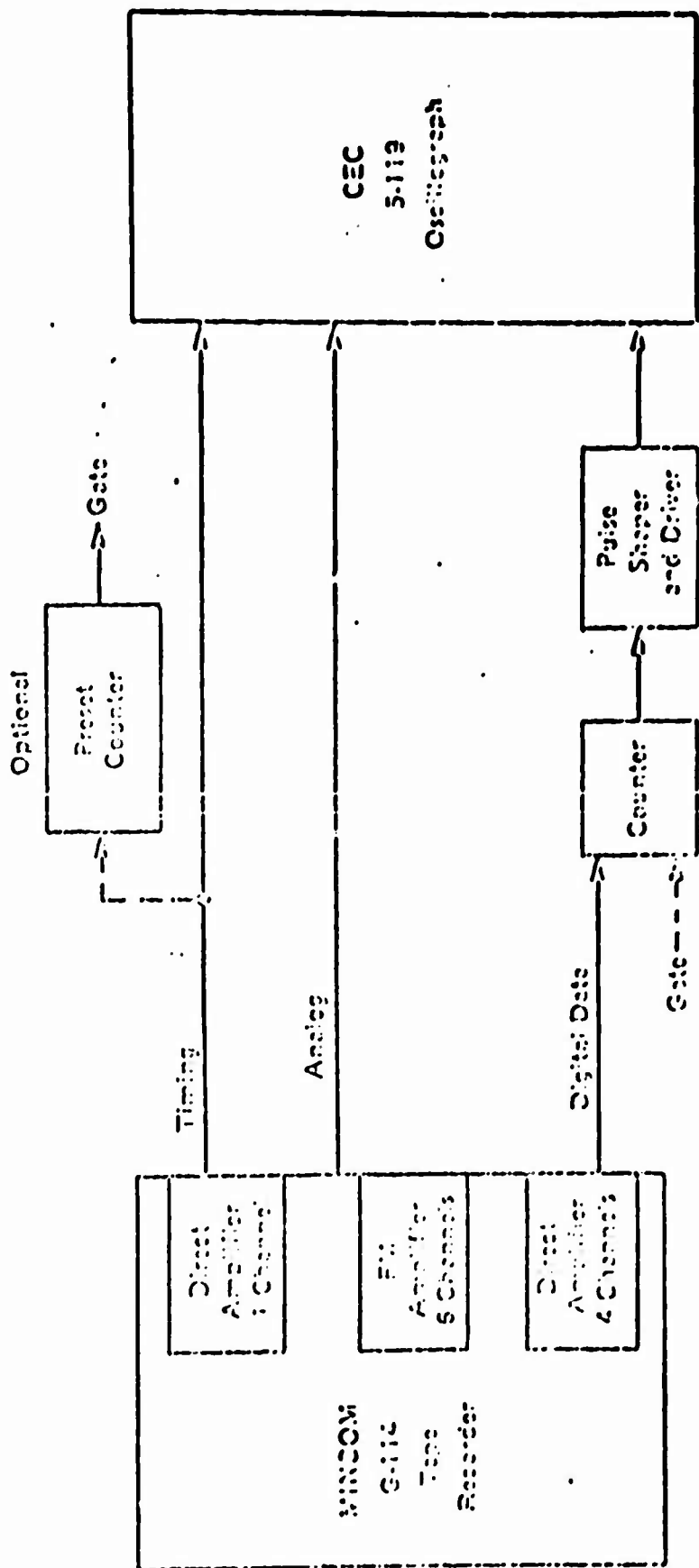


Figure 2 Oscilloscope Trigger

The Nicolet Digital Storage Oscilloscope will be used to record both accelerometer signals from the first firing in each series. Both firings will be recorded on tape for later analysis. The storage oscilloscope will allow the shock pulses to be analyzed for magnitude and frequency content immediately after each series of firings.

6.5 Firing Circuit Control

An Atlantic Research Firing Control Unit will be utilized to control the sequence and timing for the firing current pulses.

The two motors in each series will be fired one quarter of a second apart. The following section described the function of the Firing Control unit which is depicted by Figure 3.

The MMFC Control Unit is a system whose function is to fire a series of Hit motors in pre-selected sequence at the rate of 4/sec. The heart of the system is an Automatic Electric Stepper Switch. As the stepper switch moves from one position to the next, different motors are selected for firing.

A HP 202 Function Generator is used to establish the 4/sec firing rate. A square wave function will act as the system clock. The positive going waveform of the square wave will activate the 20 msec pulse generator provided the OFF-ON switch is closed. When the OFF-ON switch is activated, the stepper switch will be in a position to fire the first motor with the namma lines already properly activated. When the 20 msec pulse is generated the stepper switch routes the pulse to the proper P line and fires the first motor. At the same time that the 20 msec pulse is being generated,

the positive portion of the 4 Hz square wave energizes the stepper switch coil by cocking the ratchet. When the square wave returns to 0, the cocked ratchet will move the stepper switch to its new position and the cycle starts over again. To protect the P lines from stray transients, all the lines that are inactive are grounded by the stepper switch. This cycle will continue automatically until the OFF-ON switch is opened or until 12 cycles have occurred. Automatic shut off is assured by routing the step signal through a set of bussed contacts on the stepper switch.

As the test is in progress, the voltage of the firing capacitors will be monitored. As a firing circuit is energized, the voltage drop will be recorded on the oscillograph.

This firing system can be used to fire any number of motors at different firing rates. The IIP 202 Signal Generator has a range from 0.01 Hz to 1200 Hz.

This apparatus was designed specifically for the spin stand tests where up to twelve motors will be functioned at .25 second intervals.

For the pendulum tests the stepper switch will be wired so that only 2 motors in a row can be fired consecutively. The motors that will be fired are determined by the wiring on the stepper switch. The time between each firing is governed by the IIP 202 Function Generator.

7.0 TEST FIRINGS7.1 Sequence

The first twelve motors from the test array will be fired on the pendulum. The motors will be functioned in groups of two opposing units fired 0.25 seconds apart.

The test sequence will be as follows:

<u>Motor No.</u>	<u>Instrumentation</u>
6-34	FASTRAC
20-48	FASTRAC
8-36	High Speed Film (2)
22-50	High Speed Film (2)
7-35	High Speed Film (2), Accelerometer (2)
21-49	High Speed Film (2), Accelerometer (2)

Product of Inertia Measurements will be made after each of the six series.

7.2 Firing Procedure

- a. Mount MMA to pendulum.
- b. Hook up firing circuit to the two quadrants in which motors are to be functioned.
- c. Verify that the Firing Circuit Stepper Switch is in position 1.
- d. Connect the Firing Circuit so that the ARM voltage can be applied at T-10 seconds and the firing command activated at T_0 . These commands must come from the firing sequence in the control room.

- e. Route the Firing Command thru an interlock circuit on the firing console so that a $T + 0.85$ sec. the circuit is broken. This interlock will prevent a late firing of the second motor which could result in damage to the array.
- f. Check to see that the Nicolet Digital Storage Oscilloscope is set up to receive the signal.
- g. To fire the two motors, activate the Automatic Firing Sequencer.

8.0

DATA PLAYBACK

The accelerometer signals will be played back from the tape and an expanded analog trace will be made of each signal.

Frequency and magnitude measurements will be taken from the Nicolet Storage Oscilloscope.

APPENDIX 5

ARRAY SPIN TEST PLAN



ATLANTIC RESEARCH CORPORATION

PROPULSION

DOCUMENT NO. TS 0184
DOCUMENT DATE Sept. 13, 1973

DOCUMENT APPROVAL SHEET
FOR
TEST PLAN AND PROCEDURE
FOR
THE FUNCTIONAL SPIN TEST
OF A MANEUVER MOTOR ARRAY

AUTHORIZED ACTIVITIES		ACTIVITY APPROVALS		
REQUIRED APPROVAL	ACTIVITY	NAME	SIGNATURE	DATE
X	PREPARING	I. M. PROCOVNSKY	<i>I. M. Procovnsky</i>	9/14/73
X	PROGRAM MANAGEMENT	R. BROWN	<i>R. Brown</i>	
	QUALITY ASSURANCE			
	RELIABILITY			
	DESIGN			
X	TEST	R. E. WALLACE	<i>R. E. Wallace</i>	9/14/73
	DEVELOPMENT			
	PRODUCTION			

CHANGE HISTORY		
AMENDMENT OR REVISION	DATE OF CHANGE	AUTHORIZATION

TEST PLAN AND PROCEDURE
FOR
THE FUNCTIONAL SPIN TEST
OF A MANEUVER MOTOR ARRAY

PREPARED FOR
VOUGHT MISSILES AND SPACE CO.
DALLAS, TEXAS

SEPTEMBER 1973

1.0 SCOPE

This plan describes the sequence, procedures, and instrumentation that will be utilized in the functional spin test of 24 of the motors on a Hit MMA. It will be the purpose of this test series to fire groups of motors in succession to determine whether the spin rate and rapid firing produce any structural failures and to measure their effect on the mass balance of the MMA.

2.0 APPLICABLE DOCUMENTSVMSC Specifications

3-371-13-0-10186B	- Maneuver Motor Array, Statement of Requirements	20 March 72
3-371-04-0-10185C	- Maneuver Motor Array, Procurement Specification	20 March 72
3-371-TI-P-20021	- Maneuver Motor Firing	30 March 72
2-84500/3L-379	- MMA Dev. Program Requirements	3 August 73

Military Specifications

AMCR-385-100	- AMC Safety Manual	
MIL-C-45662A	- Calibration of Test Measurement Equipment	9 February 62

Military Standards

MIL-STD-453 Change Notice 1	- Inspection, Radiographic	26 October 62 4 September 63
--------------------------------	----------------------------	---------------------------------

Atlantic Research Corporation Drawings

A0070074	- Maneuver Motor Array Ref VMSC-T-371B100010, Rev. M	2 November 72 Rev. A
----------	---	-------------------------

3.0 TEST EQUIPMENT

Equipment to be used in the performance of the specified tests shall be as listed below, and shall exhibit evidence of calibration prior to use in any environmental or functional test.

3.1 Special Test Equipment

- 3.1.1 Spin Fixture Assembly - ARC Dwg. No. A0070136, 17 May 73.
- 3.1.2 Slip Ring, KDI Electro-Tec Corp. #11286, 22 channels.
- 3.1.3 Maneuver Motor Firing Circuit Control Unit - ARC prototype.
- 3.1.4 Magnetic Pickup, SXB-813, Power Instruments Inc.

3.2 Ballistic Recording and Computing Equipment

3.2.1 Dynamic Recording System; 12-inch width with record speeds to 160 inches/second; linearity, ± 1 percent full scale, Consolidated Electroynamics Corporation, 36-channel, Recording Oscillograph.

3.2.1.1 Recording Oscillograph, Consolidated Electroynamics Corporation, Model 5-119.

3.2.1.2 Galvanometers, Consolidated Electroynamics Corporation, Types 7-362, 7-363, 7-319 and 7-348.

3.2.2 Dynamic Recording System, 12-channel measurement with 6-inch wide analog readout on oscillograph at record speeds up to 50 inches/second; linearity, ± 2 percent of full scale, Heiland Division of Minneapolis Honeywell, Visicorder.

3.2.2.1 Oscillograph, Heiland Division of Minneapolis Honeywell, Model 906C.

NOTE: Used for "quick-look" data.

3.2.2.2 Galvanometers, Heiland Division of Minneapolis Honeywell, Models M3300T, M400-120 and M1650.

- 3.2.3 Data Acquisition System, Atlantic Research Corporation
- 3.2.3.1 Electronic Counter, Beckman Corp., Model 7360C.
- 3.2.3.2 DC Amplifier, Neff, Model 119.
- 3.2.3.3 Frequency Standard, Hewlett Packard, Model 100ER.
- 3.2.3.4 Transducer Power Supply, Computer Engineering, Model PT-214.
- 3.2.3.5 Galvo Control Panel, Atlantic Research Corporation.
- 3.2.3.6 Automatic Firing Sequencer, Atlantic Research Corporation.
- 3.2.3.7 Tape Recorder System, Mincom 3M, Model G114.

4.0 TEST PROCEDURE

4.1 Test Specimen

The test specimen will consist of a fully loaded Maneuver Motor Array and will include all the firing circuit controls as well as batteries and external accessories to simulate the structural loading of a free flying unit.

4.2 Test Facility

The tests will be performed at the Pine Ridge Plant in Gainesville, Virginia. The test assembly will be mounted to the 18" x 18" x 24" cement block on the floor of firing bay #3.

Because of the multiple test firings the enclosure that has previously been used to maintain a constant temperature environment will be removed and the tests will be conducted at ambient temperature.

4.3 Thrust Stand

The spinning thrust stand (Dwg. A0070136) consists of a two-inch diameter shaft supported at two points by a pair of high precision bearings.

The shaft is coupled to a 1/2 HP motor on one end and holds a 22-channel slip ring assembly on the other end. The drive system has a speed control for fine adjustment of the spin rate.

A non-contact magnetic sensor mounted to the frame records the passage of two bolts and provides a measurement of the spin rate.

The array is held on the shaft by means of three removable clamps which interface with the inside diameter of the nozzle ring.

4.4 Set-Up and Calibration

4.4.1 The array will be mounted on the shaft of the spin stand and hooked to the slip ring assembly by means of four jumper cables connected to each of the four quadrant firing circuit terminals that are part of the MMA.

4.4.2 The entire assembly will be bolted to the base of a Gisholt Balancing Machine and balanced to within 5 grams at 25 RPS by adding washers and bolts to the holes on the circumference of the holding shaft.

5.0 FIRING CIRCUIT CONTROL UNIT

An Atlantic Research Firing Control Unit will be utilized to control the sequence and timing of the firing current pulses.

The motors in each series will be fired one quarter of a second apart. The following section described the function of the Firing Control unit which is depicted by Figure 1.

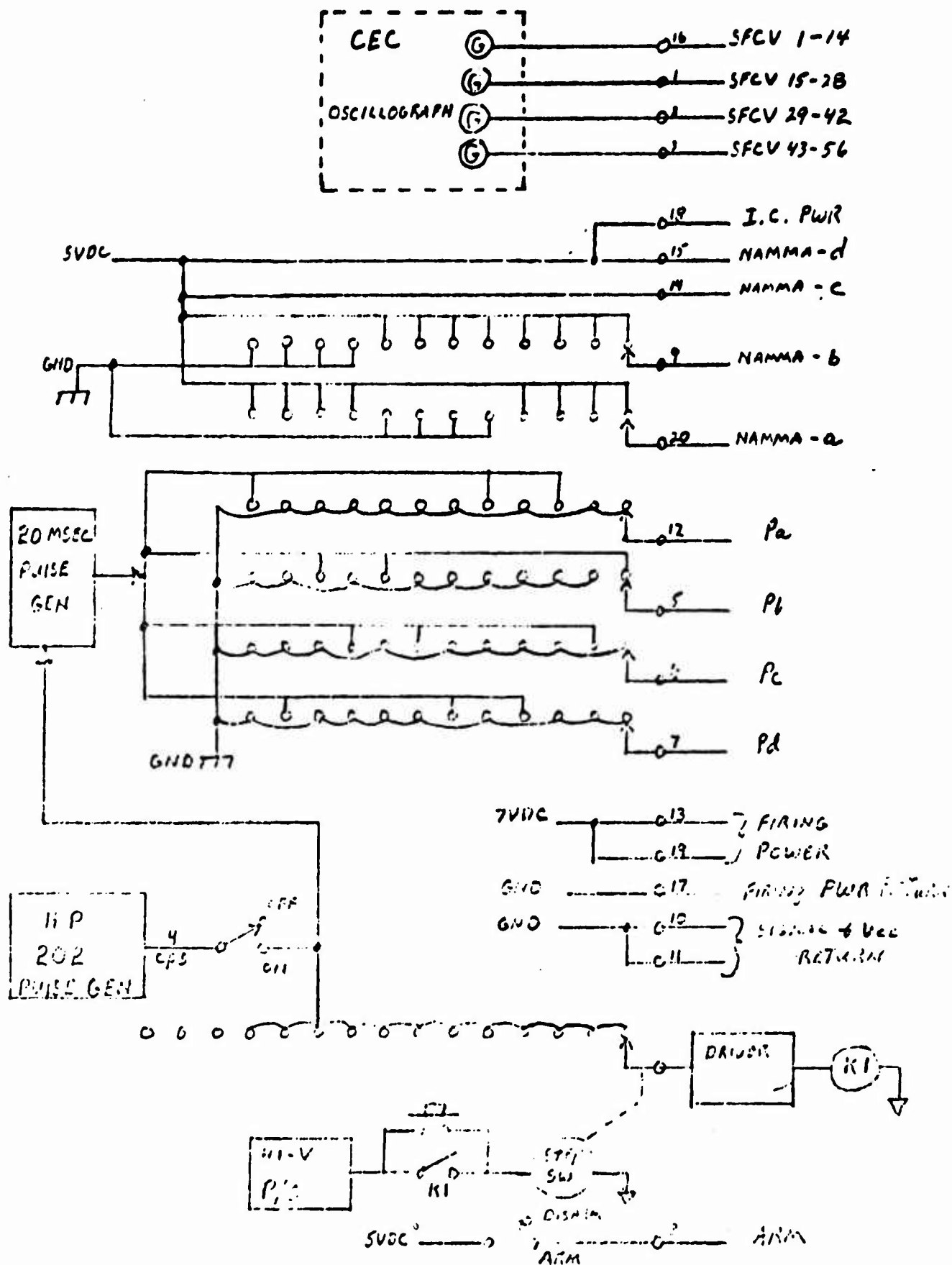


FIGURE 1 Schematic of MIMIC Control Unit.

The MMFC Control Unit is a system whose function is to fire a series of Hit motors in pre-selected sequence at the rate of 4/sec. The heart of the system is an Automatic Electric Stepper Switch. As the stepper switch moves from one position to the next, different motors are selected for firing.

A HP 202 Function Generator is used to establish the 4/sec firing rate. A square wave function will act as the system clock. The positive going waveform of the square wave will activate the 20 msec pulse generator provided the OFF-ON switch is closed. When the OFF-ON switch is activated, the stepper switch will be in a position to fire the first motor with the namma lines already properly activated. When the 20 msec pulse is generated the stepper switch routes the pulse to the proper P line and fires the first motor. At the same time that the 20 msec pulse is being generated, the positive portion of the 4 Hz square wave energizes the stepper switch coil by cocking the ratchet. When the square wave returns to 0, the cocked ratchet will move the stepper switch to its new position and the cycle starts over again. To protect the P lines from stray transients, all the lines that are inactive are grounded by the stepper switch. This cycle will continue automatically until the OFF-ON switch is opened or until 12 cycles have occurred. Automatic shut off is assured by routing the step signal through a set of bussed contacts on the stepper switch.

As the test is in progress, the voltage of the firing capacitors will be monitored. As a firing circuit is energized, the voltage drop will be recorded on the oscillograph.

This firing system can be used to fire any number of motors at different firing rates. The HP 202 Signal Generator has a range from 0.01 Hz to 1200 Hz.

The stepper switch will be wired for each series so that only the predetermined motors can be fired consecutively. The sequence in which the motors will be fired is also determined by the wiring on the stepper switch. The time between each firing is governed by the HP 202 Function Generator.

6.0 DATA ACQUISITION SYSTEM

6.1 Transducers

No ballistic data will be taken for the series of firings. The instrumentation will consist of a magnetic pick-up to monitor the spin rate and a galvanometer hookup to each of the four quadrant firing circuits that will record the discharge of current each time a firing pulse is released.

6.2 Photographic Coverage

Two HY-CAM film cameras will be used to record all firings ~~except the first two series which will be conducted in darkness.~~

The cameras will be set to run at about 1500 frames per second.

7.0 TEST FIRINGS7.1 Sequence

The twenty-four motors from the test array will be fired on the spin stand. The motors will be functioned in groups of twelve, four, four and four units and fired 0.25 seconds apart.

The test sequence will be as follows:

Motor No.	<u>Group 1</u>	<u>Group 2</u>	<u>Group 3</u>	<u>Group 4</u>
	15	02	11	10
	29	30	39	38
	01	16	25	24
	43	44	53	52
	09			
	51			
	37			
	23			
	31			
	17			
	45			
	03			

Product of Inertia Measurements will be made after each of the four series.

7.2 Firing Procedure

- a. Wire up stepper switch to fire the motors in the series
- b. Mount MMA to spin stand.
- c. Hook up firing circuit.
- d. Verify that the Firing Circuit Stepper Switch is in position 1.
- e. Connect the Firing Circuit so that the ARM voltage can be applied at $T-10$ seconds and the firing command activated at T_0 . These commands must come from the firing sequence in the control room.

APPENDIX 6

ARRAY STATIC TEST PLAN



ATLANTIC RESEARCH CORPORATION

PROPULSION

DOCUMENT NO. TS 0185
DOCUMENT DATE Sept. 14, 1973

DOCUMENT APPROVAL SHEET
FOR
**TEST PLAN AND PROCEDURE FOR
THE FUNCTIONAL STATIC TEST OF INDIVIDUAL MOTORS
IN A MANEUVER MOTOR ARRAY**

AUTHORIZED ACTIVITIES		ACTIVITY APPROVALS		
REQUIRED APPROVAL	ACTIVITY	NAME	SIGNATURE	DATE
X	PREPARING	I. M. PROCKINSKY	<i>I. M. Prockinsky</i>	9/14/73
X	PROGRAM MANAGEMENT	R. BROWN	<i>R. G. Brown</i>	9/17/73
	QUALITY ASSURANCE			
	RELIABILITY			
	DESIGN			
X	TEST	R. E. WALLACE	<i>R. E. Wallace</i>	9/17/73
	DEVELOPMENT			
	PRODUCTION			

CHANGE HISTORY		
AMENDMENT OR REVISION	DATE OF CHANGE	AUTHORIZATION

TEST PLAN AND PROCEDURE
FOR
THE FUNCTIONAL STATIC TEST
OF
INDIVIDUAL MOTORS IN A
MANEUVER MOTOR ARRAY

PREPARED FOR
VOUGHT MISSILES AND SPACE CO.
DALLAS, TEXAS

SEPTEMBER 1973

1.0 SCOPE

This procedure describes the test apparatus, calibration procedures, and instrumentation to be utilized in the functional static test of individual motors on a fully loaded MMA. Seventeen of the twenty remaining motors on the test MMA will be fired individually for ballistics data. The first three will be fired a quarter of a second apart and the instrumentation will include thermocouples to measure any cumulative effect from the close spacing of the firings.

2.0 APPLICABLE DOCUMENTSVMSC Specifications

3-371-13-0-10186B	- Maneuver Motor Array, Statement of Requirements	20 March 72
3-371-04-0-10185C	- Maneuver Motor Array, Procurement Specification	20 March 72
2-84500/3L-379	- MMA Dev. Test Requirements	3 August 73

Military Specifications

AMCR -385-100	- AMC Safety Manual	
MIL-C-45662A	- Calibration of Test Measurement Equipment	9 February 62

Military Standards

MIL-STD-453 Change Notice 1	- Inspection, Radiographic	26 October 62 4 September 63
--------------------------------	----------------------------	---------------------------------

Atlantic Research Corporation Drawings

A0070074	- Maneuver Motor Array, Ref VMSC-T-371B1000101 Rev M.	2 November 72 Rev. A
----------	--	-------------------------

3.0 TEST EQUIPMENT

Equipment to be used in the performance of the specified tests shall be as listed below, and shall exhibit evidence of calibration prior to use in any environmental or functional test.

3.1 Special Test Equipment

3.1.1 Hit Thrust Stand, Z-9005, ARC prototype.

3.1.2 Load Cell, Series 36-233-BAA, Toroid Inc., dual bridge
2000 lb.

3.1.3 Firing Circuit Control, ARC prototype.

3.1.4 Pressure Transducer, 112A03, PCB, 15,000 psig.

3.1.5 Charge Amplifier, 504A, Kistler.

3.2 Transducer Calibration Standards

3.2.1 Dead Weight Calibrator, accuracy 0.006 percent, Alinco,
Model DW 12.5-125.

3.2.2 Pressure Calibrator, Amthor S/N 10934, accuracy 0.15 percent

3.3 Ballistic Recording and Computing Equipment

3.3.1 Dynamic Recording System; 12-inch width with record speeds to 160 inches/second; linearity, ± 1 percent full scale, Consolidated Electroynamics Corporation, 36-channel, Recording Oscillograph.

3.3.1.1 Recording Oscillograph, Consolidated Electroynamics Corporation, Model 5-119.

3.3.1.2 Galvanometers, Consolidated Electroynamics Corporation, Types 7-362, 7-363, 7-319 and 7-348.

3.3.2 Dynamic Recording System, 12-channel measurement with 6-inch wide analog readout on oscillograph at record speeds up to 50 inches/second; linearity, ± 2 percent of full scale, Heiland Division of Minneapolis Honeywell, Visicorder.

3.3.2.1 Oscillograph, Heiland Division of Minneapolis Honeywell, Model 906C.

NOTE: Used for "quick-look" data.

3.3.2.2 Galvanometers, Heiland Division of Minneapolis Honeywell, Models M3300T, M400-120 and M1650.

3.3.3 Data Acquisition System, Atlantic Research Corporation

3.3.3.1 Electronic Counter, Beckman Corp., Model 7360C.

3.3.3.2 Voltage-to-Frequency Converter, Dymec Corporation, Model 2211BR-M28.

3.3.3.3 DC Amplifier, Redcor, Model 361.

3.3.3.4 Bridge Calibrator, Atlantic Research Corporation.

3.3.3.5 Frequency Standard, Hewlett Packard, Model 100ER.

3.3.3.6 Transducer Power Supply, Computer Engineering, Model PT-214.

3.3.3.7 Galvo Control Panel, Atlantic Research Corporation.

3.3.3.8 Automatic Firing Sequencer, Atlantic Research Corporation.

3.3.3.9 Tape Recorder System, Mincom 3M, Model G114.

3.3.3.10 Digital Storage Oscilloscope, Nicolet Instrument Corp., Model 9010 with dual channel plug-in Model 92.

4.0 TEST PROCEDURE

4.1 Test Specimen

The test specimen will consist of a fully loaded Maneuver Motor Array and will include all the firing circuit controls as well as batteries and external accessories to simulate the structural loading of a free flying unit.

The end plugs (A0070078) on the last seventeen motors and the middle of the first three motors to be fired will be replaced by units which have been counterbored and tapped to accept a pressure transducer.

4.2 Test Facility

The tests will be performed at the Pine Ridge Plant in Gainesville, Virginia. The test assembly will be mounted to the 18" x 18" x 24" cement block on the floor of firing bay #3.

The enclosure used during the development program will be replaced so that $70^{\circ} \pm 4^{\circ}\text{F}$ is maintained for this series of firings.

4.3 Thrust Stand

The static thrust stand will consist of a mounting bracket which clamps to the outer surface of the nozzle ring and attaches directly to the load cell.

ARC Dwg No. Z-9005 describes the apparatus. The mounting bracket uses the exit cone of the motor 180° away from the one that is to be fired to align the array. A clamp on both sides of the bracket utilizes the lightening cutouts in the nozzle ring to hold the array against the bracket.

An internally mounted clamp will be placed inside the bore of the MMA to stiffen the nozzle ring and improve the frequency response of the thrust measurement.

For the first three firings, which will be spaced a quarter of a second apart, the two side motors (#16 and #14) will be 6.4° off of the thrust axis of the load cell. The resulting side component will probably produce additional ringing on the thrust trace but will not prevent the load cell from accurately measuring the vertical component of thrust for all three motors.

4.4 Set-Up

The array will be mounted horizontally on top of the load cell. It will be rotated between firings so that the motor that is to be functioned is aligned vertically with the load cell axis.

5.0 FIRING CIRCUIT CONTROL UNIT

An Atlantic Research Firing Control Unit will be utilized to control the sequence and timing for the firing current pulses.

The three motors in the first series will be fired one quarter of a second apart. The following section describes the function of the Firing Control unit which is depicted by Figure 1.

The MMFC Control Unit is a system whose function is to fire a series of Hit motors in pre-selected sequence at the rate of 4/sec. The heart of the system is an Automatic Electric Stepper Switch. As the stepper switch moves from one position to the next, different motors are selected for firing.

A HP 202 Function Generator is used to establish the 4/sec firing rate. A square wave function will act as the system clock. The positive going waveform of the square wave will activate the 20 msec pulse generator provided the OFF-ON switch is closed. When the OFF-ON switch is activated, the stepper switch will be in a position to fire the first motor with the namma lines already properly activated. When the 20 msec pulse is generated the stepper switch routes the pulse to the proper P line and fires the first motor. At the same time that the 20 msec pulse is being generated, the positive portion of the 4 Hz square wave energizes the stepper switch coil by cocking the ratchet. When the square wave returns to 0, the cocked ratchet will move the stepper switch to its new position and the cycle starts over again. To protect the P lines from stray transients, all the lines that are inactive are grounded by the stepper switch. This cycle will continue automatically until the OFF-ON switch is opened or until 12 cycles have occurred. Automatic shut off is assured by routing the step signal through a set of bussed contacts on the stepper switch.

The voltage of the firing capacitors will be monitored. As a firing circuit is energized, the voltage drop will be recorded on the oscillograph.

6.0 DATA ACQUISITION SYSTEM

6.1 Transducers

6.1.1 Load Cell

A 2000 lbf dual bridge strain gauge load cell will be utilized.

6.1.2 Thermocouples

For the first three firings, a total of twenty-four (24) iron constantan bead thermocouples will be bonded to this array. Figure 2 shows the locations of these thermocouples.

6.1.3 Pressure Transducers

Motor pressure will be recorded on all units except #12 and #14. A PCB Model 112A03, 15,000 psig, quartz pressure transducer will be utilized.

6.2 Recording Instrumentation

The transducer signals are fed through individual shielded cables to the data system where they enter chopper-stabilized dc amplifiers. The amplifier output is then routed to the analog and semidigital recording systems. Figure 3 shows the basic instrumentation components.

Because of the short functioning time two separate analog recording systems will be utilized for these firings. The signal will be recorded on CEC recording oscillographs operating at a speed of 160 inches a second. This will be utilized only for preliminary timing information because a 10-millisecond firing will yield only a 1.6-inch long record.

The second analog data recording uses a 3M MINCOM FM tape system. Analog signals will be recorded on this system at a magnetic tape speed of 60 in/sec. They will be played back onto recording oscillographs at a tape speed of 15 in/sec with the FM amplifiers adjusted and filtered accordingly. This difference in

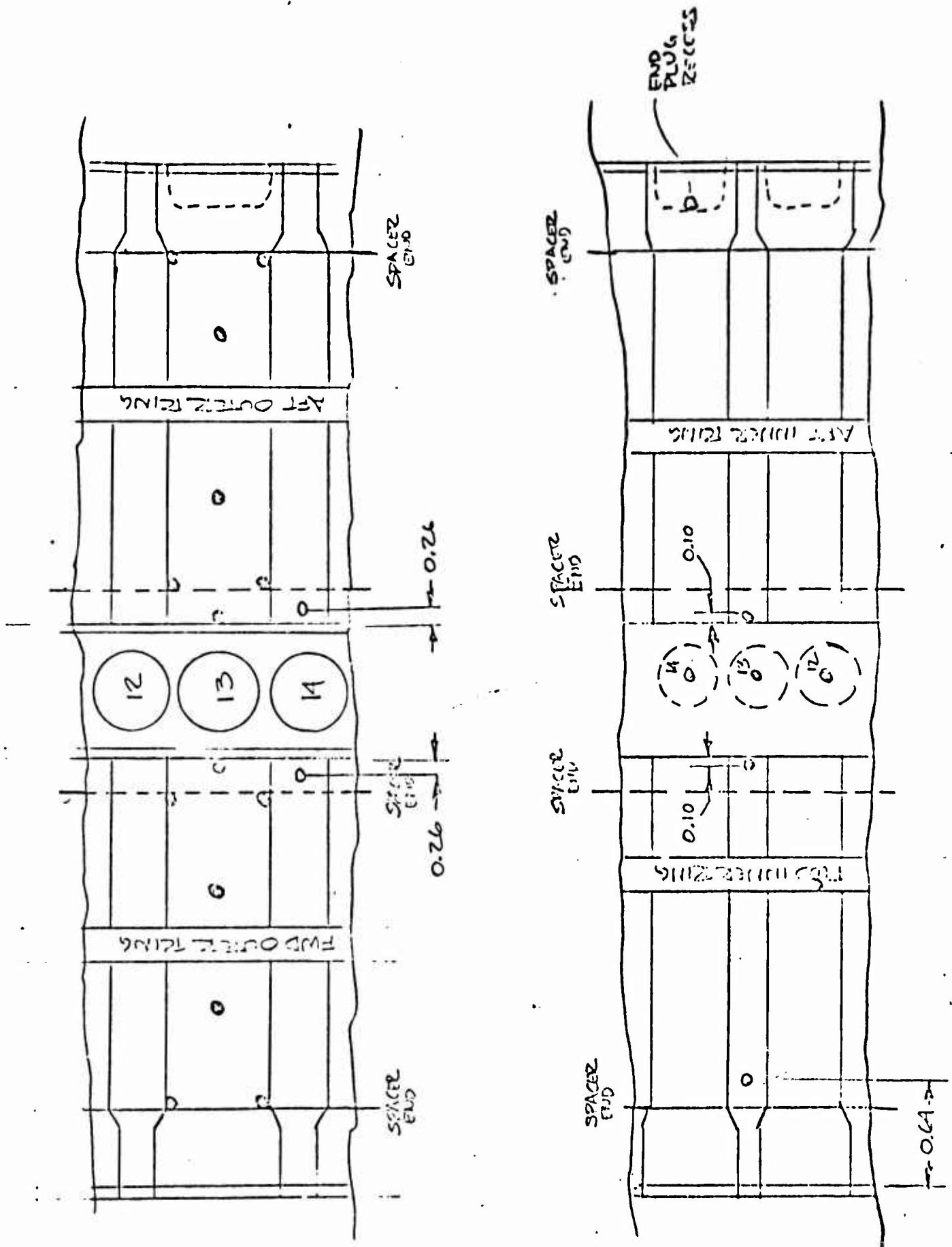


Figure 2. Thermocouple Location Diagram

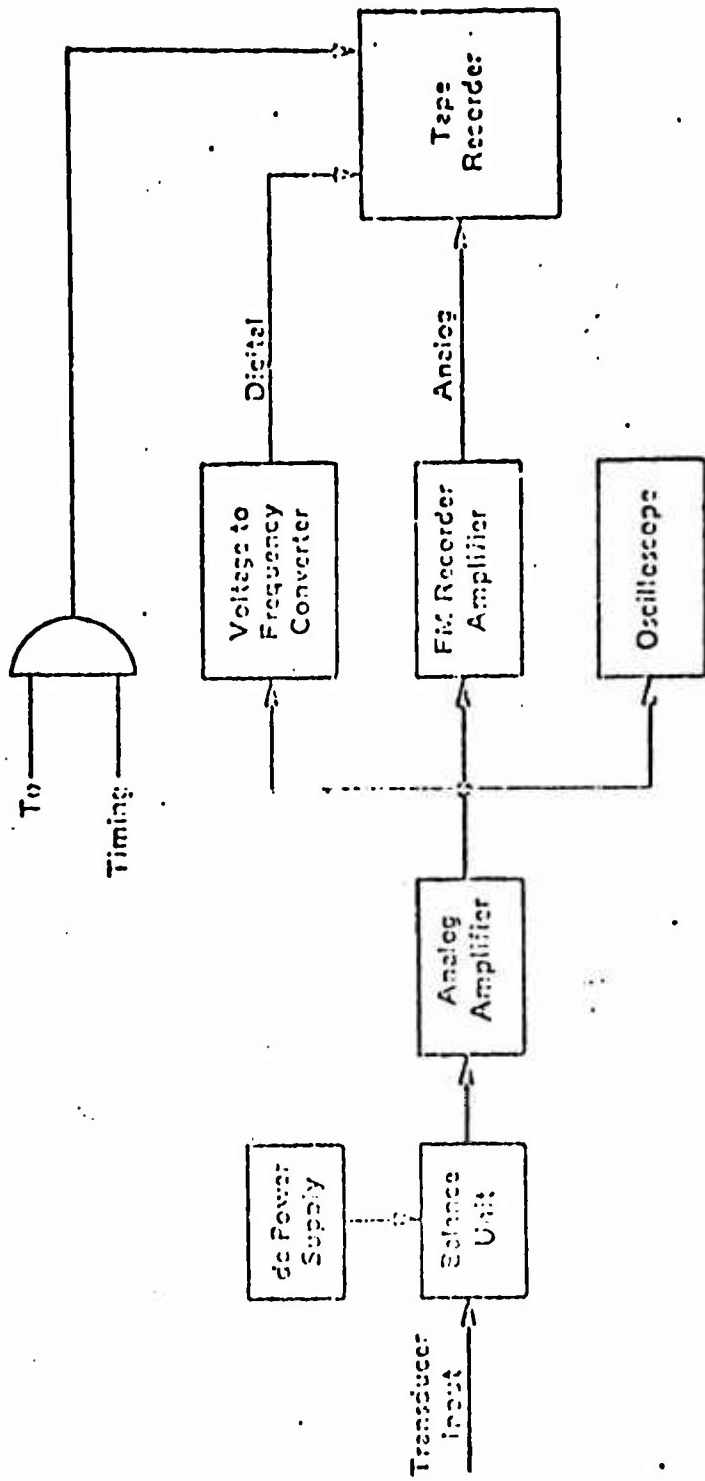


Figure 3 Record Instrumentation.

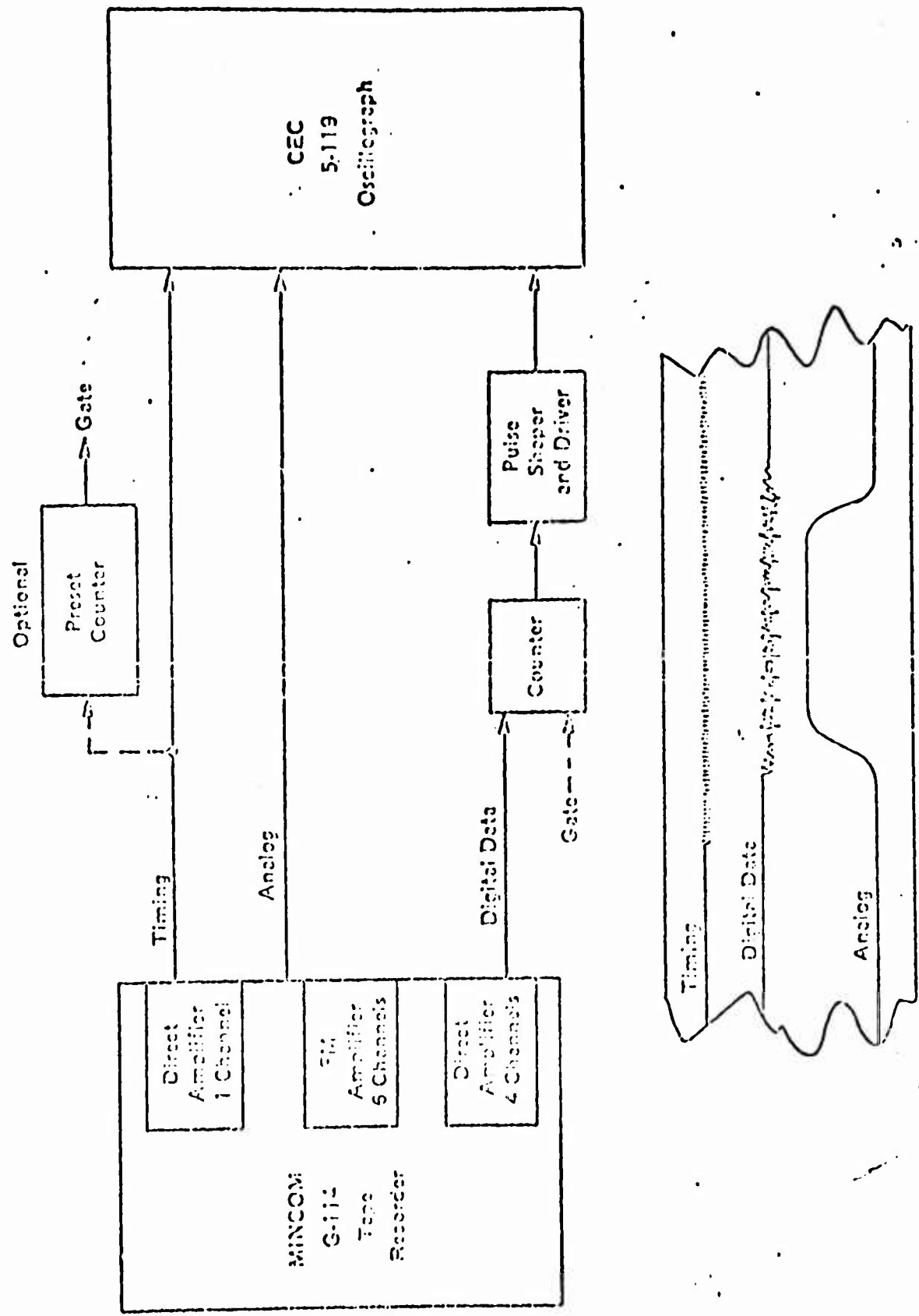


Figure 4 Oscilloscope Trace.

recording versus playback speeds will result in a 4/1 extension of the oscillograph recordings and will yield a 6.5-inch firing trace. By carefully recording calibration steps on the FM system immediately prior to firing, the data can be handled without any significant loss in accuracy. Calibrated timing will also be put on the tape so that it will appear on the expanded record at the proper intervals. A schematic of the data playback system is shown in Figure 4.

The semidigital data system is used primarily for the recording of the integral values which can be used to secure averages over selected time spans. In this system the data signal is converted into a series of pulses. These pulses range from 0 to 100,000 per second for full scale. This frequency converter is a true integrator in that it actually follows the input signal with no averaging or sampling. In terms of an analog curve, it follows the curve and emits pulses as equal area bits under the curve have been traversed. Thus, oscillations on a thrust-time curve do not affect the accuracy of the impulse measurement.

Integration of a curve requires only selection of the desired time interval and the playback of the semidigital tape over that interval. Calibration values are used to convert the pulses into an impulse integral.

6.3 Calibration Accuracy

All transducers will be calibrated physically and electrically. The physical calibration of the load cell and pressure gauge will be performed with NBS certified weights which are accurate to 0.006 percent and .15 percent respectively. Timing signals are generated by a secondary frequency standard which is accurate to at least one part in 10^8 .

The electrical calibration system is an 8-wire, double-shunt hookup in which a series of 0.005 percent resistors is shunted across two arms of the bridge. This makes errors due to changes in line resistance, transducer temperature, and contact resistance negligible.

6.4 Photographic Coverage

Two HY-CAM film cameras will be used to record all firings. The cameras will be set to run at about 1500 frames per second.

7.0 TEST FIRINGS

7.1 Sequence

The first three motors will be fired .25 seconds apart. The remaining units will be fired one at a time. The sequence and data taken will be as follows:

<u>Motor</u>	<u>Thrust</u>	<u>Instrumentation</u>		
		<u>Pressure</u>	<u>Temp.</u>	<u>Film</u>
12	X		X	X
14	X		X	X
13	X	X	X	X
05	X	X		X
33	X	X		X
19	X	X		X
47	X	X		X
41	X	X		X
27	X	X		X
55	X	X		X
04	X	X		X
32	X	X		X
18	X	X		X
46	X	X		X
40	X	X		X
26	X	X		X
54	X	X		X
42	X	X		X
28	X	X		X
50	X	X		X

7.2 Firing Procedure

- a. Wire up stepper switch to the motors that is to be fired.
- b. Mount MMA to load cell.
- c. Hook up firing circuit.
- d. Verify that the Firing Circuit Stepper Switch is in position 1.
- e. Connect the Firing Circuit so that the ARM voltage can be applied at T-10 seconds and the firing command activated at T_0 . These commands must come from the firing sequence in the control room.

8.0 DATA PLAYBACK

The analog data stored on FM tape will be played back through the Nicolet 1090 Digital Storage Oscilloscope which digitizes the signal and allows both the magnitude of the signal and the time scale to be expanded by as much as a factor of 64. This instrument also displays the magnitude and time from t_0 of any datum point in digital form.

By storing both the electrical calibration steps and the analog firing trace in the oscilloscope memory the magnitude of the signal can be determined.

This instrument will be used both to analyze the pressure signals for magnitude and frequency of oscillations at a sufficient number of points to describe any phenomenon of interest and to obtain point values of pressure and thrust. Integral values will be obtained from the frequency integrator system as usual.

APPENDIX 7

KEY PERSONNEL

LIST OF KEY PERSONNEL

Vought Systems Division

- | | | |
|-----|--|--|
| (a) | Program Manager | G. Tarnower |
| (b) | Chief Project Engineer | J. B. Griffin |
| (c) | Systems Integration
Technical Project
Engineer | R. F. Colleoni |
| (d) | MMA Propulsion
Engineer | B. L. Cockrell/A. E. Pierard |
| (e) | Structural Analysis
and Test | J. W. Farrell, C. A. Ford,
and C. L. Hudson |
| (f) | Mass Properties | D. C. Fritz |
| (g) | Thermal | W. D. Jordan |

Atlantic Research Company

- | | | |
|-----|-------------------|-------------------------|
| (a) | Program Manager | B. F. Rohrback/R. Brown |
| (b) | Project Engineer | G. J. Ripol |
| (c) | Analytical Design | C. W. Anderson |
| (d) | Process Engineer | R. O'Connor |
| (e) | Test Engineer | M. Procinsky |
| (f) | Mass Properties | D. Fisher |

ABMDA

- | | | |
|-----|--------------------|------------------|
| (a) | Program Manager | V. S. Kupelian |
| (b) | Technical Monitor | J. L. Andrews |
| (c) | Propulsion Monitor | Dr. D. C. Sayles |

Rohm and Haas

- | | | |
|-----|--------------------------|-----------------|
| (a) | Propulsion
Consultant | W. C. Stone |
| (b) | Propulsion
Consultant | Dr. H. M. Shuey |

APPENDIX 8

DD FORM 1473

Unclassified

Security Classification

14 KEY WORDS	LINK A		LINK H		LINK C	
	ROLE	WT	ROLE	WT	ROLE	WT
1. Defense Systems						
2. Ballistic Missile Defense						
3. Satellite Interceptor						
4. Miniature Homing Vehicle						
5. Homing Interceptor						
6. Exoatmospheric Interceptor						
7. Anti-Missile Missile						
8. Direct Impact Kill						
9. Hypervelocity Impact Kill						
10. Non-Nuclear Kill Mechanism						
11. HIT - Homing Interceptor Terminal						
12. HIT - Phase II						
13. Solid Rocket Motors						
14. Miniature Solid Rockets						
15. T-Burner Technology						
16. High Burn Rate Propellants						
17. Difluoramino Propellants						

Unclassified

Security Classification

DISTRIBUTION LIST

U. S. Army SAFEGUARD System Command
P. O. Box 1500
Huntsville, Alabama 35807
Attn: SSC-CS, Mr. A. M. Bolling (1 copy)

Defense Documentation Center
Cameron Station
Alexandria, Virginia 22314 (20 copies)

Advanced Ballistic Missile Defense Agency
P. O. Box 1500, Huntsville, Alabama 35807
Attn: RDMH-O (1 copy)
RDMH-M (1 copy)

Director, ABMDA, Department of the Army
1100 Commonwealth Building
Arlington, Virginia 22209
Attn: RDMD-MD (1 copy)
RDMD-D (1 copy)

Calspan Corporation
P. O. Box 235
Buffalo, New York 14221
Attn: C. Muzzey (1 copy)

Riverside Research Institute
80 West End Avenue
New York, New York 10023
Attn: J. J. Kraus (1 copy)